



## - D8.4 –Final Technical Report PART B M40

### - VERSION -

VERSION	DATE
3.1	19/04/2024

### - PROJECT INFORMATION -

GRANT AGREEMENT NUMBER	955930
PROJECT FULL TITLE	INNOVATIVE PHYSICAL/VIRTUAL SENSOR PLATFORM FOR BATTERY CELL
PROJECT ACRONYM	INSTABAT
START DATE OF THE PROJECT	01/09/2020
DURATION	3 years
CALL TOPIC	H2020-LC-BAT-13-2020
PROJECT WEBSITE	www.instabat.eu

### - DELIVERABLE INFORMATION -

WP NO.	8
WP LEADER	CEA
CONTRIBUTING PARTNERS	CEA, BMW, CNRS, FAURECIA, IFAG, INSA Lyon, UAVR, VMI
NATURE	Final REPORT
PERIODIC REPORT	2 <sup>nd</sup>
PERIOD COVER BY THE REPPORT	01/09/2020 – 31/12/2023
AUTHORS	Olivier RACCURT
CONTRIBUTORS	S. Genies, E. Villemin, C. Septet, O. Poncelet, S. Desousa-Nobre, V. Heiries, A. Laurin, R. Franchi, M. Ranieri, Y. Reynier, A. Martin, D. Buzon, L. Baggetto, M. Priour, J. Bonefacino, J.M. Tarascon, M. Nascimento, J. Pinto, L. Matuck, M. Ferreira, J. Li, M. Schmuck, T. Roessler, Talal Khan Ali Zai, P. Karayaylali, B. Antunes, F. Bribiesca-Argomedo
CONTRACTUAL DEADLINE	29/02/2024
DELIVERY DATE TO EC	19/04/2024
DISSEMINATION LEVEL (PU/CO)	PU

### - ACKNOWLEDGMENT -



This project has received funding from the European Union's Horizon 2020 research and innovation program under grant agreement No 955930.



## Deliverable Review

Reviewer #1: M. Reytier		
Answer	Comments	Type*

1. Is the deliverable in accordance with		
1.1. The Description of actions?	<input checked="" type="checkbox"/> Yes <input type="checkbox"/> No	<input type="checkbox"/> M <input type="checkbox"/> m <input type="checkbox"/> a
2. Is the quality of the deliverable in a status		
2.1. That allows it to be sent to European Commission?	<input checked="" type="checkbox"/> Yes <input type="checkbox"/> No	<input type="checkbox"/> M <input type="checkbox"/> m <input type="checkbox"/> a
2.2. That needs improvement of the writing by the originator of the deliverable?	<input type="checkbox"/> Yes <input checked="" type="checkbox"/> No	<input type="checkbox"/> M <input type="checkbox"/> m <input type="checkbox"/> a
2.3. That needs further work by the Partners responsible for the deliverable?	<input type="checkbox"/> Yes <input checked="" type="checkbox"/> No	<input type="checkbox"/> M <input type="checkbox"/> m <input type="checkbox"/> a

Reviewer #2: O. Raccurt		
Answer	Comments	Type*

3. Is the deliverable in accordance with		
3.1. The Description of actions?	<input checked="" type="checkbox"/> Yes <input type="checkbox"/> No	<input type="checkbox"/> M <input type="checkbox"/> m <input type="checkbox"/> a
4. Is the quality of the deliverable in a status		
4.1. That allows it to be sent to European Commission?	<input checked="" type="checkbox"/> Yes <input type="checkbox"/> No	<input type="checkbox"/> M <input type="checkbox"/> m <input type="checkbox"/> a
4.2. That needs improvement of the writing by the originator of the deliverable?	<input type="checkbox"/> Yes <input checked="" type="checkbox"/> No	<input type="checkbox"/> M <input type="checkbox"/> m <input type="checkbox"/> a
4.3. That needs further work by the Partners responsible for the deliverable?	<input type="checkbox"/> Yes <input checked="" type="checkbox"/> No	<input type="checkbox"/> M <input type="checkbox"/> m <input type="checkbox"/> a

\* Type of comments: M = Major comment; m = minor comment; a = advice

---

- ABSTRACT/SHORT SUMMARY -

## Summary for publication

### Summary of the context and overall objectives of the project

The increased use of batteries requires their improvement in terms of safety as well as quality, reliability and life (QRL). The EU-funded INSTABAT project aims to observe in operando essential parameters of a Li-ion battery cell to provide higher accuracy states of charge, health, power, energy and safety (SoX) cell indicators. The goal of INSTABAT is to improve the batteries' safety and Quality, Reliability and Life (QRL). The project ambition is to develop a solution of smart sensing technologies and functionalities integrated into a battery cell. This solution is to be able to perform reliable monitoring of key parameters, correlate the evolution of these parameters to the physicochemical degradation phenomena taking place at the battery cell's core and improve the battery's functional performance and safety. This ambition is aligned to the Battery 2030+ roadmap<sup>1</sup>.

To achieve this goal, INSTABAT was developing a proof of concept of smart sensing technologies and functionalities, integrated into a battery cell and capable of

- performing reliable in operando monitoring (time- and space-resolved) of key parameters (temperature and heat flow; pressure; strain; Li<sup>+</sup> concentration and distribution; CO<sub>2</sub> concentration; “absolute” impedance, potential and polarisation) by means of
  - (i) four embedded physical sensors (optical fibers with Fiber Bragg Grating and luminescence probes, reference electrode and photo-acoustic gas sensors),
  - (ii) two virtual sensors (based on reduced electro-chemical and thermal models),
- correlating the evolution of these parameters with the physico-chemical degradation phenomena occurring at the heart of the battery cell,
- improving the battery functional performance and safety, thanks to enhanced BMS algorithms providing in real-time higher accuracy SoX cell indicators (taking the measured and estimated parameters into consideration).

The main results of the project are: (1) a proof of concept of a multi-sensor platform (cell prototype equipped with physical/virtual sensors, and associated BMS algorithms providing SoX cell indicators in real time); (2) demonstration of higher accuracy for SoX cell indicators; (3) demonstration of improvement of cell functional performance and safety through two use cases for EV applications; (4) techno-economic feasibility study (manufacturability, adaptability to other cell technologies...).

INSTABAT smart cell concept aims to open up new horizons to improve cell use and performances (e.g. by reducing ageing, allowing the decrease of safety margins, triggering self-healing, facilitating second life, etc.).

### Work performed from the beginning of the project & main results

During the INSTABAT project all the objectives were partially or fully achieved.

Physical sensors development has been achieved according to the initial workplan. The definition of requirements for smart batteries and for integration of the sensors into the cell was completed (WP1) and compiled in deliverable D1.1. and D1.2.

The development of four of the 5 physical sensors was achieved in the WP2: two optical fiber sensors for temperature and one optical fiber sensor for pressure measurement, photoacoustic sensor for PAS-CO<sub>2</sub> measurement and embedded reference electrode. A Li ion luminescent probe was developed and validated on the electrolyte and open the way for the development of the Li ion sensor. Unfortunately, the development of this sensor was not fully achieved during the project. However, the proof of concept on glass substrate in electrolyte was achieved and we are confident for successful development of this kind of sensor on optical fiber in the future. For PAS-CO<sub>2</sub>, the sensor was calibrated and validate in argon atmosphere and tested embedded inside a pouch-cell. However a dependency of the signal to the cycling was observed. The analysis of the results and complementary tests conclude to an interference in detection due to the overlap of the infrared absorption between carbonate solvent of the electrolyte and CO<sub>2</sub>. We have identified

---

1 <https://battery2030.eu/research/roadmap/>

ways in which this dependency can be avoided, but it has not been possible to explore them within the framework of the project. During the second phase of the project, a size reduction of PAS CO<sub>2</sub> sensor was achieved to improve their integration into the cell.

The compatibility of these physical sensors with the cell environment was validated and the insertion of fiber-optic sensors and reference electrode sensors was successful as were the tests in cycling conditions. We have demonstrated the capability of these sensors to measure the desired physical parameters inside the cell. The evaluation of accuracy, resolution, sensitivity, response time, frequency/speed of acquisition has been done for these sensors and a proof of concept of *in-operando* measurement in cycling condition was achieved during this first period. It was found that only the FBG sensor, the OF-lumT sensor and the reference electrode are at a sufficient stage of development to be adapted to the battery environment and be integrated without affecting electrochemical performance. However, the optical sensor and reference electrode already provide valuable information for the understanding of chemical degradation phenomena. Implementation of FBGs sensors on pouch cells has allowed for calorimetric measurements (WP3) allowing not only to monitor the heat rate associated with SEI formation in cells with different electrode materials but also to benchmark electrolyte formulations. Besides, this approach has allowed for long-term monitoring during WLTP cycling, potentially paving the way for EV applications (see D3.3).

Development of the electrochemical virtual sensor has advanced as planned (D4.1) and initial validation against COMSOL models by CEA (D4.2) was done. Then the experimental data from WP3 was used to validate and adapted the model to the different type of cells. The development of indicators necessary for the BMS operation was achieved and validate. Electrochemical virtual sensors are fully parametrizable for varying resolution. Accuracy characterisation of virtual sensor was done with good results. Development of reduced electrochemical model and E-BASE algorithm considering computation time restrictions and modularity in the resolution for the real-time implementation, as well as C code generation and compilation for integration into the real-time platform. First comparisons underway for SoC in simple scenarios for single temperature point and adequate initialization using the electrochemical model (E-BASE) seem to be within the 0.5% of the reference model (CEA 1D+1D electrode model).

A first version of the multi-physics instrumentation platform was developed in WP5 to exploit the sensors signal in real time. A first demonstration of the INSTABAT lab-on-cell concept was achieved with an instrumented cell with RE and Optical fiber Luminescence Temperature sensors in cycling condition at high loading (up to 3C and 4D). Within BIGMAP<sup>2</sup>, an experimental portfolio of complementary techniques is developed towards the implementation of a multimodal and multiscale characterisation platform. *In-operando* synchrotron experiments were realised and analysed according to BIGMAP standards and protocols on INSTABAT pouch cells instrumented with different types of sensors. The spatially resolved real-time structural data obtained by X-rays diffraction (phase transitions, strain, local lithiation mechanism) will be cross-correlated to the various sensing data (temperature, local electrode potential), allowing monitoring the potential perturbations of reaction mechanisms due to sensor integration and to correlate micro-to-macro scale performance related to parameter variations along cycling. During this experiment we have validated the following steps:

- The instrumentation of cells with 2 sensors (OF LUM-T and RE).
- The cell performance was not modified by the integration of the sensors.
- The setup for, data acquisition and real-time treatment is functional with these 2 sensors
- The measurement of the internal cell parameters with sensors (Temperature, Electrochemistry).
- The local impact of sensors on the cell functioning can be characterised with operando XRD measurements.

The development of the demonstrator with the integration of all the sensors (physical and virtual) and SoX algorithm was achieved in the second part of the project (WP5). The demonstration was performed at the end of the project during abuse tests and cycling test under multi-instrumented cells and standard cells without sensors. These experiments were demonstrated the functionality and the operability of the INSTABAT lab-on-cell concept. However, due to the shorter time and the few number of samples only few experiments can be done to validate the proof of concept and measure the improvement of the performances and safety in all condition that we expected. Despite these partial results, we can conclude that the platform is functional and that it is capable of achieving the objectives set out in the project. We therefore consider that the proof of concept for this project has been achieved.



The results also demonstrate the versatility of the platform, which is capable of integrating different types of sensors (physical and virtual) as well as advanced management functions. This platform therefore also meets the BATTERY 2030+ roadmap objectives for coupling sensing and self-healing with a fully integration of all the function in the same tools.

## Progress beyond the state of the art, expected results and potential impact

New non-invasive integrated sensors based on optical fibre, reference electrode and photo-acoustic technologies was improved/developed and used in operando condition to know in real time the evolution of internal battery key parameters. Virtual sensors, based on improved electro-chemical and thermal reduced models, was developed to bring complementary data allowing a more comprehensive monitoring of the cell. BMS algorithms connecting the outputs of the physical/virtual sensors to battery physics-based models was also be developed to enable an optimised management of battery cells.

During the project we develop new innovative sensor and demonstrate their capability to catch internal parameters of the cells. The effect of sensors integration to the cell degradation and safety was studied. The results show no major impact on the insertion of optical fibre sensors and reference electrode sensors to cell performances, ageing and safety. The results from ageing test demonstrate the capability of the sensors to monitor the key parameters of the cells. The correlation between sensors signal and degradation phenomenon were achieve. These results was used to improve the development of cells models, virtual sensors and SoX algorithm integrated in BMS. The correlations between sensors signal and degradation was also bring a much better knowledge of the cell in operando internal state, opening opportunities for innovation.

One of the major results of INSTABAT is the development of the lab-on-cell concept and the associate platform. The INSTABAT platform integrate all the sensors (physical and virtual) and BMS function (SoX) for a real time cell monitoring. This platform was used in different experiment (ageing and abuse test) and in collaboration with BIG-Map project for a multi-instrumented operando measurement at ESRF.

In addition, INSTABAT was innovate by assessing the: (1) number of sensors / measurement points needed and their best positioning to provide measurements with the highest possible quality; (2) impact of the measurements provided by the physical sensors on the accuracy of the virtual sensors; (3) benefits of each physical sensor and measured parameter on the accuracy of the SoX indicators to suggest the best trade-off between the number of physical measures and model accuracy. The gain in accuracy has been also be related to the sensors cost, their potential disturbance of the cell functioning and to the manufacturing difficulties.

INSTABAT was contribute to an improvement of performance and strongly force the development of sustainable battery storage solutions for Li-ion batteries at a more competitive price. The “lab-on-a-cell” approach will be used to develop a new generation of Li-ion and post-Li-ion batteries in the future, which is aligned with the objectives of the Work Programme. Moreover, INSTABAT results will contribute to a successful mass introduction of batteries for mobility, allowing for substantial improvements leading to an ultra-high performance. The INSTABAT project was also well aligned with the specific impacts set out in the call LC-BAT-13. Finally, the progress made by INSTABAT is in line with the BATTERY 2030+ roadmap<sup>3,4</sup>.

The results obtained during the project show that there is a need for further development of sensors for monitoring internal cell parameters. In particular for the measurement of safety critical parameters and long term ageing. The integration of the sensors and their compatibility with the manufacturing processes remains a major challenge. Finally, the analysis of the long-term stability of the smart cell concept (sensors and cells) requires more effort and time. Further studies are needed to answer this ageing question.

<sup>3</sup> <https://battery2030.eu/research/roadmap/>

<sup>4</sup> J. Amici, et al. A Roadmap for Transforming Research to Invent the Batteries of the Future Designed within the European Large Scale Research Initiative BATTERY 2030+, Advanced Energy Materials, Volume 12, Issue 17 2102785

## TABLE OF CONTENTS

<b>SUMMARY FOR PUBLICATION .....</b>	<b>3</b>
<b>SUMMARY OF THE CONTEXT AND OVERALL OBJECTIVES OF THE PROJECT .....</b>	<b>3</b>
<b>WORK PERFORMED FROM THE BEGINNING OF THE PROJECT &amp; MAIN RESULTS .....</b>	<b>3</b>
<b>PROGRESS BEYOND THE STATE OF THE ART, EXPECTED RESULTS AND POTENTIAL IMPACT .....</b>	<b>5</b>
<b>TABLE OF CONTENTS .....</b>	<b>6</b>
<b>FINAL TECHNICAL REPORT – PART B .....</b>	<b>8</b>
<b>1 EXPLANATION OF THE WORK CARRIED OUT BY THE BENEFICIARIES AND OVERVIEW OF THE PROGRESS .....</b>	<b>8</b>
<b>1.1 OBJECTIVES.....</b>	<b>8</b>
<b>1.2 EXPLANATION OF THE WORK CARRIED PER WP .....</b>	<b>15</b>
WP1 - DEFINITION OF REQUIREMENT .....	15
WP2 - DEVELOPMENT OF PHYSICAL SENSORS.....	19
WP3 - CORRELATION BETWEEN MEASURED/ESTIMATED PARAMETERS AND PHYSICO-CHEMICAL DEGRADATION PHENOMENA OCCURRING IN THE BATTERY CELL.....	57
WP4 - DEVELOPMENT OF VIRTUAL SENSORS AND BMS SOX INDICATORS ALGORITHMS.....	104
WP5 - PROOF OF CONCEPT MULTI-SENSOR PLATFORM .....	116
WP6 - TECHNO-ECONOMIC FEASIBILITY, ADAPTABILITY TO OTHER CELL MARKETS AND ENVIRONMENTAL CONSIDERATIONS.....	129
PTIR545/F.....	132
DEFINED IN ROHS AND REACH DIRECTIVES .....	132
WP7 - DISSEMINATION, COMMUNICATION AND EXPLOITATION .....	138
WP8 - PROJECT MANAGEMENT .....	150
<b>1.3 IMPACT .....</b>	<b>159</b>
1.3.1 GENERAL IMPACTS.....	159
1.3.2 IMPACT ON THE PROJECT PARTNERS .....	162
<b>2 UPDATE PLAN OF THE EXPLOITATION AND DISSEMINATION RESULTS.....</b>	<b>165</b>
<b>3 UPDATE OF DATA MANAGEMENT PLAN .....</b>	<b>166</b>
<b>4 FELLOW-UP OF RECOMMENDATIONS AND COMMENTS FROM PREVIOUS REVIEW(S) .....</b>	<b>167</b>
<b>4.1 ANSWER TO THE RECOMMENDATION 1.....</b>	<b>167</b>
<b>4.2 ANSWER TO THE RECOMMENDATION 2.....</b>	<b>167</b>
<b>4.3 ANSWER TO THE RECOMMENDATION 3.....</b>	<b>167</b>
<b>4.4 ANSWER TO THE RECOMMENDATION 4.....</b>	<b>168</b>
<b>4.5 FELLOW-UP OF RECOMMENDATIONS AND COMMENTS FROM FINAL REVIEW .....</b>	<b>168</b>
<b>4.6 ANSWER TO THE RECOMMENDATION FROM THE FINAL REVIEW .....</b>	<b>169</b>
<b>5 DEVIATION FROM ANNEX 1 AND ANNEX 2 .....</b>	<b>169</b>
<b>5.1 TASKS .....</b>	<b>169</b>
<b>5.2 USE RESOURCES .....</b>	<b>173</b>
5.2.1 CEA .....	173
5.2.2 BMW GROUP .....	175
5.2.3 CNRS .....	176
5.2.4 IFAG .....	178
5.2.5 FAURECIA .....	180
5.2.6 INSA LYON .....	182



---

5.2.7	UAVR .....	184
5.2.8	VMI .....	185

## Final TECHNICAL REPORT – PART B

# 1 Explanation of the work carried out by the beneficiaries and overview of the progress

## 1.1 Objectives

The ambition of INSTABAT is to deliver a **proof of concept of a multi-sensor platform (“lab-on-a-cell”)**, capable of monitoring simultaneously multiple battery key parameters and of correlating them with battery cell physico-chemical degradation processes. The Battery Management System (BMS) receive in real-time the output data from the physical/virtual sensors of the platform, enabling the delivery of very accurate SoX cell indicators (States of Charge, Health, Power, Energy and Safety). The benefits of the improved accuracy of the SoX need to be demonstrated in the project via two critical uses cases: cycling at extreme conditions and high-power charging for EV applications. Eight objectives have been defined and are listed below:

### Objective 1:

**Perform time- and space-resolved measurements of battery cell critical parameters (Temperature and heat flow; pressure; strain; Li<sup>+</sup> concentration; CO<sub>2</sub> concentration; “absolute” potential, impedance and polarization) by means of embedded physical sensors (WP2)**

### Progress towards fulfilling objective 1:

Five different physical sensors have been developed during the project according to the initial workplan. We have demonstrated the operation of sensors technologies (OF/FBG, OF/LumT, RE) and progress to the development of OF/LumL by demonstrated the operation of Li<sup>+</sup> optical probe in the electrolyte. Insertion of 3 of physical sensors OF/FBG, OF/LumT and RE was demonstrate on full cell and tested in cycling condition. We have demonstrated the capability of sensors to measures physical parameters (temperature, heat flow, pressure, strain, “absolute” potential, impedance and polarization). Temperature monitoring of pouch cells together with heat rate monitoring has been successfully implemented, including for WLTP cycling conditions.

However the objective 1 not fully achieved at the end of the project for two of physical sensors:

- 1- The optical probe for lithium detection was developed and validate in representative medium of the cell but not on the optical fiber OF/LumL.
- 2- The PA CO<sub>2</sub> sensor have been tested inside cell. However, the measurement signal is disturbed by electrolyte vapours. The origin of this disturbance has been identified and alternative development paths proposed.

### Key performances indicators related to the objective 1:

**KPI 1: Demonstration of prototypes of sensing technologies at TRL 4 for OF/FBG, TRL 3/4 for RE, TRL 3 for OF/LumT and OF/LumL and TRL 3/4 for PA**

We have demonstrated that physical sensors are functional in the cell environment. Some of them could be tested in the cells. Each sensor has been developed and tested in representative environment to explore their capability to detect the physical parameters. It is demonstrated that OF/FBG, OF/Lum, and RE can be implemented in cells to gather critical information upon long cycling. According to the recommendation of the reviewer during after the midterm review, the dimension and architecture of the PA CO<sub>2</sub> sensor was modified for an easily integration into cell packaging.

**KPI 2: Time- and space-resolved in operando measurements according to table in section 1.4.2 for accuracy, resolution, sensitivity, response time, frequency/speed of acquisition and sensor stability over cell lifetime**

OF/FBG, OF/LumT and RE sensors have been inserted into the cells and tested under cycling conditions. We have demonstrated the capability of theses sensors to measure the physical parameter inside the different cell format in

operando at different cycling conditions. The evaluation of accuracy, resolution, sensitivity, response time, frequency/speed of acquisition has been done for these sensors and a proof of concept of operando measurement in cycling condition was achieved during this first period. The accuracy and detection limit of PAS-CO<sub>2</sub> sensors was evaluated in N<sub>2</sub> atmosphere and will be tested in the cell atmosphere in the future work when the integration rules have been resolved. The OF/LumL for the Li<sup>+</sup> is not fully operational, only optical probe was developed with good sensitivity in carbonate medium. The next step is to insert this probe on the optical fiber to develop the OF/LumLi. The OF/LumL accuracy was improved during the project up to 1°C but not up to the objective of 0.1°C. However the long-term ageing shows a very good stability of the sensor at extreme conditions and during abuse tests. OF/FBG has demonstrated a high accuracy, resolution, response time and stability during critical WLTP long-term cycling, including tests at high temperature (up to 55°C).

**KPI 3: No cross-sensitivity between measured parameters (e.g. decorrelated measurements for temperature, pressure and strain for OF/FBG)**

The development of new OF/FBG sensors technology based on high-birefringent fibers and hybrid configuration were performed. The results were demonstrating the possibility to have a decorrelated measurement of temperature and pressure and/or strain parameters. We have demonstrated for the multi-instrumented cells with RE and OF/LumT there is no cross interaction between the two sensors. During the second period of the project multi-instrumented cell with RE, OF/LumT and OF/FBG with hybrid sensor (T and pressure) was tested in cycling condition without any interference between sensors. Any interferences or cross-sensitivity was observed during multi-instrumented tests (ESRF test, WP2 and WP5 tests)

**KPI 4: No degradation of cell performance and safety due to sensor individual integration (e.g. linked to chemical reactivity, thermal aspects or geometrical disturbance)**

For this objective, the number and duration of tests with instrumented cells is too low to answer at this stage of the project. However, some of the electrochemistry tests with instrumented cells (with OF/FBG, OF/LumT and RE) have been done without degradation of the cell performances. Aging tests will be carried out during the second period of the project. From these results, we can conclude on the impact of sensors on cell degradation. The implementation of OF/FBG sensors in LiFePO<sub>4</sub> pouch cells did not show an increase in degradation during WLTP cycling at 25 °C compared to pristine cells. However, tests at 55°C showed that sensor implementation negatively impacts cell capacity retention, although no degradation on the cell electrodes was found during post-mortem analysis.

We don't observe a negative impact of the presence of a sensor inside the cell during safety tests (see WP5). However, due to the reduced number of safety tests during the project it's difficult to conclude and quantify the impact of the sensors on safety behaviour.

#### **Objective 2:**

**Perform time- and space-resolved estimations of battery cell critical parameters (Temperature and heat flow; Li<sup>+</sup> concentration and distribution; "absolute" potential and polarization) by means of virtual sensors (WP4)**

#### **Progress towards fulfilling objective 2:**

Development of Electrochemical virtual sensor has advanced as planned (D4.1 submitted) and initial validation against COMSOL model by CEA (D4.2) is underway with very positive preliminary results. In the second phase of the project, the model was adapted and validated with the experimental data. The results were a good estimation of the critical parameters of the cell by the reduced model. This has enabled us to develop high-performance SoX indicators integrated to the BMS.

#### **Key performance indicators related to the objective 2:**

**KPI 5: Demonstration of virtual sensors derived from physical-based electro-chemical and thermal reduced models at TRL 3/4 for both E-BASE and T-BASE**

Development of Electrochemical virtual sensor has advanced as planned (D4.1 submitted) and initial validation against COMSOL model by CEA (D4.2) is underway with very positive preliminary results. During the second phase of the project,

the model was adapted and validated with the experimental data from the cell used in the project. The development of a virtual sensor with a good efficiency was achieved with interfacing parameters for the BMS.

**KPI 6:** Time- and space-resolved real-time estimations according to table in section 1.4.2 for accuracy and resolution

Electrochemical virtual sensor fully parametrizable for varying resolution. Accuracy and resolution were performed in the task 4 with good results compared to the initial requirement.

#### Objective 3:

**Establish correlation between (1) cell physico-chemical degradation phenomena and (2) in operando measurements/ estimations (WP3)**

#### Progress towards fulfilling objective 3:

The ageing campaign with instrumented cell has been completed during the second period of the project. The results from these ageing tests have shown that more degradations were recorded for cells WLTP cycled at 25°C as compared with cells WLTP cycled at 55°C. Post-mortem analysis was carried out to investigate degradation mechanism and are further discussed in WP3 section. The correlation between sensors signal and degradation mechanism was achieved (see D33).

#### Key performance indicators related to the objective 3:

**KPI 7:** Correlations of thermal signature (from OF/FBG, OF/LumT, T-BASE); pressure and strain (from OF/FBG); CO<sub>2</sub> concentration (from PA); Li<sup>+</sup> concentration (from OF/LumL, E-BASE); and absolute electro-chemical potential (from RE, E-BASE), each with at least one cell physico-chemical degradation phenomena

The OF/FBG sensors developed by UAVR have proven to be available to track in real time and simultaneously decouple temperature, strain and/or pressure parameters, correlating them with internal electrochemical events in lithium cells. CNRS has demonstrated that calorimetric measurements using standard FBGs embedded in LiFUN pouch cells are a powerful tool to monitor the heat rate generated during the SEI formation, and allows for long time monitoring of the heat generated during long WLTP cycling. It was also demonstrated that such technique allows to benchmark electrolyte and electrode materials during the SEI formation. The OF/LumT sensors developed by CEA demonstrate feasibility to monitor internal temperature variation on VARTA and LiFUN cells without being affected by other parameters. RE sensors developed by IFAG and CEA, were capable to measure electro-chemical parameters on the INSTABAT cells.

#### Objective 4:

**Provide in real-time, via INSTABAT multisensory platform, (1) simultaneous monitoring of multiple battery key parameters (Temperature and heat flow; pressure; strain; Li<sup>+</sup> concentration and distribution; CO<sub>2</sub> concentration; “absolute” impedance; potential; polarization) and (2) accurate SoX cell indicators (WP5)**

#### Progress towards fulfilling objective 4:

Development of reduced electrochemical model and E-BASE algorithm considering computation time restrictions and modularity in the resolution for real-time implementation, as well as C code generation and compilation for integration into real-time platform.

#### Key performance indicators related to the objective 4:

**KPI 8:** Demonstration of multi-sensor platform (“lab-on-a-cell”) at TRL 3 (with at least 3 out of 4 physical sensors; 2 virtual sensors; data post-processing and logging; BMS on compact stand-alone prototyping unit)

Development of reduced electrochemical model and E-BASE algorithm considering computation time restrictions and modularity in the resolution for real-time implementation, as well as C code generation and compilation for integration into real-time platform.

The Lab-on-cell platform was operational and tested with 3 physical sensors, one virtual sensor and the SOC estimator in real time test condition.

**KPI 9: No degradation of cell performance due to integration of physical sensors all together**

Any test with multiinstrumented cells during the WP5 show a positive impact on the performance of the cell. The performance and safety of the cells were not affected by sensors.

However these tests were performed at the end of the project and was not long enough to conclude for the long-term impact of the sensor to the cell performances. However the results from WP3 during ageing with one sensor type inside the cell don't show a significant impact on the performance degradation.

**Objective 5:**

**Demonstrate improved performance of BMS algorithms (1) integrating measured/estimated parameters (2) based on fine electro-chemical and thermal modelling of the battery cell (WP4)**

**Progress towards fulfilling objective 5:**

In order to progress in this objective, refined versions of the P2D and P3D electrochemical and 3D thermal models have been developed by using experimental information to adapt the original parametrization of the model. These refined models have been used in the development of reduced-order models (e.g. the model used in the E-BASE algorithm, in the electrochemical case). These reduced order models and estimation algorithms have been successfully integrated into the BMS in order to provide SoX information. New SoX indicators, based on previously unavailable internal battery information have been demonstrated, such as the charge limitation due to risk of lithium plating, based on internal potential reconstruction in the battery. This proof-of-concept opens the path to exploiting the information obtained using new sensor technology, as well as tailoring new BMS indicators that go beyond the state-of-the-art limitations, such as Li-plating risk indication. This newly available information opens the door to optimizing charge and discharge profiles in real time, providing more information for the BMS to make operating decisions.

**Key performances indicators related to the objective 5:**

**KPI 10: High fidelity reproduction of cell electro-chemical and thermal behaviour using numerical simulation models:**

- 1D+1D electrode model: < SoA6 (5% error for electrode potential; <20% error for lithium concentration throughout the thickness of the electrode at different Crates and extreme temperatures)
- p3D electro-thermal cell model: < SoA (5% error for cell voltage at different Crates and temperatures; <5% error for temperature gradient)
- 3D thermal cell model: < SoA (5% for the absolute maximum temperature, temperature gradient and hot spot locations)

1. **1D+1D electrode model:** < SoA6 (5% error for electrode potential; <20% error for lithium concentration throughout the thickness of the electrode at different Crates and extreme temperatures)

This P2D electrode model has been compared to experimental results taken from WP3 for the single-layer pouch cell available for the INSTABAT project (29mAh) and shows good agreement in all operating temperatures tested, i.e. 45°C, 25°C and -10°C. Some limitations remain, in particular concerning the end-of-discharge at low temperatures. This model has not been validated in the fully instrumented multi-layer cell, where the data has not yet been processed. Therefore specific quantification of the potential error in the final cell is not available at the moment. Based on the results in the mono-layer cells, a good agreement is expected at 25°C, final performance at lower temperatures could underperform the target KPI. The lack of Li-concentration sensor in the final integrated cell means the lithium concentration error cannot be quantified throughout the battery in a direct way, so agreement in measured potentials will be used in place of direct concentration measurements. It can be seen that the model shows a good accuracy in charge, even at 2C, with the lithium plating model added to the P2D model. For discharges at 25°C, the normalized RMS error is of 0.17% (6 mV) for a 0.1C discharge and of 1.2% (41 mV) for a 1C discharge. For charges at 25°C, the normalized RMS error is of 0.25% (6 mV) for a 0.1C charge and of 1.3% (45 mV) for a 2C charge. For more details see D4.7.



2. **p3D electro-thermal cell model:** < SoA (5% error for cell voltage at different Crates and temperatures; <5% error for temperature gradient)

This P3D electrode model shows good agreement with the measured voltages of the 1Ah (multi-layer) cell in 0.2C and 4C discharge scenarios at 25°C. Little temperature heterogeneity is expected in the pouch cell format. For a 0.2C discharge at 25°C, a normalized RMS error of 2.4% between experimental and simulation results was evaluated on a full SOC range (the error is below 0.4% in the SOC range [100%;94%]). For a 4C discharge at 25°C, a normalized RMS error of 0.4% between experimental and simulation results was evaluated on a full SOC range. For a 0.2C discharge, the temperature increase was negligible. For an 4C discharge the RMS error on the temperature increase is respectively 0.2°C, 0.2°C and 1.3°C for the temperature of the casing, the temperature of the positive tabs and the temperature of the negative tabs. Those errors have to be compared to actual temperature increases measured between 6°C and 10°C during the same discharge. Temperature gradients on 1A.h pouch cells were not evaluated experimentally due to the difficulty to perform such simultaneous measurements on pouch cell prototypes clamped between solid plates. For more details see D4.8.

3. **3D thermal cell model:** < SoA (5% for the absolute maximum temperature, temperature gradient and hot spot locations)

This 3D thermal model has not been validated experimentally. It suggest high homogeneity in the temperature distribution inside the INSTABAT multi-layer cell is very small (in agreement with the p3D model expectations). It is possible that new information available after the processing of WP5 data can be used to better quantify this KPI.

#### **KPI 11:** Demonstration of improved accuracy of BMS SoX7 indicators algorithms:

- State of Charge (SoC): 0.5% accuracy over the whole temperature range (SoA:3%)
- State of Power (SoP): 2% accuracy over the whole temperature range (SoA: 10%)
- 2% accuracy for estimation time horizon of the maximum available power, as compared to the measured one (SoA: 10%)
- State of Energy (SoE): 2% accuracy over the whole temperature range (SoA: 5%)
- State of Safety (SoS) indicator allowing the cell temperature extrapolation and providing safety margin value to predict thermal runaway

1. State of Charge (SoC): 0.5% accuracy over the whole temperature range (SoA:3%)

A precise characterization of this KPI will be available after processing the results of WP5 cycling.

2. State of Power (SoP): 2% accuracy over the whole temperature range (SoA: 10%)

Quantification of this KPI will be available after processing the results of WP5 cycling, in D4.12 or an update thereof.

3. 2% accuracy for estimation time horizon of the maximum available power, as compared to the measured one (SoA: 10%)

Quantification of this KPI will be available after processing the results of WP5 cycling, in D4.12 or an update thereof.

4. State of Energy (SoE): 2% accuracy over the whole temperature range (SoA: 5%)

An SoE indicator was not developed in the final version. The underlying principle being close to the SoC and SoP indicators, a similar approach can be followed. It was decided to prioritize the development of SoC and SoP indicators, which required further adaptation of the estimators in Task 4.2 based on experimental information using the INSTABAT pouch cell materials. These two indicators serve as proof-of-principle for the overall SoX family of indicators (except for SoS).

5. State of Safety (SoS) indicator allowing the cell temperature extrapolation and providing safety margin value to predict thermal runaway

SoS indicators were not developed in this project due a number of raisons:

The first reason was the unavailability of CO<sub>2</sub> sensors that were expected to provide further information in order to detect the beginning of thermal runaway. This remains a perspective if new information becomes available through new sensor technologies.

The second reason was the delay in the project to finalize the platform and test multiinstrumented cell in abuse condition. These experiment was done very closed to the end of the project. The analysis of the results was not fully achieved. However it was not possible to develop SOS algorithm. However the results from safety test demonstrate the interest of the sensors to detect early degradation inside the cell. This early detection is the key factor to develop a performant SoS and improve the safety margin of the cells.

#### Objective 6:

**Demonstrate improvement of cell functional performance and safety through two use cases for EV applications (WP3, WP4, WP5)**

#### Progress towards fulfilling objective 6:

The results from the safety test in WP5 show the interest of the FOLum-T and RE sensor to monitor the internal parameters of the cell to increase the safety. These two sensors can be use to an early detection of the critical parameter to mitigate the thermal runaway. Unfortunately, in the project we don't have the opportunity to test the FBG sensors in safety test. However, from the result on ageing test with FBG sensors, we believe that this type of sensor should also enable early detection of the presence of a disease.

The use of OF/FBG and their application for calorimetry measurements has allowed to track the temperature and heat rate generated during cycling (WLTP-1) over a long period of time. Such approach allows for application in BMS where safety is of primary importance, while monitoring the heat generated by the cell may prove to be useful for EV cooling system.

#### Key performances indicators related to the objective 6:

**KPI 12:** Higher estimated performance for cycling at extreme conditions: increase operational temperature window by >10%; characterise impact of measurement/estimation of temperature on cell ageing

We don't have the opportunity to evaluate this KPI, the number of abuse test was too low and was perform at the end of the project. However the results from WP5 suggest that by continuing the work it will be possible to address this objective.

**KPI 13:** Optimised plans for high-power charging, while still ensuring safety: 10% less time for high-power charging from SoC 10% to 80% by utilising sensor data output compared to conventional fast charging; high-power utilising sensor data output leads to 5% less ageing compared to conventional high-power charging

We can answer we the same sentence as for the KPI12. However the results from the WP5, The results obtained are encouraging and should enable us to achieve this objective in the future. Final quantification of this KPI will be available after data processing from WP5. However, an algorithm providing proof-of-concept fast charging using sensor (physical and virtual) data in order to explicitly limit Li-plating degradation of the cell has been integrated in the experimental platform.

---

**Objective 7:**

Carry out an industrial study for a multi-sensor platform; assess manufacturability and techno-economic feasibility, including adaptability to other cell technologies and use cases; provide environmental assessment, focusing on traceability, second life and recyclability (WP6)

**Progress towards fulfilling objective 7:**

This objective is achieved successfully during WP6. The detailed explanation of each objective and how they are achieved is explained in WP6 section of this document and WP6 deliverables.

**Objective 8:**

Collaborate with other EU H2020 projects, in particular contribute to the large-scale research initiative on future Battery Technology, under the umbrella of the successful LC-BAT-15 consortium (WP7)

**Progress towards fulfilling objective 8:**

Collaboration with other EU H2020 project was already effective through the participation of the Battery2030+ initiative. Collaborative work was already started at different stages in communication and dissemination activities, experimental work and exchange and share the progress of INSTABAT work. (see WP7 and D78 for more details)

## 1.2 Explanation of the work carried per WP

### WP1 - Definition of requirement

Work package number	1	Leader	IFAG						
Work package title	Definition of requirements								
Short name of participant	BMW	VMI	CNRS	CEA	FAURECIA	UAVR	INSA	IFAG	
Person	months	per	6	8.5	0.5	0.5	0.5	0.5	3.5
participant									
Start month	M1			End month			M6		

#### Objectives

The main objectives of WP1 are to:

- Translate the goals defined in INSTABAT objectives into sets of requirements, according to the current knowledge;
- Adjust the requirements to the special needs of the selected cell;
- Correlate these requirements to the developments assessed as feasible within the consortium and the project runtime;
- Use the results obtained in WP1 as an input for the other technical WPs;
- Involve all the consortium partners in the definition of requirements, taking advantage of their technical expertise in the field.

#### Highlights of most significant results

For an alignment between all partners on the definition of requirements, a kick-off conference call was organized by WP1 leader IFAG for October 16, 2020. Between October 2020 and end of February 2021, biweekly phone conferences with a good participation by all partners took place.

As a result of these discussions, deliverable D1.1 with an encompassing definition of requirements for smart batteries was completed and submitted by BMW on March 08, 2021, with about one month delay.

Similarly, deliverable D1.2 with a complete description of the requirements for integration of the sensors into the cell was completed and submitted by VMI on February 26, 2021, right on target.

With the submission of these deliverables, milestone M1 “Smart cell requirements broken down at each WP level” was reached on March 08, 2021, with only eight days delay.

#### Summary of progress towards objectives and details for each task

### TASK 1.1 DEFINITION OF REQUIREMENTS FOR SMART BATTERIES, BROKEN DOWN AT BMS AND PHYSICAL/VIRTUAL SENSORS LEVEL

(Leader: BMW; Participants: All (M1-M5))

In extended, detailed discussions between all partners, the requirements for smart batteries were agreed on and documented in a deliverable report (D1.1) by BMW, the task leader for T1.1. For details about the requirements, please refer to this report, only an excerpt is given here.

Deliverable D1.1 states the following overarching requirements for full battery electric vehicles (BEVs) and plug-in hybrid electric vehicles (PHEVs) used for passenger vehicle applications:

- The detection or anticipation of safety-critical states and ageing mechanisms, so that countermeasures can be taken to avoid battery critical events, or at least to be able to send a timely warning signal.
- The development of adaptive “state-of-charge” (SoC), “state-of-health” (SoH) and “state-of-power” (SoP) estimators, which allows reliable performance in different environmental conditions and over the whole battery lifetime including second life application.
- Sensor-based battery operational strategies, which for example, improve fast charging and provide an adaptive “depth-of-discharge” (DoD) performance range larger than the standard range with fixed limits.

#	Requirements	Validation	Requirement Context	Priority	WP1	WP2	WP3	WP4	WP5
3	C-Rate capability: 0.3C charge/0.5C discharge continuous		Cell specifications	high					
4	Sensor must be fully functional in the following temperature ranges: Temperature range test chamber for storage: -40°C to +80°C. Temperature range test chamber for cycling tests: -25°C to +55°C. Max. Temperature of the cell core: chemistry-dependent, approx. + 80°C; Max. Temperature of cell housing: chemistry-dependent, approx. + 60 °C; Max. Temperature of cell terminal: chemistry-dependent, approx. + 70 °C	Sensor can be tested in dummy cells without active cell chemistry in the full temperature range.	Environmental condition	medium		x			x
10	Cell state of charge (SoC) must be able to be determined with a frequency of 0.1 Hz and an accuracy of 2%.	Applying a driving cycle (provided by BMW) at defined temperatures [for example 40 °C, 25 °C, 10 °C and 0 °C, -10 °C]. The cycle is stopped at certain time and the cell is discharged with a defined current (e.g. 1/ 3C) until the end-of-discharge voltage is reached. The external temperature in climatic chamber remains the same during the driving cycle and the discharge. The reference state of charge can be compared with the estimated state of charge determined by the algorithm.	BMS Functions / Use case	high				x	x
19	Cell external short circuit must be detected and communicated within 50 ms during operation	External short circuit test: The detection and communication of the short circuit event must take place within 50ms.	Safety	low			x		x
24	Sensor signals should be brought together at a central point on the cell for further evaluation	Evaluation through implementation	Demonstrator	high		x	x		x
27	Extended cycle life and calendaring life for sensor cells and electric and electronic component are required. for example, 5000 cycle life and 20 years calendaring life till battery end of service (cell dependent, therefore the definition is open)		second life application	medium					

Figure 1. Excerpt from the main table in deliverable D1.1, with functional requirements in six contexts

As documented in the detailed main table in deliverable D1.1 (see Excerpt in Figure 1), a total of 27 functional requirements in the six contexts “cell specifications”, “environmental condition”, “BMS functions / use case”, “safety”, “demonstrator”, and “second life application” were identified, each with a method for validation, a priority, and an assignment of relevance to the work packages. As one example (see Figure 1) in the category “BMS functions / use case”, requirement #10 “Cell state of charge (SoC) must be able to be determined with a frequency of 0.1 Hz and an accuracy of 2%” was given a high priority, is associated with WP5 and WP6 and will be validated in the following manner: “Applying a driving cycle (provided by BMW) at defined temperatures [for example 40°C, 25°C, 10°C and 0°C, -10°C]. The cycle is stopped at certain time and the cell is discharged with a defined current (e.g. 1/ 3C) until the end-of-discharge voltage is reached. The external temperature in climatic chamber remains the same during the driving cycle and the discharge. The reference state of charge can be compared with the estimated state of charge determined by the algorithm.”

In a second table in deliverable D1.1, the correlation of the requirements to the six physical / virtual sensors considered in INSTABAT is provided. For instance, the luminescence sensor will contribute to the determination of the cell SoC by providing information about the Li-ion concentration.

For additional information and more details, please refer to the deliverable report D1.1.

## TASK 1.2 DEFINITION OF REQUIREMENTS FOR INTEGRATION OF SENSORS INTO THE CELLS

(Leader: VMI; Participants: All) (M1-M6)

The same discussions as for T1.1 were used to work out the requirements for the integration of sensors into the cells between all partners, documented in a deliverable report (D1.2) by VMI, the task leader for T1.2. Again, details about the requirements can be found in this report, only an excerpt is given here.

As documented in deliverable D1.2, a total of 17 requirements were identified in the five categories “mechanical”, “electrical”, “environmental”, “lifetime” and “safety”. In addition, concrete tests and the corresponding passing criteria were specified for the cells with integrated sensors. For both, requirements and test results, hard exclusion criteria were defined. As one example in the category “mechanical”, Figure 2 shows the cross-section in z-direction of a sector of the stack for a tentative INSTABAT Prototype Cell for two hypIGMAP sensors, a cylindrical sensor (left) and a reference electrode (right). For this type of integration, the following hard exclusion criteria were defined:

- Sensors with a larger cross-section in the z-direction than 2 times the electrode diameter (~250µm).
- Safety-critical deposition of lithium at locations where the sensors are integrated into the stack.
- The integration of the Multi-Sensor platform increases the safety hazard level to > 4.

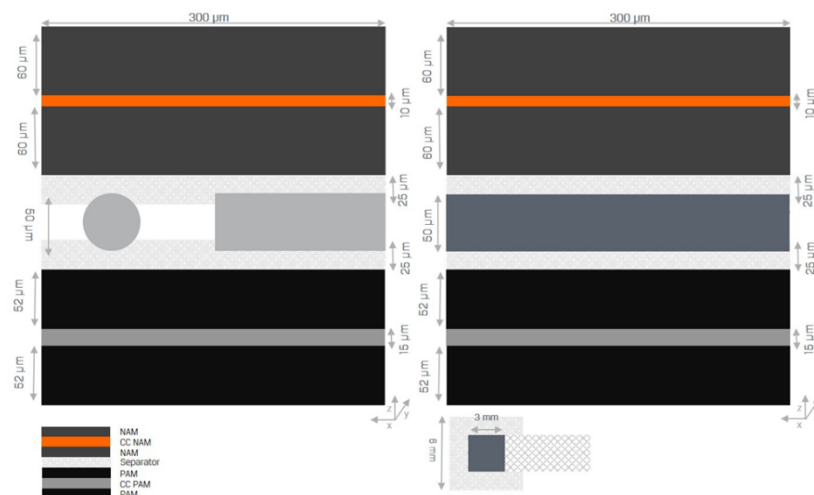


Figure 2. Cross-section in z-direction of a sector of the stack for a tentative INSTABAT Prototype Cell.  
Left - Hypothetically integrated cylindrical sensor / Right - Hypothetically integrated reference electrode.

To highlight one further example: In D1.2 concrete mechanical tests for “vibration” and “shock” of the battery cells are defined. Table 1 shows the corresponding passing criteria, differentiating for comparability between three types of cells:

- Hypothetical “state-of-the-art” (SoA) cell (TRL9)
- INSTABAT prototype base cell (TRL5)
- INSTABAT prototype cell with the integrated sensor platform (TRL4)

In addition, for the two levels of prototype cells, two different active materials are being distinguished. Here also, hard exclusion criteria for the test results are defined in D1.2:

- The integration of the Multi-Sensor platform increases the safety hazard level to > 4.
- Total failure of the sensor and/or uncontrollable shift in the sensor capabilities.

For additional information and more details, please refer to the deliverable report D1.2.



Table 1. Expected/estimated effect of vibration-test, and shock-test on industrial pouch-cell, INSTABAT prototype cell, multi-sensor platform integrated into INSTABAT prototype cell

	Industrial-Pouch-Cell*	INSTABAT Prototype-Cell**		INSTABAT Prototype-Cell***	Multi-Sensor Platform/
	C/NMC622	C/NMC622	C/Si <sub>550</sub> <sup>++</sup> /NMC622	C/NMC622	C/Si <sub>550</sub> <sup>++</sup> /NMC622
Vibration	a. no explosion/ fire b. no leakage c. cell failure (≤0.1%)	a. no explosion/ fire b. leakage (≤1.0%) c. cell failure (≤1.0%)	a. no explosion/ fire b. leakage (≤1.0%) c. cell failure (≤1.0%)	a. no explosion/ fire b. leakage (≤10.0%) c. cell/sensor failure (≤10.0%)	a. no explosion/ fire b. leakage (≤10.0%) c. cell/sensor failure (≤10.0%)
Shock	a. no explosion/ fire b. no leakage c. cell failure (≤0.1%)	a. no explosion/ fire b. no leakage c. cell failure (≤1.0%)	a. no explosion/ fire b. no leakage c. cell failure (≤1.0%)	a. no explosion/ fire b. leakage (≤10.0%) c. cell/sensor failure (≤20.0%)	a. no explosion/ fire b. leakage (≤10.0%) c. cell/sensor failure (≤20.0%)

\*TRL9, \*\* TRL5, \*\*\* TRL4, \*\*advanced (next generation) active material

Table 2. List of deliverables WP1

Deliverable Number	Deliverable Title	Lead beneficiary	Type	Dissemination level	Due date (in month)	Status
D1.1	List of requirements for smart batteries	2 - BMW GROUP	Report	Public	5	Submitted
D1.2	List of requirements for the integration of the multi-sensor platform in cells	8 - VMI	Report	Public	6	Submitted



## WP2 - Development of physical sensors

Work package number	2	Leader		UAVR
Work package title	Development of physical sensors			
Short name of participant	CNRS	IFAG	CEA	UAVR
Person months per participant	30	43	30	30
Start month	M1		End month M24	

### Objectives

The main objectives of WP2 are the following:

- Develop and characterise the following physical sensors (working on aspects such as sensor hardware development, adaptation to cell environment, sensor hardware integration and test):
- Optical fiber / Fiber Bragg Grating (OF/FBG): optical fiber sensors based on Bragg gratings will be produced, characterised and tested in the cell environment to detect accurately and in real-time internal and external temperature, heat flow and strain and pressure shifts in the cells.
- Reference electrode (RE): a reference electrode will be implemented within the cell to provide “absolute” potential, impedance and polarization.
- Optical fiber / Luminescence for Thermal and Li<sup>+</sup> Concentration (OF/LumT and OF/LumL): luminescent probes onto optical fibers will be developed to measure internal temperature and Li<sup>+</sup> concentration inside the cells.
- Photo-Acoustic sensor (PA): a photo-acoustic CO<sub>2</sub> gas detector will be adapted to the cell environment and provide
- CO<sub>2</sub> concentration measurements.
- Adapt sensors to the cell environment, considering aspects such as electro-chemical reactivity and thermal design, and carry out in situ lab-scale tests.
- Manufacture pouch cells to be used for sensor implementation and carry out in situ lab-scale tests.
- Validate the sensor technologies and deliver sensor prototypes for integration in the INSTABAT platform.

### Highlights of most significant results

WP2 intends to develop and to characterize four different physical sensors that will be used for specific cell parameters monitoring. Aspects such as the adaptation to the battery/cell environment will be considered in this WP. To successfully achieve the proposed WP2 objectives, different physical sensors have been developed, adapted and characterized to the specific sensing parameters. In this way, UAVR partner developed OF/FBG sensors based on Bragg gratings inscribed in standard and special fibers (polarization maintenance (PM) fibers) and hybrid sensing configurations. All the OF/FBG sensors were specifically calibrated to real time temperature, strain, and pressure detection. OF/FBGs with higher reflectivity and good signal stability were produced and a linear dependence to all parameters were attained. Addressed to this, hybrid sensing configurations based on Bragg gratings and Fabry-Perot interferometers were developed with impressive sensitivity values to simultaneous decouple pressure and temperature parameters. Several publications resulted from these physical sensors instrumented in the battery cells. The OF/FBG designed presents lower dimensions (from 5.0 to 8.0 mm length) and very good chemical stability and resistance, after 24 months submerged in the INSTABAT electrolyte solution. From the SEM and EDS analysis, the optical fiber surfaces were not etched, where just some precipitation of crystals (Phosphorous and Fluorine electrolyte compounds) was observed. The OF/FBGs developed with higher reflectivity were shipped to CNRS and CEA for cell battery integration during their manufacturing (WP3) and operation (WP5). Regarding the Reference Electrode (RE) sensor, several samples were developed by IFAG, targeting the “absolute” potential, impedance and polarization cell measurements. Gold and Aluminium with different thickness (100 nm, 50 nm, and 300 nm) and geometries (square, fork, and antenna) samples were tested and performed. From the experimental cell integration tests, the samples with gold films with antenna geometry and 100 and 300 nm thickness shows to be the better option as a RE sensor, due their present a stable potential after several hours of usage and higher conductivity. However, an LFP coating was necessary to be performed on the gold film. In this way, the RE sensors coated with gold, and LFP materials were selected as the INSTABAT RE sensors.

Optical fiber Luminescence thermal probes were successfully performed to temperature monitoring in the cells. Electrochemistry test of instrumented cell was used to demonstrate the no impact of the optical fiber on the cell up from C/10 to 4C cycling. During these tests didn't was observed any degradation on the cell and on the response of the

thermoluminescence sensor. We can conclude the good operation of the thermoluminescence. The OF/LumT was inserted in 1.1Ah cell and we demonstrated the linear dependence between optical signal to the cell temperature. The accuracy of the sensor is currently of 1.0 °C after a data treatment.

OF/LumL sensors based on luminescent probes for to detect the Li<sup>+</sup> concentration has been developed. It was demonstrated the efficiency of this luminescent probe to detect lithium ions in aqueous and carbonate medium (electrolyte) with a concentration around 1M. This optical probe was successfully deposit on glass substrate by covalent bounding without degradation of sensitivity for Li<sup>+</sup> detection. This probe was deposit on optical fiber but as an increase of the material quantity was required. For that, an adaptation of the tests bench should be performed and it is out of the INSTABAT timeline.

IFAG has adapted and provided different versions of a PA-CO<sub>2</sub> sensor based on the photoacoustic principle for cell integration and real time CO<sub>2</sub> monitoring. In the course of the integration tests, some further adaptations were performed, e.g., the installation of a completely new emitter and filter package, separation of the sensing chamber from the other electronics and the implementation of a connection between sensing chamber and electronics via a Flex PCB, and significant size reduction. From the calibration tests in a pre-fabricated CO<sub>2</sub> chamber, the sensor shows a good accuracy above 5 ppm and a detection limit up to 2 ppm. However, the PA-CO<sub>2</sub> sensor signal is also affected by other cell electrolyte solvents which compromise the CO<sub>2</sub> detection inside the cells environment.

*Summary of progress towards objectives and details for each task*

## **Task 2.1: PHYSICAL SENSOR HARDWARE DEVELOPMENT AND ADAPTATION TO BATTERY CELL ENVIRONMENT**

(Leader: UAVR; Participants: CNRS, CEA, IFAG) (M1- M24)

- **Subtask 2.1.1. Optical fiber / Fiber Bragg Grating (OF/FBG) sensor development and characterisation**

An inherent drawback of using FBG sensors in a standard photosensitive optical fiber as sensing technology is that it suffers from a large cross sensitivity from external parameters, such as: temperature, pressure and/or strain. In this way, alternative solutions to solve this drawback should be designed and they should also be tailored accordingly to the proposed application. Getting this in mind, UAVR partner has proposed to use two different approaches regarding the parameters of interests of monitoring in the INSTABAT Li-ion cells. For temperature and strain discrimination and tracking, FBG sensors recorded in commercial (PM) fibers were envisaged (OF/FBG – PM-FBG). For pressure and temperature discrimination, a hybrid sensing configuration based on FBGs and intrinsic Fabry-Perot interferometers (FPI) in the fibers tip were developed (OF/FBG – Hybrid sensor).

### **Temperature and strain decouple and tracking**

Simultaneous discrimination of temperature and strain parameters can be achieved by recording FBGs in high-birefringent (Hi-Bi) fibers. The basis for measuring two parameters with an FBG is to have a different sensitivity of the Bragg wavelength to each parameter. This is achieved in Hi-Bi FBGs because the shift of the reflection bands, for each polarization, is different and depends on the angle of the application of the external load. The displacement of both Bragg wavelengths can be used in a matrix equation to determine the two physical parameters: temperature and strain. As a consequence of the internal stress profile, the optical reflection spectrum of an FBG written in Hi-Bi fibers, with non-polarized light focused on the fiber, has a two-peak structure corresponding to the two orthogonal polarization modes of the fiber (see Figure 3); the X and Y polarizations of the LP<sub>01</sub> modes are split and each one has a different refractive index. These linear polarizations are the slow (X-axis) and fast (Y-axis) modes associated with the principal directions of the refractive index profile of the fiber. To use an optical fiber sensor composed of FBG in Hi-Bi fiber it is necessary to characterize the FBG properties in the presence of the parameters to be measured, as the specific dependence of these properties can induce.

Between the different type of commercial Hi-Bi fibers, the PANDA fibers were selected as to be better option to perform all the process, since the FBG sensors recording up to the cell battery integration, due to their easier fiber handling, simplicity of the recording process and very good FBG peaks reflectivity's and reproducibility. Also, FBG sensors recorded on standard Photosensitive (PS) fibers were also produced and used attached to the surface of the cylindrical or pouch

cells for external temperature monitoring, or internally for calibrations proposes. Some of the sensors produced, after a pre-calibration step, were shipped to CNRS and CEA partners to pouch cell integration during the battery manufacturing process.

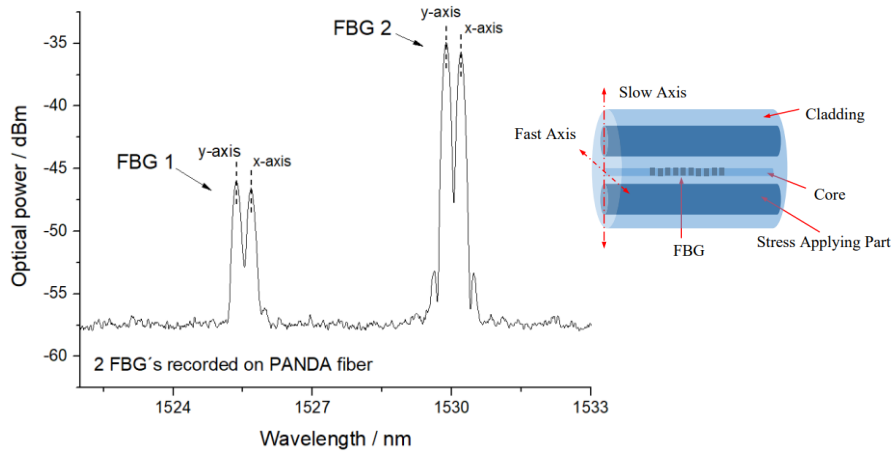


Figure 3. Optical reflection spectrum from the structure with two superimposed Bragg gratings in commercial Photosensitive PM PANDA Hi-Bi fiber. FBGs were inscribed using different phase masks by pulsed Q-switched Nd:YAG UV laser installed in the UAVR lab.

OF/FBG - PM-FBG fabrication:

- Several FBG sensors recorded on PM PANDA Hi-Bi fibers with higher reflectivity were performed after a pre-hydrogenation step for 1 week. This step of fiber hydrogenation was applied because the PM PANDA fiber is not photosensitive, and to get a very good reflectivity value of the FBG peaks. From Figure 3, can be observed that all FBGs presents peaks values near of -20 dBm, which is a very good result, with a birefringence value around  $4.2 \times 10^{-4}$ .

OF/FBG fabrication in standard PS fibers:

- Several FBG sensors were also recorded in standard PS fibers and a very good reflectivity and reproducibility has been achieved. To multipoint monitorization, different wavelength peaks were used.

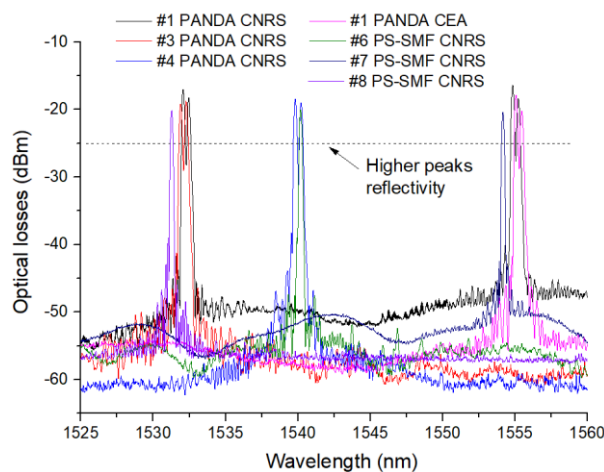


Figure 4. Spectral response of some FBG sensors recorded in PM Hi-Bi PANDA and PS fibers at UAVR lab, by using the UV laser, after the fiber hydrogenation, and shipped to CNRS and CEA. Double FBG peaks reflectivity higher than -25 dBm.

- Temperature and strain calibrations:

All the OF/FBG – PM-FBG sensors performed were calibrated to temperature and strain, by using a climatic chamber (between 5.0 °C and 60.0 °C) and a micrometre translation stage (between 0 and 2000  $\mu\epsilon$ ), respectively. As expected, different sensitivities were obtained for the two FBG peaks (x and y). Regarding the temperature sensitivities, values

around 9.0 pm/°C were obtained, in which higher values were register on the y-axis (fast) peak, with a difference near of 0.5 pm/°C for the x-axis (slow) peak. From the strain calibration, sensitivities around 1.20 pm/μϵ were determined, however with higher values on the x-axis (slow) (~ 0.05 pm/μϵ). All these sensitivities will be used on the simultaneous discrimination of both parameters through the matrixial method, as following described (Eq. 1):

$$\begin{bmatrix} \Delta\lambda_{FBGf} \\ \Delta\lambda_{FBGs} \end{bmatrix} = \begin{bmatrix} k_{FBGf\epsilon} & k_{FBGfT} \\ k_{FBGs\epsilon} & k_{FBGsT} \end{bmatrix} \begin{bmatrix} \Delta\epsilon \\ \Delta T \end{bmatrix} \quad (Eq. 1),$$

where  $k_{FBGf\epsilon}$ , and  $k_{FBGfT}$  are the strain and temperature sensitivities of the FBG fast peak, respectively, and  $k_{FBGs\epsilon}$  and  $k_{FBGsT}$  are the strain and temperature sensitivities of the FBG slow peak, respectively. A sensitivity matrix for simultaneous measurement of strain and temperature can be derived as (Eq. 2):

$$\begin{bmatrix} \Delta\epsilon \\ \Delta T \end{bmatrix} = \frac{1}{M} \begin{bmatrix} -k_{FBGsT} & k_{FBGfT} \\ k_{FBGs\epsilon} & -k_{FBGf\epsilon} \end{bmatrix} \begin{bmatrix} \Delta\lambda_{FBGf} \\ \Delta\lambda_{FBGs} \end{bmatrix} \quad (Eq. 2),$$

where  $M = k_{FBGs\epsilon} \times k_{FBGfT} - k_{FBGsT} \times k_{FBGf\epsilon}$  is the determinant of the coefficient matrix, which must be non-zero for possible simultaneous measurement.

### Pressure and temperature decouple and tracking

To simultaneous discriminate and track pressure and temperature variations during cell operation, UAVR have developed new and highly sensitive optical fiber sensors based on an in line FBG recorded near an intrinsic FPI cavity, forming and hybrid configuration (OF/FBG – Hybrid sensor). These sensors were performed by splicing a single mode fiber (SMF) to a hollow core silica tube (~ 200 μm), with a very small section of a UV curable polymeric material in the fiber tip (see Fig 5.d). This small portion created by the silica tube and the polymer will perform a triple light interference. The first one between the SMF and the 1<sup>st</sup> polymer surface (M1). The second one between the two surfaces of the polymer (M2), and the third one between the SMF and the end face of the polymer (fiber tip) (M3). This constructive interference will promote a sensitivity increase in the resultant spectral response, which can be followed by performing appropriate data analysis on the final spectral responses. By following the peaks or valleys from the filter signal produced after the correspondent Fast-Fourier Transform analysis, was possible to attain the pressure and temperature shifts of the FPI cavity. In this case, the simultaneous discrimination of both parameters, will be obtained by recording FBG sensors near of this region. As the FBG sensors presents different pressure and temperature sensitivities, by using the matrixial method (Eq. 3), both parameters can be simultaneously tracked.

$$\begin{bmatrix} \Delta\lambda_{FBG} \\ \Delta\lambda_{FPI} \end{bmatrix} = \begin{bmatrix} K_{P,FBG} & K_{T,FBG} \\ K_{P,FPI} & K_{T,FPI} \end{bmatrix} \begin{bmatrix} \Delta P \\ \Delta T \end{bmatrix} = \mathbf{K} \begin{bmatrix} \Delta P \\ \Delta T \end{bmatrix} \Leftrightarrow \begin{bmatrix} \Delta P \\ \Delta T \end{bmatrix} = \frac{1}{D} \begin{bmatrix} K_{T,FPI} & -K_{T,FBG} \\ -K_{P,FPI} & K_{P,FBG} \end{bmatrix} \begin{bmatrix} \Delta\lambda_{FBG} \\ \Delta\lambda_{FPI} \end{bmatrix} \quad (Eq. 3)$$

These coefficients include the temperature sensitivity coefficients ( $K_{T,FBG}$  and  $K_{T,FPI}$ ) measured in picometers or nanometers per degree Celsius (nm/°C or pm/°C) for the FBG and the FPI, respectively, as well as the pressure sensitivity coefficients ( $K_{P,FBG}$  and  $K_{P,FPI}$ ) measured in picometers or nanometers per bar (nm/bar or pm/bar) for the FBG and FPI, respectively.  $\Delta\lambda_{FBG}$  and  $\Delta\lambda_{FPI}$  (measured in picometers, pm) denote the wavelength variations for the FBG and FPI, respectively.  $\Delta P$  (measured in bar) and  $\Delta T$  (measured in degrees Celsius) represent the pressure and temperature variations, respectively.

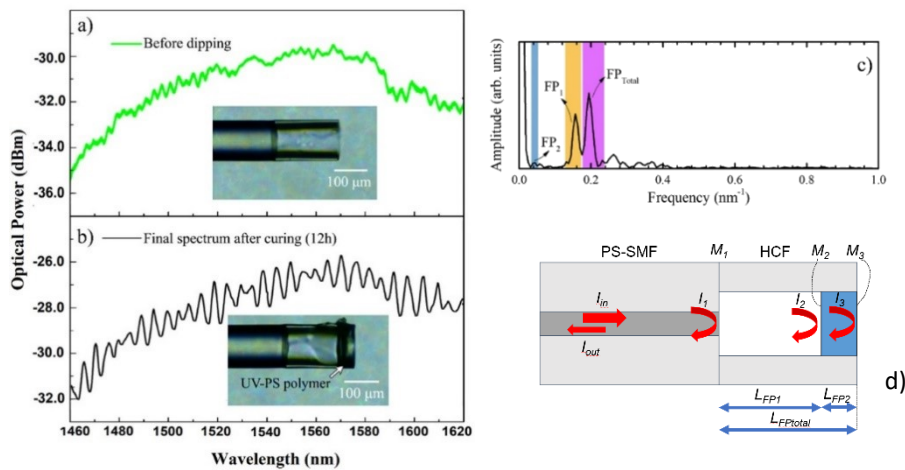


Figure 5. The spectrum response of the FPI sensor before (a) and after (b) the dipping. c) Fast-Fourier transform of the FPI response spectrum after curing. d) Schematic diagram of the internal FPI sensor on the fiber tip.

- OF/FBG - Hybrid sensor temperature and pressure calibrations:

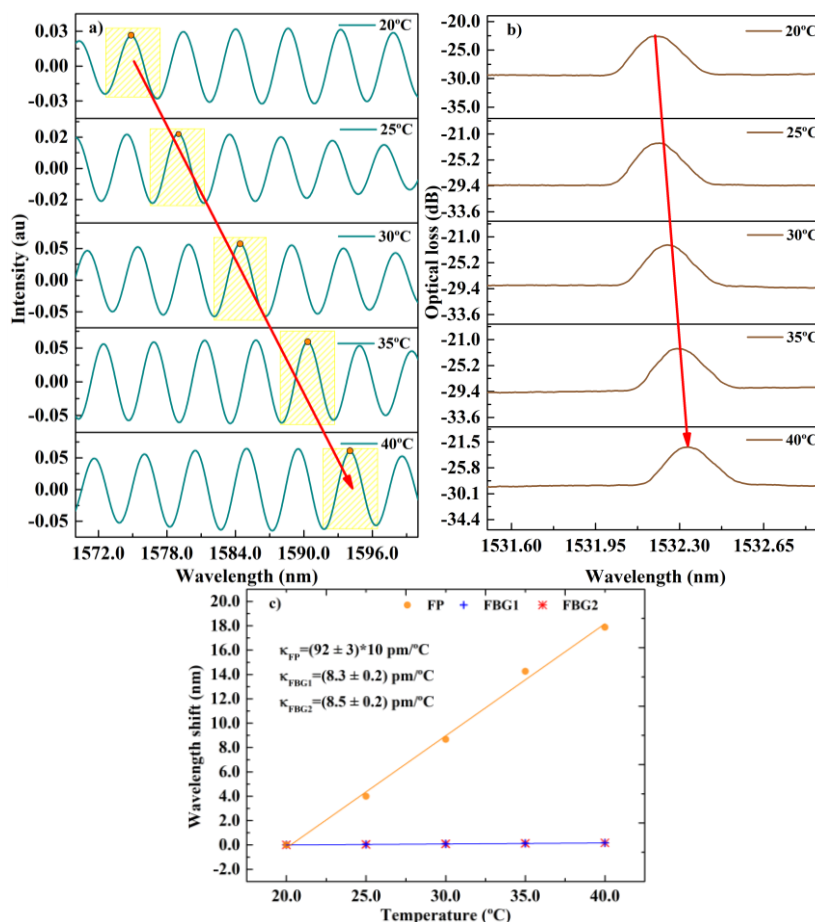


Figure 6 a) Spectral response of the FP1 cavity at each temperature step; b) Spectral response of the FBG1 at each temperature step; c) Temperature characterization.

The temperature calibration was performed in a climatic chamber (Model LC64, from WeissTechnik®, Supplylab, Lisbon-Portugal, with an operating range between -70.0 °C and 180.0 °C), in steps of 5.0 °C, from 25.0 °C to 50.0 °C. Two types of data were recorded: the spectral responses after stabilizing the chamber internal temperature, approximately 25 minutes apart, and the FBGs wavelength peaks at an acquisition rate of 1 s. The pressure calibration was performed by using a stainless-steel pressure chamber, controlled with a digital manometer, in a range between 0.0 and 3.0 bar, with steps of 0.2 bar. In both cases, the spectral responses were acquired with the previously mentioned optical interrogator and processed with Enlight® software. The arrows in each graph of Figure 6 and Figure 7, represent the selected interference fringe used to calibrate the FPI sensor and the FFT bandpass filter signal to each physical parameter. The FBG sensors were calibrated by analysing the Bragg wavelength shift in each temperature and pressure step. From these values, standard sensitivities were achieved for the FBG sensors to temperature and pressure. For pressure characterization, as the wavelength shifts of FBGs were inside of the optical interrogator resolution, it can be inferred that the FBGs sensitivity to pressure is null, so, a zero value will be utilized for subsequent calculations. Regarding the FP1 an outstanding negative pressure sensitivity of -11.4 nm/bar were determined. For temperature, also a higher value of 0.92 nm/°C was attained. In order to analyse if any hysteresis to pressure is presented on the hybrid sensor developed, a consecutive pressure variation ranging from 0 to 3.0 bar was applied. A very residual hysteresis was determined during the cycles. However, we can neglect this behavior for the operando cycling results.

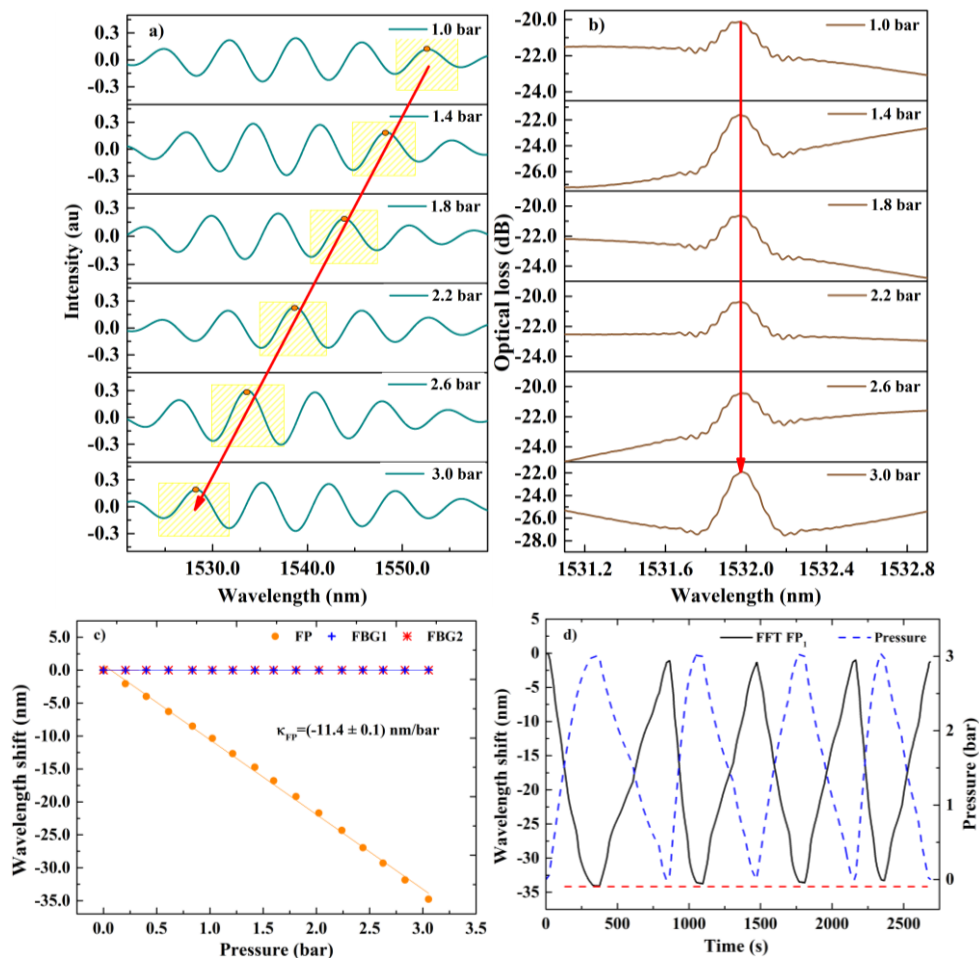


Figure 7 a) Spectral response of the FP1 cavity at each pressure step; b) Spectral response of the FBG1 at each pressure step; c) Pressure characterization; d) Hysteresis test conducted on the OF/FBG - hybrid sensor, consecutive pressure variations ranging from 0 to 3.0 bar was applied to the sensor to assess its response characteristics, a residual hysteresis can be observed during the cycles.



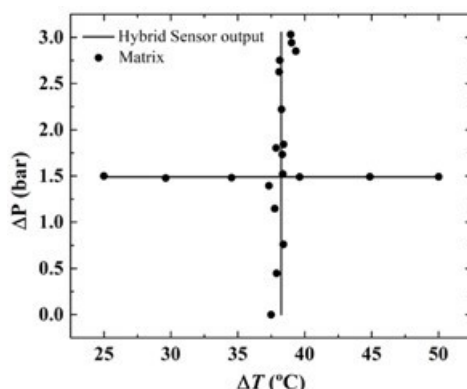


Figure 8 OF/FBG - Hybrid sensor output values determined by Equation 3 for applied pressure at constant temperature and temperature shifting at constant pressure. The resolution of the OF/FBG - Hybrid sensor was determined when the sensing head was subject to pressure and temperature changes of 3.0 bar and 25.0 °C, respectively. The spread of the data in this figure presents root mean square deviations of  $\pm 0.6$  °C and  $\pm 8$  mbar for temperature and pressure measurements from the simultaneously discrimination.

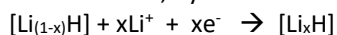
From Equation 3, the sensors output can be determined as presented in Figure 8 From the matrix method, rms errors for temperature and pressure of  $\pm 0.6$  °C and  $\pm 8$  mbar was respectively determined for the OF/FBG - Hybrid sensor developed.

## • Subtask 2.1.2 Reference Electrode (RE) sensor development

The reference electrode (RE) will provide measurements of “absolute” potential, impedance and polarization. Currently, there is no reference electrode is present on the market for lithium-ion systems. This explains why the literature reports the use of “homemade” reference electrodes based on different materials supported on tabs or metal grids <sup>1,2</sup>. Three main families of materials can be used: insertion materials such as  $\text{Li}_{(1-x)}\text{FePO}_4/\text{LiFePO}_4$  (LFP) <sup>5</sup> or  $\text{Li}_4\text{Ti}_5\text{O}_{12}/\text{Li}_{(4+x)}\text{Ti}_5\text{O}_{12}$  (LTO) <sup>6</sup>, lithium alloy metals (e.g.  $\text{Li}_x\text{Al}/\text{Al}$  <sup>7</sup> or  $\text{Li}_x\text{Au}/\text{Au}$  <sup>8</sup>. They are identified as a possible reference material because:

1 - Their thermodynamic potential is independent of the lithium ion concentration in the electrolyte. It is fixed:

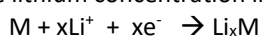
- For biphasic insertion materials, by the ratio between delithiated active sites and lithiated active site:



$$\text{Nernst Law: } E = E^0 + \frac{RT}{nF} \ln\left(\frac{1-x}{x}\right)$$

with H = insertion structure, x = insertion rate

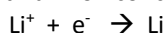
- For alloys, by the lithium concentration in the solid phase



$$\text{Nernst Law: } E = E^0 + \frac{RT}{nF} \ln\left(\frac{1}{x}\right)$$

with x = lithium concentration in the solid phase

This is not the case for the  $\text{Li}^+/\text{Li}$  couple, which is nevertheless widely used as a reference electrode<sup>9</sup>, its redox potential being dependent on the lithium ion concentration in the electrolyte:



$$\text{Nernst Law: } E = E^0 + \frac{RT}{nF} \ln\left(\frac{[\text{Li}^+]}{1}\right)$$

The appearance of a lithium concentration gradient in the inter-electrode space can then modify the potential of the electrode.

<sup>5</sup> F. La Mantia, C.D. Wessells, H.D. Deshazer, Yi Cui, *Electrochemistry Communications*, Vol. 31,2013, 141-144

<sup>6</sup> I. Jiménez Gordon, S. Grugeon, A. Débart, G. Pascaley, S. Laruelle, *Solid State Ionics* 237 (2013) 50-55

<sup>7</sup> I.G. Kiseleva, L.A. Alekseeva, A.V. Chekavtsev, P.I. Petukhova, *Soviet Electrochemistry*, 18 (1982) 114-117.

<sup>8</sup> J. Zhou, P. H. L. Notten, *J. Electrochem. Soc.*, 151 (12) A2173-A2179 (2004)

<sup>9</sup> J. Hou, R. Girod, N. Nianias, T.-H. Shen, J. Fan, V. Tileliz, *J. Electrochem. Soc.* 167 (2020) 110515



2 - Their lithium insertion/disinsertion curves show a potential plateau over a wide range of lithiation (Figure 9). This implies, before their use, a prior electrochemical step of delithiation (LFP) or lithiation (LTO, metal alloy) to place the insertion potential of the material on the plateau.

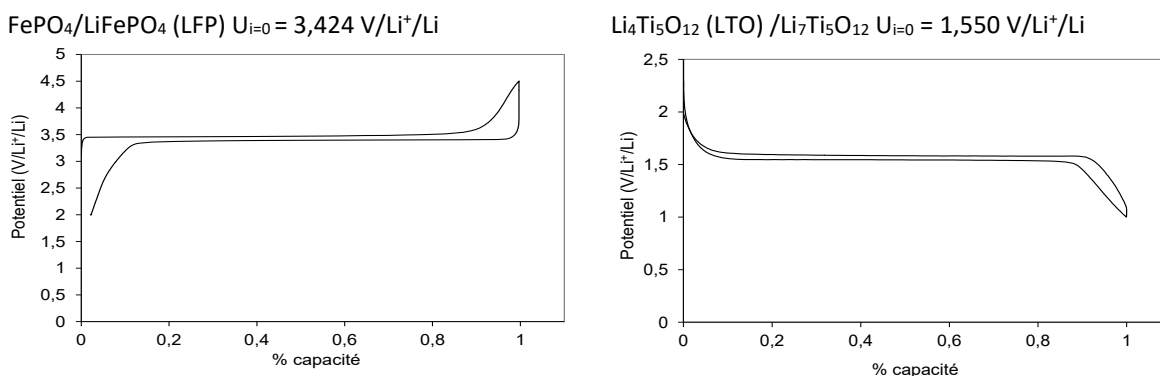


Figure 9. Galvanostatic curves in lithiation/delithiation of LFP and LTO (at C/10).

During cell operation, the electrochemical profiles provided by the reference electrode could be used to control the end of charge, no longer by the cell voltage, but by the potential of the negative electrode. The appearance of metallic lithium could thus be avoided leading, consequently, to gains in lifetime. But this therefore implies that the reference electrode can then be easily integrated into commercial cells and be able to provide a reliable and stable response over time. In the INSTABAT project, three electrochemical couples have been chosen:

- Au alloy (LixAu/Au )
- Aluminum alloy (LixAl/Al)
- LiFePO4 (LFP)

In discussions between the partners CEA, CNRS and IFAG, it was agreed, based on experience and the fundamental physical properties, that the most promising metallic materials for RE sensors were Gold (Au) and Aluminium (Al). Furthermore, the partners decided that three different design variants for the end of the RE sensor reaching into the cell would be considered: “Square”, “fork” and “antenna” (see Figure 10 - Left). Also, a general thickness of 100nm for the structures was targeted, with additional variants of 50nm and 300nm thickness for the RE sensor made from Au.

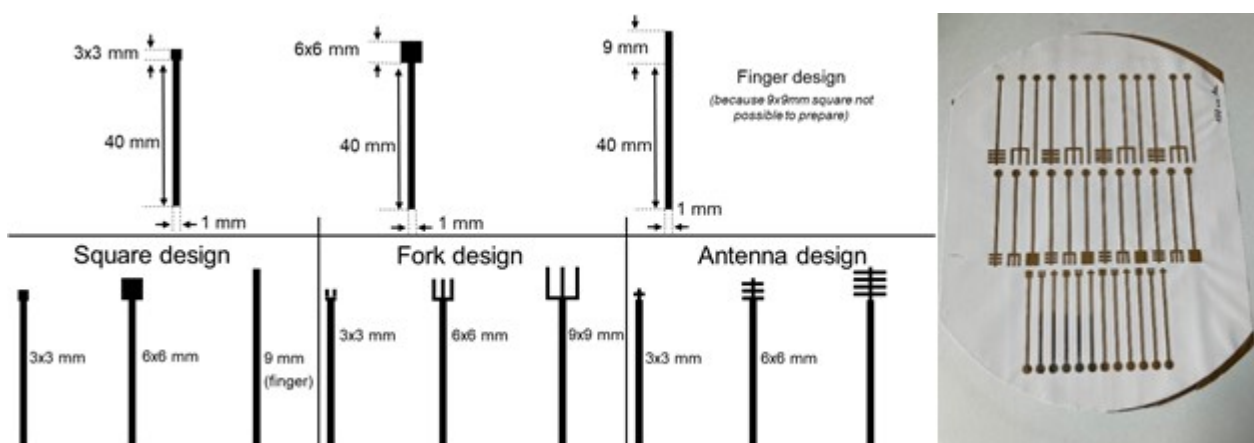


Figure 10. Left - Final design variants for the RE sensor made from metallic materials. Width (1mm) and length (40mm) of the finger were fixed. For Au samples, different thicknesses were used. For the end of the RE sensor inserted into the cell, a square, fork, and antenna design were chosen. Right – Samples manufactured with an 8 inch wafer backend sputtering process directly onto the separator sheet.

In order to sputter the metals via hard mask directly onto the separator sheets from Celgard© provided by VMI, IFAG established a backend process for 8 inch wafers adapted to these geometries. After an optimization of the design, avoiding large open areas in the hard mask which lead to excessive heat generation destroying the separator sheets, IFAG was eventually able to manufacture the desired RE sensor variants (see an example in Figure 10- Right). Achievement of the target thickness was controlled using a profilometer, indicating a variation of merely 4-6% between

the centre and the edge of the wafer. In addition, resistivity measurements of the samples were performed via 4-point probe, confirming a low standard deviation of 10%. IFAG delivered a first batch with 4 pieces of each variant (i.e., a total of 144 RE sensors) to both, CEA and CNRS, in July 2021 for integration into the battery cell and testing at cell level. A second batch consisting of 12 pieces of each design variant only for the 100nm and 300nm RE sensors made from Au (i.e., another 216 RE sensors) was delivered to CEA in February 2022.

According to the primary tests, we have seen that:

- the potential of  $\text{Li}_x\text{Au}$  (with various tested thicknesses) are not stable after lithiation.
- the conductivity of aluminum was not sufficient to have an usable  $\text{Li}_x\text{Al}$

Gold sample with LFP coating has been finally retained as reference electrode. A stability study of the potential of the  $\text{FePO}_4/\text{LiFePO}_4$  couple was carried out to determine the validity of its response over time. This study was carried out by following the open circuit potential (OCV) of  $\text{Li}_{0.5}\text{FePO}_4$  against lithium over time and at three temperatures 25°C, 45°C and 55°C. Before launching the temperature test, the delithiation of  $\text{LiFePO}_4$  is carried out electrochemically to place the potential of the material at mid-plateau ("activation" step) (Figure 11).

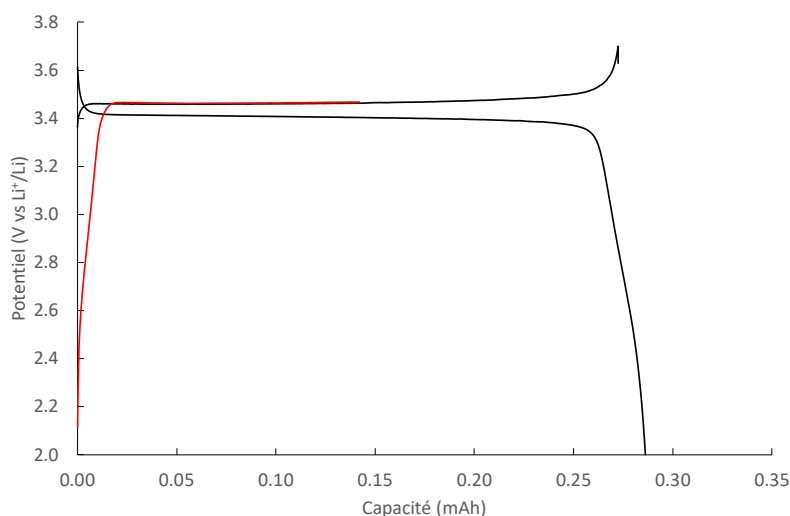


Figure 11. Lithiation and delithiation curves of LFP reference electrode (black line) and delithiation at 50% of the lithiation capacity to place the potential in the middle of the plateau (red line) (activation step)

### • Subtask 2.1.3 Optical fiber / Luminescence (OF/LumT and OF/LumL) sensors development

From the literature review, different type of optical probes for temperature measurement and Lithium concentration measurement were identified. We detail the work for each probe below.

#### Thermoluminescent probe (OF/LumT)

There is a large amount of literature on thermoluminescent phosphors. To find the more appropriate candidate for INSTABAT, some requirements were fixed (see D1.1 and D1.2):

- The optical probe must be stable and compatible with the electrolyte and the electrochemistry environment of the cell.
- The sensitivity and the temperature range must be compatible with the application.
- The excitation wavelength used to measure doesn't induce photo degradation of polymeric material inside the cell.
- The luminescence of probe must be easily detectable.

We identified a first promising candidate for the thermoluminescent probe based on  $\text{Gd}_2\text{O}_2\text{S}$  particles doped with  $\text{Er}^{3+}$  and  $\text{Yb}^{3+}$ . Thereafter, we started to work on a second candidate based on  $\text{GdV}_2\text{O}_4$  particles doped with  $\text{Er}^{3+}$  and  $\text{Yb}^{3+}$ . Calibration tests have been carried out on  $\text{Gd}_2\text{O}_2\text{S}$  and  $\text{GdV}_2\text{O}_4$  powder to determine its sensitivity to temperature. Then we are developing coating protocols to perform a deposition of these particles onto the optical fiber tip. Different

formulations (sol-gel and polymer) were studied to optimize the powder deposition and the luminescence intensity of the probe on fiber. Tailored sol-gel formulations have been synthesized for both phosphors. The goal is to deposit phosphor particles as close to the optical fiber tips as possible to optimize the optical and the mechanical performances (the modified fibers must be robust enough to be put and sealed inside the pouch cell battery).

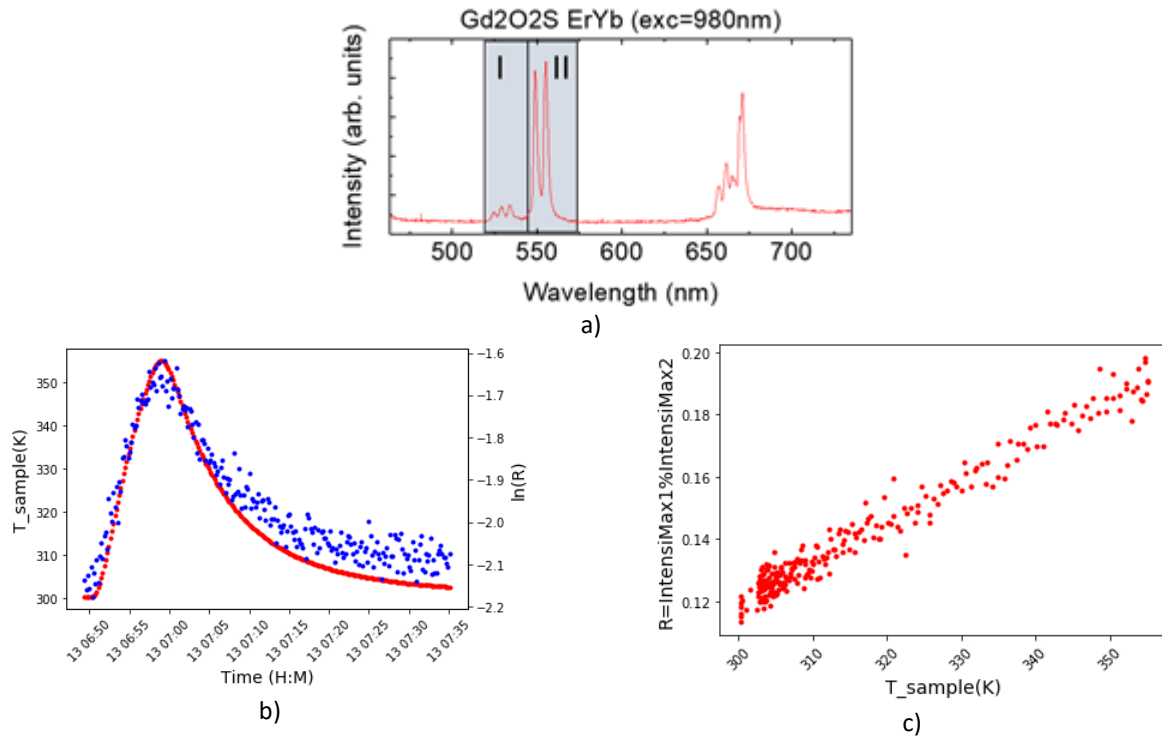


Figure 12: Gd<sub>2</sub>O<sub>2</sub>S:ErYb – a) Luminescence spectra with the two pics used for thermoluminescence ratiometry ( $I_I/I_{II}$ ), b) Variation of luminescence intensity ratio in temperature, c) Calibration curve.

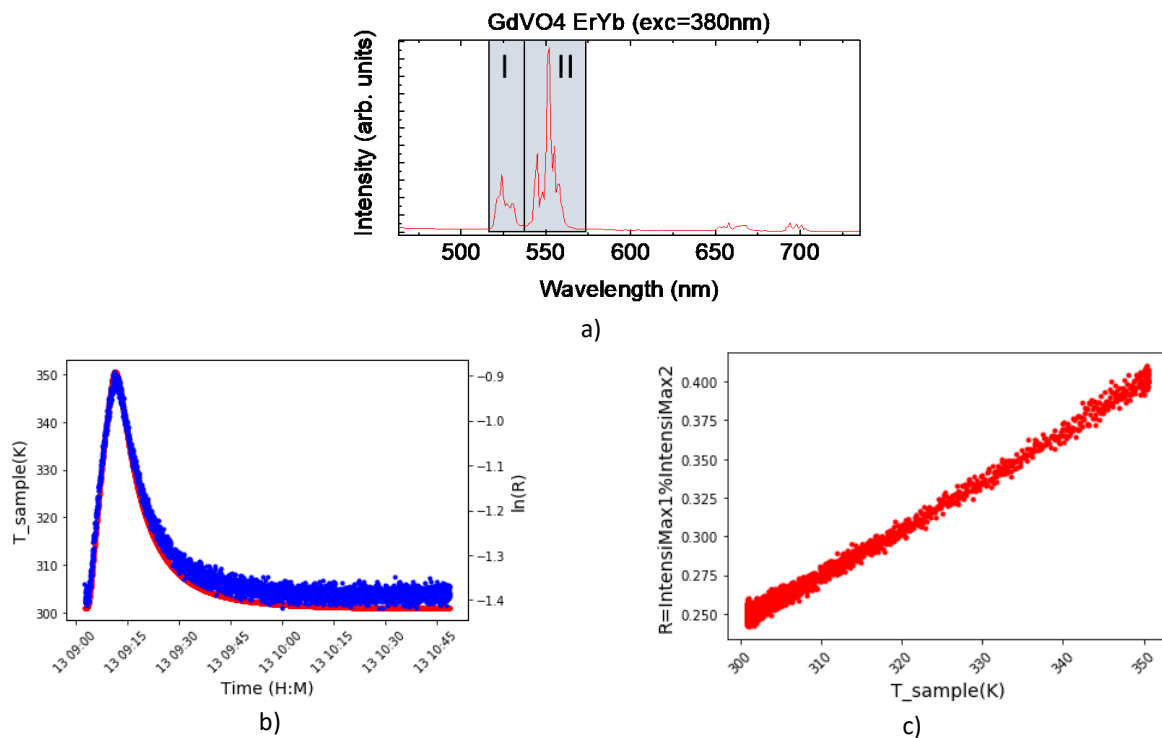


Figure 13. GdVO<sub>4</sub>:ErYb - a) Luminescence spectra with the two pics used for thermoluminescence ratiometry ( $I_I/I_{II}$ ), b) Variation of luminescence intensity ratio in temperature. c) Calibration curve.

Sol-gel formulation has been modified to enhance the gelification time by acting on the catalyst choice. All the experiments have been carried out at room temperature. Finally, a PMMA varnish have been locally applied to wrap and protect the active sensing zone. PMMA has been chosen because it can work in carbonate based electrolyte (the thickness of this protective layer does not impact the thermal measurement). At this time, the sol-gel formulation performed very well for  $Gd_2O_2S$  phosphor. Several samples have been tested (all of them showing equivalent thermal sensing performances).

An innovative deposition technique was developed during this work and patented. The fibers are calibrated in temperature prior to using as thermal sensors for cell monitoring (see subtask 2.3).

The thermal sensitivity of  $Gd_2O_2S$  phosphor is below the KPI's of the project ( $0.1^\circ C$ ). Then, we are testing the second promising probe material with a higher thermal sensitivity from literature:  $GdVO_4:Er,Yb$ . This material was synthesized by CEA and tested in powder. The results confirm the higher thermal sensitivity for this phosphor. However, the deposition of the powder on optical fiber require to adjust the protocol. This work still under progress.

For the WP3 we decide to use the  $Gd_2O_2S$  phosphor for preparing the OF/LumT sensor.

### Lithium luminescent probe (OF/LumL)

In this part of the deliverable, we resume the development of the luminescent lithium probe during INSTABAT project. The most challenging part was to identify fluorescent chelating complexes of Lithium able to survive in the organic carbonates based electrolytes. Several families of molecules have been evaluated. All complexes or molecules containing metals (lanthanides, alkaline earth) or very basic reactive groups have been discarded. The lithium complexes have been solubilized in fresh battery electrolyte containing lithium salts. Fluorescent measurement has been performed (excitation 350 to 420nm), those losing their fluorescent properties were discarded. Then the samples has been stored in dark at room temperature for several weeks. Again, samples showing versus time a loss of fluorescence or a change of colours and/or a formation of precipitates were discarded.

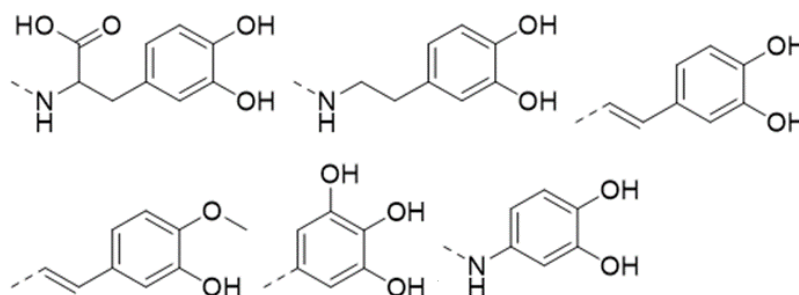
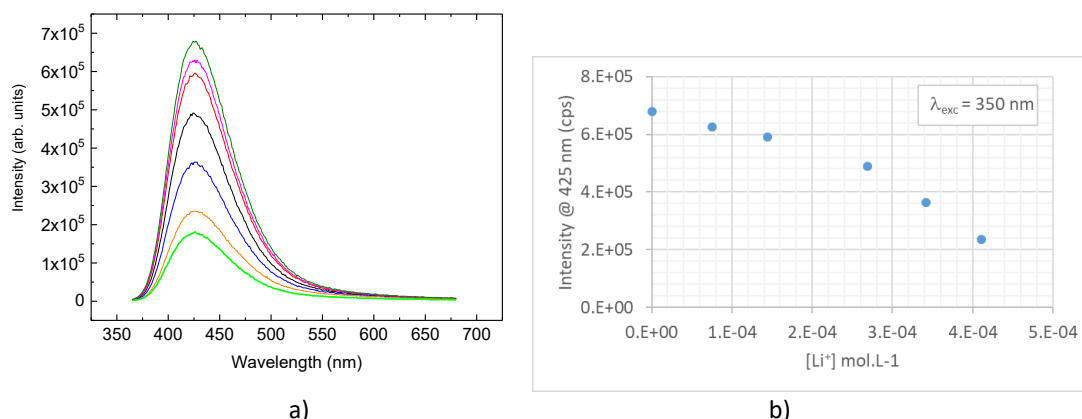


Figure 14. Relevant catechol function.

Among them, the lithium catecholates (Figure 14) showed quickly a good stability in terms of fluorescence signal. So, a new study wherein pure catechols instead of lithium salts has been set in fresh battery electrolyte first without Li salts and with gradual addition of  $LiPF_6$  (Figure 15). The catechols showed a good stability in fresh organic carbonates electrolyte and were able to monitored the concentration in  $LiPF_6$ . A third study has started to check the stability of catechols in aged electrolytes (aged electrolytes containing a large number of chemicals able to interact with catechols). After a few weeks of keeping at room temperature, only slight changes of colours have been observed.

Finally, catechols being known to be photosensitive so some samples has been stored at room temperature under argon at day light for several weeks. Only slight changes of colours were observed. Probably a similar study will have to be done using a UV irradiation.



### Choice of the chemical bonds in order to graft the fluorescent chelating agents on optical fibers

For this task, the challenge was to identify chemical bonds that are able to survive during long periods of time in organic carbonates electrolytes. Based upon the obtained data for the design of thermal sensors wherein the isocyanate chemistry has been successfully used to design coatings able to survive in battery electrolytes.

Three kinds of chemical linkage have been studied:

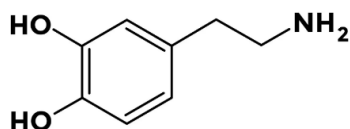
- Urethane linkage allowed to modify the surface (silanol pending groups) of optical fibers

$\text{Si-OH} + \text{RNCO} \rightarrow \text{Si-O CONHR}$

R could be advantageously a diisocyanate (e.g; Hexamethyldiisocyanate)

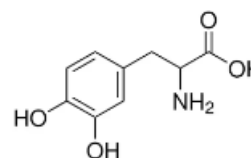
Forming a reactive surface: **Si-OCOHN(CH<sub>2</sub>)<sub>6</sub>NCO**, able to react with catechols bringing reactive moieties.

Among them, those bringing a primary amino group were the most reactive:



Dopamine

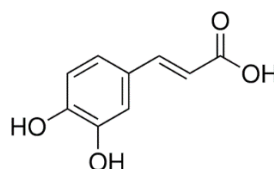
and



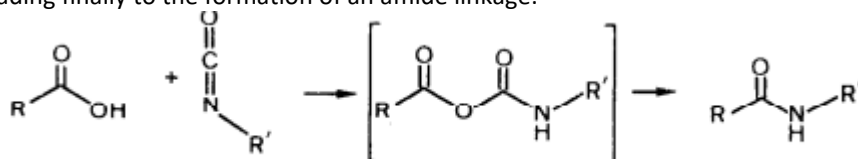
3,4-Dihydroxy-DL-Phenylalanine

These two chemicals reacting at room temperature in aprotic solvents without requiring any catalysts leading to the formation of an urea linkage: **Si-OCNH(CH<sub>2</sub>)<sub>6</sub>NHCONHR**

The second one was caffeic acid:



This chemical reacting at 50.0 °C in aprotic solvents on pending isocyanate groups (using triethylamine as catalyst) leading finally to the formation of an amide linkage:



Urethane, urea and amide linkage were able to survive in battery electrolytes (fresh or aged).

Grafted fluorescent catechols (on quartz, polymers, optical fibers) were able to monitor lithium concentration in electrolyte. The calibration curve of the lithium sensor in electrolyte is shown in Figure 16 for the probe function and grafted on glass substrate.

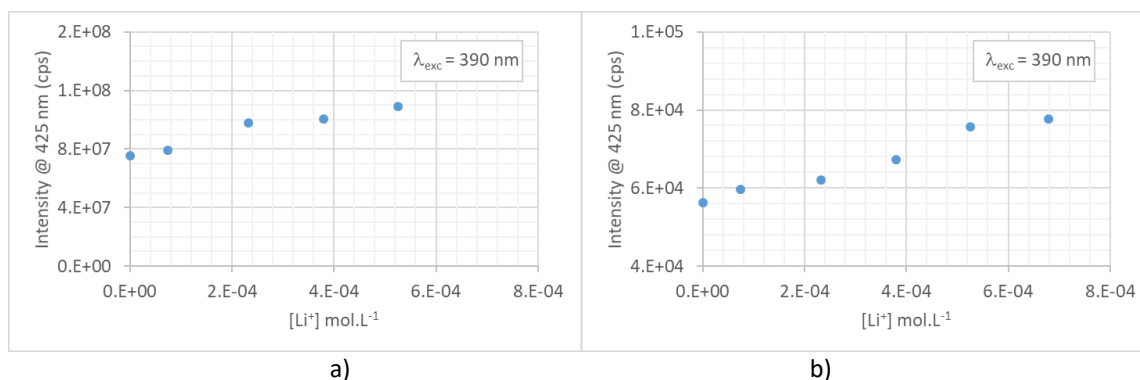


Figure 16 Variation of the luminescence intensity of the optical probe as function of the  $\text{LiPF}_6$  concentration in electrolyte: (a) optical probe (catechol function) grafted in low MW PVA (b) Optical probe functionalized with low MW PVA grafted on glass substrate.

Ageing stability tests have been carried out over the three years of INSTABAT project and it was performed these tests both on grafted and/or free catechols. At this time, fluorescent catechols seemed to “work” efficiently in organic carbonates electrolytes. We also grafted the optical probe (catechol) on the tip of optical fiber. However, the signal from the optical probe was low and requires future improvement:

- 1- Optimize the optical bench for increase the ratio signal to noise;
- 2- Increase the surface density of optical probe grafted in the fiber tip.

However, we did not make tests inside the cell “operando measurement” in true battery wherein the charge/discharge cycles could induce a chemical reactivity. This has to be done.

#### OF/LumL sensor development – Main conclusions

A family of fluorescent chelating agents able to monitor the Lithium concentration in organic carbonates has been identified. These fluorescent chelating agents are still able to monitor the lithium concentration after covalent grafting on silanol groups of optical fibers and/or polymers. Long term keeping tests showed a correct stability in organic carbonate electrolytes. In this way, **two patents** describing the technology has been filed (no publish yet) and one publication is under preparation to disseminate these results.

#### Remaining works which have to be done in the future to achieve the goals of the project:

Several improvements of the technology have been prepared: these addresses particularly the following points:

- ✓ Increase the number of fluorescent catechols grafted on fiber surfaces in order to manage a possible saturation of lithium probe;
- ✓ Improve the optical test bench to increase the signal to noise ratio for optical fiber measurement;
- ✓ Protect catechol function during the charge/discharge cycles.

- **Subtask 2.1.4 Evaluation and adaptation of a  $\text{CO}_2$  sensor based on the photo-acoustic principle (PA)**

After a careful joint analysis of the requirements, IFAG provided several samples of what was considered the most suitable existing engineering prototype of a PA-based  $\text{CO}_2$  sensor (denoted as “PAS Gen 1.0” in Figure 17) to CEA and CNRS in December 2020, for a basic evaluation of the usability in the context of a LIB cell. The open architecture implementation of this PAS prototype consists of a gas measuring cell with an infrared (IR) emitter, a microphone with a high “signal-to-noise-ratio” (SNR) as the acoustic detector, and an XMC™ microcontroller for data processing (see Figure 18). The diffuser port on the top side of the measuring cell allows for efficient gas exchange while maintaining dust protection. The sensor module allows for integration via surface mount soldering via the pads on the bottom side of its PCB. All the key components were developed in-house at IFAG. To ensure efficient and quick evaluation, the sensor



was provided to CEA and CNRS together with an evaluation kit (ensuring communication to a PC GUI via micro USB and a 12V power supply for the IR emitter) and an easy-to-use PC graphical user interface. A series of tests was performed on these early samples by CEA and CNRS, using different approaches to emulate the incorporation of these PA-based CO<sub>2</sub> sensor into an operating cell. These tests confirm the basic gas sensing functionality during battery operation, successfully concluding Phase 1 of subtask 2.1.4. However, the tests also revealed certain deficiencies of PAS Gen 1.0.



Generation	PAS Gen 1.0	PAS Gen INSTABAT special 1.0	PAS Gen INSTABAT special 2.0
Status	Engineering Prototype 13.8 x 14 x 7.5 mm <sup>3</sup>	INSTABAT special release 1.0 13.8 x 14 x 7.5 mm <sup>3</sup>	INSTABAT special release 2.0 13.8 x 7 x 7.5 mm <sup>3</sup>
Facts and purpose	<ul style="list-style-type: none"> <li>• CO<sub>2</sub> sensing only</li> <li>• Smallest CO<sub>2</sub> sensor available in the market</li> <li>• Learnings in the field</li> <li>• Dual power supply (3.3V + 12V)</li> </ul>	<ul style="list-style-type: none"> <li>• CO<sub>2</sub> sensing only</li> <li>• High performance then PAS Gen1.0</li> <li>• With new and powerful emitter/filter package</li> <li>• Capability of temperature feedback loop</li> <li>• Updated firmware/software capabilities</li> <li>• Dual power supply (3.3V + 12V)</li> </ul>	<ul style="list-style-type: none"> <li>• CO<sub>2</sub> sensing only</li> <li>• Same performance as INSTABAT special release 1.0</li> <li>• Cost / size down are the main focus</li> <li>• Dual power supply (3.3V + 12V)</li> </ul>

Figure 17. Different generations of the PAS CO<sub>2</sub> sensor by IFAG, as detailed in the text.

Based on these test results, IFAG implemented several improvements of the PA-based CO<sub>2</sub> sensor. The main change in the hardware consisted in the installation of a completely new emitter and filter package. More concretely, the emitter package was changed from a “liquid crystal polymer” (LCP) to a ceramic package, including an upgraded filter and sealant glue. This change is fundamental to enable the required measurement of extremely low CO<sub>2</sub> values (at about 2ppm) with relatively low noise and generally increases the reliability of the sensor. IFAG also introduced a temperature feedback loop to the sensor system, to improve the stability of the output values. In order to fully support these hardware changes and the related added functionality, an upgrade of the firmware was required, both on the level of the microcontroller and on the level of communication. Finally, the software was upgraded to allow a calibration of the PA-based CO<sub>2</sub> sensor in the actual battery environment. The resulting version is included as “PAS Gen INSTABAT Special 1.0” in the overview in Figure 17. Two samples of this version were provided to CEA in September 2021 and six more in February 2022.



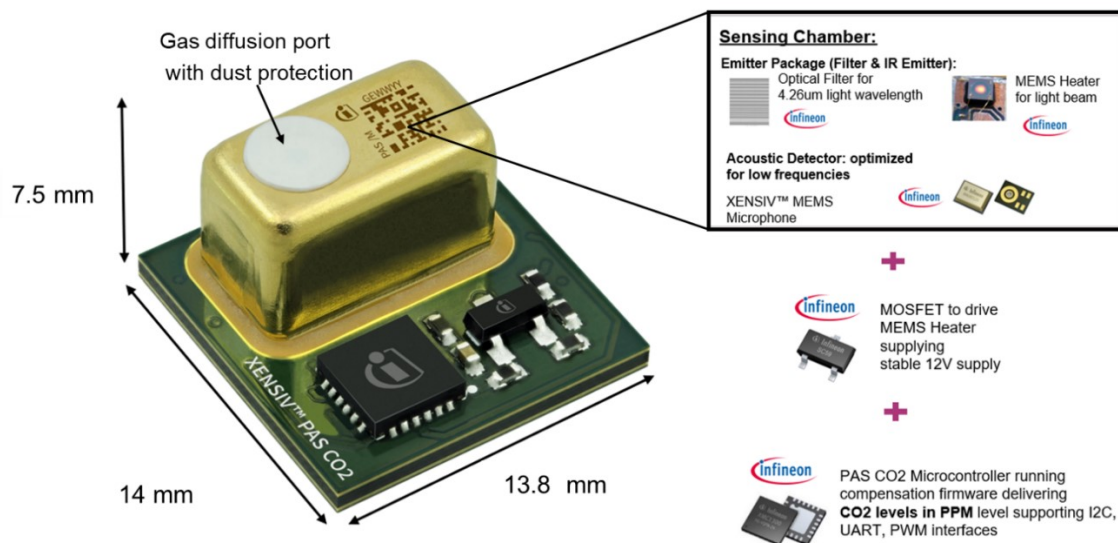


Figure 18. Basic components of the PAS CO<sub>2</sub> sensor Gen 1.0 by IFAG

Experiments performed by CEA (see Subtask 2.2.4 below) revealed “physical limitations” of the PA-based CO<sub>2</sub> sensor to its integration into the cell. In order to reduce these limitations, IFAG developed a completely new generation of the sensor, denoted as “PAS Gen INSTABAT Special 2.0”, also included in the overview in Figure 17. For this new generation, IFAG separated the single PCB used for previous generations into two parts, one part containing only the sensing chamber with the emitter package and acoustic detector (see upper right in Figure 18) and the other part containing the remaining electronics components. For the transmission of current and data, these two PCBs were connected by a so-called “Flex PCB”. The overall architecture of this generation is shown in Figure 19, where the lid of the sensing chamber (on the left) has been removed for illustration purposes. With this approach, the volume of the part of the PA-based CO<sub>2</sub> sensor which actually needs to be integrated into the cell (i.e., the sensing chamber itself) could be reduced by a factor of 2. At the same time, this architecture now allows the realization of the connection between inside and outside of the cell with the Flex PCB. The height of the Flex PCB is much less than that of the somewhat bulky USB cable which was required for the previous generations and should be compatible with the cell sealing process, according to CEA (PCB thickness = 0.12mm, USB cable diameter = 3.80 mm). Four samples of this version were provided to CEA in July 2022 and two more in January 2023.

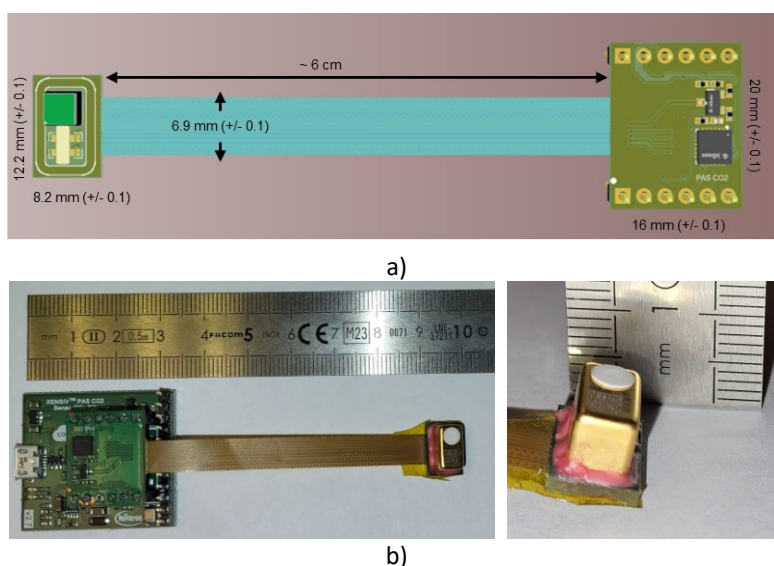


Figure 19. (a) Overall architecture of the PAS CO<sub>2</sub> sensor Gen 2.0 by IFAG. (b) Photo of the Gen 2.0 PAS sensor.

Further experiments performed by CEA suggested that the PA-based CO<sub>2</sub> sensor in the present realization of the sensing chamber using a wavelength of 4.2 μm to detect CO<sub>2</sub> exhibits a cross-sensitivity with certain components of the electrolyte vapor (for more details, see Subtask 2.2.4 below). Figure 20 b) show the infrared absorption band overlapping between CO<sub>2</sub> and electrolyte carbonates component (EC, DEC, DMC). This would result in an overestimation of the CO<sub>2</sub> concentration in the presence of such vapor, which is normally the case inside a cell. A possible solution to avoid this cross-sensitivity would be the utilization of a wavelength of 2.6-2.7 μm. This value corresponds to a different absorption band of CO<sub>2</sub>, at which, however, the electrolyte vapor shows no absorption.

IFAG carefully evaluated this possibility, but eventually concluded that this would not provide a reasonable solution, at least not within the scope of the INSTABAT project. The main arguments for this conclusion are:

- Since the absorption of CO<sub>2</sub> at 2.6-2.7 μm is about one order of magnitude lower than at 4.2 μm, the sensitivity of the sensor would be reduced correspondingly.
- Utilization of 2.6-2.7 μm would introduce an at least equally undesirable cross-sensitivity with humidity (see Figure 20), for which no solution approaches were readily available.
- For the switch to a different wavelength, an entire development cycle of the optical filter, including the steps of modelling and simulation, fabrication and assembly, hardware assessment and finalization, would be required, with an expected duration of 5-6 months and significant efforts, not planned by IFAG for INSTABAT.

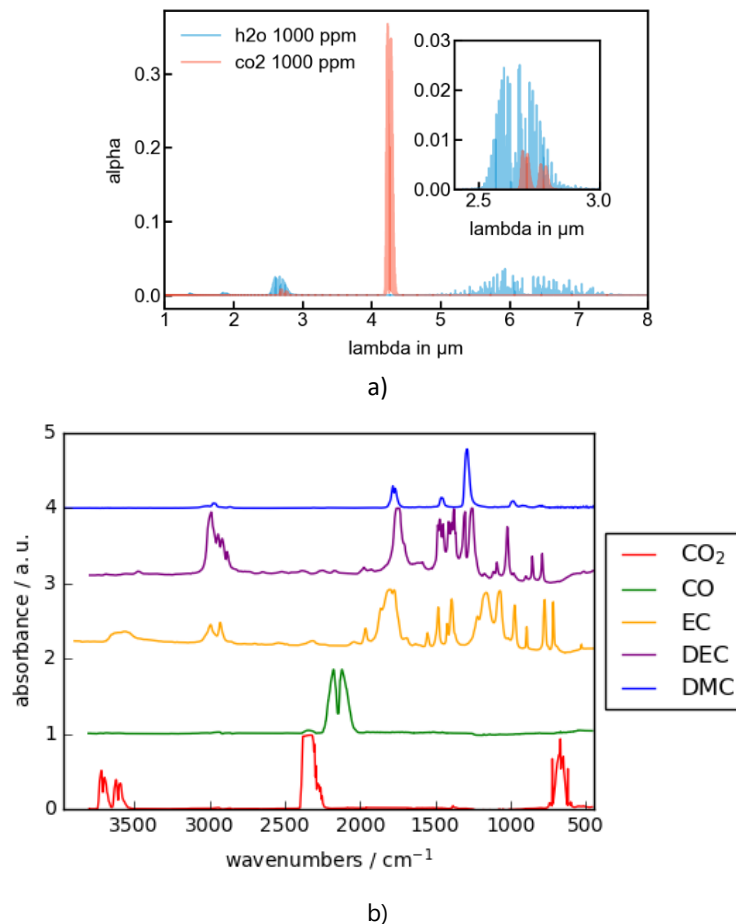


Figure 20. (a) Comparison of the absorption bands of water (H<sub>2</sub>O, blue) and CO<sub>2</sub> (red); (b) Comparison of the absorption band of CO<sub>2</sub> (red), CO (green), EC (yellow), DEC (purple), DMC (blue).

Finally, the experiments by CEA on PAS Gen 1.0 also revealed an apparent dependence of the output of the PA-based CO<sub>2</sub> sensor on both, temperature and pressure (see Subtask 2.2.4 below). The temperature feedback loop implemented in PAS Gen INSTABAT Special 1.0 in combination with a calibration including the temperature would in principle allow a compensation of the temperature dependency. Furthermore, a compensation of the pressure dependence can also be triggered manually, by setting the values in the corresponding registers of the sensor. However, this was not actually tested within INSTABAT.

- **Subtask 2.1.5. Sensors stability and adaptation related to the battery cell environment**

### OF/FBG sensor - Testing the chemical stability of optical fibers in electrolyte

The optical fiber sensors that will be used to monitor temperature, strain, and pressure variations inside the cells, will be manufactured in different types of optical fibers (as previous described on D2.2). These optical fibers are typically composed by silica, and as they will be integrated into the pouch cells, together with the INSTABAT electrolyte solution (EC/EMC (3:7 vol.) 1M LiPF<sub>6</sub> + 2%w VC, Sol-Rite™), stability and adaptation tests were carried out. In this way, stability tests were started to be designed with a row number of samples. Different types of optical fibers were prepared and inserted in aluminium flasks (50 mL capacity), submerged in the INSTABAT electrolyte (~25 mL). In total, 14 samples were prepared, 6 with SMF fibers, 6 with PANDA fibers, and 2 with FBG sensors inscribed on PM fibers (Figure 21). These flasks were placed within a nitrogen-pressurized chamber to create a controlled environment, at room temperature. The assessment of degradation in both the single-mode fiber (SMF) and OF/FBG sensors was conducted in response to exposure to corrosive chemical environments present within the battery. Additionally, an optical fiber with two FBG sensors was strategically placed at different points along an optical fiber line, where one FBG sensor ( $\lambda_B = 1537$  nm) was exposed to the battery liquid electrolyte solution while the other ( $\lambda_B = 1551$  nm) was placed on the gas phase of the electrolyte, as shown in Fig. 16 left. During the experimental time (24 months), the flasks were safely stored inside a fume hood in an air-sealed container with a nitrogen-dense atmosphere to minimize oxidation and maintain the stability of the samples. Additionally, the fibers exposed to the liquid electrolyte were periodically rescued and subjected to scanning electron microscopy (SEM) and energy dispersive X-ray spectroscopy (EDX) analysis to assess the extent of corrosion and chemical deposition (Figure 23). These measurements were performed in a TESCAN Vega3 SBH SEM microscope equipped with a Bruker Xflash 410 M Silicon Drift X-ray Detector, characterized by an energy resolution of 133 eV @ MnK $\alpha$  (100 k cps). The ESPRIT software (Bruker) was used to produce elemental mappings and perform elemental quantification via incorporated standard less P/B ZAF algorithm.

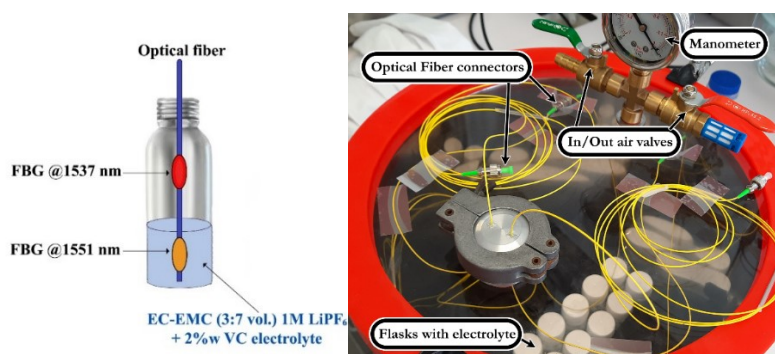


Figure 21. Left) Representation of the FBGs arrangement in a flask partially filled with EC-EMC (3:7 vol.) 1M LiPF<sub>6</sub> + 2%w VC electrolyte. The objective is to expose one of the FBGs to the electrolyte and compare its optical response with the other FBG, which is not directly exposed to the electrolyte. Right) Photograph shows the air-sealed container along with the flasks and external instrumentation used to control the internal pressure and to connect the sensors inside the aluminium flasks.

Periodic measurement of the FBG spectral response was performed over 24 months (Figure 22) using an optical interrogator (Hyperion si155, LUNA®, Atlanta, GA, USA) with a spectral range spanning from 1460.0 to 1620.0 nm. These experiments aimed to detect any potential changes in the sensors spectral characteristics attributable to chemical exposure. The wavelength shifts observed are associated with the environmental temperature changes over time (see Figure 22). Also, the FBG that was immersed in the electrolyte solution ( $\lambda_B = 1551$  nm) perfectly follows the other FBG that was not immersed. It is important to mention that this experiment was not performed in a controlled temperature environment, so it was dependent on external temperature variations, as can be observed in Figure 22.

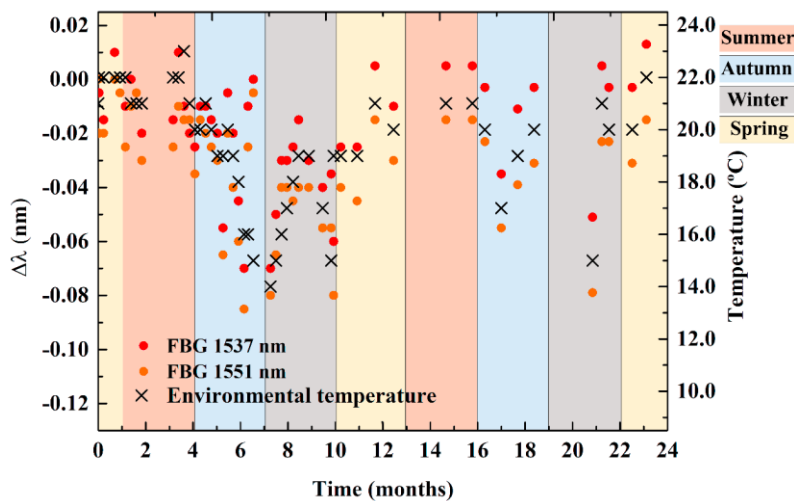


Figure 22. FBG sensors wavelength shift over 24 months of exposure to the electrolyte solution.

Several optical fibers were periodically submitted to the SEM/EDX analysis to evaluate the chemical deposition on the fiber and the possible degradation of the silica material. It is clearly seen in Figure 23 a progressive formation of deposits originated by the decomposition of the battery electrolyte (EC/EMC (3:7 vol.) 1 M LiPF<sub>6</sub> + 2 %w VC), likely from the release of hydrogen fluoride (HF), phosphorus pentafluoride (PF<sub>5</sub>), and phosphoryl fluoride (POF<sub>3</sub>). The orange color on the mappings reflects the presence and superposition of F and P in the deposits (due to the combination of F in red and P in yellow, Figure 23 f-j). Note that the fact that some deposits or crystal facets do not show any superimposed color is due to the shadowing effect, i.e. obstructed or limited line-of-sight regarding the X-ray detector. In the 3<sup>rd</sup> month, cubic-shaped deposits are formed showing sharp edges and facets, which tend to grow in size as immersion duration is increased (Figure 23 k-o). Semi-quantitative point EDX measurements on these crystals reveal the presence of F and P in a stoichiometry consistent with that of LiPF<sub>6</sub> (measured average F/P ratio of 8.99±4.97), which is known to crystallize in a cubic structure. On the other hand, a second morphology with smaller, amorphized grains also develops (see Figure 23 l-o). For these deposits, the measured F/P atomic ratio varies greatly but it is in general increased, reaching up to 30 and above, which is reflected in the redder contrast in the EDX mappings. Regardless of the extensive coverage of the fiber surface by these deposits, no signs of silica degradation were observed, and the integrity of the optical fiber and the FBG was maintained throughout the whole analyzed period. By an EDX analysis, it was possible to conclude that these precipitates are composed by phosphorus (P) and fluorine (F) elements, as shown on Figure 23. However, no degradation/etching phenomena were observed on the fiber surfaces. After 9 months, crystal dimensions of ~ 5.0 μm can be observed.

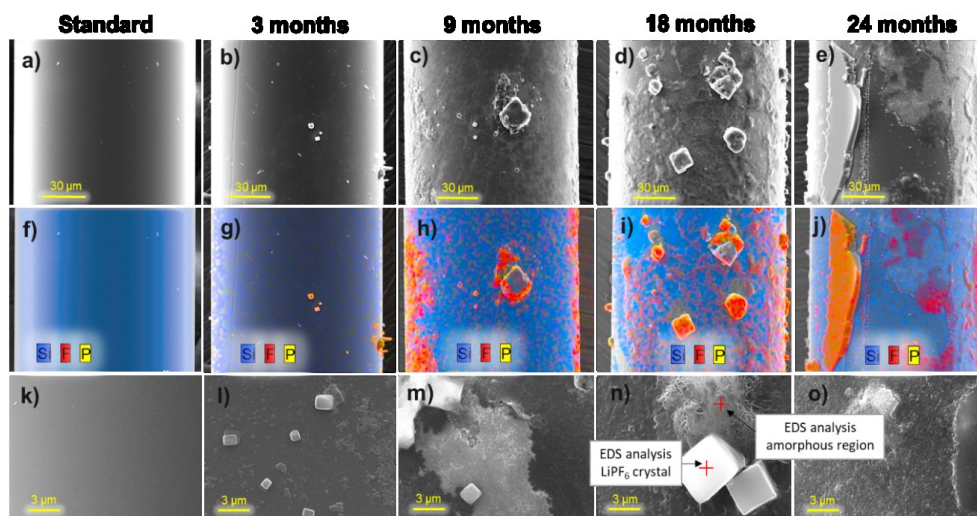


Figure 23. SEM analysis of the optical fibers chemical exposure over time. a, b, c, d, and e are the secondary electron (SE) images of the fiber at 0, 3, 9, 18, and 24 exposure months, respectively. f, g, h, i, and j are the EDS mapping images of the fiber over time. k, l, m, n, and o are magnified SE images of the deposits on the fiber surface.



## Optical fiber (OF/LumT sensor)

The optical fiber used (FT200EMT) presents an external coating of Tefzel (a fluoropolymer with a high chemical and mechanical resistance), which protects the fragile cladding and the core of the wave guide. The integration of this specific optical fiber in pouch cells has been carried out by a thermo-sealing step. The preliminary tests have demonstrated the good operation of the optical fiber after this integration step. Furthermore, the mono-stacked pouch cells instrumented with a temperature sensor have presented the same thermoluminophore emission spectrum than the temperature sensor alone before insertion, indirect proof of a correct integration of this sensor inside the pouch cell.

The presence of the electrolyte did not degrade the optical fiber during a short time (< 2 months). The stability tests are currently performed for a longer time at two temperatures ( $T = 25.0\text{ °C}$  and  $T = 55.0\text{ °C}$ ). The integrity of the thermoluminophore deposit on the end of the optical fiber has been indirectly proved by the conservation of the emission intensity of the thermoluminophore on the temperature sensor inserted inside the mono-stacked pouch cell. We performed this test after formation and after 4 months (note that this sample was conserved at the fridge at  $5.0\text{ °C}$  between the two experiments).

The stability of the sensor OF-LumT in cell environment was confirmed and demonstrated with the ageing test performing in the WP3 (see next part of the report)

## RE sensor

We have followed the OCV potential of  $\text{Li}_{0.5}\text{FePO}_4$  over time and then proceeded to re-lithiation to evaluate the capacity consumed during the elapsed period. The percentage of capacity lost per hour of storage at  $25.0\text{ °C}$ ,  $45.0\text{ °C}$  and  $55.0\text{ °C}$  is shown in Figure 24. Capacity loss is very small at  $25.0\text{ °C}$  and is doubled at  $45.0\text{ °C}$ . At  $55.0\text{ °C}$ , the loss of capacity is very rapid, implying a potential drift in the shorter term, which reduces its useful life.

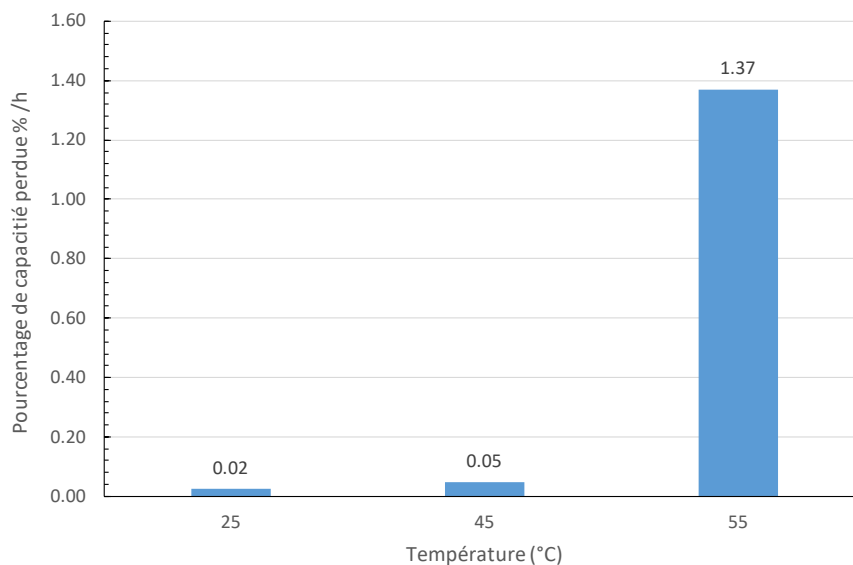


Figure 24. Percentage of capacity loss per hour at different temperatures.

This loss of capacity is not irreversible as we have shown by reactivating the LFP stored at  $55.0\text{ °C}$  after its potential has drifted. Figure 25 shows that the effective capacity of the LFP RE before and after storage at  $55.0\text{ °C}$  is not impacted and the potential profile still shows a very stable plateau. Thus, after reactivation, the LFP RE is functional again.

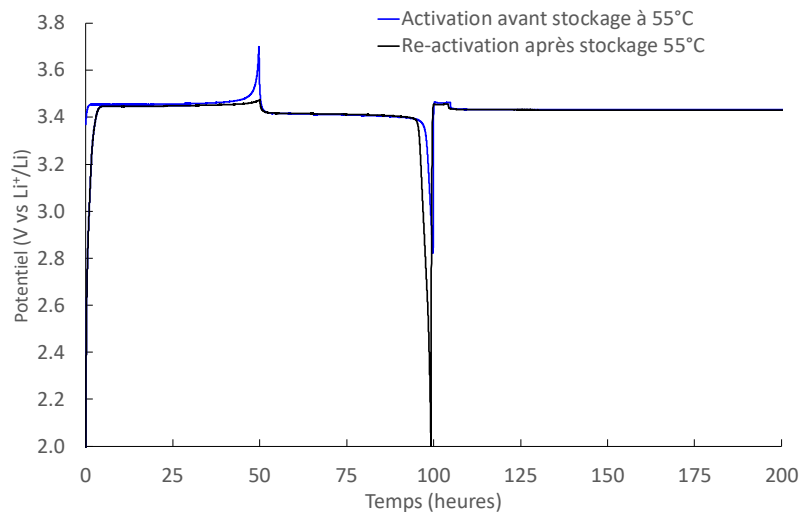


Figure 25. Re-activation of the RE after drifting of the potential by storage at 55.0 °C: delithiation/lithiation curves of LFP and delithiation at 50% of the lithiation capacity to place the potential in the middle of the plateau before (blue line) and after storage (black line).

To conclude, the stability of the LFP potential over time could be achieved at cell scale by reactivating the RE before the appearance of a drift of its potential.

## TASK 2.2: SENSOR HARDWARE INTEGRATION AND TEST

(Leader: CNRS; Participants: UAVR, CEA, IFAG) (M6-M24)

The sensor integration in the battery cell environment is being performed, by execution of long-term chemical resistance tests to certify that all physical sensors are adapted. Ageing tests will be performed: OF/FBG by UAVR and standard FBGs by CNRS, RE and PA by CNRS; OF/LumT, RE, OF/LumL and by CEA. Three main features will be covered:

- 1) Impact on the cell performance and safety of batteries containing the different sensors;
- 2) Impact on the performance of the different sensors when implanted in the battery cells;
- 3) Sensor positioning in the cell.

- **Subtask 2.2.1. Optical fiber / Fiber Bragg Grating (OF/FBG) sensor integration and test**

### OF/FBG sensors

The OF/FBG sensors were tested and integrated in different battery configurations to evaluate their feasibility, reliability, and performance during battery cells operation. At UAVR, these sensors started to be instrumented and tested on commercial rechargeable cylindrical (18650) lithium-ion batteries. Between all the studies performed with these sensors, we can highlight four. Two of them were already published on the *Batteries*<sup>10</sup> and *Advanced Sensor Research Journals*<sup>11</sup>. Another one about the simultaneous discrimination of pressure and temperature by using highly sensitive OF/FBG - Hybrid sensors it was submitted and is under the review step (when we write this report). On the published works, the OF/FBG - PM sensors were used for simultaneously discriminate temperature and strain variations during battery operation, on longitudinal (Figure 26) and radial (Figure 28) configurations.

<sup>10</sup> Matuck, L.; Pinto, J.L.; Marques, C.; Nascimento, M. Simultaneous Strain and Temperature Discrimination in 18650 Li-ion Batteries Using Polarization-Maintaining Fiber Bragg Gratings. *Batteries* 2022, 8, 233. DOI: 10.3390/batteries8110233.

<sup>11</sup> Matuck, L.C., Cabrita, P.D., Pinto, J.L., Marques, C.A. and Nascimento, M.S. (2023), Customized Optical Fiber Birefringent Sensors to Multipoint and Simultaneous Temperature and Radial Strain Tracking of Lithium-Ion Batteries. *Adv. Sensor Res.*, 2: 2200046. DOI: 10.1002/adsr.202200046.

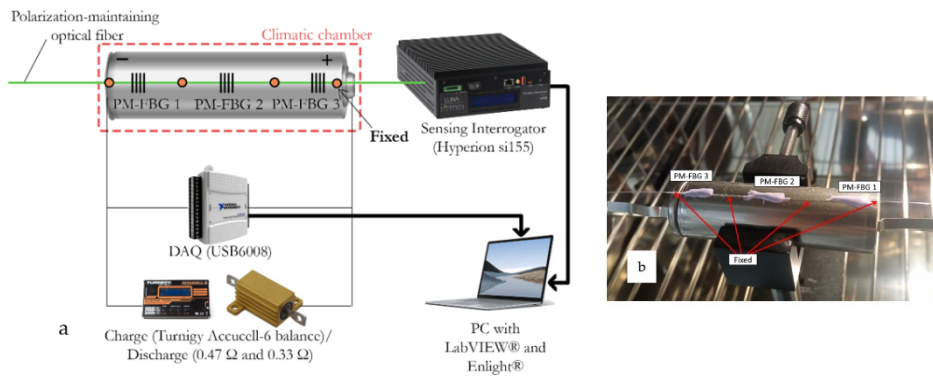


Figure 26. (a) Illustrative scheme of the experimental setup used for simultaneously decoupling longitudinal strain and temperature variations on three different areas on the battery surface. (b) The optical fiber and the OF/FBG - PM-FBG sensors fixed to the battery cell. The optical fiber was fixed to the battery after temperature calibration; thus, the experimental probe was in near-initial strain conditions.

Figure 27 shows the temperature and strain variations over voltage performance at charge/discharge cycles for the PM-FBGs placed in positions close to negative terminal (PM-FBG1), middle of battery (PM-FBG2), and positive terminal (PM-FBG3). The different steps of the experiment are separated by dashed lines, where D, C, and R represents discharge, charge, and rest steps, respectively. Both charge and discharge processes presented greater temperature and strain variations when the battery was operated at higher C-rates. For both charge steps, the temperature increased in the first half of the process and then decreased until the end of the charge, due to the current adjustment charging mode of the charger used.

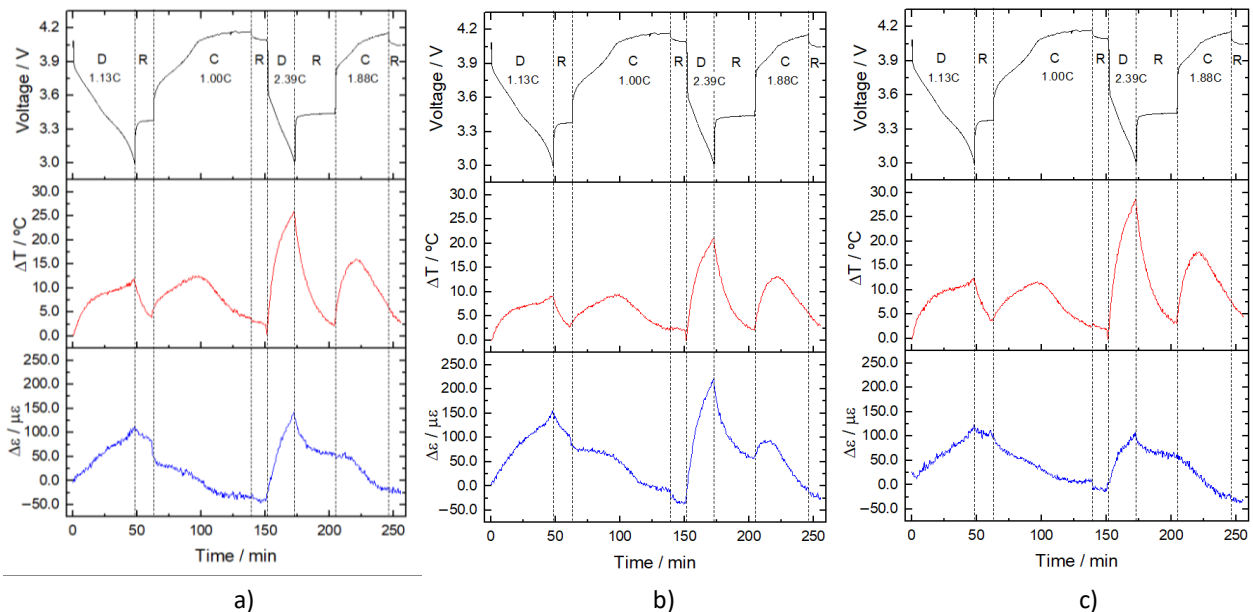


Figure 27. Temperature and strain variations detected over voltage performance for a) negative terminal (PM-FBG 1), b) middle (PM-FBG 2), and c) positive terminal (PM-FBG 3) of the battery.

The results obtained are in accordance with previous studies regarding battery cell strain behavior during charge/discharge cycles, using strain gauges placed in different spots of 18650 batteries. In this way, future work regarding the application birefringent PM optical fibers in other battery configurations (pouch cells) may be approached using these types of sensors, enabling the simultaneous measurement of internal temperature and strain variations in different battery points or multi-stack layers.



The proposed approach promotes a non-invasive, multipoint, and real-time monitoring of battery cell safety parameters. Such a technique has no influence on the safety or performance of the battery cell, once neither the interior nor the battery housing is damaged by the optical sensors.

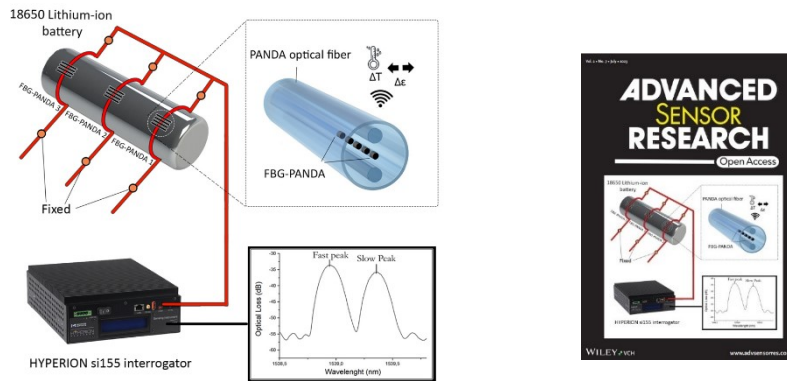


Figure 28. Left) Representative scheme of the experimental setup used for simultaneous radial strain and temperature tracking on three different zones during an 18650 LiB operation. Right) Journal front cover of the volume 2, issue 7, 2023.

Aiming to obtain greater thermal and radial variations of the battery, the galvanostatic cycles were executed at high charge and discharge rates. In total, 8 cycles were performed, all on the same battery, the first 4 of them were performed with a 2.5 C discharge rate and the other 4 with a 3.5 C discharge rate. Aiming to achieve thermal and volumetric stabilization of the battery, a rest time of 15 and 20 min was established after charging or discharging processes, respectively. To better visualize temperature and radial strain behavior during the battery operation, different thermal and radial strain color maps were developed for the moments of the end of charge and discharge steps through the MATLAB® software.

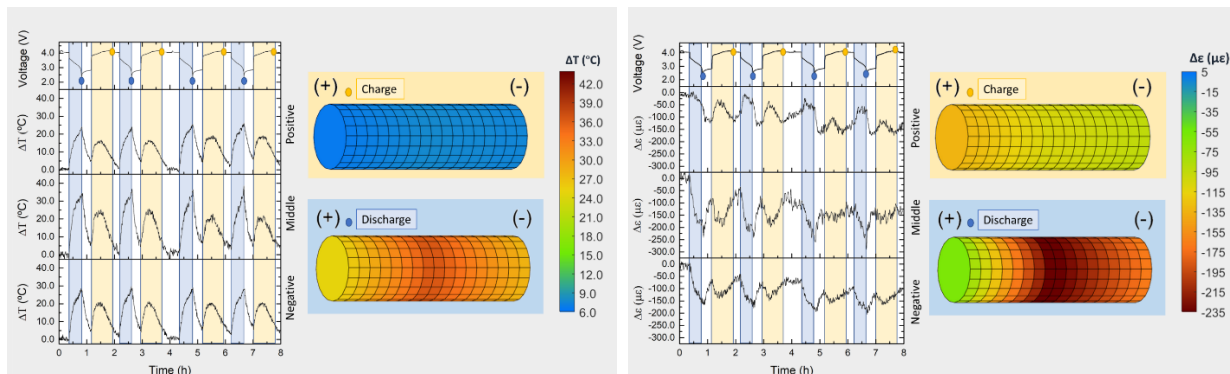


Figure 29. Left) Temperature variations of the 18650 LiB while submitted to a 1.9 C charge and 2.5 C discharge processes. The charge processes are represented by a beige color background, the discharge, by blue color, and the rest interval between procedures, by white color background. The higher temperature variations were achieved in the end of the discharge processes and in the middle location, as can be observed in the thermal mapping. Right) Radial strain variations of the 18650 LiB while submitted to a 1.9 C charge and 2.5 C discharge processes. The higher radial strain variations (contraction) were achieved in the middle location, and during the discharge process up to their ending. The positive terminal presented a different behavior when compared to the other locations.

In Figure 43 left, it is presented the results of the temperature variations tracked by all the FBG-PANDA sensors at different points of the battery during the 1.9 C charge and 2.5 C discharge cycles over time. A thermal mapping of the mean temperature variation values registered by the sensors on the end of charge and discharge steps is also presented. An accentuated increase in the temperature variation is achieved when the battery discharges (blue color) up to the lowest voltage (2.0 V), reaching the maximum temperature variation at the minimum battery terminal voltage. It should be noted that these maximum values of temperature variations during charging were achieved when the highest current

was applied to the battery. Figure 29 right, shows the radial strain variations detected by all the sensors at different points of the battery during the 1.9 C charge and 2.5 C discharge cycles over time. A radial strain mapping of the mean radial strain values registered by the optical fiber sensors on the end of charge and discharge steps is highlighted.

The results obtained from the temperature variations detected by the FBG-PANDA sensors at the different locations of the battery during the galvanostatic cycles at 3.5 C discharge and the correspondent thermal mapping at the end of charge and discharge steps, are represented in Figure 25, left. It was possible to observe similar behavior if compared to the 2.5 C discharge cycles. However, a greater temperature variation is achieved at the end of the discharge processes. Figure 30 right, represents the radial strain variation tracked by all the FBG-PANDA sensors during the galvanostatic cycles at the higher discharge rate and the correspondent radial strain mapping. From all the cycles performed in this experiment, we observed a very good feasibility and reproducibility in the FBG-PANDA sensors performance. With that, we can assume that these approaches, by using the optical fiber sensing technology to track and discriminate specific parameters in LiBs, are a reasonable tool to improve the safety of next batteries generation.

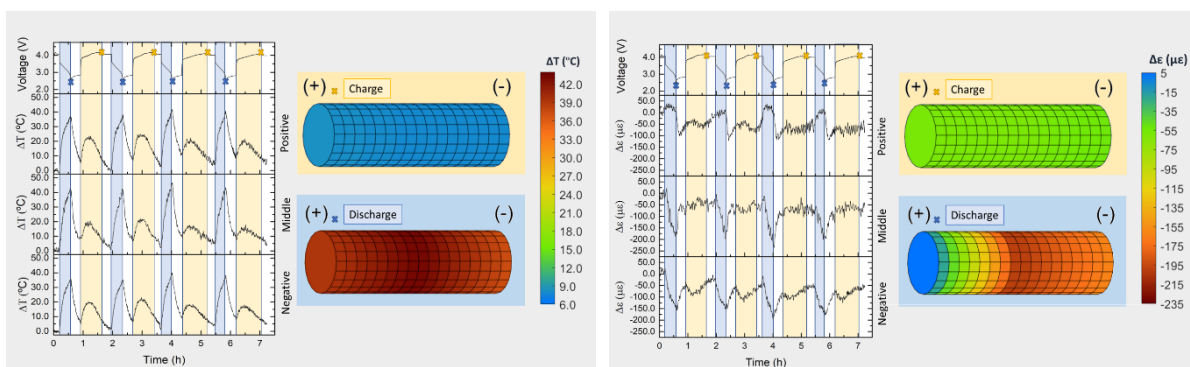


Figure 30. Left) Temperature variations of the 18650 LiB while submitted to a 1.9 C charge and 3.5 C discharge processes and respective thermal mapping detected in the end of charge and discharge steps. The higher temperature variations were achieved in the end of the discharge processes and in the middle location, as can be observed in the thermal mapping. Right) Radial strain variations of the 18650 LiB while submitted to a 1.9 C charge and 3.5 C discharge processes. The higher radial strain variations (contraction) were achieved at the end of the discharge processes.

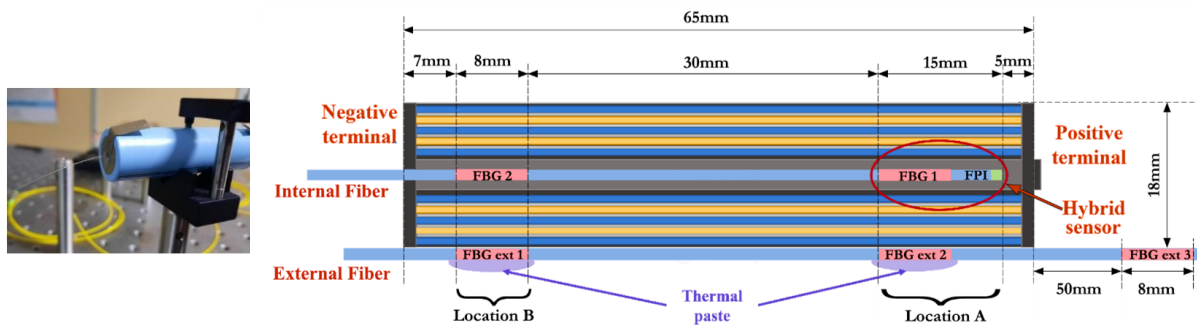


Figure 31. Schematic of the sensing setup of the instrumented 18650 LiB used for simultaneous decouple pressure and temperature changes during cell operation. The internal hybrid sensor was placed in location A (close to the positive terminal), the FBG2 was used to monitor the temperature near the negative terminal (location B). An external optical fiber line was used to monitor the surface temperature of the battery in the same location as the internal ones (FBG<sub>ext1</sub> and FBG<sub>ext2</sub>) and the environmental temperature of the climatic chamber (FBG<sub>ext3</sub>). Not on scale.

For the internal temperature and pressure decoupling, the OF/FBG – Hybrid sensors were internally located in the cylindrical battery cell, as it is illustrated on Figure 31, by performing a central hole of the negative terminal. To preserve the cell performance and structural integrity without the need for disassembly, a specialized drilling technique tailored for 18650 format cells was employed, following established methodologies previous used in the literature, and the negative terminal was selected as the preferred entry point for OF/FBG sensors instrumentation. On the same location, but externally, were also used standard FBG sensors for surface (FBG<sub>ext1</sub> and FBG<sub>ext2</sub>) and room (FBG<sub>ext3</sub>) temperature sensing.

To perform the optical fiber integration in safety conditions, the battery was firstly discharged up to 3.35V, to decrease their energy and the drilling process was performed in a glovebox with controlled nitrogen atmosphere. After that, an epoxy resin was used to seal the battery hole. After and before the battery drilling and optical fiber integration, the voltage value was not affected, registering also 3.35V.

The battery equipped with the sensors underwent galvanostatic cycling tests using the SP-150e potentiostat from Biologic®, France. To operate the battery under different conditions, charge/discharge cycles at  $\pm 1000$  mA and  $\pm 65$  mA were applied, corresponding to the C-rates of approximately C/3 and C/20, respectively, considering the LiB capacity of 3200 mAh. A 15-minute resting period was implemented at the conclusion of each charge/discharge step to ensure the thermal stabilization of the battery. The test at C/3 comprised eight consecutive charge/discharge cycles, with the charging phase initially conducted through a galvanostatic (constant current) step, followed by a potentiostatic (constant voltage) step. The discharging phase exclusively employed a galvanostatic step. These experiments were conducted at two distinct environmental temperatures: one at 25.0 °C, simulating normal operating conditions, and another at 40.0 °C, simulating more extreme and abnormal conditions.

Throughout the tests, the sensors spectral responses were recorded at 20 second intervals, and the peak reflection of each FBG was measured every 2 seconds using a si155 optical interrogator. Comprehensive data related to the battery's parameters, including voltage, capacity, and current, were recorded using the EC-Lab® software, interfaced with the SP-150e potentiostat.

In Figure 32, a charge/discharge cycle for the battery is presented at a C/20 rate. This initial experiment serves multiple objectives, including the validation of sensor functionality within the battery, the elucidation of the LiB electrochemical behavior in alignment with existing literature, and an exploration of potential variations when conducting the procedure at temperatures of 25.0 °C and 40.0 °C. As observed in the accompanying charts, the proposed hybrid sensor demonstrated its capability to consistently discriminate and monitor both temperature and pressure throughout the galvanostatic steps. Importantly, it should be noted that the spectral responses were converted into temperature and pressure values using the method previously described in Subtask 2.1.1.

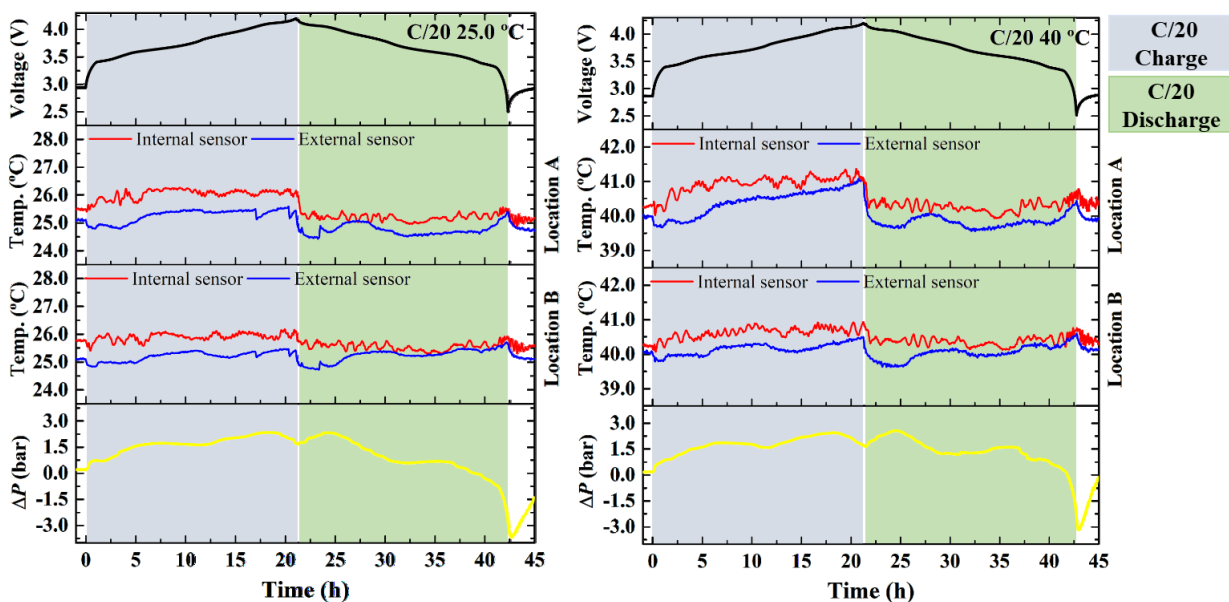


Figure 32. Temperature and pressure evolution over a C/20 charge/discharge cycle, for 25.0 °C (left) and 40.0 °C (right).

Particularly, the pressure evolution exhibited a consistent pattern, while both external and internal temperatures followed similar profiles. This synchronized data collection offers valuable insights into the battery performance and behavior under different environmental conditions. Regarding the temperature variations during each step, similar behavior was observed between the internal and external sensors. However, higher, and consecutive thermal fluctuations were internally achieved, being a significant insight into the internal battery instability during operation.

Comparing both sensing locations, higher  $\Delta T$  were detected on location A, over the charging process at 40.0 °C. In terms of pressure variation, during the CC charge and CC discharge steps,  $\sim 3.0$  bar and  $\sim 6.0$  bar was achieved, respectively. In Figure 33, an overview of the voltage behavior during the charge and discharge cycles is presented. The figure also includes the temperature and pressure variations of the battery throughout these procedures.

From a general perspective of temperature evolution, there are several considerations to be pointed out: (1) higher temperature variations were detected on the cycling tests at 25.0 °C; (2) the temperature detected by the internal sensors followed the tendency of the external FBGs data but with a greater magnitude, fact that can be attributed to the lithiation and delithiation processes occurring within the internal materials of the battery, which result in internal heat generation; (3) superior internal thermal instability (fluctuations of near 0.2 °C) was tracked by the internal sensors which means that the battery is more prone to temperature variations than externally.

Notably, the temperature fluctuations measured by the external sensors closely followed the trend observed by the internal sensors. It is worth emphasizing that the temperature values recorded by the hybrid sensor align with those obtained in eight cycling tests performed on another instrumented LiB, utilizing internal and external FBG sensors to monitor temperature variations during battery operation at both 25.0 °C and 40.0 °C room temperatures. In both experiments, greater temperature fluctuations were registered at 25.0 °C, particularly by the internal FBG sensors. Both sensor locations exhibited a similar signal behavior, thereby validating the reliability of the developed optical fiber hybrid sensor.

The fluctuations in internal pressure remained remarkably consistent across all galvanostatic cycles, regardless of the environmental temperatures. Mainly the pressure tends to increase during the charge and decrease during the discharge steps behaving as a “breathing” profile. This behavior is in accordance with the literature, which confirms again the reliability and feasibility of the optical hybrid sensor developed. In general, a pressure double peak was tracked for each charge/discharge cycle. However, during the consecutive cycles, a variation appears (slow decrease at 25.0 °C and slight increase at 40.0 °C), and the justification for that is, at this stage, unknown. The maximum  $\Delta P$  are similar for all cycles during the same environmental temperature, reaching values between  $\sim 3.0$  and  $\sim 4.0$  bar, for 25.0 °C and 40.0 °C, respectively. This discovery holds significant importance as it elucidates that at elevated external temperatures, the battery exhibits an increased propensity to accentuate internal volume changes, leading to consequential superior pressure variations. Comparing the SOC evolution (Figure 34) over the cycles with the temperature and pressure values detected by the OFS sensors it does not seem to exist a linear correlation between both parameters.

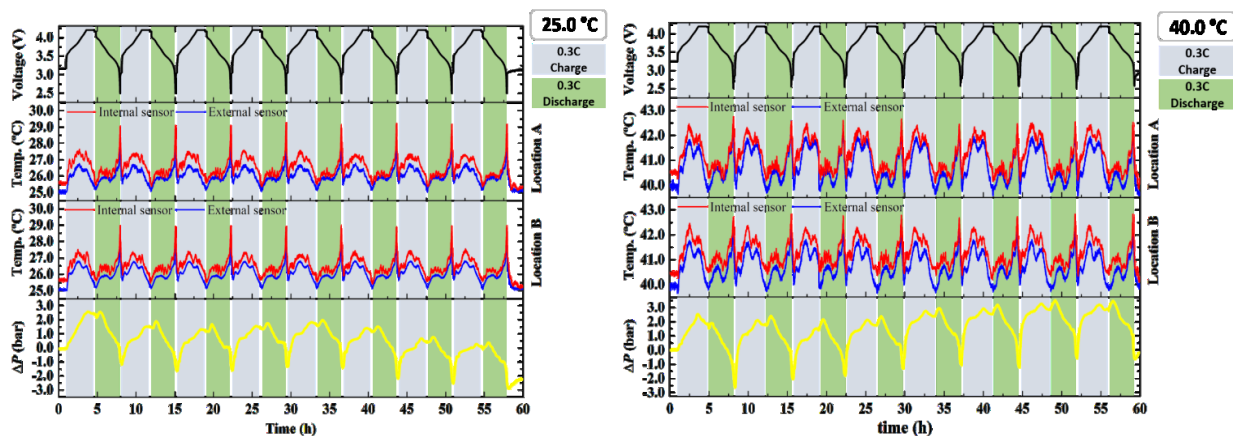


Figure 33. Temperature and pressure variation evolution for the eight galvanostatic cyclic test performed at 25.0 °C and 40.0 °C, with each charge (blue area) and discharge steps (green area), and the resting steps (white areas) represented. The first plot refers to the voltage profile, while the second and third are related to location A (close to the positive terminal) and location B (close to the negative terminal) temperature shifts, respectively (internal variation - red; external variation – blue). The fourth plot demonstrates the pressure variation inside the battery (yellow) over operation.



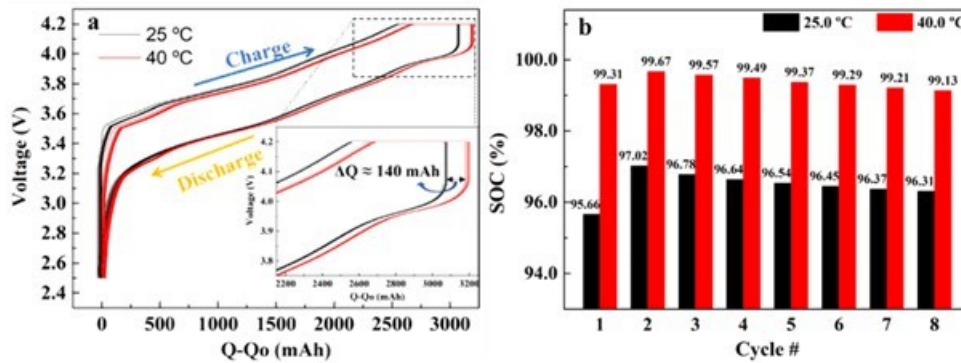


Figure 34. a) Voltage evolution with the battery's capacity during the galvanostatic cyclic test at 25.0 °C and 40.0 °C. It was observed higher battery performance at 40.0 °C, b) SOC evolution in function of the cycle number for each environmental temperature.

Figure 35 offers a comparative analysis between ICA and pressure variation as a function of voltage signals during both charge (a) and discharge (b) steps, conducted at C/20 and C/3 rates, and at temperatures of 25.0 °C and 40.0 °C. In both charge and discharge steps, a clear and robust correlation emerges between pressure variation and the ICA curves. During the charging process, as the  $dQ/dV$  signal increases, there is a simultaneous rise in  $\Delta P$ . It is also evident the impact of the environmental temperature and C-rate on the battery performance in terms of pressure evolution and electrochemical behaviour.

In a broader context, higher temperatures accelerate the increase in  $\Delta P$  signals, and higher C-rates result in lower  $\Delta P$  during charge steps and higher  $\Delta P$  during discharge steps. This means that during cycling, electrochemical performance, as reflected in lithiation and delithiation processes, is influenced by external factors such as temperature and the applied C-rate.

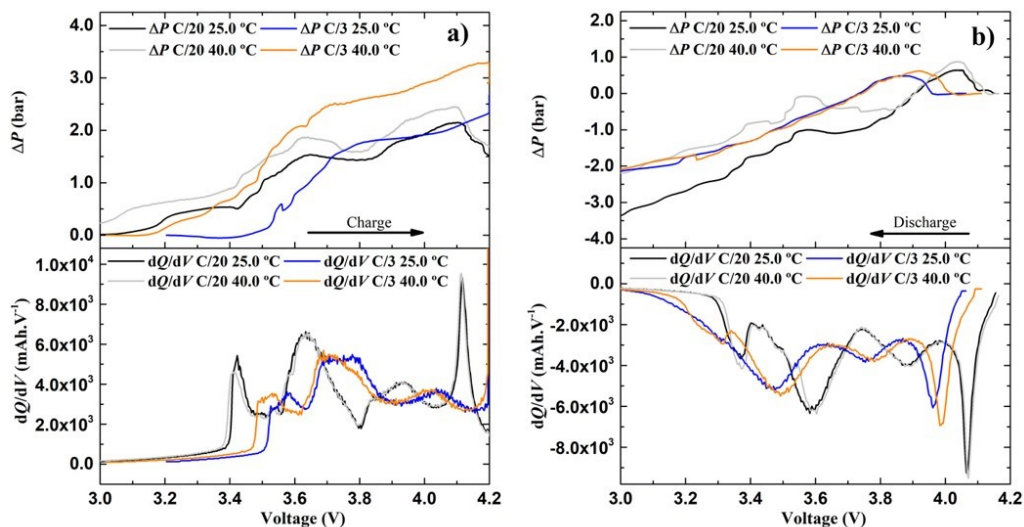


Figure 35. Comparison between the ICA analysis and pressure variation in function of voltage signal during the charge (a) and discharge (b) steps at C/20 and C/3 over 25.0 °C and 40.0 °C.

The OF/FBG sensors developed by UAVR, were also integrated in LiFUN pouch cells at CEA (Figure 36). For that, two pouch cells were instrumented with these optical sensors and tested at different operating conditions (including WLTP test). The optical fibers with OF/FBG PM-FBG and OF/FBG – Hybrid sensors were placed between the separator and negative electrode materials. This experimental configuration enabled the internal and real time temperature, strain, and pressure monitoring during cell operation. The main results are shown in Figure 37 and Figure 38. The temperature and strain data recorded and discriminated by the OF/FBG-PM-FBG sensors are presented in Figure 38. The data registered by the external thermocouple is also shown and served in this way as a comparison and validation that the optical sensors data are in accordance with them. Internally, higher temperature values and more thermal fluctuations were recorded. Regarding the strain data, the changes sensed by the optical sensors are well aligned with

the voltage signal and respective lithiation and delithiation Li-ion cell processes, where the electrode volume changes occurs.

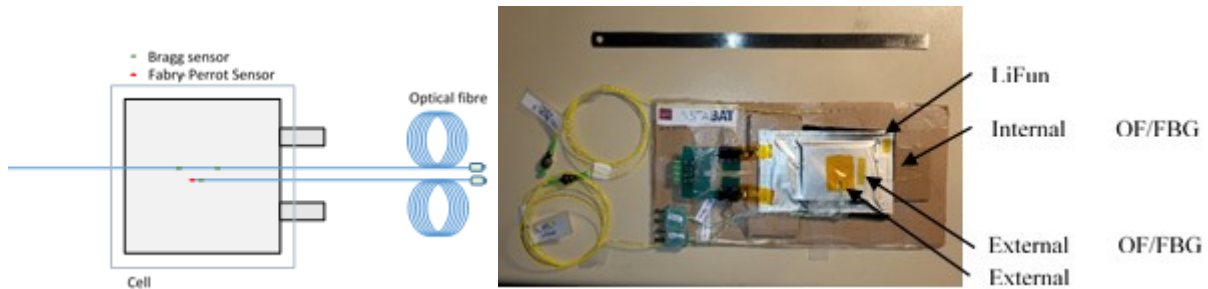


Figure 36. OF/FBG sensors integration and cycling test performed in the LiFUN pouch cells at CEA for internal temperature, strain, and pressure monitoring.

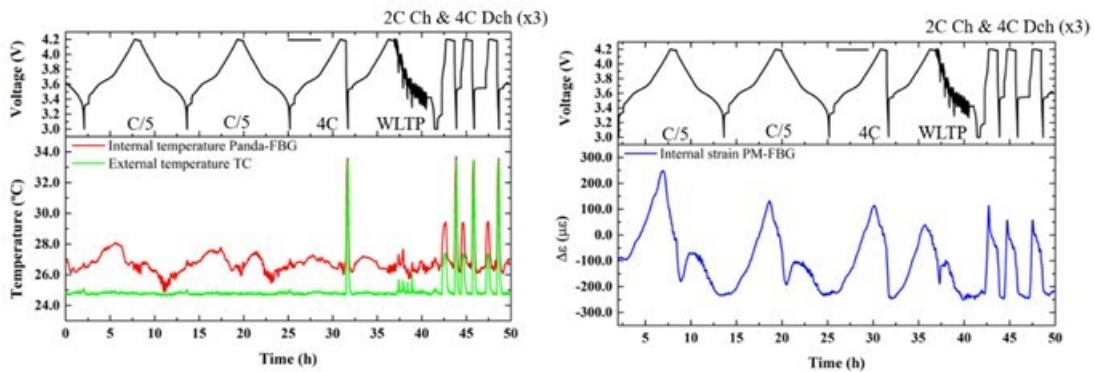


Figure 37. Left) Temperatures sensed in the LiFUN cell by the internal OF/FBG sensors and external Thermocouples during the cycling tests. Right) Strain variations monitored by the OF/FBG-PM-FBG sensors.

In Figure 38 are presented the temperatures sensed in the LiFUN cell by the internal OF/FBG sensors and external thermocouples and pressure variations tracked by the OF/FBG-Hybrid sensors from the simultaneous discrimination during the WLTP test. In this case, the pressure data is also well aligned with the voltage signal, in which, the four drop peaks of the WLTP test promoted an inversion/change on the internal pressure of the LiFUN cell. A total variation of near 12.0 bar was sensed during the discharge of the WLTP test.

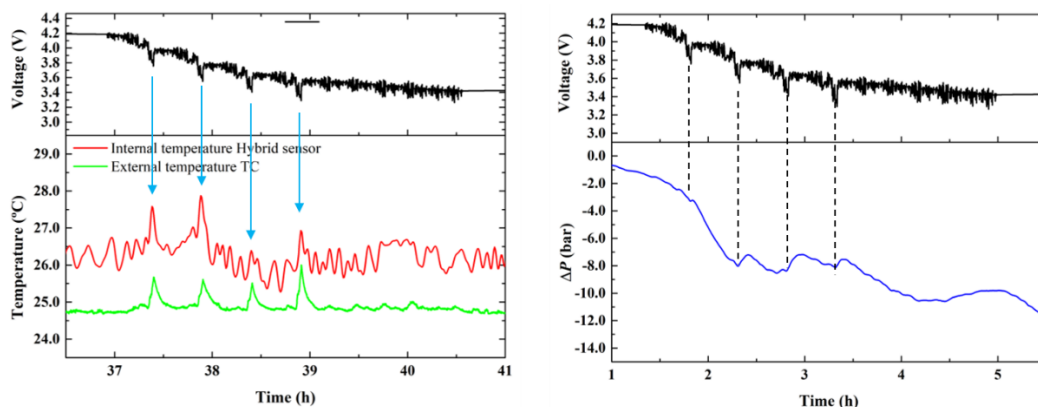


Figure 38. Left) Temperatures sensed in the LiFUN cell by the internal OF/FBG sensors and external Thermocouples during the WLTP test. Right) Pressure variations tracked by the OF/FBG-Hybrid sensors.

## Other type of OF/FBG sensors developed in the scope of INSTABAT - Tilted Fiber Bragg Grating sensors

Tilted Fiber Bragg Gratings (TFBGs) have a similar structure than classical FBGs but differ by the fact that the periodic refractive index modulation inscribed in the core of the fiber is tilted by a certain angle, allowing part of the light to travel in the fiber cladding as seen on Figure 39.

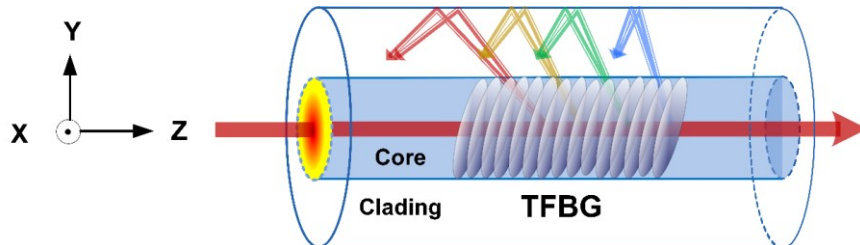


Figure 39. Schematic illustration of the TFBG.

The TFBGs used by CNRS were fabricated by Jacques Albert's group from Carleton University and have the following specifications: Each 10 mm-long, 556.015 nm period TFBG with 7° internal tilt angle was inscribed in hydrogen-loaded CORNING SMF-28 fiber (core diameter: 8.2 μm; clad diameter: 62.5 μm, attenuation: 0.05 dB/km at 1550 nm wavelength) by laser irradiation based on phase-mask method. Hydrogen loading of the fibers, enhancing their photosensitivity to ultraviolet light, was performed at room temperature and a pressure of 15.2 MPa for 14 days. The input light from KrF pulsed excimer laser (model PM-848 from Light Machinery, Inc., emitting at 248 nm and 100 pulse/second) was cylindrically focused along the fiber axis with energy of ~40 mJ over the grating region and also having passed through a 1078.4 nm period phase mask to produce a permanent periodic refractive index modulation in the core of the fiber. Rotating the fiber and phase mask, the tilt of grating fringes was obtained at an angle in the core as 7°.

The sensors were implemented in Swagelok cells as followed: A ring made of PEEK (12.8mm diameter, 2mm thick to fit 10mm length fiber sensor, storing 250 μL of electrolyte for immersion and electro-chemical testing) is fixed in the middle of 19mm diameter Swagelok cell where fiber sensor can go through by drilling two holes. The Li metal foil (0.38mm thickness, 14mmdiameter) is attached to one side of PEEK ring as anode, and on the other side of ring there is a steel grid to hold one Whatman separator beneath cathode composite. The cells were assembled in an argon-filled glovebox. An overview of the Swagelok with the fiber is given in Figure 40.

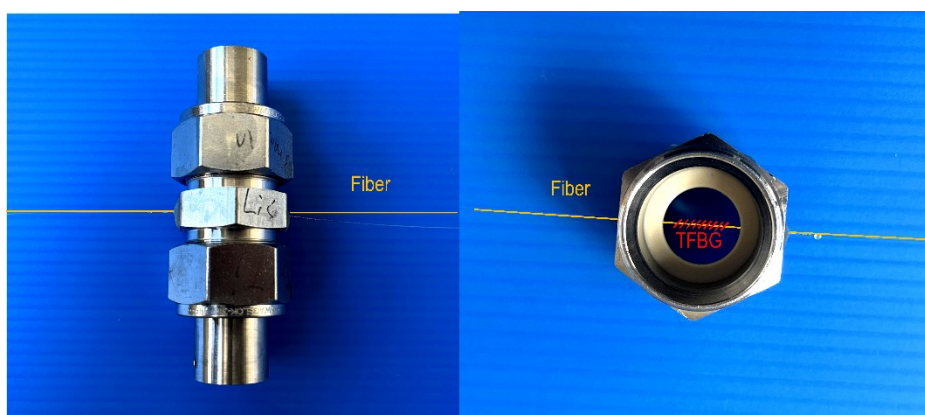


Figure 40. Photography of the assembled Swagelok with TFBG sensor.

The batteries investigated were Lithium sulfur batteries (LSBs) which is one of the most promising next-generation energy storage devices giving the merit of the batteries with overwhelming energy density of 2600 Wh/kg, abundance reserves and non-toxicity. While they are still not commercialized due to a number of unresolved challenges, including the insulating nature of sulfur and lithium sulfides, large volume expansion (80%) of the solid sulfur cathode during the formation of Li<sub>2</sub>S, and the shuttle effect caused by soluble polysulfide in electrolyte. Therefore, it is meaningful to clarify



the underlying science of LSBs during operation in terms of complicated kinetics and thermodynamics of the dissolution/precipitation of polysulfides.

In laboratory, numerous characterization technique (XRD, rotation-ring disk, UV-vis spectroscopic) has been developed to untangle the underlying science of LSBs. However, these analytical techniques rely on special equipment and cell designs that cannot be deployed directly in cells. Optical fiber gratings sensors could fill the gap by taking advantage of compactness (1 cm in length), remote sensing capabilities, simple integration into batteries without interfering its internal chemical reaction, which offers intriguing opportunities to build a “lab-on-fiber” platform for deeper chemistry and practical applications.

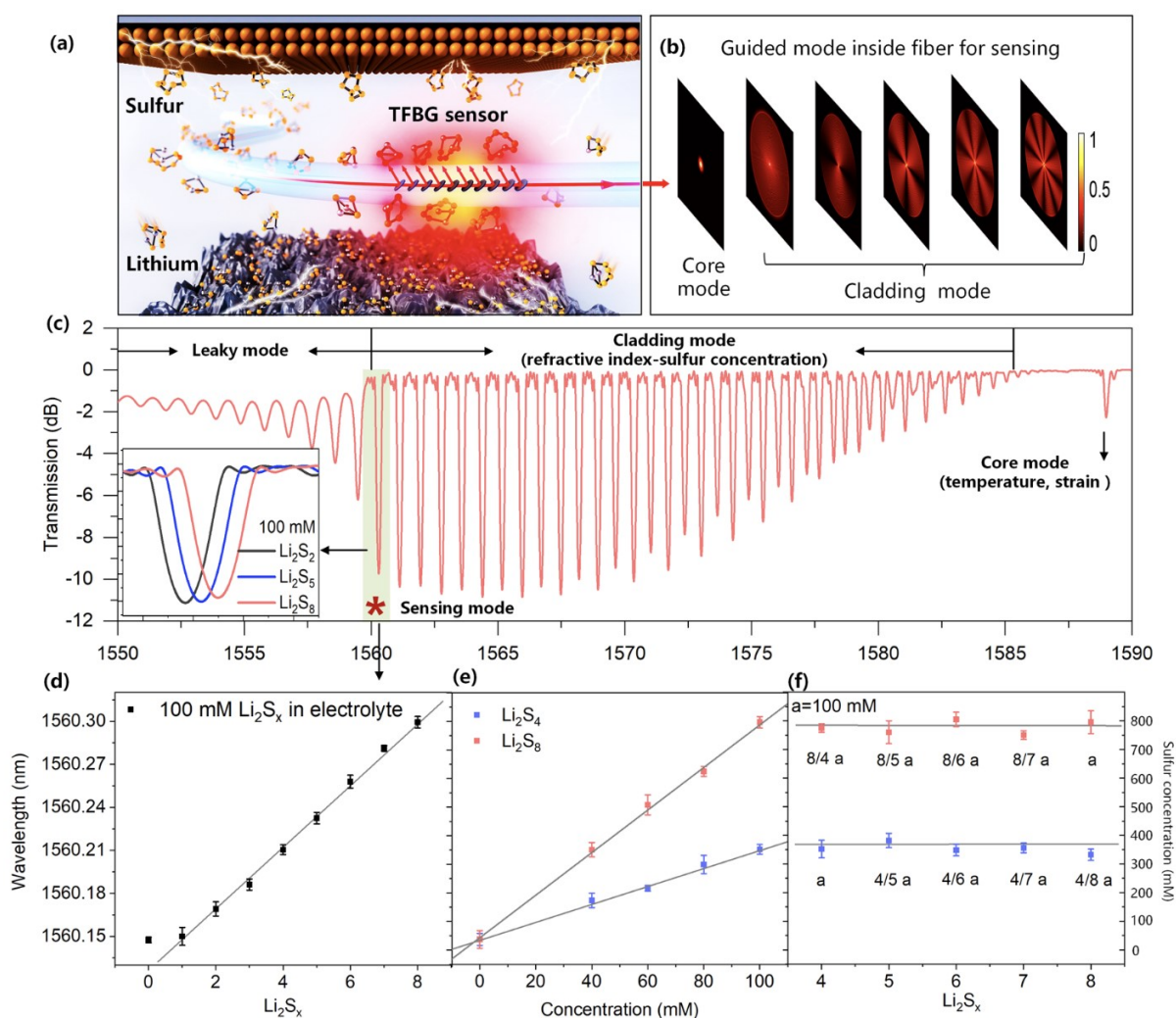


Figure 41. Concept of optical fiber sensing for LSB. a Schematic of a fiber optic sensor immersed in electrolyte for in-situ detection of sulfur concentration originating from the generated dissolved polysulfide and their transport activities (i.e., shuttle effect). b Backward-propagation guided modes inside fiber for sensing. c Experimental spectra response to polysulfide. d. The wavelength shifts of cladding mode resonance at ~1560nm to 100mM polysulfide  $\text{Li}_2\text{S}_x$  ( $x=1, 2, 3, \dots, 8$ ), shaded in green; (e) to concentration variation of  $\text{Li}_2\text{S}_4$  and  $\text{Li}_2\text{S}_8$  from 0mM to 100mM; (f) to same sulfur concentration of polysulfide  $\text{Li}_2\text{S}_x$  ( $x=4, 5, 6, 7, 8$ ). The error bars represent the measurement error (test 3 times continuously) resulting from the surrounding temperature change and electrolyte solvent evaporation.

The TFBG sensors, enabling the excitation of hundreds of discrete cladding mode resonances that are sensitive to a wide array of parameters including refractive index, temperature and strain, are proposed to operando track the chemical

dynamics/states of the LSB via electrolyte sulfur concentration<sup>12</sup>. We demonstrate that the capacity fading is strongly correlated with the dissolution/precipitation of polysulfides throughout cycling and hence, with respect to cycling rates. By exploiting the kinetic and thermodynamic responses of soluble sulfur in the electrolyte, the nonlinear net transport flux clarifies the invisible disproportionation process and the origins of its dynamic evolution. With this understanding, we show that altering the nucleation pathway of the crystalline Li<sub>2</sub>S and sulfur can be attributed to real improvements in cell cycling performance. Subsequently, it is noted that TFBGs have the ability to obtain key chemical-physical-thermal metrics in operando with notable time and spatial resolution that may extend beyond LSBs.

Prior to in operando battery inspection, it is appropriate to first briefly visit the suitability of TFBG sensing for such chemistries, as related to fundamental principles of their operation. The experimental spectra are presented in Figure 41 c, where the core mode resonance (i.e., Bragg resonance) is located at the longest wavelength around 1590nm (sensitive to temperature and strain ( $T, \epsilon$ )). The cladding mode resonances guided by the fiber cladding (beside  $T, \epsilon$ , also sensitive to refractive index (RI) of the surrounding media) are shown on the left of Bragg resonances. The leaky modes are located at the region where there is a discontinuity in the cladding mode envelope, indicating the loss of total internal reflection at the point where the cladding mode effective index becomes equal to or smaller than the surrounding RI. Therefore, with respect to soluble polysulfides which perturb electrolyte density, and hence the refractive-index, we focus on the cut-off guided cladding mode near the leaky mode region (around 1560nm wavelength) which is insensitive to unpolarized input light (i.e. can be probed without a polarizer, which simplifies sensing system and still ensures that detection is both stable and repeatable) and shows the highest refractive index sensitivity. To investigate the response of TFBG to polysulfides, depicted in Figure 41 c, it was thoroughly immersed in a series of 100mM polysulfide containing electrolytes in a modified Swagelok cell. Bearing this in mind, the Bragg resonance remains stable because any strain and temperature variation were eliminated during the measurements, indicating that the cladding mode wavelength shift is only related to refractive index variation. When the chain length of polysulfides is increased while keeping the polysulfide concentration the same, the guided modes on the left side of cladding mode at 1560nm become leaky due to the increased refractive index. This is a result of the number sulfur atoms in solution becoming larger and perturbing the corresponding mode effective refractive index, while guided modes on its right side are linearly shifted to longer wavelength (Figure 41 d, e).

- **Subtask 2.2.2 Reference electrode (RE) integration and test**

After a preliminary test on the RE samples with different shapes and coatings, it was selected the antenna shape with gold coating and an additional LFP layer. The RE sensor was located in a central position on the active area of the cell. To analyze if the lithiation/delithiation of gold was reversible, it has been performed 10 galvanostatic cycles (Figure 42 A). That is an important aspect to consider in the perspective of taking to reinitialize the RE periodically in the event of a drift of its plateau potential. A capacity fading was observed cycles (Figure 42 B), however without a strong degradation of the plateaus, making it possible to provide for reactivation of the RE in the event of a shift of its potential.

The electrochemical protocol applied consisted to a first delithiation/lithiation cycle at 42  $\mu$ A/day and 67  $\mu$ A/day to evaluate the LFP capacity. A partial delithiation step was then performed to fix the state of lithiation of LFP at 50%. The potential of LFP was recorded to evaluate its stability over time (Figure 43). It can be seen that the potential was stable over time. Therefore, for the integration in pouch cells, electrodes with a gold deposit coated with LFP will be used.

---

<sup>12</sup> Liu, F., Lu, W., Huang, J., Pimenta, V., Boles, S.T., Demir-Cakan, R., Tarascon, J-M. Detangling electrolyte chemical dynamics in lithium sulfur batteries by operando monitoring with optical resonance combs. Nature communications, 14 (1), 2023. DOI: 10.1038/s41467-023-43110-8

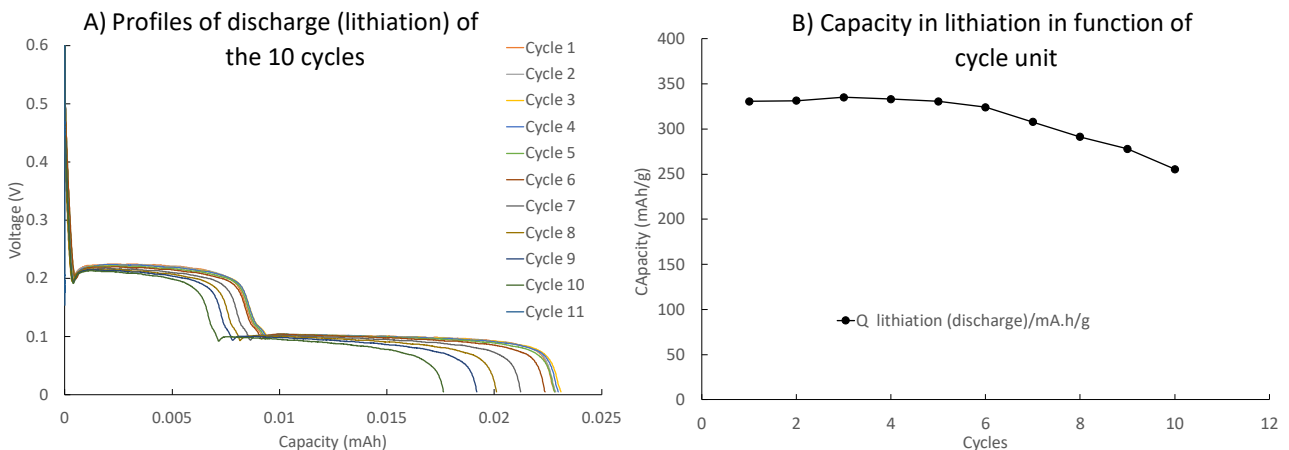


Figure 42. Lithiation/delithiation cycles of Gold ( $I = 6 \mu\text{A}$ ,  $[1\text{V} - 10 \text{mV}]$ ). A) Profiles of discharge during the 10 cycles. B) Capacity in lithiation in function of cycle number.

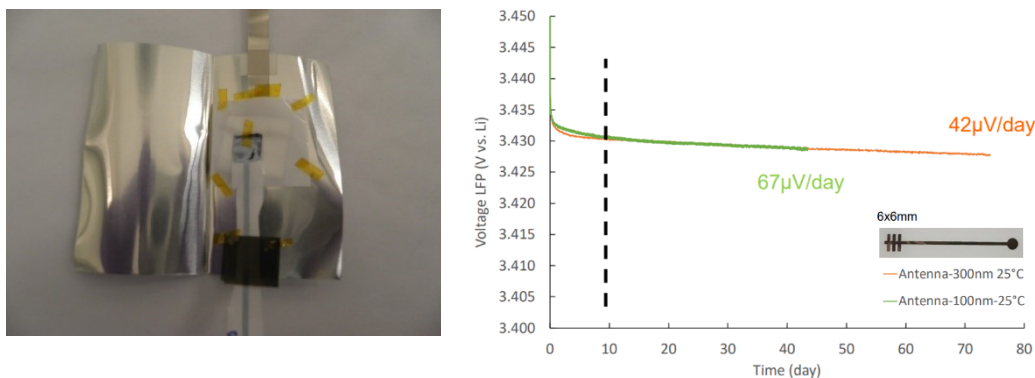


Figure 43. Left - Pouch-cell with LFP/Au film electrode before sealing. Right – Stability test of LFP/Au during 75 days for two different Au thickness (100 and 300 nm) (state of lithiation = 50%).

### • Subtask 2.2.3. OF/LumT and OF/LumL integration and test

We demonstrated in the Deliverable D3.1 (Figure 11, page 14) that the instrumentation of pouch cells with optical fibers does not modify the percentage of irreversibility (1st cycle of formation protocol) :  $15.1 \pm 1.3\%$  for non-instrumented pouch cells and  $15.1 \pm 1.1\%$  for instrumented pouch cells. The electrochemical protocols used on these non-instrumented and instrumented cells were similar. A small decrease on the discharge capacity per gram of NMC and the discharge capacity per surface of NMC (positive electrode) was observed in comparison with non-instrumented pouch cells (see Figure 9, page 13 in Deliverable D3.1):  $155.7 \pm 1.1 \text{ mA.h/g}$  for non-instrumented pouch cells and  $149.2 \text{ mAh/g}$  for instrumented pouch cells. However, this small variation can be explained by the experimental variability between the samples. It is mainly due to the manual assembling protocol of mono-stacked pouch cells. We give on an example of the formation curves for a pouch cell instrumented with an optical fiber and for a non-instrumented mono-stacked pouch cell.(see Figure 45). Figure 44 show instrumented cell use for this characterisation.

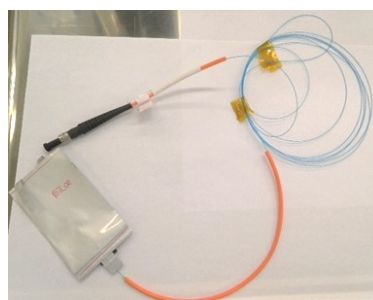


Figure 44. Integration of an OF-LumT sensor in a pouch cell (monolayer).

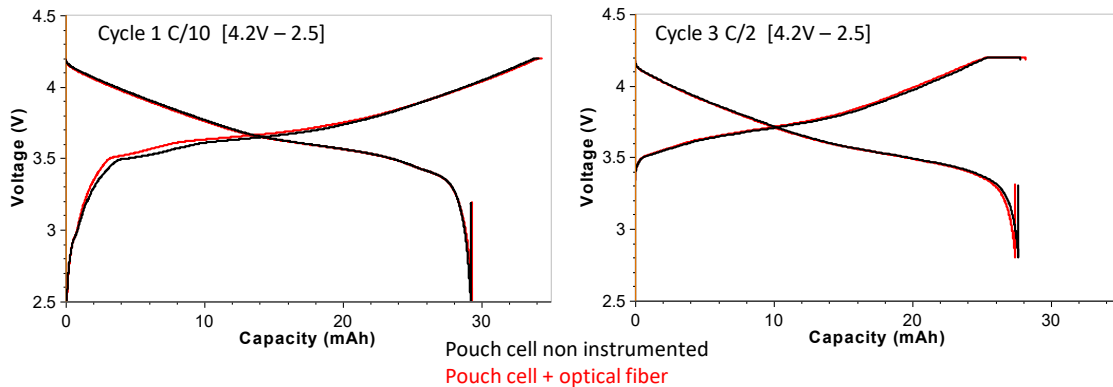


Figure 45. Example of the formation curves for the first cycle at C/20 and the third cycle at C/2 for a pouch cell instrumented with an optical fiber and for a non-instrumented pouch cell.

Regarding the capacity and internal resistance measurement, a variability in C/5 capacity and internal resistance at 25.0 °C were observed for instrumented and non-instrumented pouch cells, which is explainable by the experimental reproducibility of assembly (Figure 48). Comparatively, the charge and discharge capacities and internal resistance remained in the same range. The integration of the optical fiber on pouch cells does not really modify the electrochemical properties of the pouch cells.

	Non-instrumented pouch cell	Instrumented pouch cell
Internal resistance ( $\Omega$ )	$1.39 \pm 0.03$	$1.28 \pm 0.19$
Capacity C/5 (mAh)	$28.76 \pm 0.67$	$27.96 \pm 0.21$

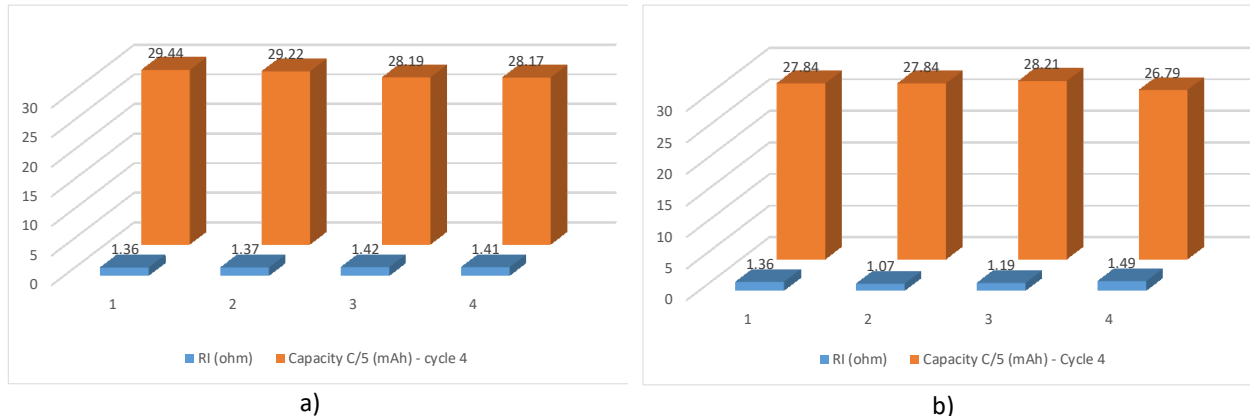


Figure 46. Comparison of the charge and discharge capacities of charge and discharges for non-instrumented pouch cells (a) and pouch cells instrumented with thermoluminescent optical fibers (b).

The instrumented cell with OF/LumT sensor has been tested in cycling condition with a C/2 charge and C/2, C and 2C discharges. External cell temperature was measured with a thermocouple (K-type) is used as reference temperature. In Figure 47 are shown the results. We can clearly show the variation of luminescence spectra during the high discharge rate is correlated to the cell temperature increase. Unfortunately, the increase of cell temperature is low (less than 2.0 °C). In this case, the sensor accuracy is too low. To improve the sensor, we need to work on the optical probe to improve the accuracy.

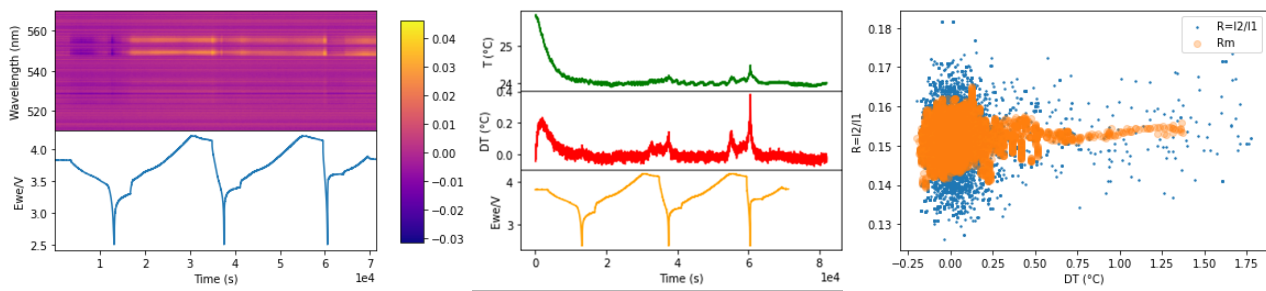


Figure 47. Test of OF/LumT sensor inside a pouch cell (monocell) under cycling condition: Optical spectra variation and cell potential over the time (left). Absolute and relative surface temperature as function of time compared to cell potential (center). Calibration curve of luminescent signal (peak ratio) versus relative temperature with and without noise reduction (right).

A first experiment with external measurements (OF/LumT sensor placed in the center of the cell surface and outside the cell) with a charge rate of  $C/2$  and discharge rates of 1D, 2D, 2D and 4D has shown a temperature increase from 3.0 °C to 17.0 °C in discharge (depending on the regime). We observe a good detection of the temperature increase by the OF/LumT sensor (see yellow curve in Figure 48) with a linear dependence on the temperature. The sensor shows a good resolution for a temperature variation of 1.0 °C.

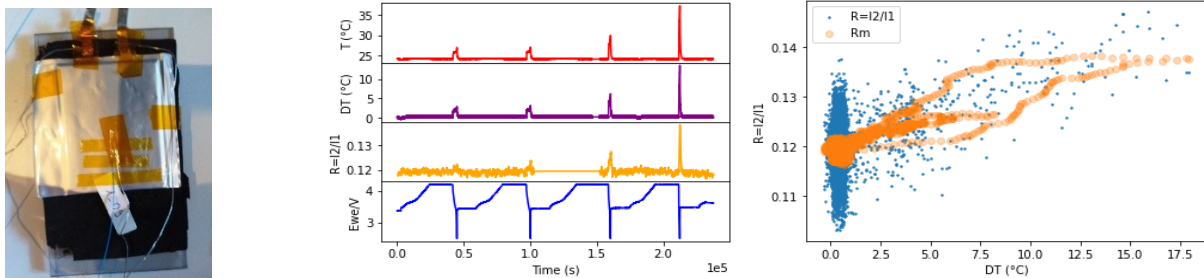


Figure 48. Test of OF/LumT sensor outside a pouch cell (1.1 Ah) (left) under cycling condition ( $C/2$ ; 1D, 1D, 2D and 4D): Absolute and relative surface temperature variation, response of OF/LumT sensor placed on the cell surface and cell potential over the time (center). Calibration curve of luminescent signal (peak ratio) versus relative temperature with and without noise reduction (right).

To qualify the sensor and have a reliable proof of concept, we have decided to test cells with higher capacities. Therefore, we also used commercial cells (LIFUN 1.1 A.h NMC622/graphite) provided by CNRS. This cell was instrumented with OF/LumT in the center of the electrode stacks and tested in cycling conditions:

The sensor was calibrated before insertion and inside the cell was done between 272 and 312 K. The Figure 49 present the calibration of the sensor before insertion inside the cell (a) the variation of the luminescence, (b) the comparison between temperature and the sensor signal ( $\ln(\text{FIR})$ ), (c) the calibration curve and (d) the relative sensitivity as function of temperature. Figure 50 show the same results for sensor inside the cell before cycling.



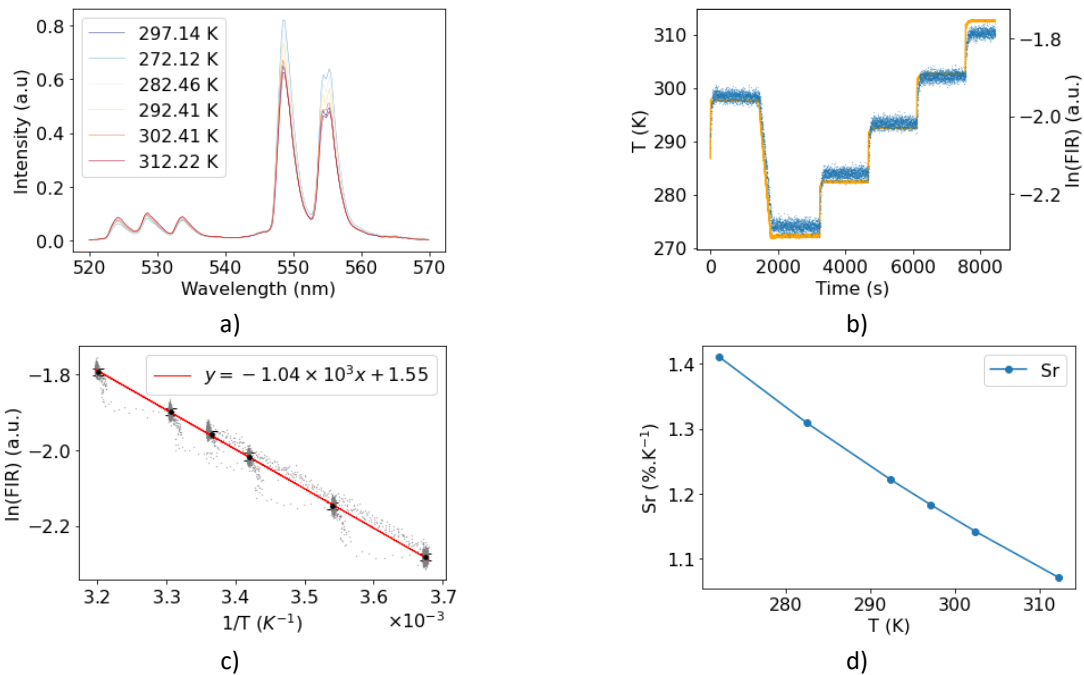


Figure 49. Thermoluminescence of optical fiber with Gd<sub>2</sub>O<sub>2</sub>S (Er<sup>3+</sup>, Yb<sup>3+</sup>) PTIR545UF powder in silica matrix and PMMA coating inside the Li-ion cell: a) Luminescence spectra evolution between 272 to 312 K, (b) Ln(FIR) (blue point) and Temperature (orange line) variation as a function of time during calibration, (c) Linear variation of ln(FIR)=f(1/T): measure (grey), mean and error bar correspond to the root mean square RMS (dark) and linear regression (red). (d) Relative sensitivity (S<sub>r</sub>) as a function of temperature calculated from the linear regression coefficient (ln(FIR)=f(1/T)).

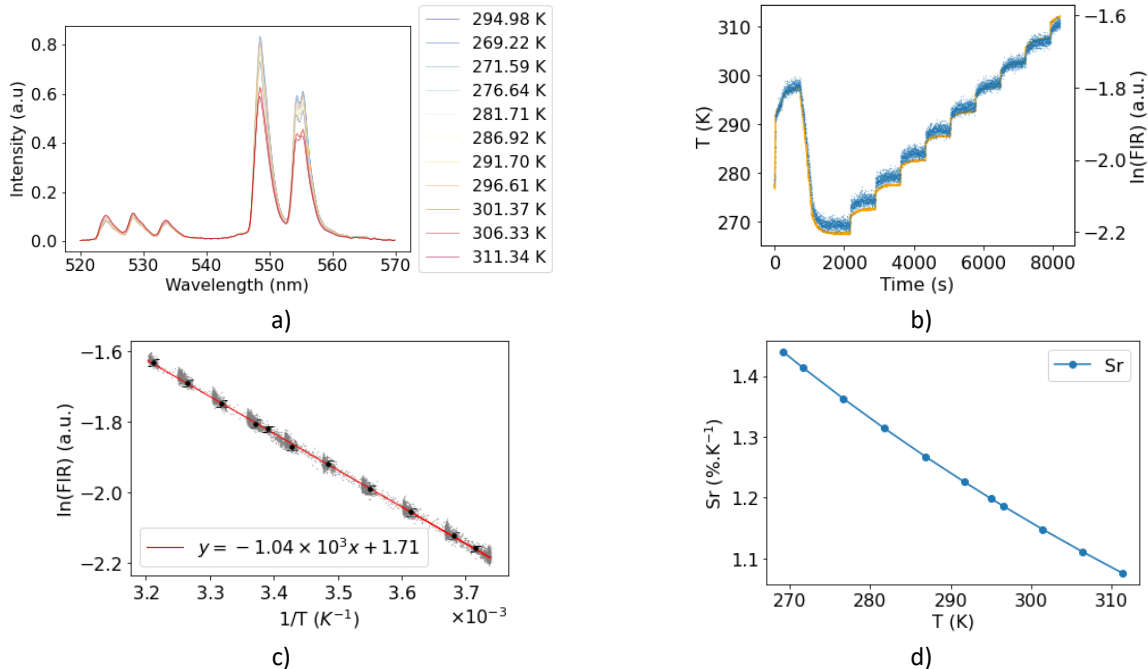


Figure 50. Thermoluminescence of optical fiber with Gd<sub>2</sub>O<sub>2</sub>S (Er<sup>3+</sup>, Yb<sup>3+</sup>) PTIR545UF powder (in the silica matrix) and PMMA coating: a) Luminescence spectra evolution between 272 to 312 K, (b) Ln(FIR) (blue point) and Temperature (orange line) variation as a function of time during calibration, (c) Linear variation of ln(FIR)=f(1/T): measure (grey), mean and error bar error bar correspond to the root mean square RMS (dark) and linear regression (red). (d) Relative sensitivity (S<sub>r</sub>) as a function of temperature calculated from the linear regression coefficients (ln(FIR)=f(1/T)).

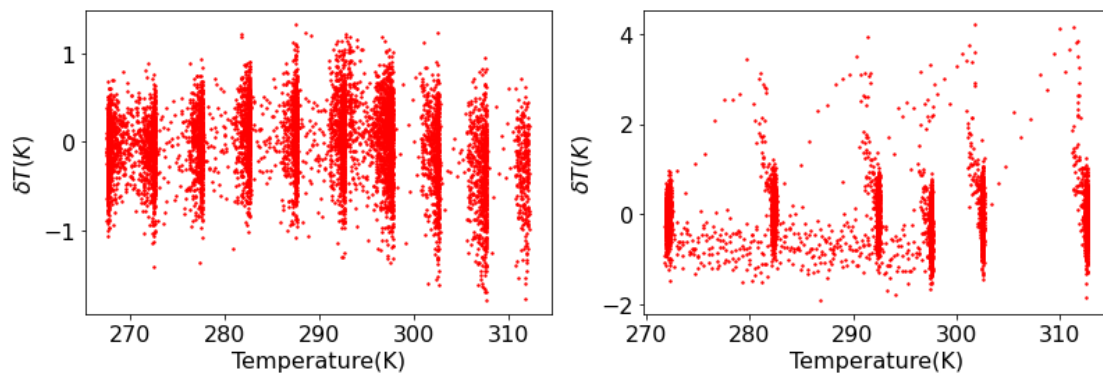


Figure 51:  $\delta T$  as function of temperature for sensor calculate from calibration curves (left) sensor alone, (right) sensor inside the cell.

The accuracy of the sensor was calculate from the calibration data outside and inside the cell (see Figure 51). The uncertainty of the temperature  $\delta T$  is about +/- 1°C over the range tested. A higher value for the error between two constant temperature plateaus is shown in Figure 51 for the sensor inside the cell. This error is not related to the sensor but to the thermal gradient between the sensor temperature inside the cell and the reference temperature measured in the climate chamber during the temperature transition. These points are outliers. They are not considered for evaluating the accuracy of the sensor.

Four cycles at rates of 4D + D/5 and C, then at rates of C/2, D/5, C, D/5, 2C). The Figure 52 shows the comparison between the luminescent signal and the surface temperature variation over the cycling protocol. We observe then a good correlation between these two signals. The signal from the sensor is linearly dependent on the temperature with a reduced noise after data treatment. This data treatment improves the accuracy of the sensor around 1.0 °C.

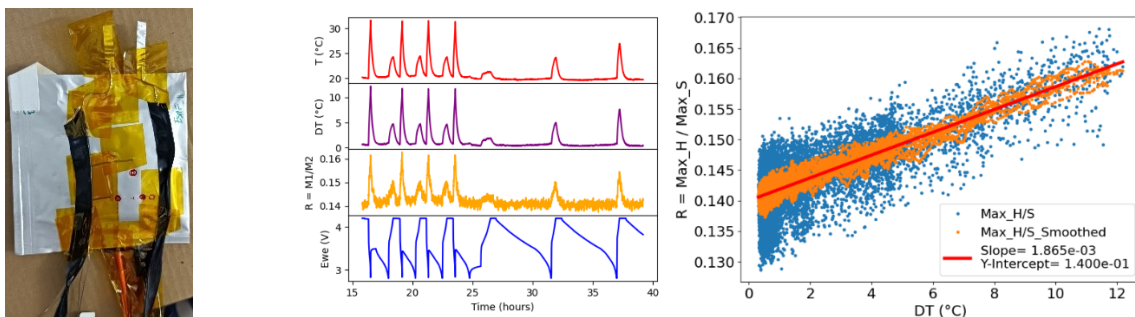


Figure 52. Test of OF/LumT inside a pouch cell (1.1A.h) (left) under cycling condition (C, 4D + D/5, C/2+D/5, C+D/5 and 2C/D/5): (left) Absolute and relative surface temperature variation, response of OF/LumT sensor inside the cell and cell potential variation (left). Calibration curve of luminescent signal (peak ratio) versus relative temperature with and without noise reduction (right).

To conclude this part, the integration of the OF/LumT sensor inside the cell has no impact on the cell performances. These results show the operability of the sensor inside the cell. The optical response inside and outside the cell have the same temperature dependency. Accuracy of the OF/LumT is around 1.0 °C with appropriate data treatment and is in the way fitted with the requirements of the project. Finally, these results validate the sensor integration inside the cell and this sensor was used for the ageing tests on multilayer cells (WP3).

- **Subtask 2.2.4. PA sensor integration and test**

Two versions of IFAG PA CO<sub>2</sub> sensors have been tested at CEA institute (see Figure 17 and Figure 18). For both versions, a dedicated software developed by Infineon is necessary to collect the data measured by each sensor. These sensors are designed to perform CO<sub>2</sub> measurements in air atmosphere. Furthermore, they must operate in conditions close to the atmospheric pressure. Then, these sensors must be calibrated in neutral atmosphere and in harsh atmosphere with electrolyte vapour. Their sensibility and detection limits in these atmospheres must also be determined. We first performed calibration and sensitivity tests in Ar environment.



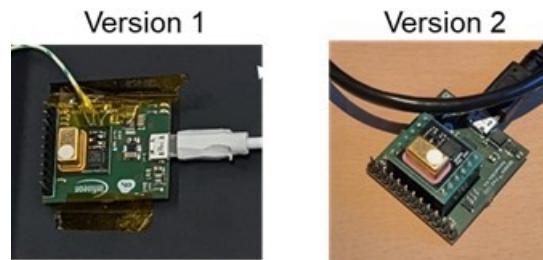


Figure 53. Two versions of Infineon PA CO<sub>2</sub> sensor tested (version 1=PA GEN 1.0, version 2= PA Gen INSTABAT special 1.0 cf Figure 17).

A hermetic chamber was specially designed by CEA and manufactured to perform gas concentration measurements on opened cells under cycling condition (see Figure 54). This chamber has been also used to perform sensors calibrations. Two different approaches have been used to perform sensors calibration: 1- with gas cylinder at different concentration; 2- with an Alytech Gasmix™ Nomad dilution bench (see Figure 55).

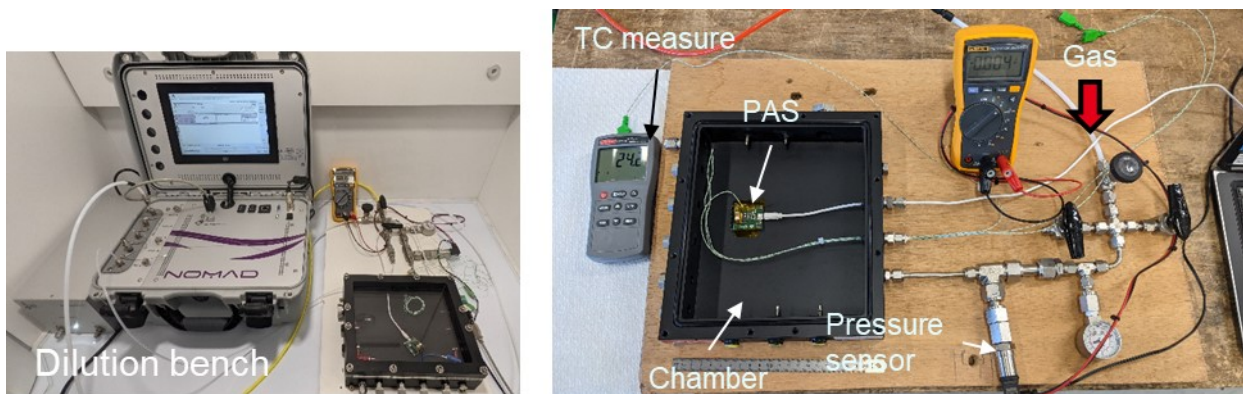


Figure 54. Setup for CO<sub>2</sub> sensors calibration: dilution bench (on the left) and hermetic chamber with inlet pipe circuit.

The gas cylinders had calibrated CO<sub>2</sub> concentrations from 100 ppm to 5000 ppm. The dilution bench is used to calibrate sensor at decreasing concentrations from 50 ppm to 2 ppm. Results are shown in Figure 55. The post processing of these data gives us the calibration in Ar for the first version of PA CO<sub>2</sub> sensors as shown in Figure 56. PA CO<sub>2</sub> sensors measure CO<sub>2</sub> in Ar with a good correlation to CO<sub>2</sub> in air with a monotonic variation. The detection limit is detected up to 2 ppm with relatively low error. However, we did not test the sensors below 2 ppm during this campaign. Calibration tests are currently performed on sensors from a PA Gen INSTABAT special 1.0 version.

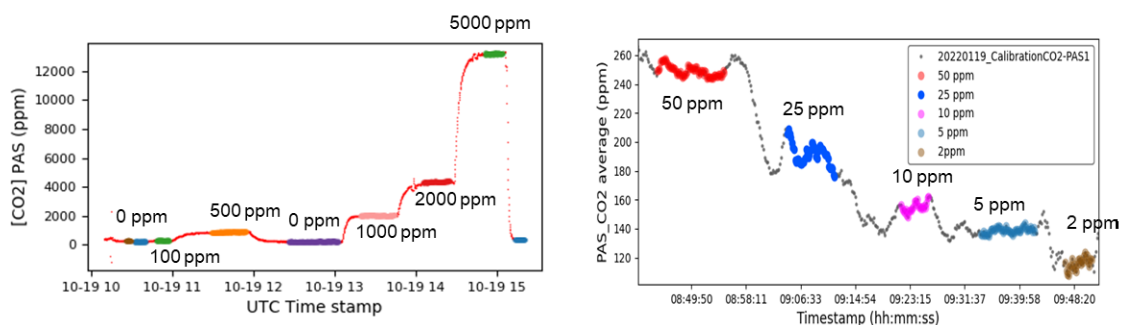


Figure 55. Calibration data from the first version of PA CO<sub>2</sub> (PA Gen 1.0) sensor using gas cylinders (left) and gas dilutor (right).

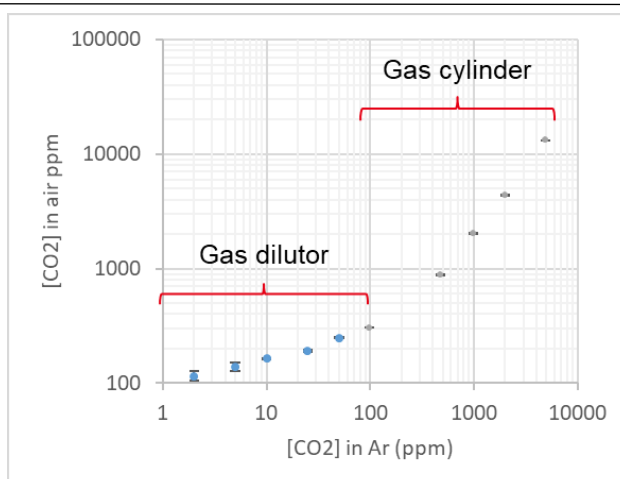


Figure 56. Calibration curve between CO<sub>2</sub> concentration in Ar (from the gas dilutor and gas cylinders) and CO<sub>2</sub> concentration in air (measured by the sensor) for the first version of PA CO<sub>2</sub> sensor (PA Gen 1.0).

The PA Gen 1.0 sensor provided by IFAG has been implemented in battery by CNRS using a different strategy. The first one, shown in Figure 57a, consists of placing the bag containing the electrolyte and the jelly roll and the PA sensor in a larger pouch bag. In this case, the sensor is not directly in contact with electrolyte and can sense the gas passing through the hole drilled in the pouch cell in glovebox. A hole is drilled in the big pouch bag to allow the large USB cable to power the PAS sensor. It is then covered with epoxy resin cured for 24 hours to avoid leaks. In this configuration, the cell cannot be vacuum sealed or degassed after the formation cycles, which is likely to affect cell performances. However, as observed in Figure 57b and c, the performances of the cell instrumented with PA CO<sub>2</sub> sensor are only slightly lower than the pristine cell performances. Then this configuration can be used for the implementation of the PA sensor inside cells since the different parameters influencing its values can be decoupled.

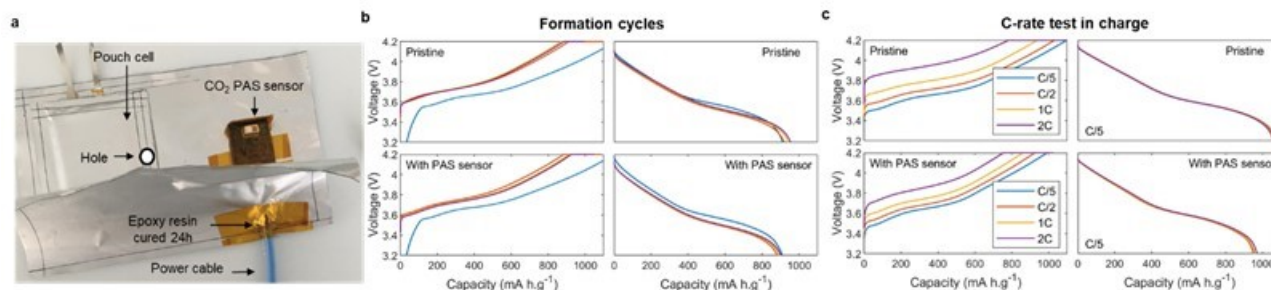


Figure 57. (a) Picture of the instrumented bag with a pouch cell and the PA CO<sub>2</sub> sensor. To allow contact between the gas and the sensor, a hole is drilled in the pouch cell in glovebox. The power cable passes in the bag through a hole covered with epoxy resin cured for 24 hours to avoid leaks. Formation cycles (b) and C-rate test in charge (c) at 25.0 °C for pristine LiFUN cell (top) and LiFUN cell instrumented with CO<sub>2</sub> PA sensor.

Indeed, different parameters seem to influence the value of the sensor. As demonstrated in Figure 58a, when the cell is cycled, the sensor responds with an increase of the CO<sub>2</sub> concentration during charge and a decrease during discharge. However, the value of 6000 ppm is not realistic. By reproducing the measurements, the same variation is observed but the value of -25000 ppm was obtained. Regarding the variation, the influence of other parameters has been confirmed. Indeed, by changing the temperature of the oven containing the cell, we observe an important variation of the CO<sub>2</sub> concentration given by the sensor (see Figure 58.b). The sensor is then also sensitive to pressure. As described in WP2, Infineon is now working on a new version of its sensor. More investigations are required in the future to understand the impact of the protocol of sample preparation to the sensor response. The impact of the pressure during the sample preparation and cycling must be study in deeper way to manage the response of the sensor.

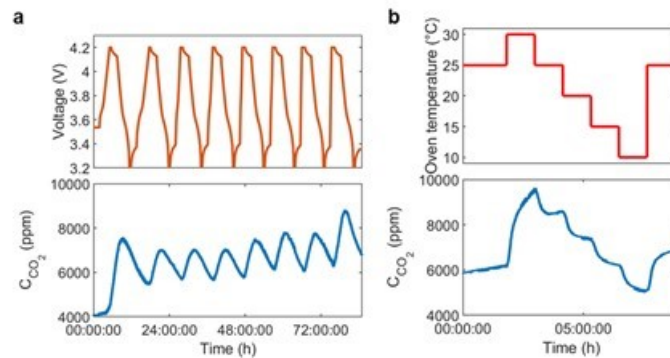


Figure 58. (a) C-rates in charge test and CO<sub>2</sub> concentration given by PA sensor. (b) Variation of the CO<sub>2</sub> concentration given by the sensor in function of the temperature of the cell.

Beyond highlighting the basic functionality, the tests performed at CEA and CNRS on the PA Gen 1.0/ PAS Gen INSTABAT Special 1.0 samples also clearly demonstrate that the implementation of the PA CO<sub>2</sub> sensor still imposes severe physical limitations for future integration into the cell. The size of the sensor system (refer to Figure 17 for the dimensions) and the connection via a USB cable were identified as the main hurdles in this regard. To overcome these obstacles, IFAG has started to work on another design, denoted as “PA Gen INSTABAT Special 2.0” in the overview in Figure 19. As indicated there, the main improvements targeted in this version consist in a separation of the sensing chamber from the other electronics (thereby instantly halving the size of the part of the sensor to be integrated into the battery cell) and the implementation of a connection between sensing chamber and electronics via a Flex PCB. The work on this new generation is still in progress at IFAG. Due to these limitations, CNRS has stopped performing tests using the PA sensor to focus on standard FBGs implementation for calorimetric measurements.

Table 3. *List of deliverables WP2*

Deliverable Number	Deliverable Title	Lead beneficiary	Type	Dissemination level	Due date (in month)	Status
D2.1	Report on present state-of-art for sensors in Liion batteries	7 – UAVR	Report	Public	3	Submitted
D2.2	Protocol for sensors fabrication	7 – UAVR	Report	Confidential	12	Submitted
D2.3	Protocol for sensors adaptation to cell environment	7 – UAVR	Report	Confidential	15	Submitted
D2.4	Report on sensor integration feasibility and impact on cell and sensors performance	3 – CNRS	Report	Confidential	30	Submitted
D2.5	Prototypes of each finalised sensor	7 – UAVR	Demonstrator	Public	30	Submitted

Table 4. Relevant Milestones associate to WP2

Milestone Number	Milestone Title	Lead beneficiary	Due date (in month)	Status
MS3	Sensors prototype available and validated in battery cell environment	7 – UAVR	30	Validate

## WP3 - Correlation between measured/estimated parameters and physico-chemical degradation phenomena occurring in the battery cell

Work package number	3	Leader	CNRS						
Work package title	Correlation between measured/estimated parameters and physico-chemical degradation phenomena occurring in the battery cell								
Short name of participant	UAVR	CEA	CNRS						
Person months per participant	7	11	35						
Start month	M6			End month			M32		

### Objectives

The objective of WP3 is to correlate the physical sensor measurements (sensor signals output) and the virtual sensors estimations with the physico-chemical phenomena occurring in Li-ion battery cells. The main objectives of this WP are the following:

- Characterise the electro-chemical performance of pristine and instrumented cells;
- Identify the significant physical sensor outputs during cycling conditions;
- Characterise significant physico-chemical phenomena of the battery cells, in particular signals correlated to degradation;
- Validate virtual sensors values with respect to the reference Newman model and outputs from sensors in instrumented cells;
- Correlate physical/virtual sensor output signals to physico-chemical phenomena of the battery cells.

### Highlights of most significant results

Batteries are evolving systems, throughout their life the electrolyte and material will degrade to form interfaces, soluble products and gas. By using sensors developed in WP2, these phenomena can be detected and understood providing unique information about degradation mechanism.

The first challenge of WP3 is to implement the different sensors to battery without affecting the electrochemical performances. In this context, pouch cells have been tested with or without sensors. In order to compare results between the different partners of the project, we agreed on material, electrolyte and electrochemical protocol (detailed in task 3.1). In doing so, electrochemical tests on pristine cells at different temperatures have been performed. Moreover, experimental conditions have defined to reproduce the extreme conditions that batteries can undergo during their life (temperature, current). These tests will later be used as a reference for comparison with instrumented pouch cells and highlight the good performance of the material/electrolyte combination, giving confidence in their potential use in real applications.

Knowing this, different tests of sensor integration have been carried out. Regarding the optical fibers, their small diameter, their good chemical stability in organic electrolytes (see WP2) and their robustness allow their integration directly during the sealing of the pouch bag. Indeed, it is possible to place the fiber between the upper and lower part of the bag, during the welding at high temperature, the polymer covering the bag will melt slightly ensuring a good sealing. Thanks to this easy integration, optical fiber sensors have been integrated into pouch cells without affecting the electrochemical performances. Using the same strategy, reference electrode sensor can be implemented at different position inside the cell without any problems and without affecting the cells performances. The greatest difficulties concern the integration of the CO<sub>2</sub> PAS sensor. Indeed, the evaluation of the sensitivity of the PAS sensor to temperature, pressure and humidity demonstrated that the implementation of such sensor in pouch cell was not possible. Therefore, it was decided to not use such sensor for the rest of the project.

Only the standard FBG, the OF/LumT and the reference electrode RE sensors were at a sufficient stage of development to adapt to the battery environment and be integrated without affecting electrochemical performance. The optical fiber sensors and RE have provided valuable information for the understanding of chemical degradation phenomena. Indeed, we have shown that FBG sensors are mostly temperature sensitive and by using a thermal capillary to protect the sensor from deformation or change in curvature during the pouch cell cycle, we were able to measure the temperature inside pouch cells in operando with very good accuracy. In addition, by placing optical fibers with FBG

sensors inside, on the surface, and within a few centimetres of the pouch cell, heat transfer can be measured during the formation cycles of the cells, and during long cycling. In this context, a thermal model can be solved allowing to calculate heat, enthalpy and entropy. These energies are directly related to the chemical phenomena and allow accurate identification and characterization of SEI formation and cell aging. Furthermore, it was demonstrated that LiFUN cell cycled at 25°C experienced more damage than cell cycled at 55°C, presumably due to the fact that more cycle was performed at 25°C. SEM, EDX, and XRD measurements support those findings.

Using the OF/LumT sensor in VARTA multilayer cell, aging tests were performed at different temperature. Such sensor has the advantages of not being sensitive to strain, pressure, or curvature. It was shown that the sensor can track the temperature inside the cell over 150 cycles. Besides, the implementation of such sensor has also been made in LiFUN cell where very good stability was achieved, even at high C-rates. It was shown that cycling the cell at -10°C was the worst-case scenario has the cell died within a few cycles. Post-mortem analysis performed on those cells showed clear evidence of lithium plating, particularly at the edge of the electrode for high temperature tests, and on the full electrode at low temperature test. Concerning reference electrode, their used is well known since decades. The reference allows the distinction of contribution to current and voltage of each cell component to the overall battery performance and to study the degradation mechanism of individuals electrodes. The results of RE implemented in VARTA monolayer cells show that the gold film deposited on a separator and covered with a LFP can be used as a stable reference electrode without affecting the electrochemical performance. WLTP cycling at temperature ranging from -10°C to 45°C shows no impact compare to pristine cells cycled within those conditions. No significant damages were monitored at room temperature. At 0°C and 45°C, Loss of Lithium Inventory (LLI) were the major degradation mechanism as demonstrated through SEM and EDX measurements. Those findings were corroborated with half cell measurements using recovered electrode from cycled cells.

*Summary of progress towards objectives and details for each task*

### **TASK 3.1 ACCELERATED TESTS ON INSTRUMENTED CELLS**

(Leader CEA, participants CNRS, UAVR) (M6-M30)

CNRS and CEA have defined in the beginning of the project the electrochemical test protocols used to characterize the instrumented cells. To remind, two formats of cells have been tested:

- Standard CEA lab format with VARTA positive and negative electrodes (nominal capacity 29.6 mAh at C/5, RT)
- Li-FUN cell (nominal capacity 1170 mAh at C/5, RT)

The specifications of both cells are given in Table 5. They are almost similar in terms of nature of active materials and electrode coatings but the particle sizes and electrode porosities are not known that will influence their respective performances.



Table 5. Cell specifications

	Li-FUN cell	Standard CEA lab format
Nominal capacity (mAh) at RT (C/5)	1170	29.6
Voltage range (V)	4.2 – 3.0	4.2 - 2.7
<b>Cathode</b>		
Cathode material	LiNi <sub>0.6</sub> Mn <sub>0.6</sub> Co <sub>0.2</sub> O <sub>2</sub>	
Coating weight (mg/cm <sup>2</sup> )	16.7	17.5
Active material loading (wt%)	0.964	/
Mass active material (g)	7.083	/
Real capacity (mAh/cm <sup>2</sup> )	2.8	2.9
Coating thickness (µm)		61
<b>Anode</b>		
Anode material	Artificial Graphite	Graphite
Coating weight (mg/cm <sup>2</sup> )	10.0	9.3
Active material loading (wt%)	9.948	/
Mass active material (g)	/	/
Real capacity (mAh/cm <sup>2</sup> )	/	3.2
Coating thickness (µm)		55

- Formation protocol**

The formation protocol is conformable to the protocol proposed by VARTA. The test conditions are given in Figure 59 and Table 6.

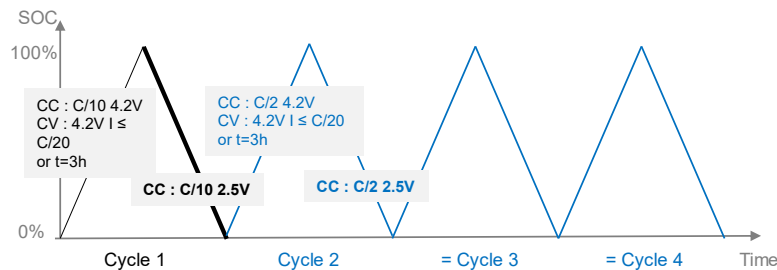


Figure 59. Schematic diagram of the formation protocol

Table 6. Formation protocol

Cycle	Value	Type	Limit
0		Rest	2h
1	C/10	CC charge	4.2 V
	4.2 V	CV charge	$I \leq C/20$ or $t=3h$
	C/10	CC discharge	2.5 V
		Rest	5h
2-4	C/2	CC charge	4.2 V
	4.2 V	CV charge	$I \leq C/20$ and $t=3h$
		Rest	5 min
	C/2	CC discharge	2.8 V
		Rest	5 min
5 (→ if storage after)	C/2	CC charge	SOC 30%

Note: The voltage limit in discharge will be 3.0V for Li-FUN cell.

- Capacity and internal resistance measurement**

The capacity and internal resistance measurement protocol is given in Figure 60 and Table 7. The internal resistance is measured at 50% of SOC.



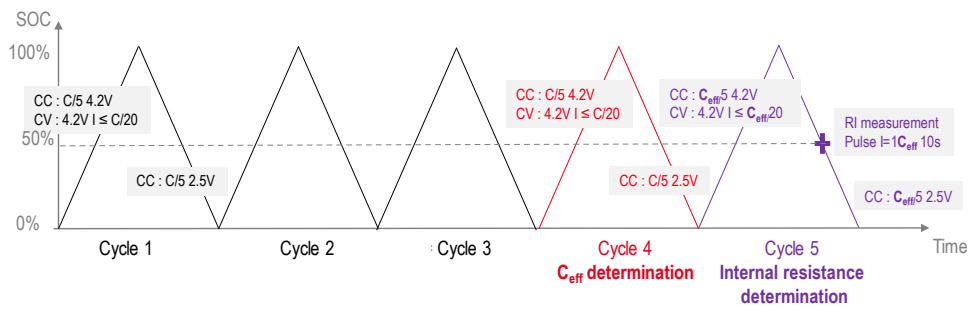


Figure 60. Schematic diagram of the capacity and internal resistance measurement protocol

Table 7. Capacity and internal resistance measurement protocol

Cycle	Value	Type	Limit
0		rest	5 min
1-3	C/5	CC charge	4.2 V
	4.2 V	CV charge	$I < C/20$
		rest	30 min
	C/5	CC discharge	2.5 V
4		rest	30 min
	C/5	CC charge	4.2 V
	4.2 V	CV charge	$I < C/20$
		rest	30 min
5	C/5	CC discharge	2.5 V → Effective capacity $C_{eff}$
		rest	30 min
	$C_{eff}/5$	CC charge	4.2 V
	4.2 V	CV charge	$I < C_{eff}/20$
		rest	1 h
	$C_{eff}/5$	CC discharge	2h30 → SOC 50%
		rest	30 s
	$C_{eff}$	CC discharge	10s → Internal resistance calculation
6 (if storage after)	$C_{eff}/5$	CC discharge	2.5V
		rest	30 min
	$C_{eff}/5$	CC charge	1h30 SOC 30%

Note: The voltage limit in discharge will be 3.0V for Li-FUN cell.

### • C-rate test

The C-rate tests are given in Figure 61 and Table 8 for discharge and in Figure 62 and Table 9 for charge. The test will be performed at 3 different temperatures: 25°C, 45°C and at -10°C. The value of the low temperature was chosen according to the test results performed on instrumented pouch cells with LFP reference electrode at -10°C.

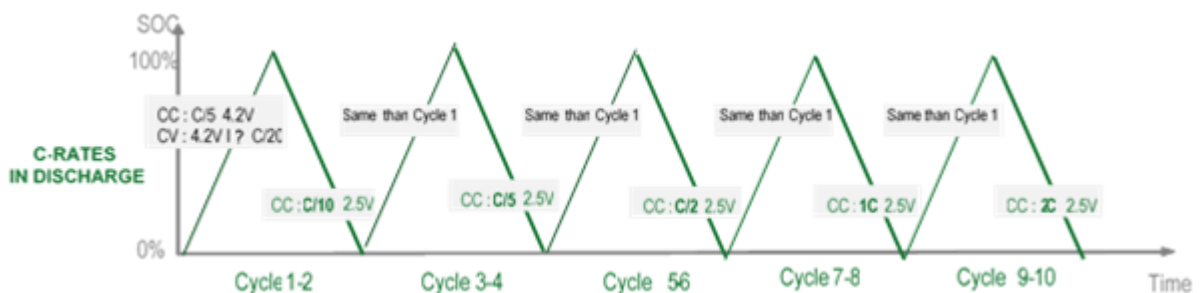


Figure 61. Schematic diagram of the C-rate test in discharge

Table 8. C-rate test in discharge

Cycle	Value	Type	Limit
0		rest	5 min
1-2	C/5	CC charge	4.2 V
	4.2 V	CV charge	$I < C/20$
		rest	240 min
	<b>C/10</b>	<b>CC discharge</b>	<b>2.5 V</b>
		rest	240 min
3-4	C/5	CC charge	4.2 V
	4.2 V	CV charge	$I < C/20$
		rest	240 min
	<b>C/5</b>	<b>CC discharge</b>	<b>2.5 V</b>
		rest	240 min
5-6	C/5	CC charge	4.2 V
	4.2 V	CV charge	$I < C/20$
		rest	240 min
	<b>C/2</b>	<b>CC discharge</b>	<b>2.5 V</b>
		rest	240 min
7-8	C/5	CC charge	4.2 V
	4.2 V	CV charge	$I < C/20$
		rest	240 min
	<b>1C</b>	<b>CC discharge</b>	<b>2.5 V</b>
		rest	240 min
9-10	C/5	CC charge	4.2 V
	4.2 V	CV charge	$I < C/20$
		rest	240 min
	<b>2C</b>	<b>CC discharge</b>	<b>2.5 V</b>
		rest	240 min

Note: The voltage limit in discharge will be 3.0V for Li-FUN cell.

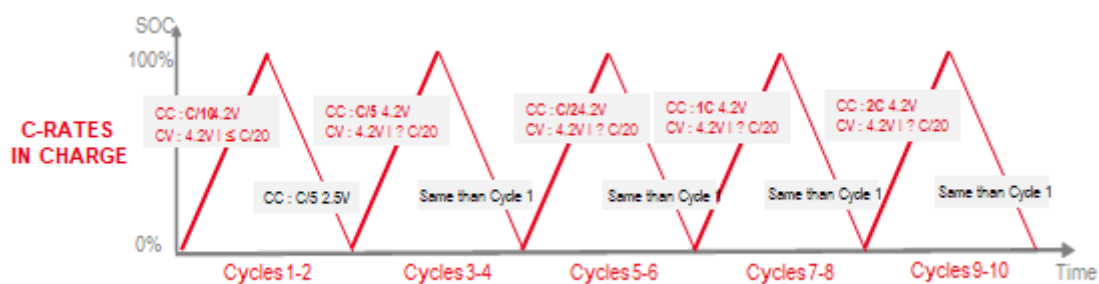


Figure 62. Schematic diagram of the C-rate test in charge

For each current rate, 2 cycles will be performed in order to verify if the thermal profile changes between the first to the second cycle. Note that the rest of 240 min between the charge and discharge step is required allowing the cell temperature to do back at the regulated temperature and thus to control the good response of the temperature sensor.



Table 9. C-rate test in charge

Cycle	Value	Type	Limit
0		rest	10 s
1-2	<b>C/10</b>	<b>CC charge</b>	<b>4.2 V</b>
	4.2 V	CV charge	$I < C/20$
		rest	240 min
	C/5	CC discharge	2.5 V
		rest	240 min
3-4	<b>C/5</b>	<b>CC charge</b>	<b>4.2 V</b>
	4.2 V	CV charge	$I < C/20$
		rest	240 min
	C/5	CC discharge	2.5 V
		rest	240 min
5-6	<b>C/2</b>	<b>CC charge</b>	<b>4.2 V</b>
	4.2 V	CV charge	$I < C/20$
		rest	240 min
	C/5	CC discharge	2.5 V
		rest	240 min
7-8	<b>1C</b>	<b>CC charge</b>	<b>4.2 V</b>
	4.2 V	CV charge	$I < C/20$
		rest	240 min
	C/5	CC discharge	2.5 V
		rest	240 min
9-10	<b>2C</b>	<b>CC charge</b>	<b>4.2 V</b>
	4.2 V	CV charge	$I < C/20$
		rest	240 min
	C/5	CC discharge	2.5 V
		rest	240 min
5 (if storage after)	C/5	CC charge	1h30 SOC 30%

Note: The voltage limit in discharge will be 3.0V for Li-FUN cell.

- **Fast ageing protocol**

CNRS has proposed to qualify some sensors a specific test described in Table 10. It consists of evaluating the sensor response during overcharging at 4.4 V for 24 h and at 55°C. These conditions allow to produce heat, gas and lithium-plating, that will be identify respectively by thermal fiber, gas sensor and reference electrode.

Table 10. Fast ageing protocol

Lab		Cycle	Value	Type	Limit	
CNRS	25°C	1-5	1C	CC charge	4.2 V	
				Rest	240 min	
			1C	CC discharge	3 V	
				Rest	240 min	
	25°C	+ Pulse 1C and 1.5C for FBG/OF thermal model calibration				
	55°C	6-16	1C	CC charge	4.4 V	
			4.4 V	CV charge	t=24h	
				rest	240 min	
			1C	CC discharge	3 V	
				rest	240 min	
	25°C	17	+ GITT at 1C for OF/FBG entropy calculation			
	25°C	18-22	1C	CC charge	4.2 V	
				Rest	240 min	
			1C	CC discharge	3 V	
				Rest	240 min	

- **Cycling protocol**

CEA has proposed to develop a cycling protocol (Figure 63) in charge and according to a discharge protocol based on the World harmonized light vehicles test procedure (WLTP)<sup>13</sup>. This discharge profile is representative of a worldwide statistic study realized on real driving profiles. The methodology applied to calculate the WLTP cycle for the two formats of cells is presented schematically in the Figure 64. It consists of converting the WLTP cycle corresponding to the ZOE electric vehicle for which the characteristics of the cell present in the battery pack are known in power per surface area of the positive electrode. The WLTP cycle can be thus calculated for the LiFUN cell and the CEA lab standard format for which the positive electrode surfaces are also known. Note that CEA has proceeded to the dismantling of a LiFUN cell to measure the electrode dimensions.

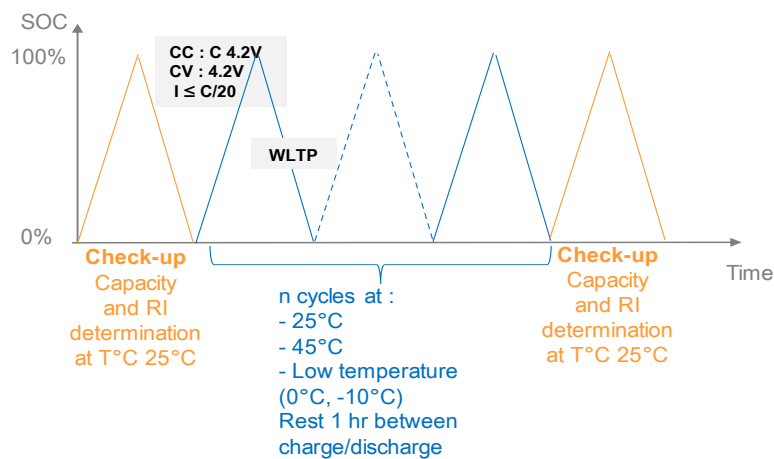


Figure 63. Schematic diagram of the cycling protocol

<sup>13</sup> Addendum 15: United Nations Global Technical Regulation No. 15. United Nations; 2019. <https://unece.org/transport/documents/2021/01/standards/addendum-15-united-nations-global-technical-regulation-no-15-spreadsheet> <http://www.unece.org/fileadmin/DAM/trans/doc/2012/wp29grpe/WLTP-DHC-12-07e.xls>

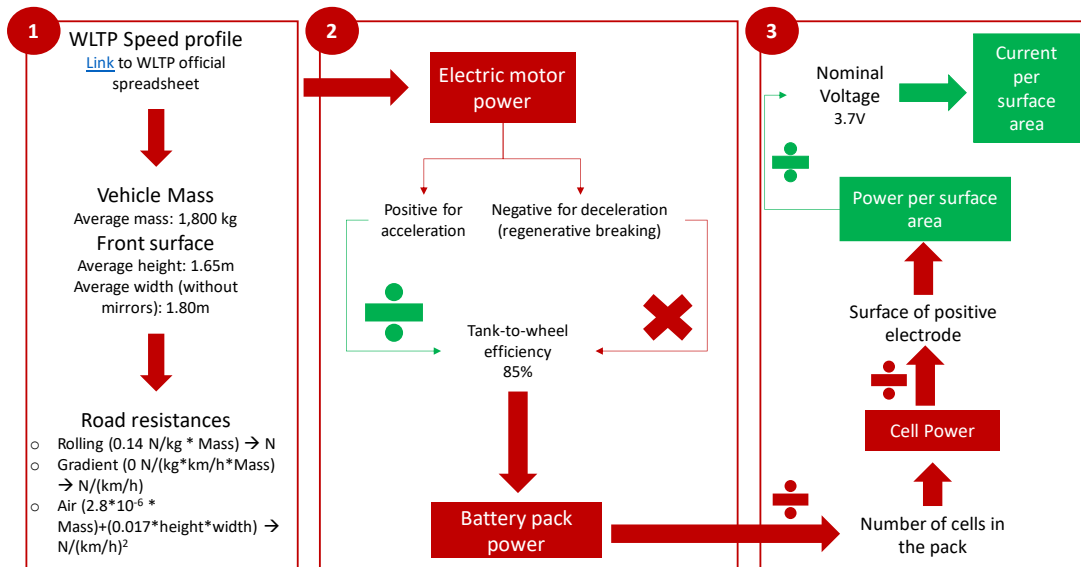


Figure 64. Illustration of the WLTP Power calculation procedure

The protocols for Li-FUN and mono cells prepared with VARTA electrodes are reported in the Figure 65 and Figure 66.

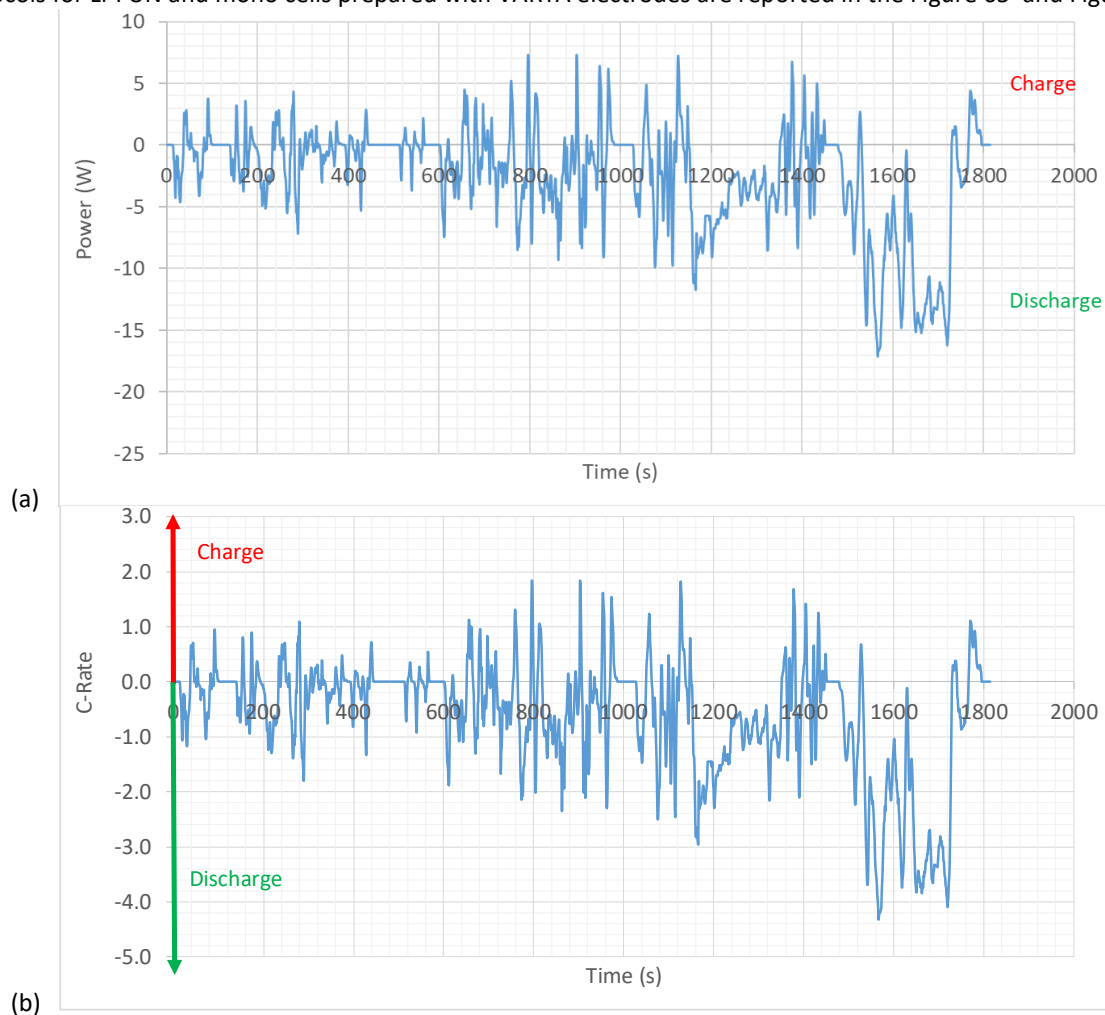


Figure 65. (a) WLTP protocol for Li-FUN cell in power. The corresponding current rates are given in (b).

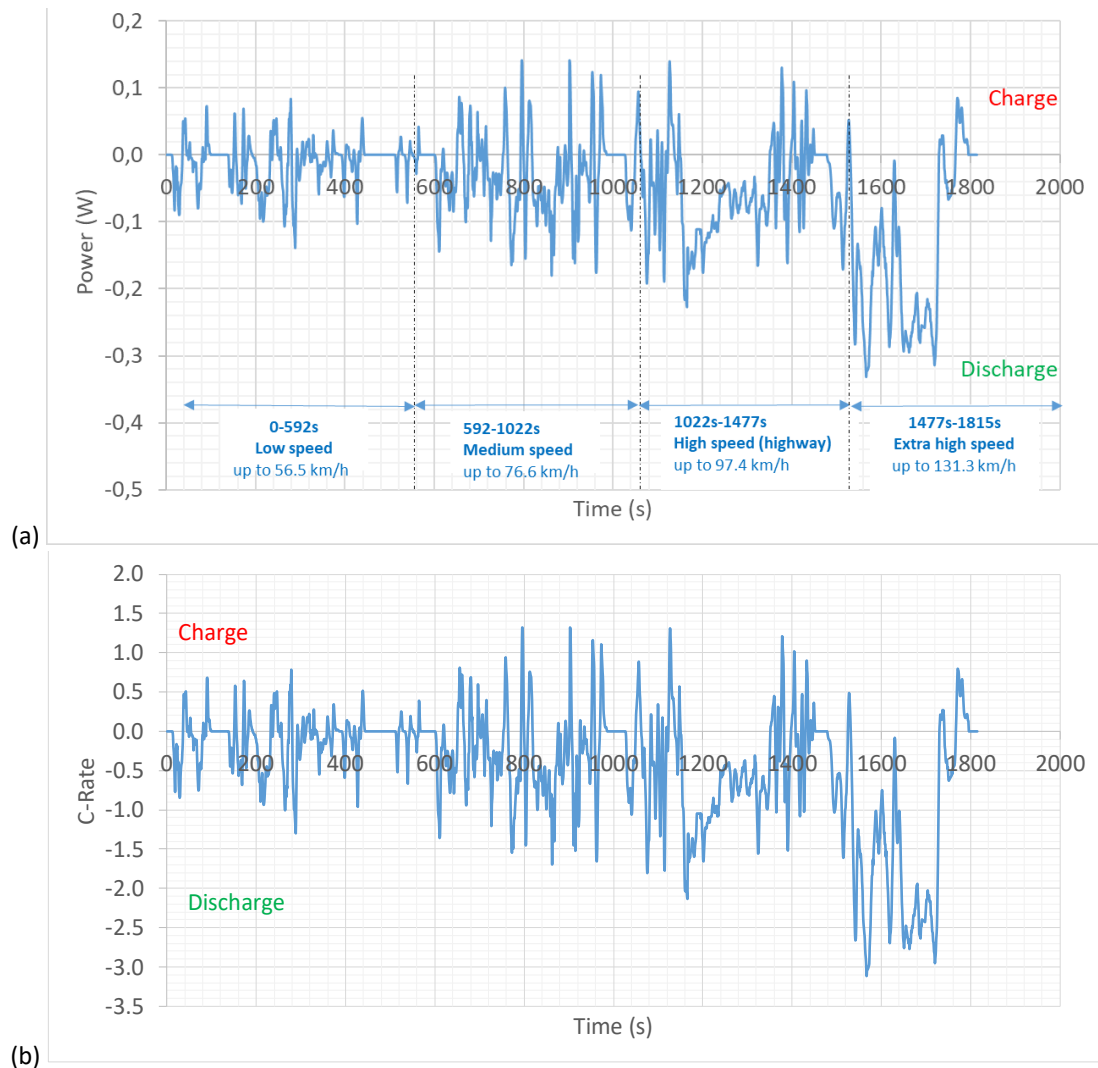
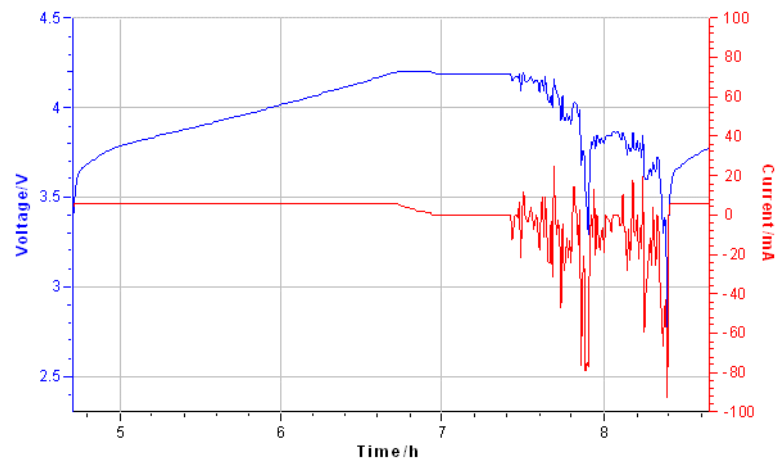


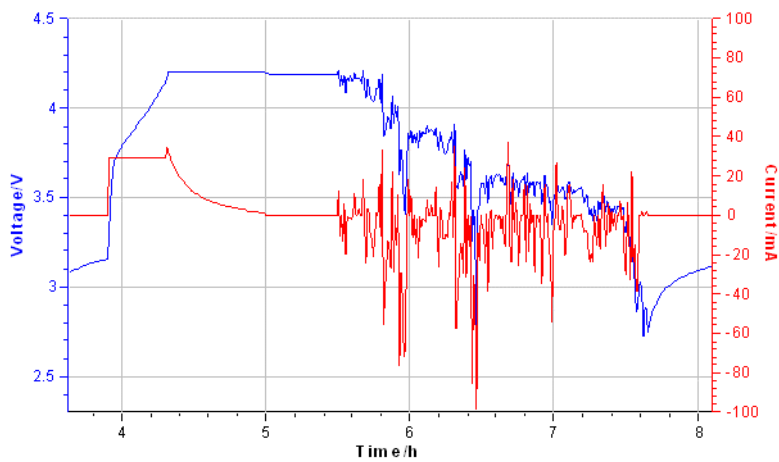
Figure 66. (a) WLTP protocol for mono cells prepared with VARTA electrodes in power. The corresponding current rates are given in (b).

We proposed to apply successive WLTP cycles in the aim to cycle the cell on a deep range of state of charge. Indeed, we have observed that if we launch two WLTP cycles (profile 1), the limit in low voltage (2.5V) is reach during the second cycle when the cell is submitted to the highest power peaks in discharge. The state of charge of the cell is only of 58.7%. By looping x full WLTP cycle up to 2.6V, x Medium speed WLTP cycle up to 2.5V and x Low speed WLTP up to 2.5V (Profile 2), it is possible to decrease greater the state of charge up to 35.2% allowing to accelerate the cell aging.





(a) Profile 1



(b) Profile 2

Figure 67. WLTP protocols : Profile 1 (2 full WLTP), Profile 2 (loop : x full WLTP cycle up to 2.6V, x Medium speed WLTP cycle up to 2.5V and x Low speed WLTP up to 2.5V (Profile 2)).

Table 11. State of charge reached after profile 1 and profile 2

Nominal capacity at C/5 (mAh)		28.8
Capacity at C/0.8 (= mean current = 37mA during WLTP cycle)		16.179
<b>Profile 1</b>		
Charge capacity 1C (mAh)		11.907
WLTP cycle - Profile 1 (mAh)	Charge capacity (mAh)	2.348
	Discharge capacity (mAh)	14.234
Discharge capacity WLTP (mAh)		11.886
SOC reached considering the capacity at C/0.8		26.5%
SOC reached considering the capacity at C/5		58.7%
<b>Profile 2</b>		
Charge capacity 1C (mAh)		18.569
WLTP cycle - Profile 2 (mAh)	Charge capacity (mAh)	4.319
	Discharge capacity (mAh)	22.977
Discharge capacity WLTP (mAh)		18.658
SOC reached considering the capacity at C/0.8		-15.3%
SOC reached considering the capacity at C/5		35.2%

- **Standard for material and battery testing**

### LiFUN cell

In order to allow the comparison of results between the different groups and sensors, integration material chemistry and electrolytes are common across the different WP. The material defined in this project is  $\text{LiNi}_{0.6}\text{Mn}_{0.2}\text{Co}_{0.2}\text{O}_2$  (denoted NMC622 in the rest of this document), as a positive electrode, in combination with graphite, as negative electrode. To ensure reproducibility of results, electrode from only two suppliers will be used (Varta and LiFUN). The electrodes supplied by Varta are assembled at CEA to form a single-layer stacked pouch cell with a capacity of 29.6 mAh. LiFUN provides wounded pouch cell with a capacity of 1000 mAh. The cells geometry is highlighted in Figure 68. The electrolyte used throughout the project is a commercial mixture of Ethylene Carbonate (EC) and Ethyl Methyl Carbonate (EMC) in a weight ratio of 3:7 with 1M  $\text{LiPF}_6$  conductive lithium salt and 2% of vinyl carbonate (VC) additive (denoted LP57+2% VC in the rest of this document) provided by Sol-Rite (Mitsubishi).

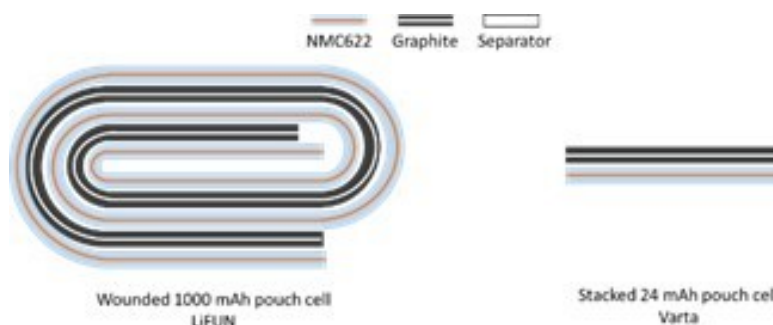


Figure 68 : Cells format used in INSTABAT project

Following the recommendations of the equipment supplier and the need of the partners for characterization and modelling, a list of protocols has been established within INSTABAT. Formation protocol is performed at 25°C following Varta's recommendation. After the formation cycles, a degassing step will be performed for LiFUN cells. This step is essential to achieve the maximum capacity of LiFUN cells but is not necessary for Varta cell due to their low mass of material producing a small amount of gas. Then capacity and internal resistance measurement protocol will be used by the modelling team to calibrate their model and a pulse test protocol will be used by CNRS to calibrate the thermal parameters such as the internal resistance ( $R_{in}$ ), the external resistance ( $R_{out}$ ) and the thermal capacity ( $c_p$ ) to be able to solve the thermal model and to calculate heat and enthalpy. Then, C-rate test in charge and discharge will be performed at 25°C and 55°C. For cell ageing, CEA has proposed a cycling protocol with a 2C (or 1C) charge and a discharge protocol based on the worldwide-harmonized test procedures for light vehicles (WLTP). This discharge profile is representative of a worldwide statistical study performed on real driving profiles. However, by choosing an excellent electrode material and electrolyte, the degradation of materials can take years. Consequently, a fast ageing protocol inspired by the work of Dahn et al. was proposed by CNRS<sup>14</sup>. By overcharging the cell and maintaining the voltage, heat generation, gas formation, and lithium plating are expected, which should be trackable by sensors. Detailed of the electrochemical protocol is provided in deliverable D3.1.

### VARTA cell

The preparation of monolayer and multilayer cells was made by CEA with raw materials provided by VARTA. The description of the cell design and the fabrication of the cell was detailed in the deliverable D3.1 chapter 2. The mono cell design is based on the CEA's standard cell format and is given in Figure 69 together with the implementation scheme of the LFP RE.

<sup>14</sup> J. H. Cheng *et al* 2020 *J. Electrochem. Soc.* **167** 130529, DOI: 10.1149/1945-7111/abbb0a

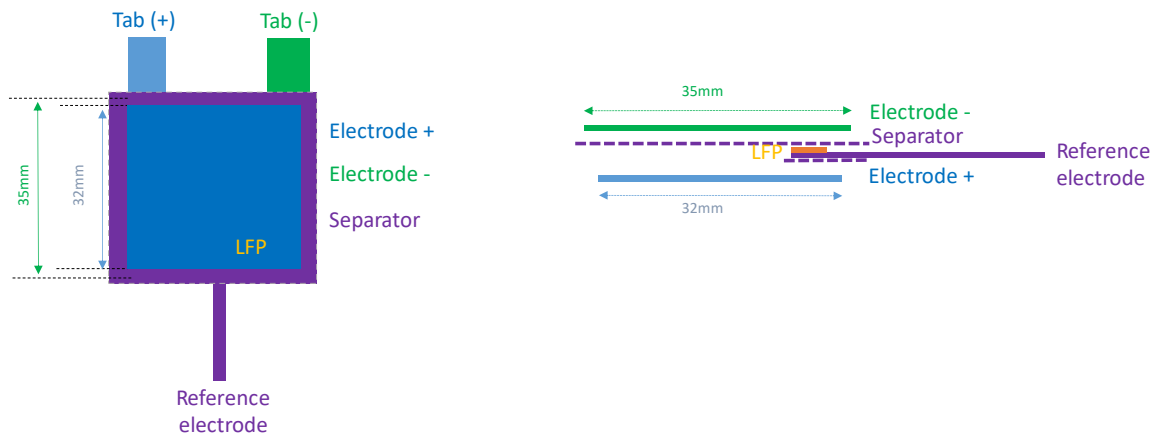


Figure 69 : Schematic illustration of the CEA's standard pouch cell design and instrumentation of the RE.

Its real electrochemical characteristics are as follow:

- Discharge capacity at C/5 (25°C) =  $28.3 \pm 0.6$  mAh
- Internal resistance (25°C) =  $1.4 \pm 0.4$   $\Omega$

For multilayer samples (see Figure 70), cells assembled at CEA with VARTA's electrodes are a standard stacked design pouch cell with Z-folded separator, allowing easy access for sensor insertion. Note that extra pouch at the bottom is needed to accommodate sensor connections. The separator used is a standard trilayer PP/PE/PP Celgard 2325 separator (25  $\mu$ m thick, 54 mm width). The formation capacity (at C/10) is 1.0 Ah, with 7 double sided positive electrodes (NMC622) and 8 double sided negative electrodes (Gr). Each positive electrode format is 50x50mm and the negative electrode is 52x52mm. The cells average thickness is 2.7 mm before formation. Cells are filled with the reference electrolyte (LP57+2% VC) and formed at C/10 [2.5-4.2V] (CC-CV and C/20 for current limit condition) at 25°C, followed by 3 cycles at C/2 [2.8-4.2V] (CC-CV and C/20 for current limit condition). 6 cells were assembled to test their performances.

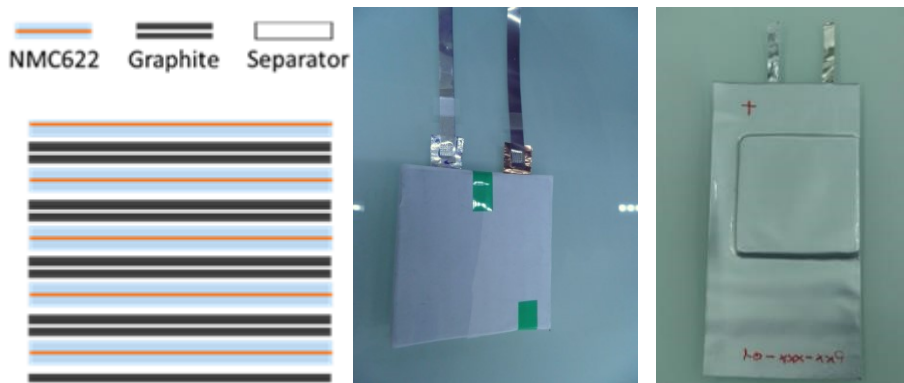


Figure 70 : Multistacked 1000 mAh pouch cell VARTA (schematic view and photo of sample)

The implementation of the OF/Lum sensor in VARTA multilayer pouch cell is presented in Figure 71.

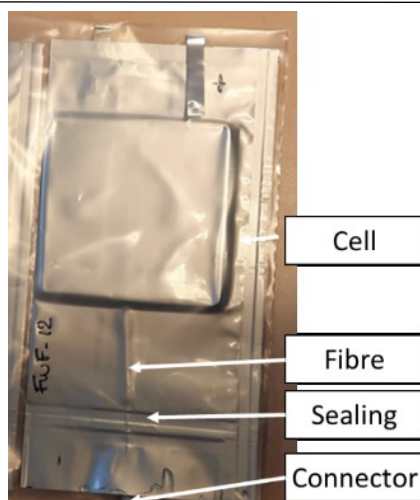


Figure 71 : Photography of one instrumented pouch cell with OF/LumT sensor

- **Test performed on LiFUN cells using optical fibers with standard FBG sensor (OF-FBG)**

## C-rates characterisation

LiFUN pristine cells were tested according to the protocol defined between the partners. In addition, C-rate tests were performed at 25°C and 55°C in order to observe the degradation related to cycling in extreme conditions. As shown in Figure 72, the performances of the cells are impacted by both current density and temperature. The extreme condition being particularly detrimental during discharge.

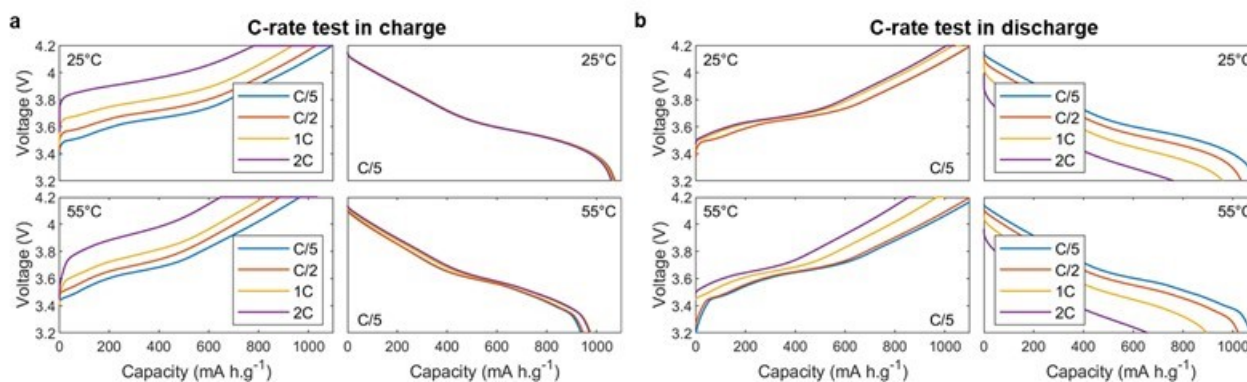


Figure 72 : C-rate test in charge (a) and discharge (b) at 25°C (top) and 55°C (bottom) of LiFUN cells.

## Overview of FBG sensor tests in LiFUN cells

Standard OF-FBG sensors have been bought from SAMYON by CNRS in order to be implemented into pouch cell. To do so, firstly, the OF-FBG sensor was protected with a stainless sheath to avoid contribution from strain and curvature. Then the optical fiber with FBG sensor was attached to the pouch bag with a droplet of epoxy cured 24 hours. Inside glovebox, the sensor is placed in the middle of the jelly roll of LiFUN's cell previously dried at 55°C under vacuum overnight. Two sides of the bag are then sealed with a sealing machine at 180°C and the bag is filled with electrolyte and left for 12 hours. Finally, the bag is closed under vacuum. The pouch cell is connected inside an isothermal cabinet and two other fibers with sensors (surface and ambient) were placed on top of the pouch and on top of the cabinet Figure 73.c. The instrumented cell has been then cycled in the same condition as the pristine cell. As observed in Figure 73.b and c, during the formation cycles and C-rate tests, the pristine and instrumented cells show exactly the same behaviour. Therefore, we can be confident that the optical fiber with FBG sensor does not affect the electrochemical performance of the cell.

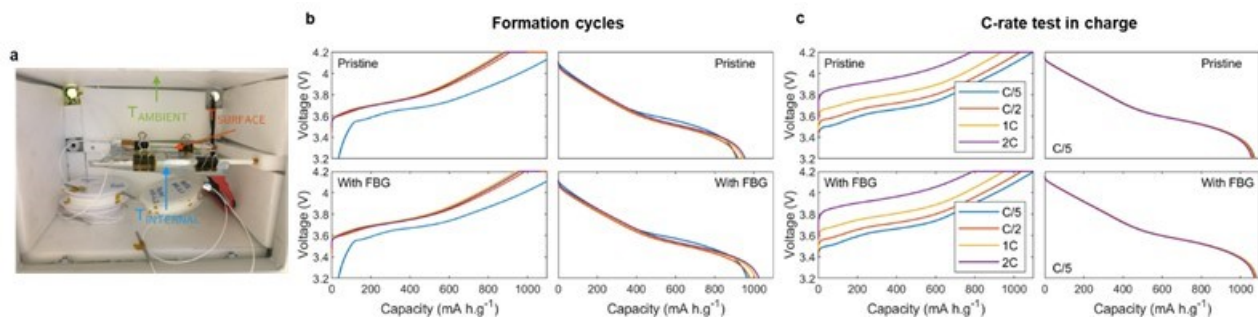


Figure 73 : (a) Picture of the isothermal cabinet instrumented with the pouch cell and optical fiber with the FBG sensor. The cabinet is placed in an oven to avoid any external temperature variation. Unless specified, the temperature of the experiments is maintained at 25°C. Formation cycles (b) and C-rate test in charge (b) at 25°C for pristine LiFUN cell (top) and LiFUN cell instrumented with optical fiber with the FBG sensor.

- Test performed on VARTA multistack cells using OF/LumT sensors

### SOH estimation during ageing test using OF/LumT sensor

Two sets of cells were prepared and tested with WLTP-3 cycling protocol by the CEA: standard cells (STD) and cells equipped with optical fiber for thermo-luminescence measurements (OF/LumT). Three sets of STD and OF/lumT cells were subjected to three different temperatures: -10°C, 25°C, and 45°C during the WLTP-3 cycle tests. Cells with OF/LumT sensor was referenced FOTL in the graphs.

A total of 11 cells were tested, grouped as follows:

- Two standard cells (STD01 and STD05) that cycled at 25°C
- Two standard cells (STD02 and STD06) that cycled at -10°C
- Two standard cells (STD03 and STD04) that cycled at 45°C
- Two instrumented cells (FOTL02 and FOTL03) that cycled at 25°C
- One instrumented cell (FOTL04) that cycled at -10°C
- One instrumented cell (FOTL05) that cycled at 45°C

State of health (SOH) and cell capacity measurements, were consistently conducted at 25°C. Of course, a waiting period of several hours was allowed for cells that were not undergoing cycling at this temperature to stabilize. More precisely, SOH and capacity measurements were derived through data analysis using a specific procedure referred to as the "Check-up" (CU). The CU procedure consists in four sections: two C/5 full cycles, one C/10 full cycle and a last cycle that can be decomposed in three parts, which are a C/5 charge, a 4C discharge and a C/5 discharge until the lowest admitted voltage level. Relying on this CU profile, it was stated that:

- The **cell capacity** has to be measured as the **discharge capacity** of the third cycle (the one at **C/10 C-rate**);
- The **internal heating** has to be measured during the **4C discharge** with thermocouple on the cell surface for both type of cell and OF/LumT sensor inside the cell for instrumented cell.
- Optionally, the **C/5 discharge** can be used to measure the cell capacity, but care must be taken not to compare it with the C/10 discharge, as they naturally give different results.

Then, the SOH of a cell is simply calculated as a ratio of the current capacity over the capacity measured at the Beginning of Life (B.O.L.) of the cell, expressed in percentage.

As demonstrated in Figure 74 and Figure 75, no clear impact of the sensor implementation was recorded for the three temperatures investigated. Cell cycled at 10°C died after a few cycles and interestingly, it is demonstrated that the OF-Lum can be operational in the cell even at high temperature without damaging the cell performances.

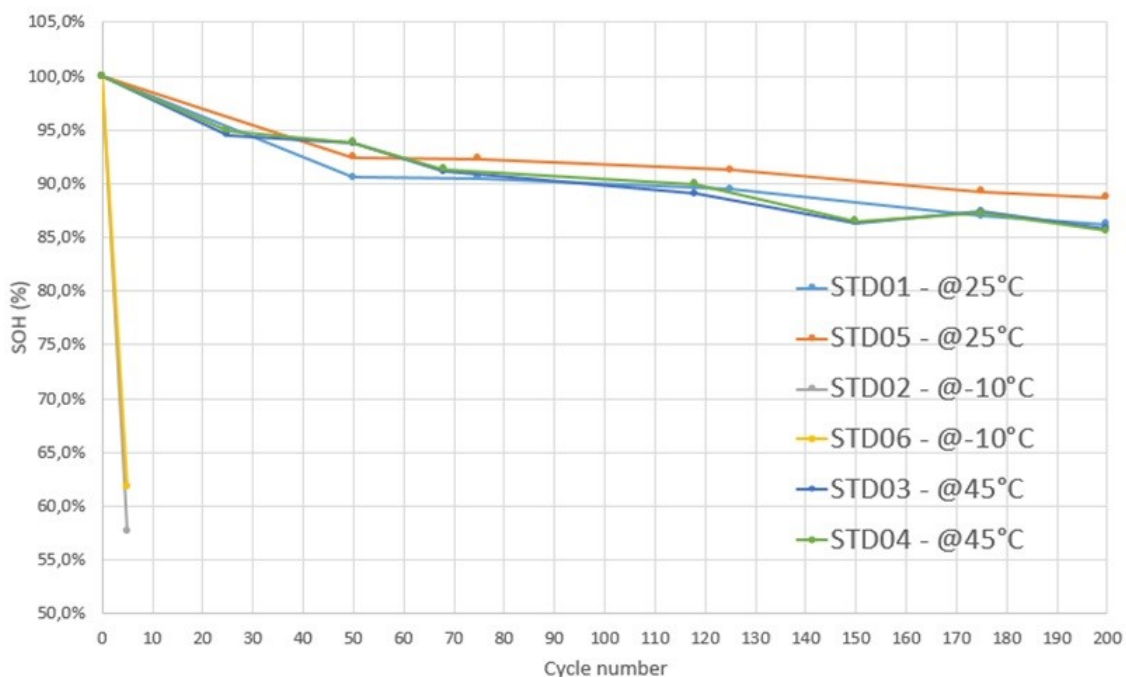


Figure 74 : Graph summarizing the SOH evolution of the tested STD cells over 200 cycles.

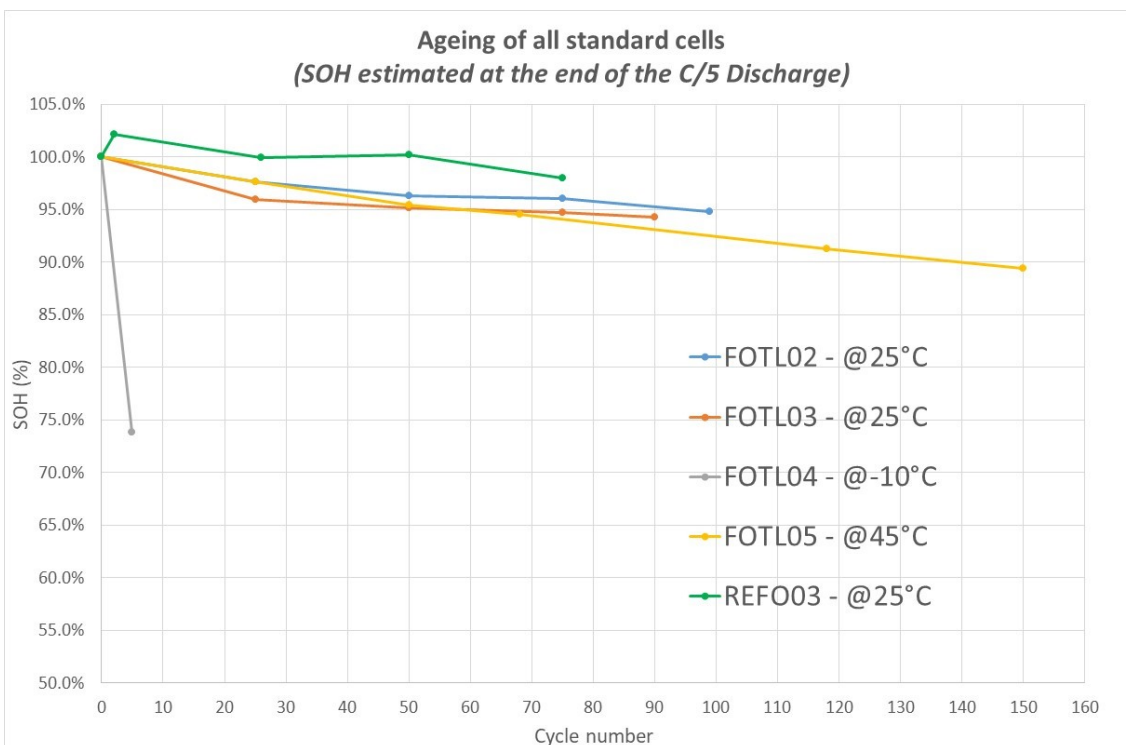


Figure 75 : Graph summarizing the SOH evolution of the tested OF/LumT (instrumented) as far as the cycles went.

A summary of the data collected can be found in Table 12 below.



Table 12 : Detailed values of standard and instrumented multistack VARTA cells, which underwent the ageing protocol.

Cell name	WLTP-3 temperature	BOL Capacity (Ah)	Performed cycles	Reached Capacity (Ah)	Reached SOH	Post-mortem analysis
<b>STD01</b>	25°C	0.984	200	0.848	86,21%	x
<b>STD02</b>	-10°C	0.979	5	0.563	57,57%	x
<b>STD03</b>	45°C	0.977	200	0.839	85,81%	x
<b>STD04</b>	45°C	0.983	200	0.842	85,60%	
<b>STD05</b>	25°C	0.969	200	0.860	88,72%	
<b>STD06</b>	-10°C	0.980	5	0.605	61,75%	
<b>FOTL02</b>	25°C	0.954	99	0.905	94,85%	x
<b>FOTL03</b>	25°C	0.950	75	0.900	94,74%	x
<b>FOTL04</b>	-10°C	0.946	5	0.699	73,80%	
<b>FOTL05</b>	45°C	0.940	150	0.841	89,46%	
<b>REFO03</b>	25°C	0.912	75*	0.893	98,0%	

## • Tests performed on VARTA monolayer cell using RE sensor

### Methodology

The reference electrode sensor is able to detect operando the excursion of the negative and positive electrodes in some critical ranges of potential where some degradation mechanisms are favored.

To validate this ability, an experimental design has been launched. It consists of cycling instrumented pouch cells at high and low temperature to exacerbate some degradation mechanisms that will be identified by using:



- A diagnosis tool developed in the lab.
- A post-mortem analysis consisting of (i) a visual inspection of the electrodes, (ii) Scanning Electronic Microscopy (SEM) observations and (ii) capacity measurement of the electrodes in half-coin cell.

As a reminder, Table 13 associates some degradation phenomena with the range of potential favoring them. For comparison, 8 instrumented cells and 8 non-instrumented cells were cycled at 45°C, 25°C, 0°C and -10°C as specified in Table 14. To evaluate the reference electrode response, 8 instrumented cells and 8 non-instrumented cells were cycled with WLTP-3 cycling protocol at 45°C, 25°C, 0°C and -10°C as specified in Table 14.

Table 13 : Range of potential favoring some degradation phenomena.

	Degradation phenomenon	Potential domain of appearance	Conditions of cell operation favorable to their appearance	Effect
<b>Positive electrode</b>	Dissolution of transition cations	> 4.35V vs Li	High temperature, high current	LAM positive and negative
	Crystalline disorder	> 4.35V vs Li	High temperature	LAM positive
<b>Negative electrode</b>	Lithium deposition	< 0 V vs Li	Low temperature, high current	LLI and LAM negative (isolated particle of the bulk)
	SEI growth	High state of lithiation (< 50mV vs Li)	high temperature	LLI

Table 14 : Experimental design

Cell format		Cycling test
Name	Picture	Disch. WLTP/ Charg. = 1C
Mono cell Nominal capacity (29.6 mAh)	STD cell 	2 cells / 45°C 2 cells / 25°C 2 cells / 0°C 2 cells / -10°C
	REF cell 	2 cells / 45°C 2 cells / 25°C 2 cells / 0°C 2 cells / -10°C

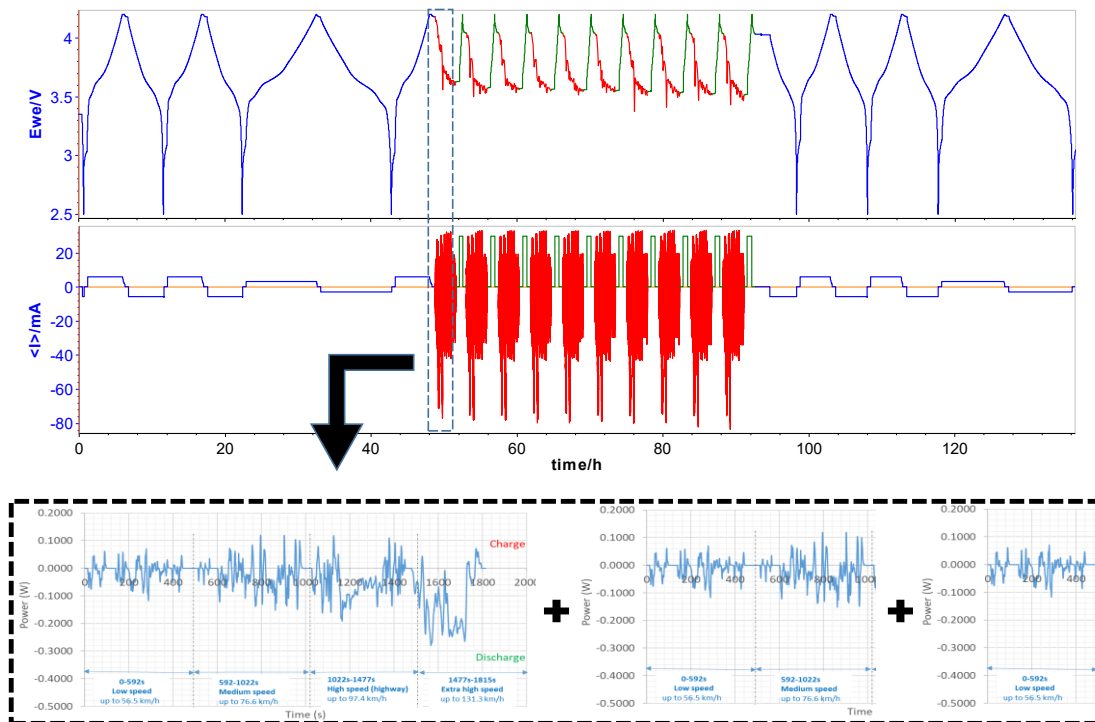


Figure 76 : Protocol of cycling

The sequence of cycling is reminded in Figure 76. The discharge is a modified WLTP profile that consists of chaining n full WLTP cycles up to 2.6V + n Low + Medium speed WLTP cycles up to 2.55V + n Low speed WLTP cycles up to 2.5V. The charge is a CC-CV charge at 1C up to 4.2V and C/20. A rest of 30 min is applied between every charge and discharge. Every 10 cycles, a checkup is performed (2 cycles at C/5 and 1 cycle at C/10) to measure the capacity of the cell and evaluate its SOH.

## Cycling performance

The cycling performance of the instrumented (REF) and non-instrumented (STD) is reported in Figure 77. It is noteworthy that the discrepancy between the non-instrumented and instrumented cells is greater at room and high temperatures which could be due to the presence of the RE that can create side effects on the electrode surface surrounded it, as it has been confirmed by visual inspection of the electrodes.

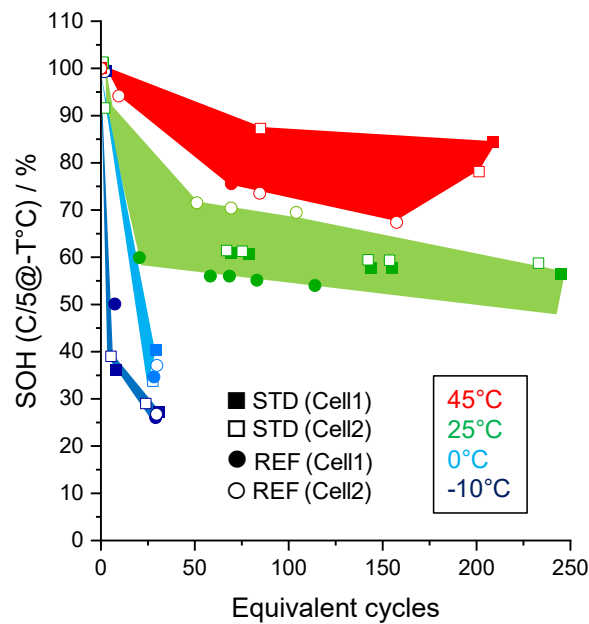


Figure 77 : Cycling performance

## Correlation with the electrochemical signals at electrode scale

In the figures below, the charging CC-CV profile at 1C of the negative electrode has been plotted in function of the capacity and the time.

At 45°C (Figure 78), the potential of the negative electrode does not pass below 0 V vs Li. The evolution of the potential during the rest that starts when the potential shifts a few millivolts suddenly (around after 1.6h) shows a linear evolution without marking a shoulder linked to lithium stripping.

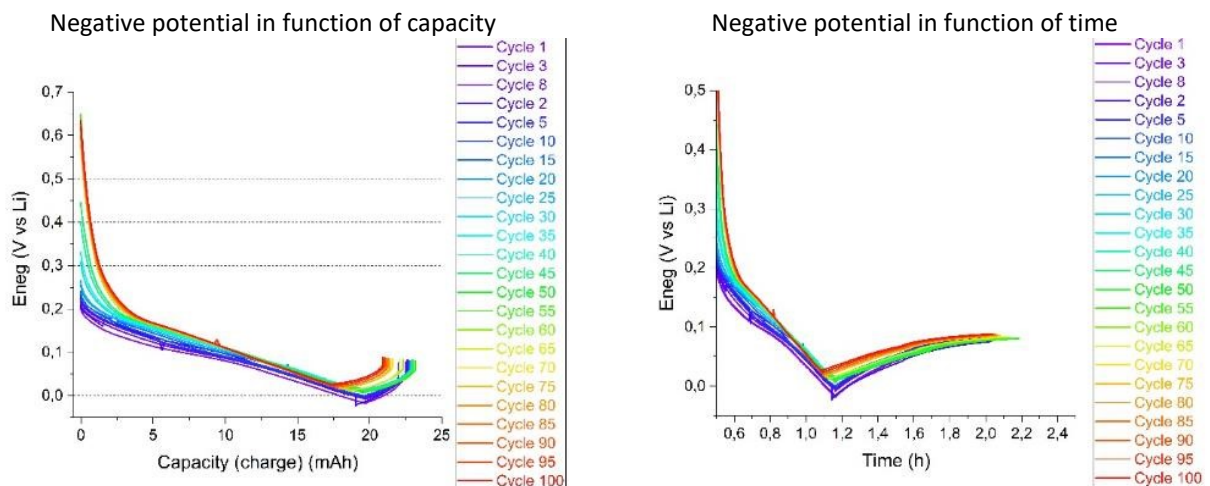


Figure 78 : Profile in CC-CV charge at 1C at 45°C of the negative electrode

At 25°C (Figure 79), the potential of the negative electrode does not pass also below 0 V vs Li. No shoulder is observable on the potential during the rest.

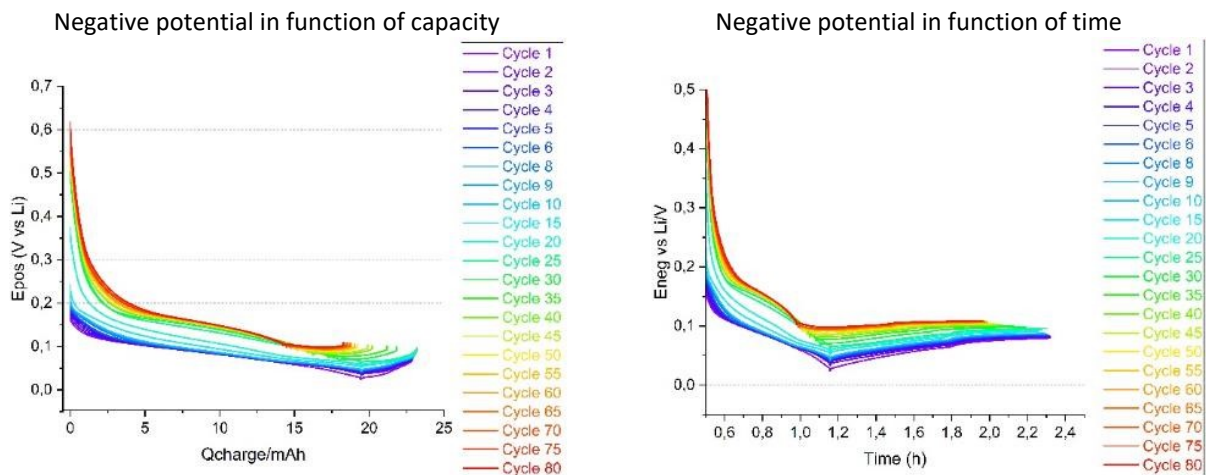


Figure 79 : Profile in charge at 1C at 25°C of the negative electrode

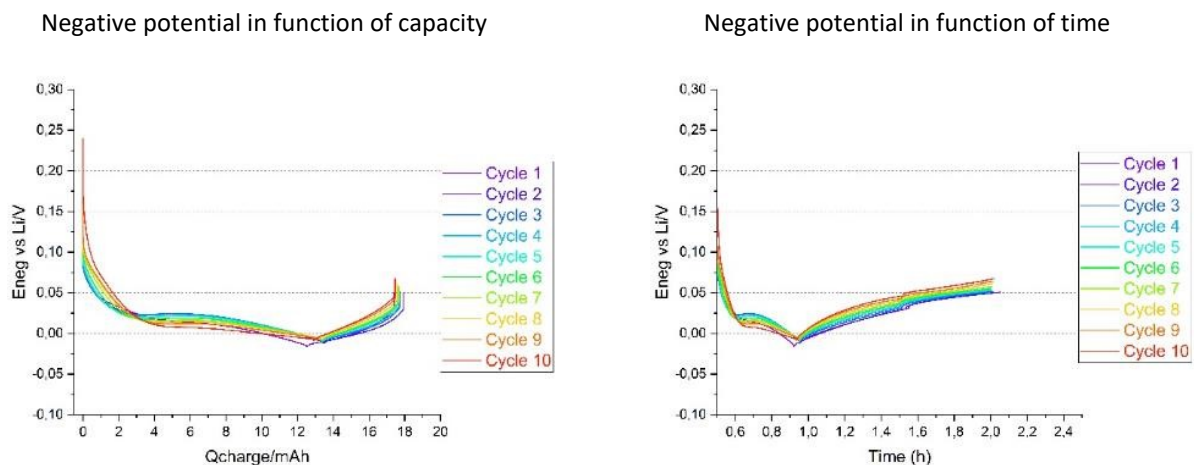
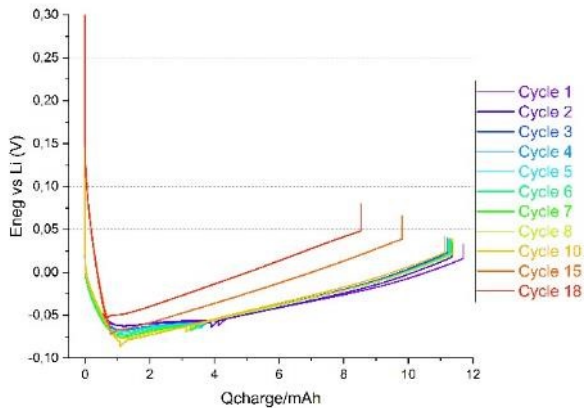


Figure 80 : Profile in charge at 1C at 0°C of the negative electrode

At 0°C (Figure 80), the potential of the negative electrode reaches 0 V vs Li with the establishment of a plateau around 0V vs Li. The evolution of the potential during the rest is normal.

The data recorded at -10°C are shown in Figure 81. At low temperature (0°C and -10°C), the potential of the negative electrode decreases below 0V with the establishment of a plateau that can be associated without a doubt to lithium deposition. At 25°C and 45°C (Figure 79 and Figure 78, respectively), the potential reaches 0V vs Li at the end of the charge process at the beginning of the cycling. As soon as the consumption of exchangeable lithium exceeds a certain value, the duration of the constant current charge is shortened and consequently the potential of the negative electrode no longer drops below 0V.

Negative potential in function of capacity



Negative potential in function of time

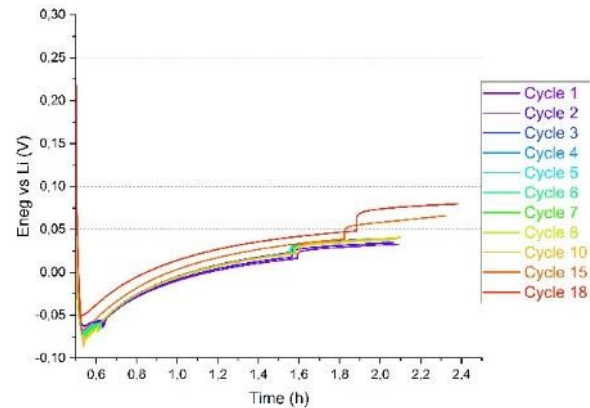


Figure 81 : Profile in charge at 1C at -10°C of the negative electrode

## TASK 3.2 IDENTIFICATION OF DEGRADATION MECHANISMS BY IN OPERANDO AND POST-MORTEM ANALYSIS

(Leader: CNRS; Participants: UAVR, CEA) (M6-M32)

- In operando measurements in LiFUN cell using standard FBG sensors (OF/FBG)

### SEI formation

Optical fibers with standard FBG sensor can be implemented inside pouch cell to measure temperature without affecting the electrochemistry. Moreover, by using three sensors positioning inside, at the surface and far from the pouch we are able to solve the thermal model and calculate the heat (Figure 82). The explanation of the thermal model and its resolution is described in Deliverable D3.2. The heat being directly connected to the amount of energy involve during the electrochemical reaction is very useful for comprehension of battery degradation.

Calorimetry measurement in pouch cell

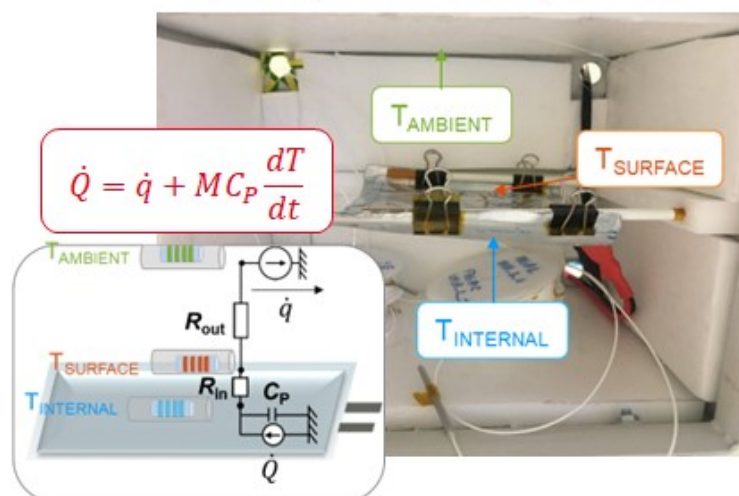


Figure 82: Test set up with the three FBGs and summary of the equivalent circuit to calculate the heat generated



To prove the ability of FBG sensors to give valuable information on pouch cells during formation, we decided to realize three different instrumented cells with three different electrolytes: (i) the one of the project the LP57+2%VC which is expected to be the most stable thanks to VC additive, (ii) LP57 to investigate the influence of the additive during the first charge and (iii) LiPF<sub>6</sub> EC/DMC (1/1 v/v) (called LP30) an electrolyte well known in the literature but expected to be less stable than LP57. As provided in Figure 83, the heat released during the first cycle is proportional to the electrolyte decomposition. LP30 is known to decompose into various carbonates and alkoxides. In the case of LP57, decomposition is reduced as well as heat. Finally, the VC additive must decompose first to avoid solvent reduction. In agreement with this pathway in Figure 83c, a small peak at the beginning of the charge and no further decay are observed.

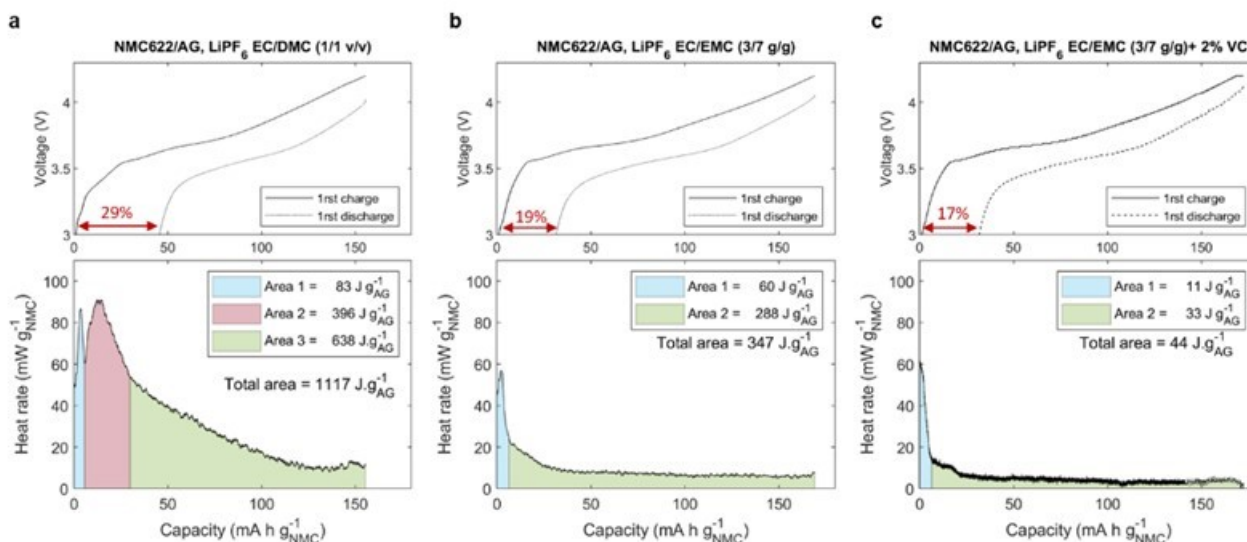


Figure 83 : 1st formation cycle of NMC622/AG pouch cell instrumented with FBG and heat generated during the first charge with LiPF<sub>6</sub> EC/DMC (a) LiPF<sub>6</sub> EC/EMC (b) and LiPF<sub>6</sub> EC/EMC+2%VC (c).

Furthermore, such technique is not only limited to electrolyte screening but can be apply to benchmark cells with exactly the same electrolyte, but different electrodes material as seen in Figure 84 , taken from 15 . Figure 84a show the voltage curve and the heat rate generation ( $Q'$ ) as a function of the capacity of the first and second charges at C/10. The electrolyte was classical LP30 (1M LiPF<sub>6</sub> in ethylene carbonate (EC)/dimethyl carbonate (DMC) (1/1, v/v)). As recommended by the manufacturer, the NMC622/AG and the NMC811/AG cells are cycled between 3 V and 4.2 V, while the NMC532/AG is tested between 3 V and 4.4 V. The NMC811/AG and NMC622/AG cells exhibit an irreversibility of 53 mAh g<sup>-1</sup> NMC (28%) and 47 mAh g<sup>-1</sup> NMC (30%), respectively, between the first charge and discharge. Compared to the other two, NMC532/AG only has an irreversible capacity of 38 mAh g<sup>-1</sup> NMC (22%). Similarly, a larger amount of heat is released during the first cycle for NMC622/AG and NMC811/AG than for NMC532/AG cells, which is likely due to SEI-related parasitic reactions. In agreement with this assumption, for all cells, the significant heat release is not observed during the second charge, indicating that the SEI is mostly formed during the first cycle as expected. Such approach is extremely useful as it is well-known that it is the formation cycle that govern the rest of the life of a cell.

To interpret further our data, we decided to check the contribution of each electrode to the irreversibility of the first cycle by assembling Li coin cells based on each positive and negative electrode that was cycled at C/10. For clarity, the electrodes extracted from the NMC622/AG cell are named NMC622 for the cathode and AG(622) for the anode, with the same referencing being applied to electrodes pertaining to NMC532/AG and NMC811/AG cells. Those data are presented in Figure 84b where it is showed that all the cathodes exhibit first similar cycle irreversibility, but higher polarization is observed between the first charge and discharge in the case of NMC622 and NMC811 compared to NMC532. As for the anodes, a significant difference was observed between the voltage profile of AG(523) and those of AG(811) and AG(622), most likely due to a lack of repeatability between the batches of AG used by the manufacturer in the cells specified as identical. The difference is particularly evident during the first discharge, where AG(811) and AG(622) exhibit around 45 mAh g<sup>-1</sup> AG of capacity above 0.2 V, while AG(532) exhibits only 18 mAh g<sup>-1</sup> AG.

<sup>15</sup> Gervillié-Mouravieff, C., Albero Blanquer, L., Alphen, C., Huang, J., & Tarascon, J.-M. "Unraveling SEI formation and cycling behavior of commercial Ni-rich NMC Li-ion pouch cells through operando optical characterization," J Power Sources (2023).



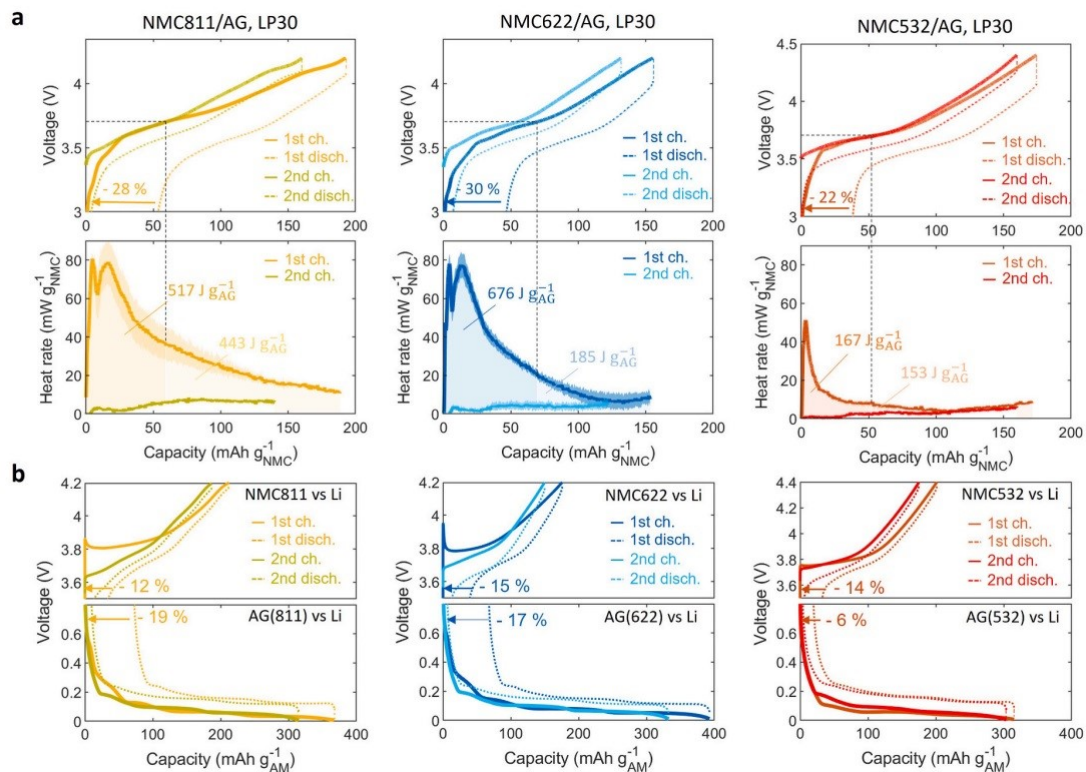


Figure 84: Heat release during the formation cycle. a) Voltage (top) as a function of the capacity of the 1st and 2nd charges and discharge of NMC811/AG, NMC622/AG, and NMC532/AG pouch cells at C/10. The average heat generation (bottom) calculated from three cells are given together with the corresponding error bars of the experiment (shadings) for the 1st and 2nd charges. b) Half cells cycling of the NMC and AG electrodes versus lithium at C/10.

### Identifying the SEI:

To corroborate the significant role of AG anode to the irreversible capacity and heat generation of the cell during the formation cycles, two dry cells have been disassembled and reassembled following the instructions and illustrations schematized in Figure 85.a and Figure 85.b. Since the negative electrode specifications provided by the manufacturer were identical for NMC622/AG and NMC532/AG cells, we deemed it reasonable to perform this exchange.

Figure 85.c shows that the first charge and discharge irreversibility for NMC622/AG(532) have been reduced to 33 mAh g<sup>-1</sup> NMC (25%) and the second charge almost completely overlaps with the first one. Additionally, the heat generation has been drastically reduced to one main peak at the beginning of the charge, alike what has been previously observed for the NMC532/AG cell. In the case of NMC532/AG(622), an irreversibility of 53 mAh g<sup>-1</sup> NMC (33%) is observed between the first charge and discharge, which is of the same magnitude as what has been previously observed for NMC622/AG (Figure 85.a). Those results confirm that the AG anode is the main cause of heat generation and first cycle irreversibility in lithium-ion cells.

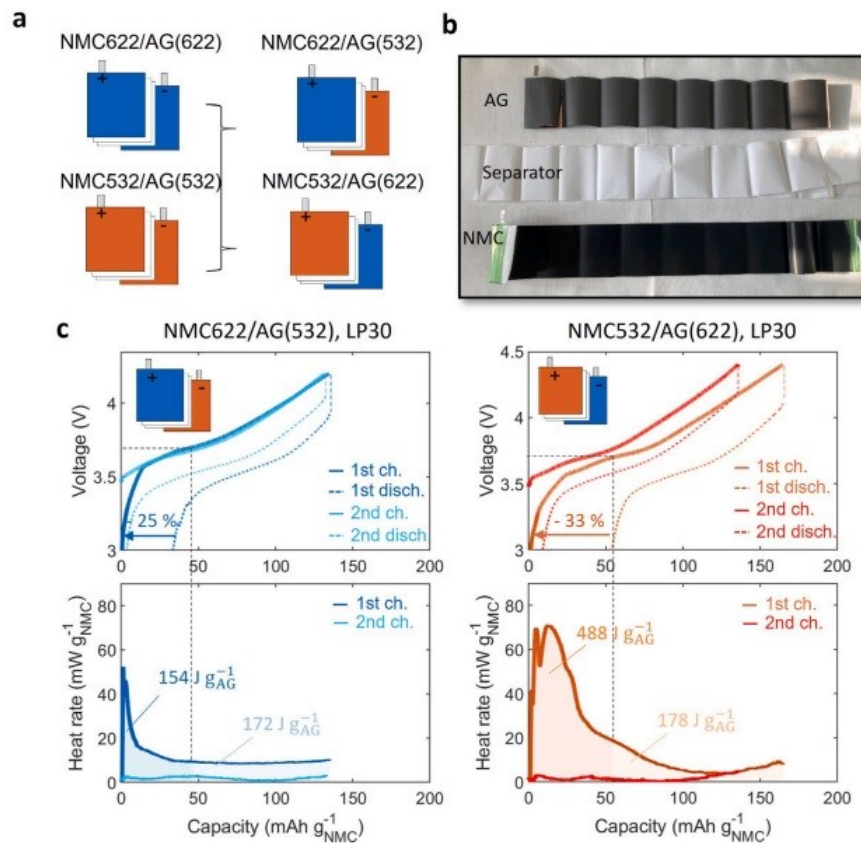


Figure 85: a) Schematic description of the negative electrode exchange between NMC622/AG and NMC532/AG cells. B) Picture of NMC622/AG cell fully opened. C) Voltage (top) as a function of the capacity of the 1<sup>st</sup> and 2<sup>nd</sup> charges and discharges at C/10 of cells NMC622/AG(532) and NMC532/AG(622) with NMC622 and NMC532 as a cathode and the artificial graphite recovered from NMC532/AG and NMC622/AG cells, respectively. Heat generation rate (bottom) for the 1<sup>st</sup> and 2<sup>nd</sup> charges.

## Temperature variation during C-rate tests

The sensing of cells by using FBG sensors can also be helpful to study the influence of C-rate on the battery life. The Figure 86 a. give the maximum temperature reached during charging at different C-rates in charge for a NMC622/AG LiFUN cell instrumented with standard FBGs. It is interesting to note that the surface temperature and the internal temperature are close, the design of the pouch-cell being favourable to the heat exchange with the outside. By looking at the Figure 86 b, at C/5, C/2 and 1C the voltage and heat profile appear as similar.

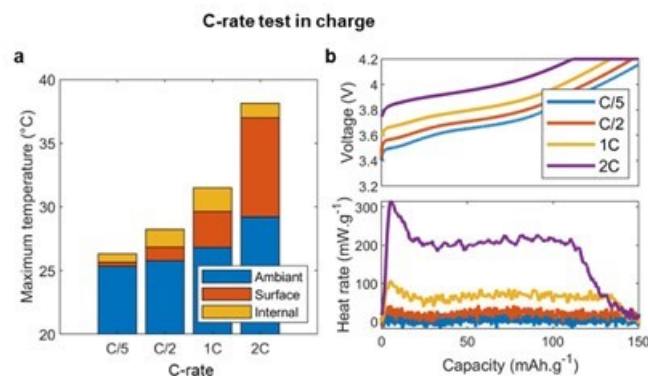


Figure 86. Study of the C-rate influence on charge. (a) Maximum temperature reached during charging at different C-rates. (b) Voltage profile and heat rate profile in charge in function of capacity at different C-rate.

However, at 2C a significant decrease in capacity is observed as well as the appearance of a low voltage heat peak similar to that observed for SEI formation and which could correspond to a degradation of the electrolyte. Post-mortem characterization will be done on cells after high C-rate cycling to confirm the electrolyte degradation.

## Long cycling of LiFUN cell with OF/FBG using WLTP-1

Two implemented cells were fabricated (NMC622/AG) and cycled at 25°C and 55°C (harsh condition) to study the impact of WLTP-1 cycling on the performance of the cells (Figure 87). Interestingly, the cell with OF/FBG did not show significant difference compared to pristine cell for cycling at 25°C, whereas an impact was noted for test performed at 55°C. Indeed, at 25°C both implemented and non-implemented cell retained 90% capacity after 500 cycles. However, the capacity decay of cells cycled at 55°C was more than 10% after 180 and 260 cycles, for implemented and non-implemented cell, respectively.

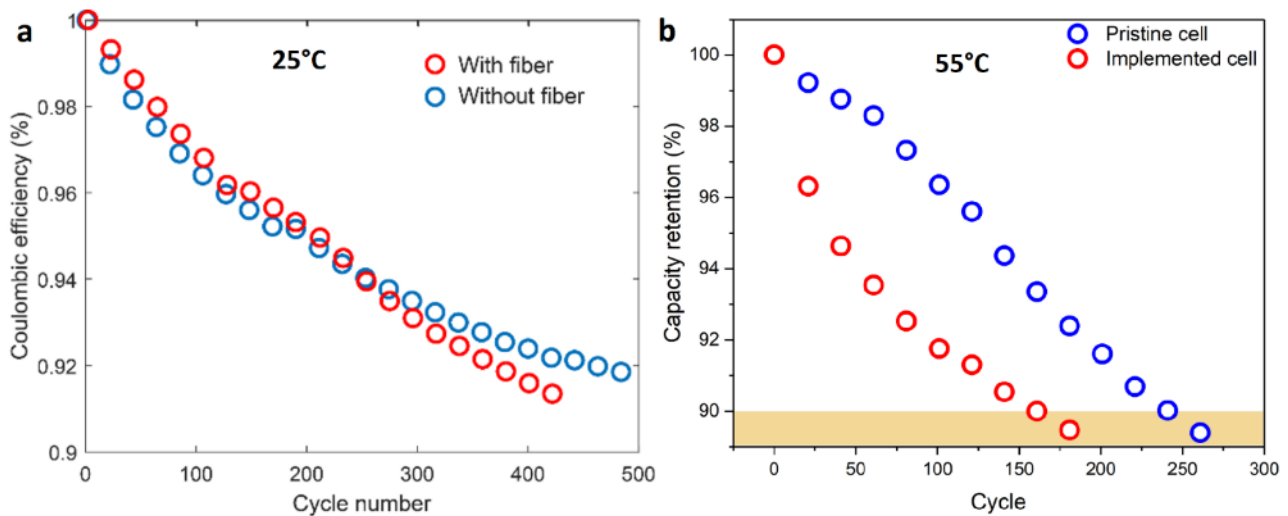


Figure 87 : Impact of the sensor implementation on the coulombic efficiency/capacity retention for cells cycled at 25°C (a) and 55°C (b).

Thermal measurements during those WLTP cycling were performed and showed that significant heat was generated internally and at the surface of the cell for test performed at 25°C (Figure 88a). As expected, the heat was increasing with the speed of the WLTP cycling (Figure 88b). Interestingly, during WLTP-1 cycling at 55°C (Figure 89), it was noticed that the difference of temperature between the inside of the cell and the surface of the cell was only 1°C, whereas it was of 4°C for test performed at 25°C.

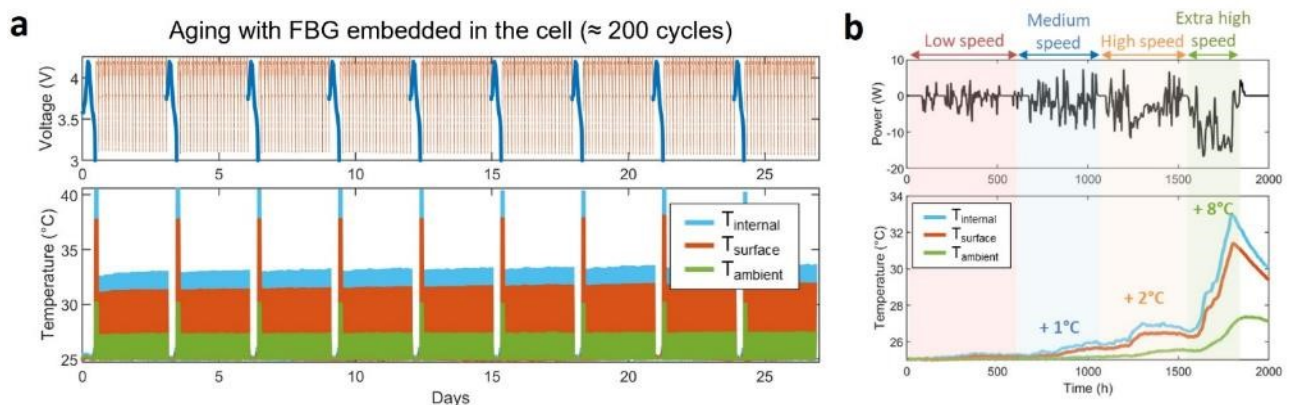


Figure 88: (a) Overview of temperature measured inside, at the surface, and at the ambient for the first 200 cycles for LiFUN pouch cell cycled at 25°C. (b) Close view of the heat recorded inside, at the surface and at ambient in function of the WLTP cycle speed.

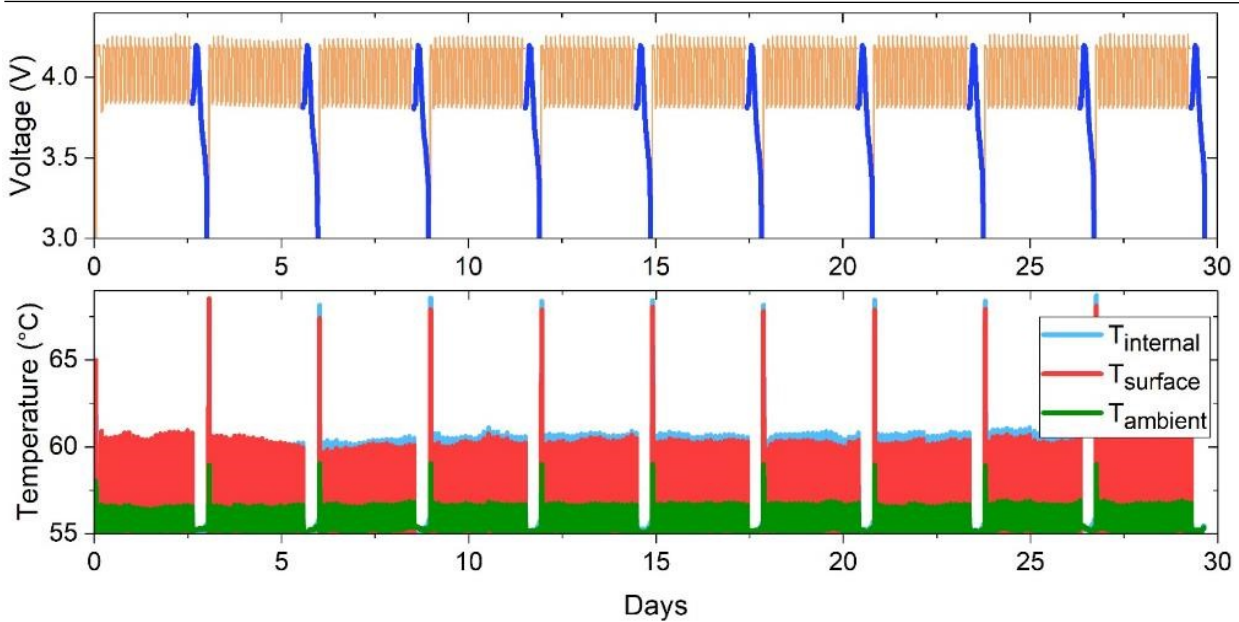


Figure 89 : Overview of temperature measured inside, at the surface, and at the ambient for the first 180 cycles for LiFUN pouch cell cycled at 55°C.

Finally, the robustness of the calorimetric measurements performed for WLTP cycling protocol can be summarized in Figure 90, where cells with different cathode material were benchmarked and where it can be clearly seen that the heat-rate they are generating upon cycling is like a fingerprint, allowing to differentiate the material used.

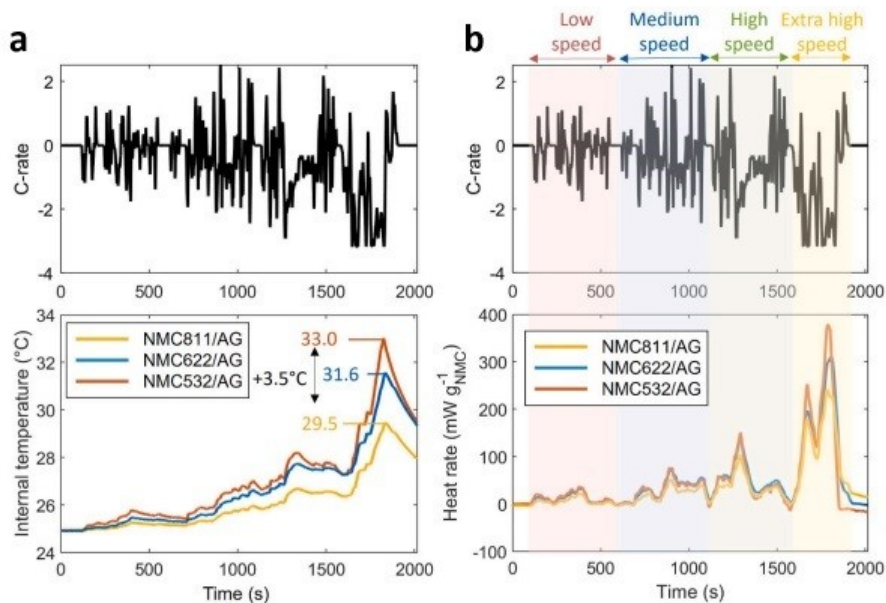


Figure 90 : a) Temperature changes during a single WLTP discharge cycle of NMC811/AG, NMC532/AG and NMC622/AG cells. b) Heat rate changes during one WLTP discharge cycle of the NMC811/AG, NMC532/AG, and NMC622/AG cells.



- **Post-mortem analysis of OF/FBG instrumented LiFUN cells after ageing**

## SEM measurements

### Investigation on cells cycled at 25°C:

After WLTP cycling, the cells were dismantled in the glove box and the electrodes were recovered. The procedure consisted of carefully opening the cell and wash the electrode three time in DMC. The electrodes were then dried overnight in the vacuum chamber.

No significant damages were observed on the NMC side for implemented and non-implemented cell compared to pristine cell, as seen on Figure 91.

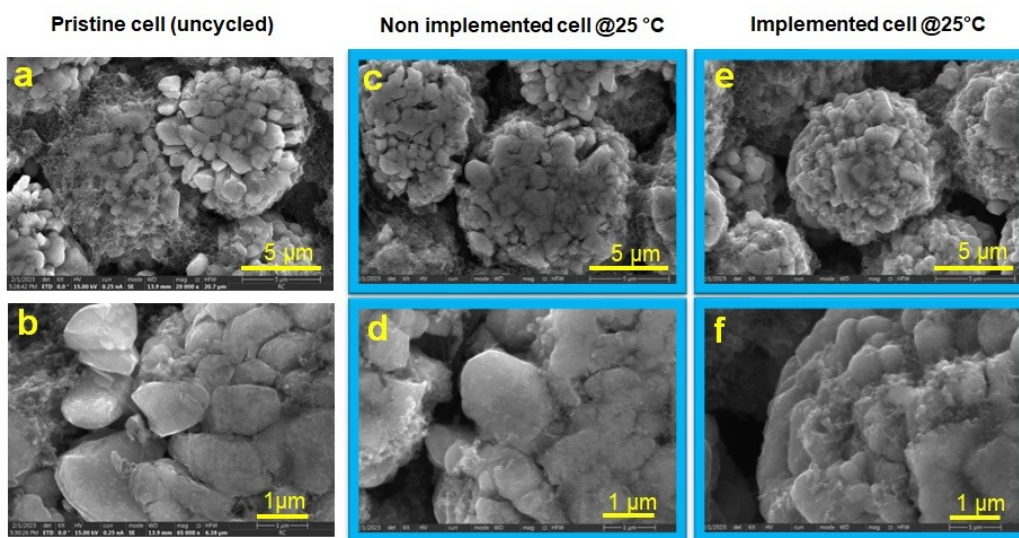


Figure 91: SEM images of recovered NMC 622 electrodes for: (a, b) pristine cell, (c,d) non-implemented cell cycled at 25 degrees, and (e,f) implemented cell cycled at 25 degrees, with focus on undamaged region.

The story is very different for AG compared to NMC 622, as seen on Figure 92. For both non-implemented cell (Figure 92c-d) and implemented cell (Figure 92 e-f) cycled at 25°C, the presence of damage is clearly evident, with slightly more pronounced damage recorded for the implemented cell.

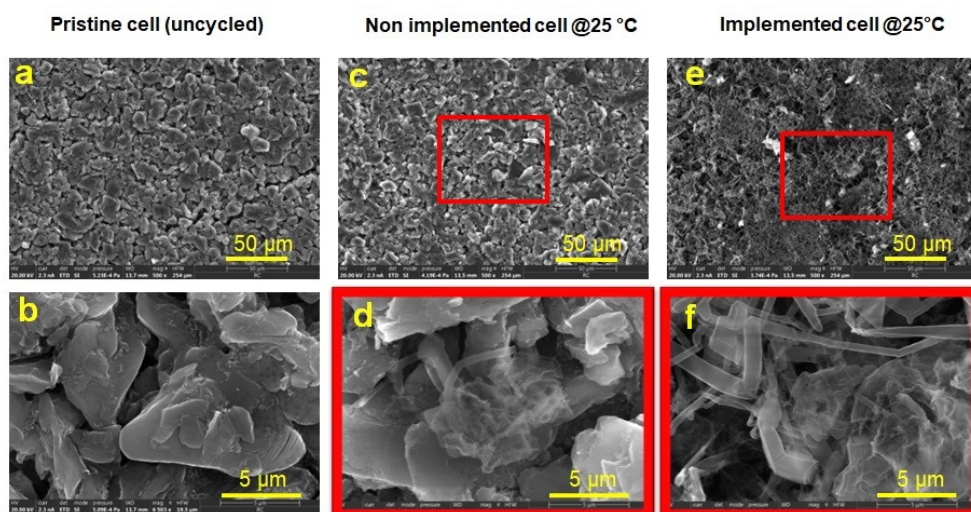


Figure 92: SEM images of recovered AG electrodes for: (a, b) pristine cell, (c,d) non-implemented cell cycled at 25 degrees, and (e,f) implemented cell cycled at 25 degrees.

## Investigation on cells cycled at 55°C:

The procedure for those investigation was the same as the one described above for the cell cycled at 25°C, e.g. recovering the electrode in the glove box after cell disassembly, and wash them three time in DMC before drying them. Very interestingly, no significant damage was seen among the cycled cells (both non-implemented and implemented with FBG) on the NMC side (Figure 93) and on the AG side (Figure 94).

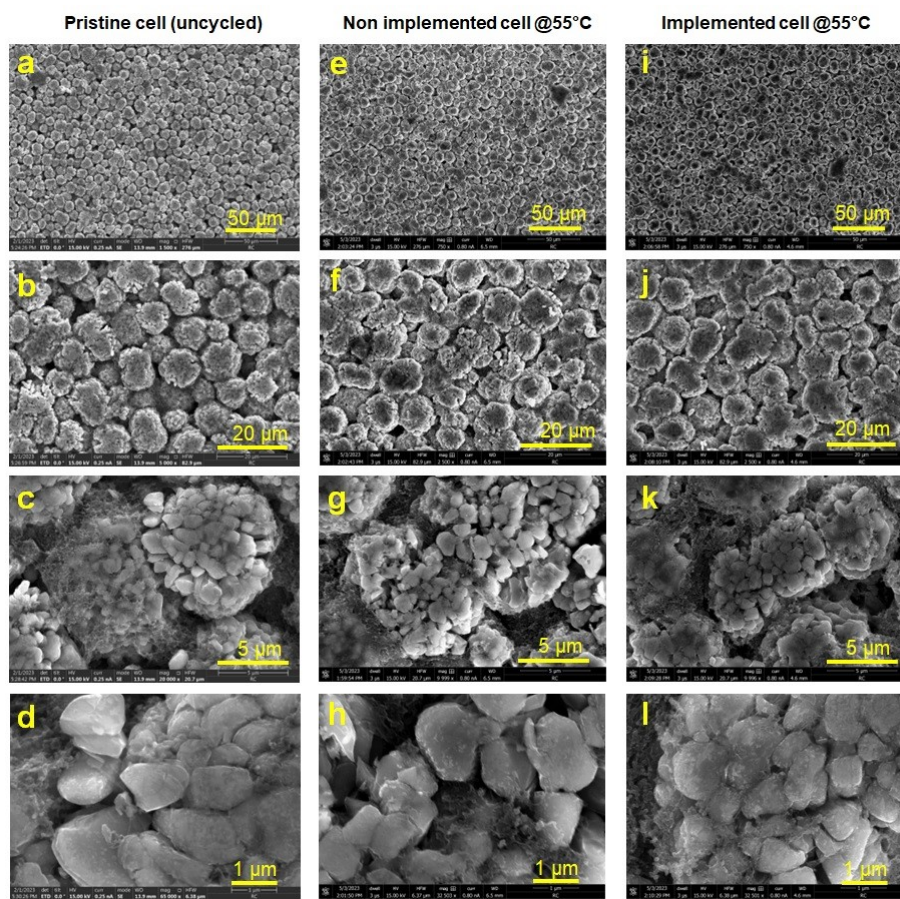


Figure 93: SEM images of recovered NMC 622 electrodes for: (a, b, c, d) pristine cell, (e, f, g, h) non-implemented cell cycled at 55 °C, and (i, j, k, l) implemented cell cycled at 55 °C.

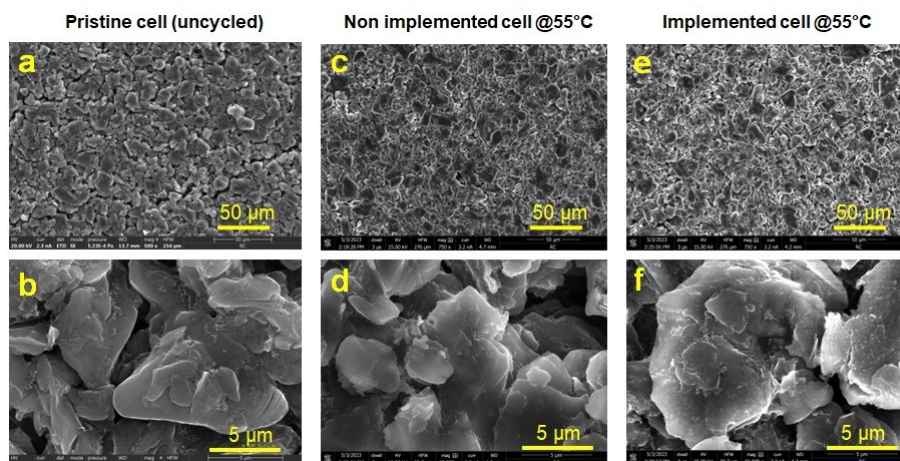


Figure 94: SEM images of recovered AG electrodes for: (a, b) pristine cell, (c,d) non-implemented cell cycled at 55 degrees, and (e,f) implemented cell cycled at 55 °C.



From the SEM results presented in the above Figures, we were not able to detect any significant influence of the OF/FBG sensor on the electrodes, which may be due to the fact that the fiber was placed between the 2 separators. Furthermore, it was interesting to note that the cells cycled at 55°C did not show any obvious degradation. In the other hand, for the cell cycled at 25°C, although we did not observe significant damage at the positive electrode (NMC 622), we however recorded very obvious damage on the negative electrode (see Figure 87) for both non-implemented and implemented cells. Those observations tend to indicate that the OF/FBG sensor did not affect the electrodes. Lastly, as the damage for cell cycled at 25°C were only present on the negative electrode side, it may be an indication of changes in the SEI or lithium plating.

## EDX measurements

### Investigation on cells cycled at 25°C:

Complementary to SEM, EDX measurements were performed on the recovered electrodes. It is interesting to note in Figure 95 a-c, that in the case of NMC 622, we observed a growth of the Phosphorous peak. The same Phosphorous peak growth was also observed for the AG (see Figure 95 d-f). More interestingly, we also observed a growth of the Fluorine (peak F) for both the electrodes of the cell that was cycled at 25°C with OF/FBG sensor.

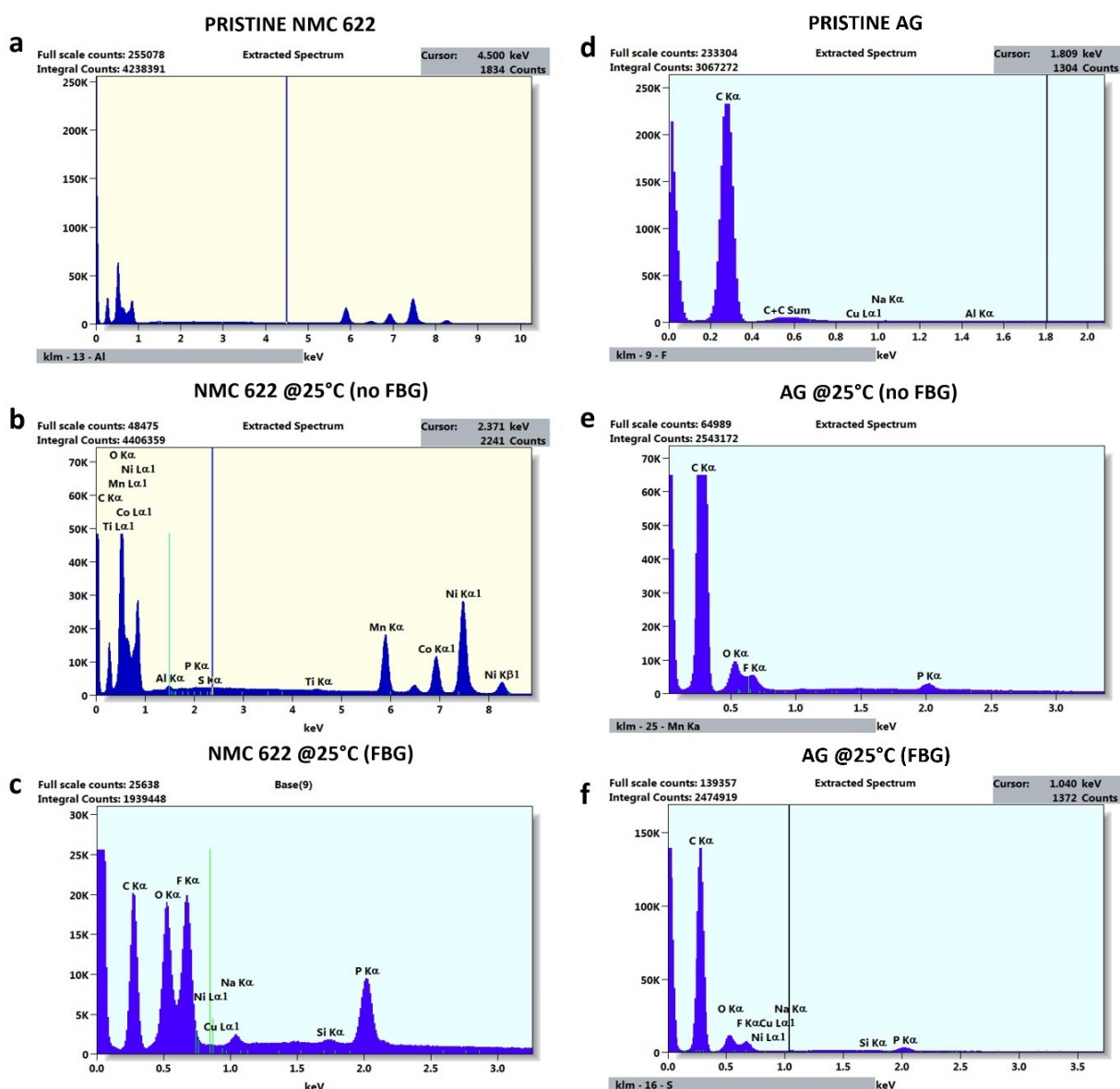


Figure 95: EDX measurements of recovered electrodes for: (a, d) pristine NMC 622 and pristine AG, (b,e) NMC 622 and AG for the non-implemented cell cycled at 25 °C, and (c,f) NMC 622 and AG for implemented cell cycled at 25 °C.

## Investigation on cells cycled at 55°C:

The measurement performed on both NMC 622 and AG for the non-implemented cell and implemented cell cycled at 55°C are shown in Figure 96. In addition to our comment for the SEM images, we could not observe significant changes for the non-implemented and implemented cell cycled at 55°C, for both NMC 622 and AG. It also seems that the peaks are relatively similar than the one recorded for the pristine cell (Figure 96.a and Figure 96.d).

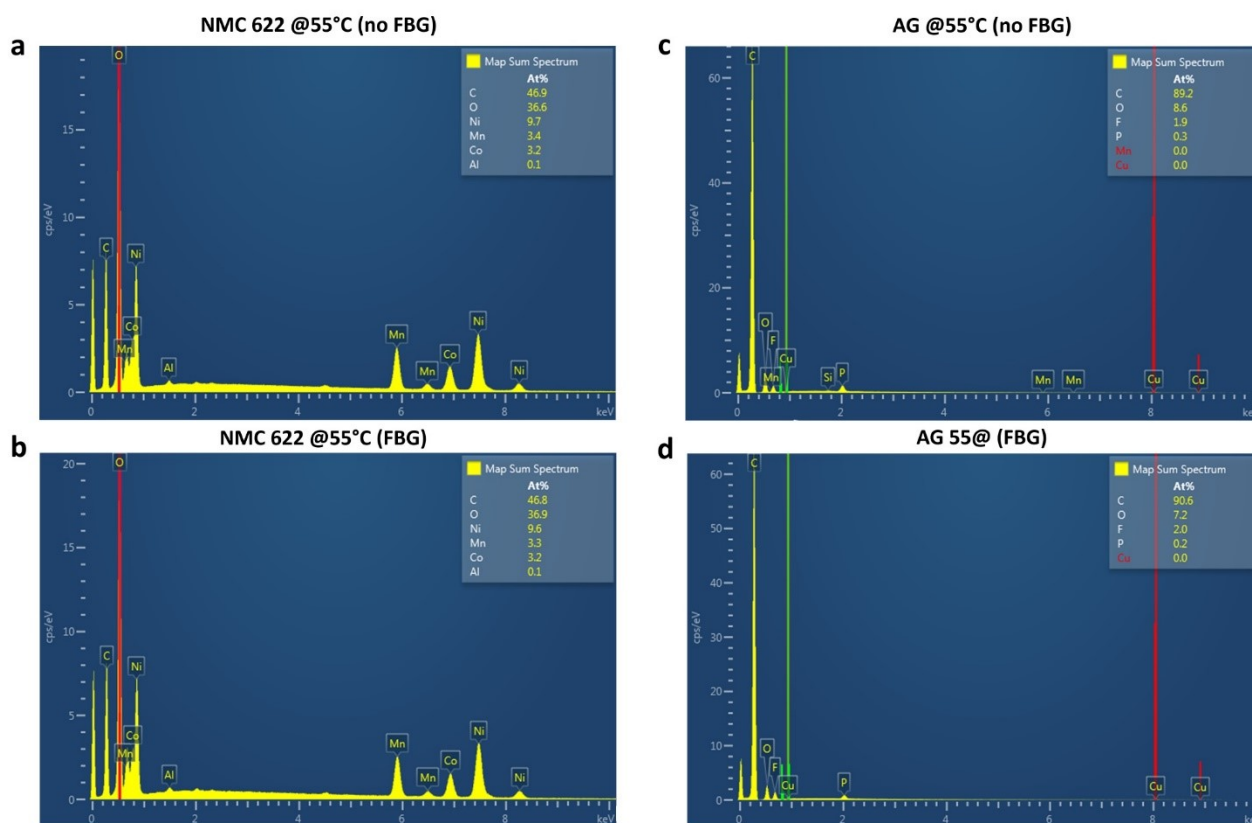


Figure 96: EDX measurements of recovered electrodes for cell cycled at 55 °C. (a) NMC 622 of the non-implemented cell, (b) NMC 622 of the implemented cell, (c) AG of the non-implemented cell, and (d) AG of the implemented cell.

## XRD measurements

To conclude our investigation, CNRS launched a series of XRD measurement to study the crystallography of the electrode material recovered. The intensity of the peaks was normalized to the highest intensity peak of the pristine material, as it is commonly done.

In the case of NMC 622 (Figure 97), we noticed at first glance that surprisingly, the cells that cycled at 55°C (both implemented and non-implemented, in green and orange respectively) do not show much difference with the pristine material. In the other end, both cells that cycled at 25°C show very different XRD pattern compared to the pristine cell. This would be indicative that the temperature plays a minor role in the degradation process in our case, and that the cycle number would be the major contributor to the cell degradation (500 cycles at 25°C vs ≈200 cycles at 55°C).

Concerning the peaks of the cell cycled at 25°C, the peak 003 exhibited a huge shift to the left for both the cell cycled at 25°C, which is indicative of an increase of the 'c' parameter in the lattice. The peak 101 is seen to increase in both case (red and blue), which is evidence of the decrease of the 'a' parameter of the lattice, which is supported by the shift observed on peaks 102 and 104. Besides, we noticed that the intensity of all the peaks decreased compared to the pristine NMC 622, which indicate that the atoms are not at the same position.

Concerning the peaks of the cell cycled at 55°C, we did not observe significant shift for all the peaks, which might indicate that the lattice parameter did not change much.

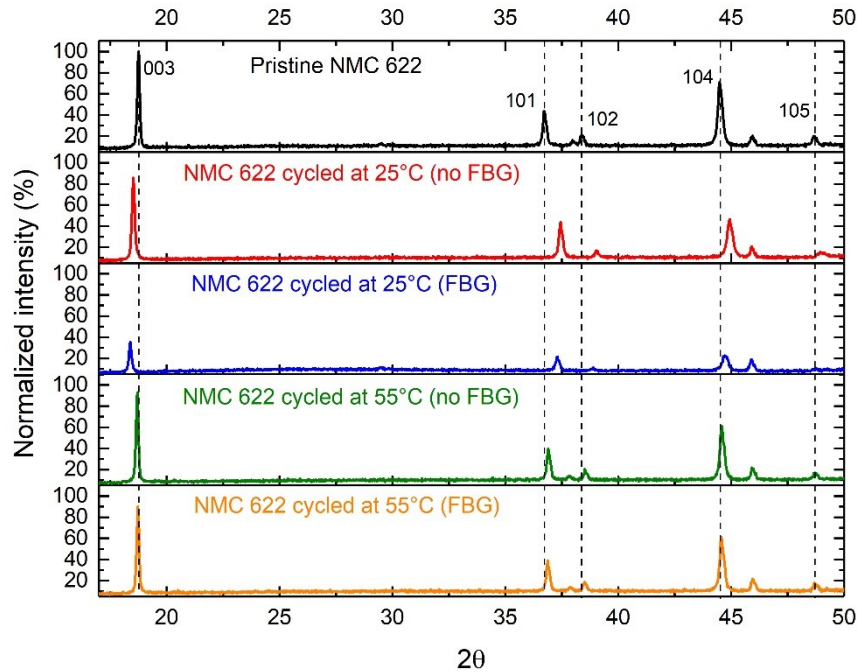


Figure 97: XRD measurements of recovered NMC 622 electrodes.

In the case of AG, the same conclusion than for the NMC electrodes could be made in the sense that more changes were observed for the cells cycled at 25°C than the cells cycled at 55°C (see Figure 98).

Concerning the peaks of the cell cycled at 25°C, the peak 002 exhibited a huge shift to the left for both the cell cycled at 25°C (red and blue), which is indicative of an increase of the 'c' parameter in the lattice. Besides, we observed a small peak at  $2\theta = 24^\circ$  for the cell cycled at 25°C without OF/FBG sensor (red), which indicate that another phase is present, and which confirm that the cell was not totally discharged when dismantled.

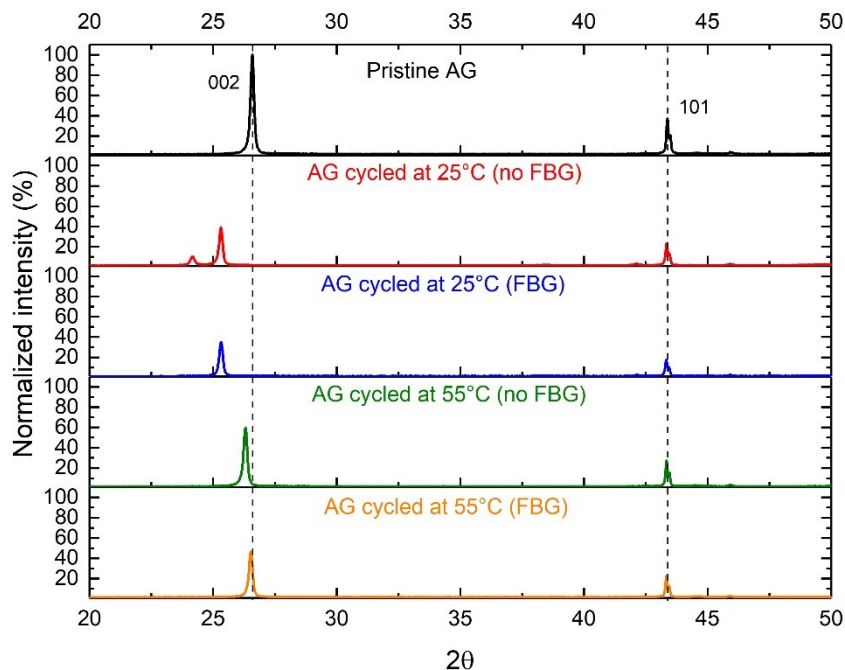


Figure 98: XRD measurements of recovered AG electrodes.

To summarize the finding made using XRD, we used the software Fullprof and the Rietveld method to calculate the lattice parameters. We were not able to do the measurement for AG but we obtained a very nice set of data for NMC 622, presented in Table 15 below, where the number highlighted in red shows a decrease of the lattice parameter, and those in bold show an increase of the lattice parameter.

Table 15: Calculation of the lattice parameter of NMC 622

Lattice parameter	NMC 622 Pristine	NMC 622 cycled at 25°C (no FBG)	NMC 622 cycled at 25°C (FBG)	NMC 622 cycled at 55°C (no FBG)	NMC 622 cycled at 55°C (FBG)
<b>a</b>	2.87104(7)	<b>2.81626(9)</b>	<b>2.82527(19)</b>	2.85820(7)	2.86110(7)
<b>b</b>	2.87104(7)	<b>2.81626(9)</b>	<b>2.82527(19)</b>	2.85820(7)	2.86110(7)
<b>c</b>	14.23882(32)	<b>14.41213(36)</b>	<b>14.51701(70)</b>	14.28368(32)	14.26079(33)

- In operando measurements in VARTA multistack cell using OF/LumT sensor**

Similarly to internal temperature monitoring with OF/FBG sensor, luminescence was used to track internal temperature of the cell. OF/Lum-T sensor was located in the middle of the electrode stack to measure the internal temperature. Cells are instrumented with thermocouple on the external side in contact with the pouch material at the same location. This external temperature measure is used to correlate the internal and external measurements. Due to the very low temperature increase during the first checkup phase (at C/10) only the discharge at 4C was analyzed.

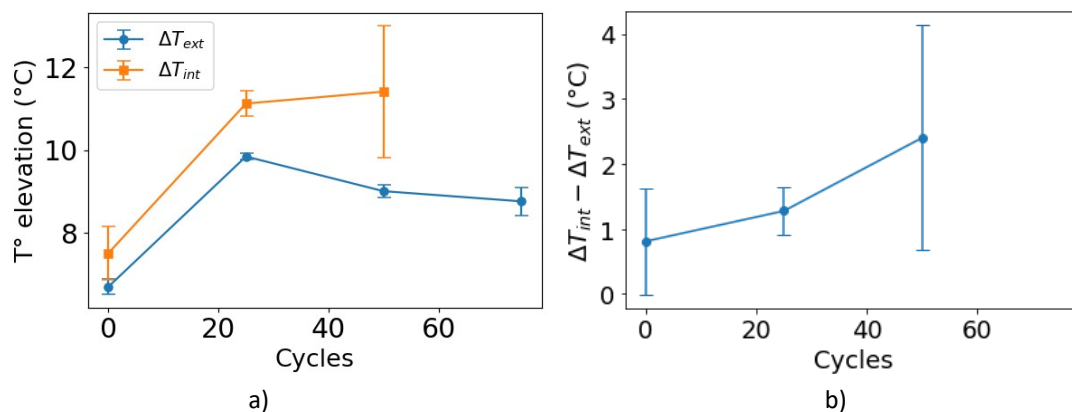


Figure 99 : (a) External temperature variation ( $\Delta T = T_{cell} - T_{ambiant}$ ) during the discharge at 4C measured by thermocouple for instrumented LiFUN cell with OF/Lum-T tested at 25°C (b) Temperature difference between internal and external temperature of the cell

The variation of the maximum temperature on the external surface and inside the cell during the discharge at 4C for WLTP cycling at 25°C is shown in Figure 99. It can be observed that the external temperature measured at the surface of the cell increased by 7°C during the initial check-up and grew to 9-10°C for the others check-up. If we compare this temperature variation to the SOC, the thermal evolution is similar to the SOC variation. Indeed, there is a good correlation between temperature variation and SOH of the cell, which is confirmed at different temperature as seen on Figure 100 (-10°C) and Figure 101 (45°C). In conclusion, OF/LumT sensor did not have an impact on the cell cyclability and was able to operate for up to 150 cycles.

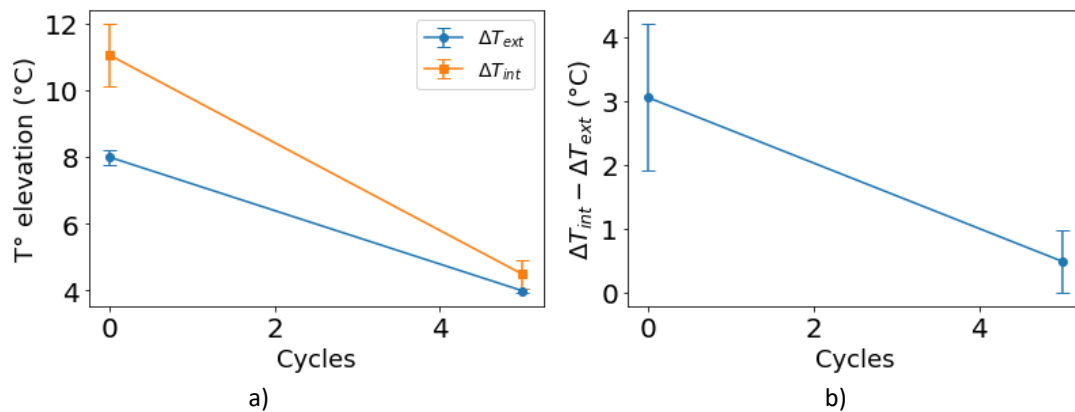


Figure 100 : (a) External temperature variation ( $\Delta T = T_{cell} - T_{ambient}$ ) during the discharge at 4C measured by thermocouple for instrumented LiFUN cell with OF/Lum-T tested at -10°C (b) Temperature difference between internal and external temperature of the cell

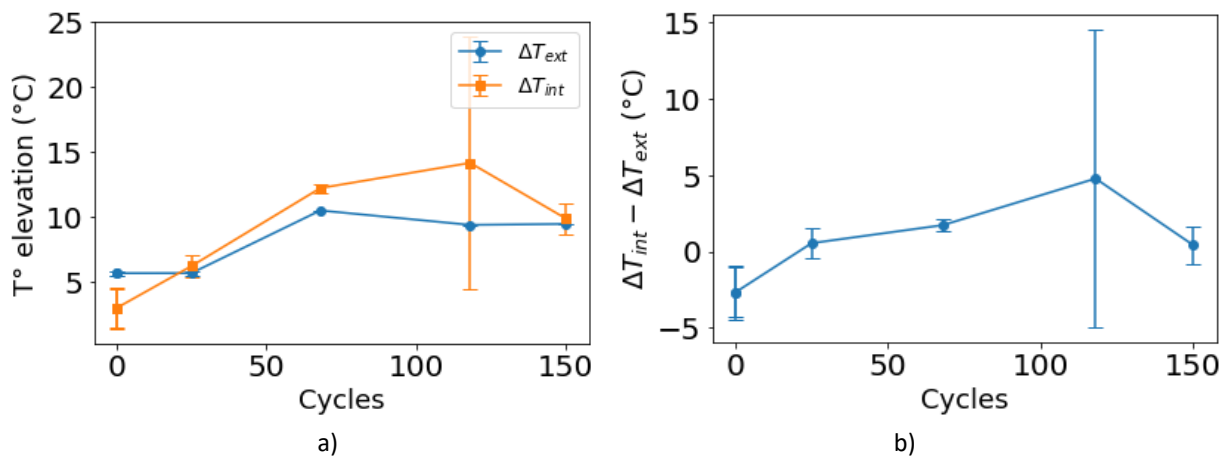


Figure 101 : (a) External temperature variation ( $\Delta T = T_{cell} - T_{ambient}$ ) during the discharge at 4C measured by thermocouple for instrumented Lifun cell with OF Lum-T tested at 45°C (b) Temperature difference between internal and external temperature of the cell

## • Post-mortem analysis of OF/Lum instrumented VARTA cells after ageing

In this part, as we demonstrated previously that sensors implementation didn't have effect on the cell, it was decided to pick up three cells for postmortem analysis, namely:

- FOTL02: cycled at 25°C (99 cycles, SOH =94.85%)
- FOTL03: cycled at 25°C (99 cycles, SOH =94.85%)
- STD02: cycled at -10°C (5 cycles, SOH =57.57%)
- STD03: cycled at 45°C (200 cycles, SOH =85.81%)

The cell reference OF/LumTO2 correspond to an instrumented cell with FO/LumT sensor.

### OF/LumT02 cell (cycled at 25°C, 99 cycles, SOH = 94.85%)

The cells were disassembled as shown in Figure 102 (FOTL02).



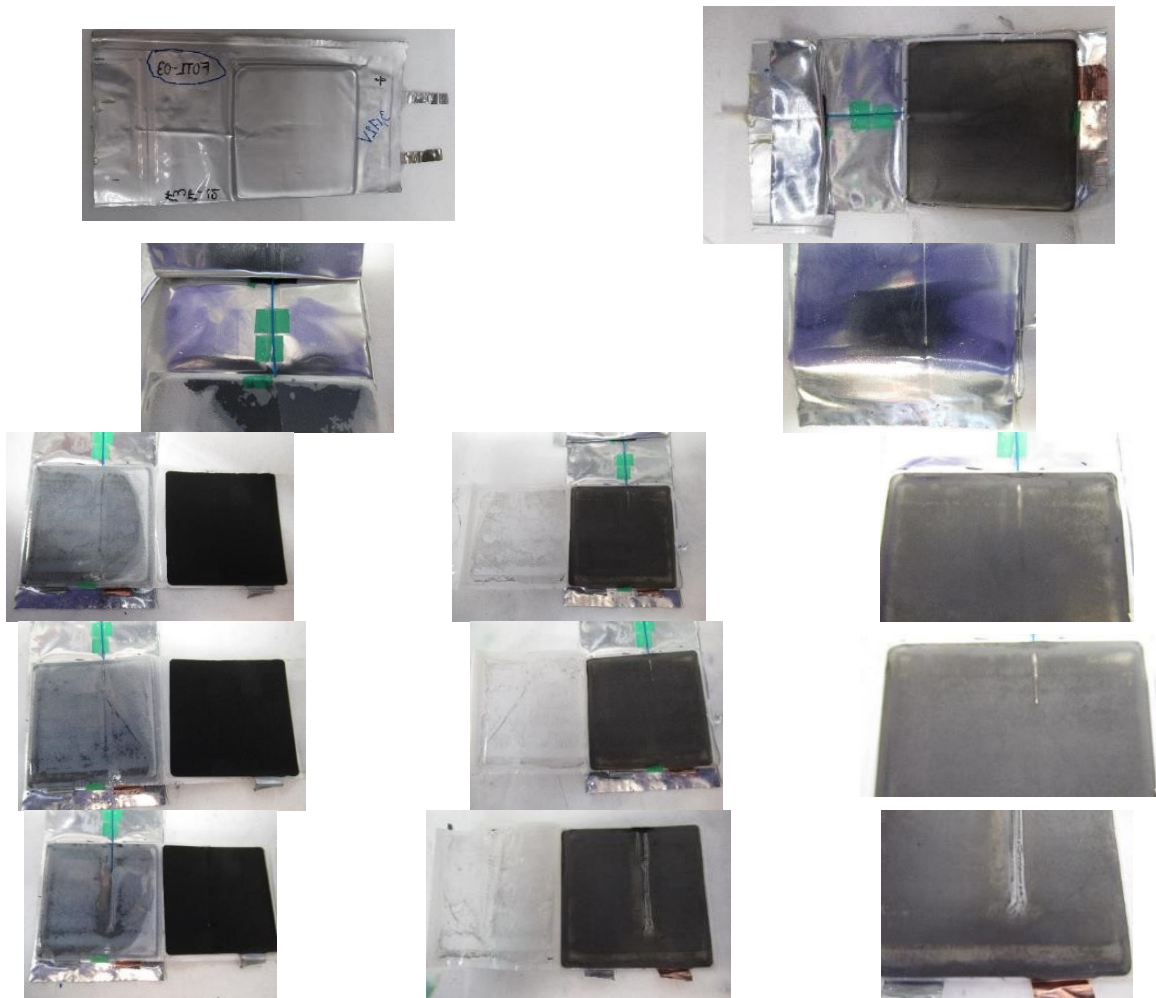
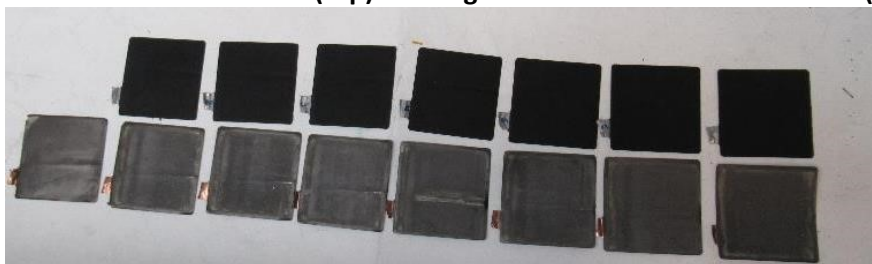


Figure 102 : Photos of the internal components of the instrumented FOTL02 cell (cycled at 25°C, 99 cycles, SOH = 94.85%) taken during the disassembly of the cell

**(a) Positive electrodes – internal side (top) and negative electrodes – external side (bottom)**



**(b) Positive electrodes – external side (top) and negative electrodes – internal side (bottom)**

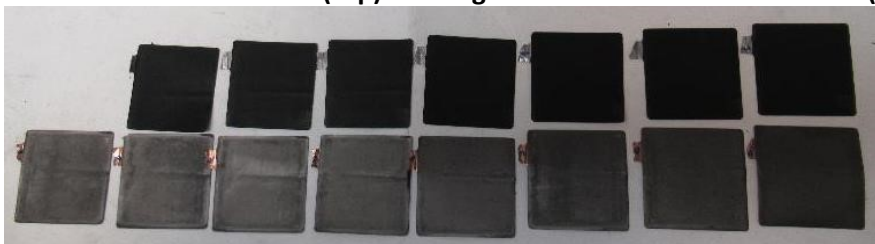


Figure 103 – Photos of all the positive and negative electrodes in alignment of the instrumented FOTL02 cell (cycled at 25°C, 99 cycles, SOH = 94.85%)



On the negative electrode where the fiber is, the deposit has a thicker and whiter appearance. The Figure 103 shows all the electrodes of the stack. They are aligned to better distinguish the fiber impact. The same impact of the fiber was observed in a second cell (FOTL03). Besides, cell STD01 (non-instrumented cell) was also disassembled and visual aspect of the negative electrodes was similar, with grey deposition on the electrode edges.

The area on the negative electrode surrounded the fiber has been observed by SEM (Figure 104). The sample was rinsed with DMC twice for 10 seconds before observation. The deposit remains on the electrode surface, indicating that it is not crystallized lithium salt from the electrolyte, but an insoluble component. The photo of the sampled area is given below. The electrode area on which the fiber was easily identified by the black straight line. Either side of this line, we see an increasingly thicker deposit toward the fiber. The edge of the image in the middle column shows graphite particles in the frontier part of the area where lithium metal was deposited. The shape of the deposit is characteristic of lithium metal deposition.

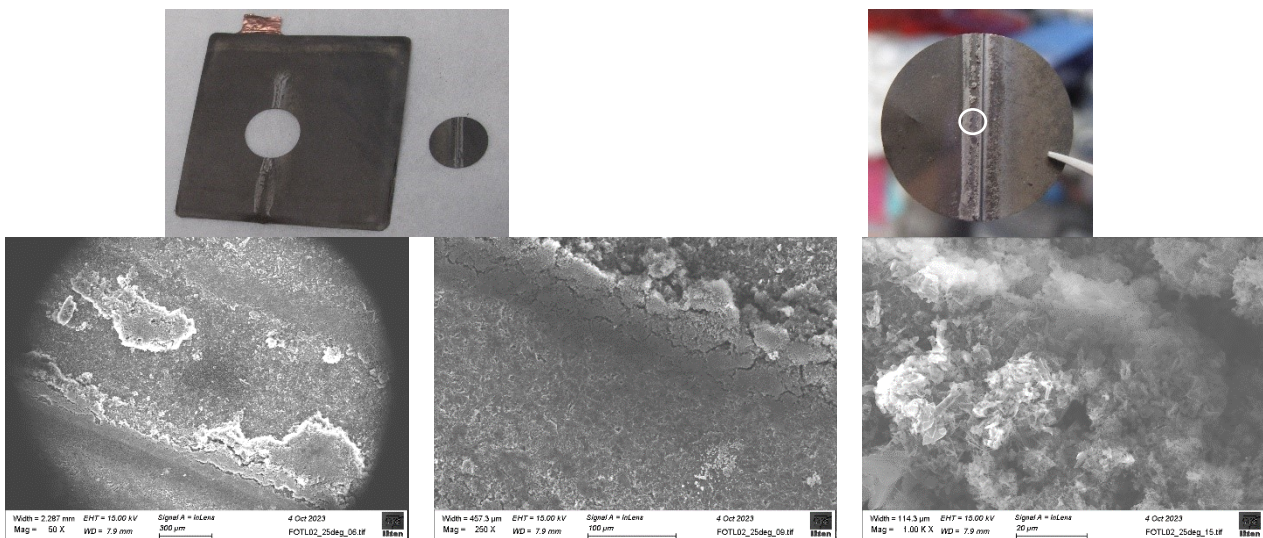


Figure 104 : Images of the fiber periphery (top view)

Figure 105 shows the cross-section of the electrode in the area where the fiber has been implemented. It is possible to distinguish the double-layer coated electrode and the collector. The deposit of lithium is clearly visible on the side where the fiber is present. In the thickest part, its thickness is about 60  $\mu\text{m}$ .

At the fiber periphery, the lithium metal is deposited exclusively. Figure 106 gives the SEM images of the electrode at a distance from the fiber periphery. Lithium plating is not seen.

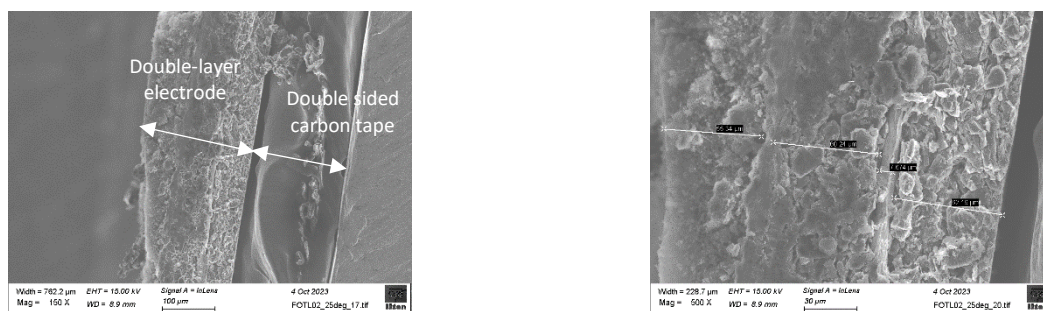


Figure 105 : Images of the fiber periphery (cross section view)

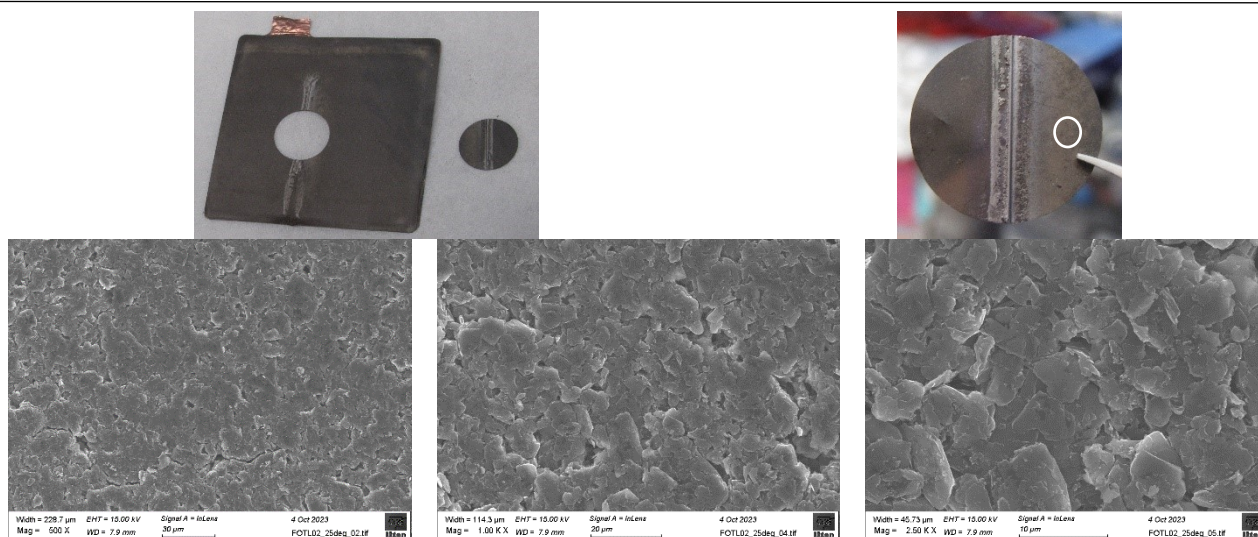


Figure 106 : Images taken on the electrode at a distance from the fiber periphery (top view)

This phenomenon of the deposition of lithium plating around the fiber was already observed in the literature<sup>1,16</sup> with other cell technology. For example, the recent paper from Hedman and al. shows the same pattern of the Li plating around the optical fiber.

Monolayer electrode disks on the negative electrode and on the positive electrode were sampled in the area of the fiber implementation where lithium metal was deposited and in an area away from the fiber periphery. To determine the Loss of Lithium Inventory (LLI) and Loss of Active Material (LAM) for the positive and negative electrodes, the disks were characterized in half coin cell. The results are summarized in Table 16. They are compared with data from fresh electrodes. LLI is not the main cause of the loss of capacity at the cell level. It is almost similar of the initial value in both the areas, even if locally lithium ions have been consumed by lithium plating. Regarding the data of the disks sampled at a distance from the fiber periphery that corresponds to the global behaviour of the electrodes, the cause of capacity of the cell is linked to the positive active material degradation that is in the same magnitude that the loss of capacity of the cell. Locally, on the area at the fiber periphery, the negative active material is more damaged or less accessible because of the deposit comparatively to the other part of the electrode.

Table 16. LLI and LAM for the positive and negative electrodes extracted from FOTL02 cell and from a fresh cell  
(a) In capacity

	SOH of the cell / %	NEG -Crev / mAh	POS-Crev / mAh	POS-Cres / mAh
Fresh	100	4.77	4.61	0.53
Disk sampled at a distance from the fiber periphery	95.6	4.67	4.39	0.41
Disk sampled at the fiber periphery		4.28	4.51	0.49

(b) In percentage of capacity loss

	Loss of cell capacity (%)	LAM neg / %	LAM pos / %	LLI / %
Disk sampled at a distance from the fiber periphery	4.4	2.1	4.7	-2.62
Disk sampled at the fiber periphery		10.4	2.2	-0.91

<sup>1</sup> Hedman, J., Mogensen, R., Younesi, R. & Björefors, F. Fiber Optic Sensors for Detection of Sodium Plating in Sodium-Ion Batteries. *ACS Applied Energy Materials* (2022) doi:10.1021/acsaem.2c00595.

<sup>2</sup> Hedman, J., Mogensen, R., Younesi, R. & Björefors, F. Fiber Optical Detection of Lithium Plating at Graphite Anodes. *Advanced Materials Interfaces* **10**, 2201665 (2023).

## STD02 cell (cycled at -10°C, 5 cycles, SOH = 57.57%)

The images of the internal components of the STD02 cell cycled at -10°C are summarized in Figure 107. After 5 cycles, the SOH of the cell is 57.57%. The color of the negative electrode does not have the expected color of a discharged negative electrode. It appears grey with some spots darker.



Figure 107 : Photos of the internal components of the STD02 cell (cycled at -10°C, 5 cycles, SOH = 57.57%) taken during the disassembly of the cell

SEM images of the surface of the negative electrode in Figure 108 shows that the electrode is entirely covered by a deposit. Some cracks are visible in surface. The LLI and the LAM of the negative electrode are the main causes of the degradation of the cell. However, the loss of capacity at the cell scale (41.9%) is higher than the loss of LLI (17.5%). The loss of LAM is not to be considered at the cell scale because the amount of lithium ions that can still be exchanged is not sufficient to have to consider the limitation of the electrode capacity in any case. This means that lithium ions may be trapped in the graphite particles, but this is not enough to fully explain the loss of cell capacity (10.6%). Some electrodes in the stack are more damaged.

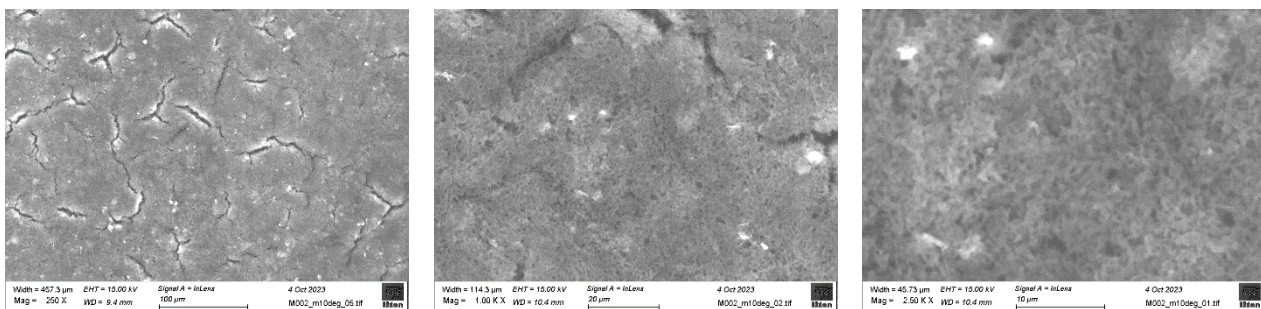


Figure 108 : Images of the negative electrode of the STD02 cell (top view)

Table 17. LLI and LAM for the positive and negative electrodes extracted from -STD02 cell and from a fresh cell  
(a) In capacity

	SOH of the cell / %	NEG -Crev / mAh	POS-Crev / mAh	POS-Cres / mAh
Fresh	100	4.77	4.61	0.53
STDM02	58.1	4.27	4.44	1.34

(b) In percentage

	Loss of cell capacity (%)	LAM neg / %	LAM pos / %	LLI / %
STDM02	41.9	10.6	3.7	17.47



## STD03 (cycled at 45°C, 200 cycles, SOH = 85.81%)

The images of the internal components of the STD03 cell cycled at 45°C are summarized in Figure 109. After 200 cycles, the SOH of the cell is 85.81%. The color of the negative electrode in the center is the expected color of a discharged negative electrode. The electrode edges show a gray surface deposit due to lithium plating.

Postmortem analysis of the cell was performed on the ageing cells at 25°C, -10°C and 45°C. The results from surface imaging (SEM analysis) confirm the presence of Lithium plating for sample aged at low and high temperature. The results from the electrochemistry characterization on each electrode (positive and negative) give an information of the ratio in Loss of Active Material (LAM) and Loss of Lithium Inventory (LLI). This analysis highlights also the effect of the optical fiber on the local degradation phenomenon. Lithium plating was detected around the fiber and is due to the geometrical effect. We also observe lithium plating in the edge of electrodes at high temperature and in the full electrode surface at low temperature. This difference is already known in the literature: the morphology of the lithium plating is generally not the same at low and at high temperature.



Figure 109 : Photos of the internal components of the STD03 cell (cycled at 45°C, 200 cycles, SOH = 85.81%) taken during the disassembly of the cell

- **Identification of degradation mode in monolayer VARTA cells with RE**

### Diagnosis tool

The diagnosis tool is based on a comparison of the experimental cell voltage curves at low current with the simulated profile obtained by summing the positive and negative potential curves. The positive and negative potential curves used are obtained in half-coin cells. The methodology is illustrated in the Figure 110. This tool attributes the loss of capacity to three main degradation modes: LLI (Loss of Lithium Inventory), LAMn (Loss of Negative Active Material) and LAMp (Loss of Positive active material) as explained by C.R. Birkel et al<sup>17</sup>.

<sup>17</sup> Birkel, C. R., Roberts, M. R., McTurk, E., Bruce, P. G., Howey, D. A. Degradation diagnostics for lithium ion cells. Journal of Power Sources (2017) 10.1016/j.jpowsour.2016.12.011

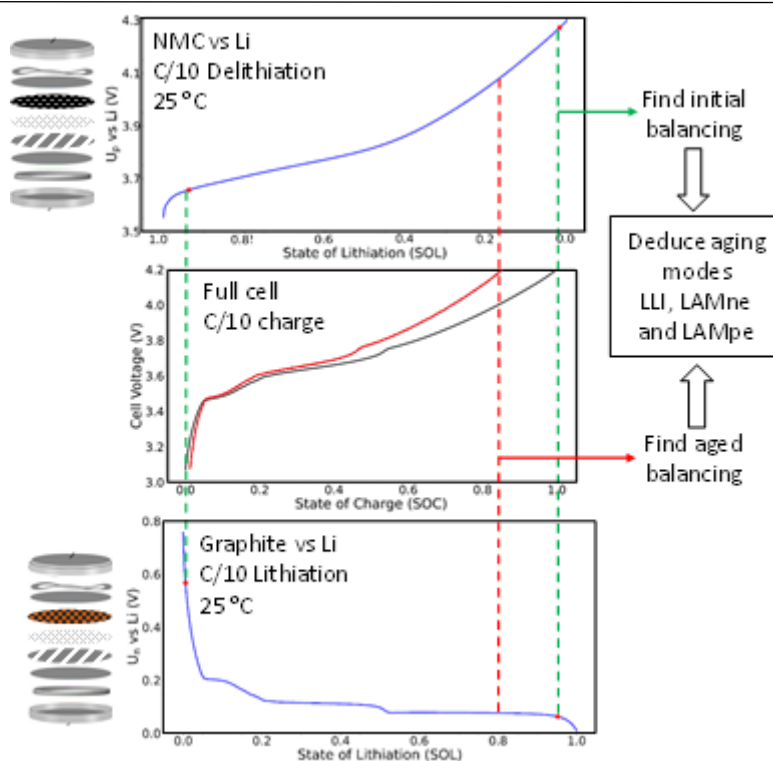


Figure 110 : Method used for the cell diagnosis

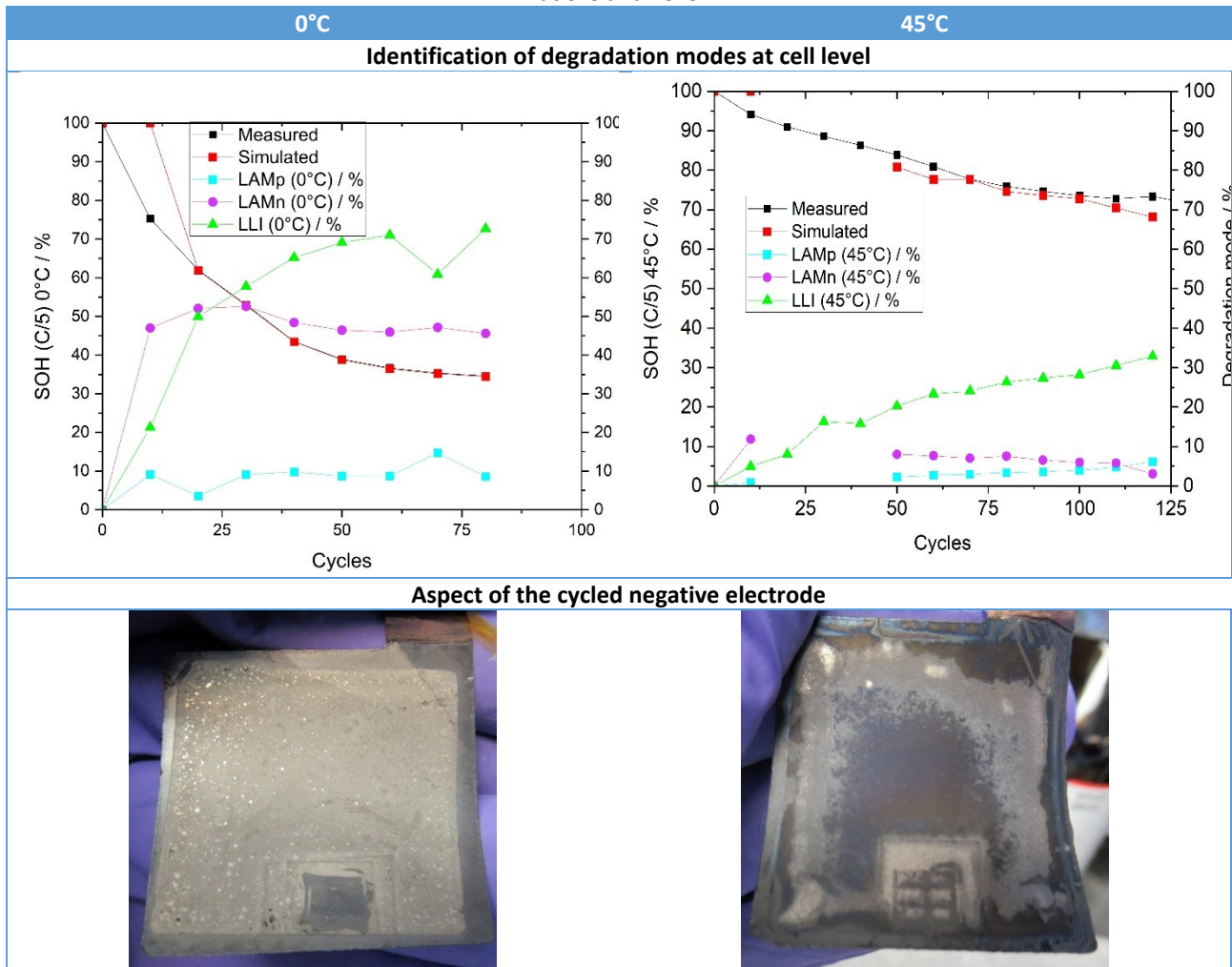
## Results on degradation modes

We will focus here more particularly on the cells tested at 0°C and 45°C. In Table 18 are given the degradation modes over cycling identified at cell level:

- LLI (Lithium Loss Inventory)
- LAMn (Loss of negative active mass)
- LAMp (Loss of positive active mass)

At 0°C, the decay of the capacity was very fast and was caused by the LLI. Visually, the negative electrode appears to be completely covered with a thin deposit of gray color. At 45°C, LLI is also the main cause of capacity decay. However, capacity decays more progressively along the cycling test. Visually, the negative electrode appears to be covered with a deposit of gray color also but only the edges. The deposition is not homogeneous but has been deposited preferentially on the edges. There is no visible defect on the positive electrode. More information such as  $dQ/dV$  can be found in Deliverable D3.3. The conclusion on this study was that monitoring the charging process using the negative electrode potential provided by the reference electrode, lifetime extension can be expected due to the fact that lithium deposition is avoided. The LFP-based reference electrode provides a reliable response over a long period of time.

Table 18 : Identification of degradation mode at cell level and aspect of the cycled negative electrode after cycling test at 0°C and 45°C



- **Post-mortem analysis of VARTA monolayer cell with RE sensor**

The methodology of characterization is illustrated below (Figure 111).

Visual inspection of the electrodes was performed and the same conclusions than the one made for the VARTA multistack cell implemented with OF/Lum could be made: the negative electrodes shows that LLI is due to lithium metal deposition that is observed on the negative electrode surface, which is totally covered, except for 45°C. At that temperature, the deposition is heterogeneous and principally localized on the edge of the electrode



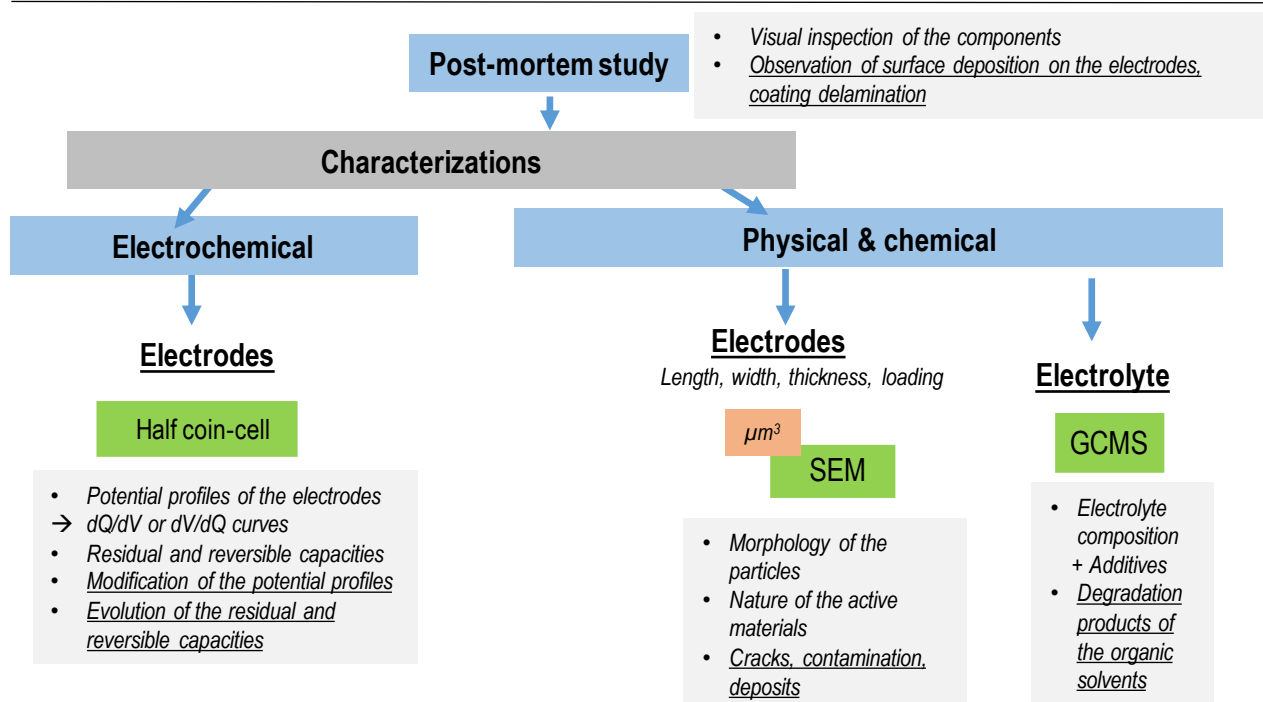


Figure 111 : Post-mortem characterization (underlined text indicates degradations that can be identified after aging)

## SEM and EDX observations

SEM measurements of cycled electrodes at different temperature were performed. Focus was made on the negative electrode where apparent damages were spotted. For each anode, SEM measurements were focused on their crossed section. Measures of the thickness of the lithium plating and thickness of the electrode (SEI measurement by comparing with pristine cell) were performed. For clarity, we will not present all the measurements here and will direct the reader to the Deliverable D3.3 where all the results are presented. We will give below the example of an SEM measurement of the AG anode at different locations of a cell cycled at 45°C (Figure 112). However, the main finding of this study are summarized in Table 19, at the end of this post-mortem study.

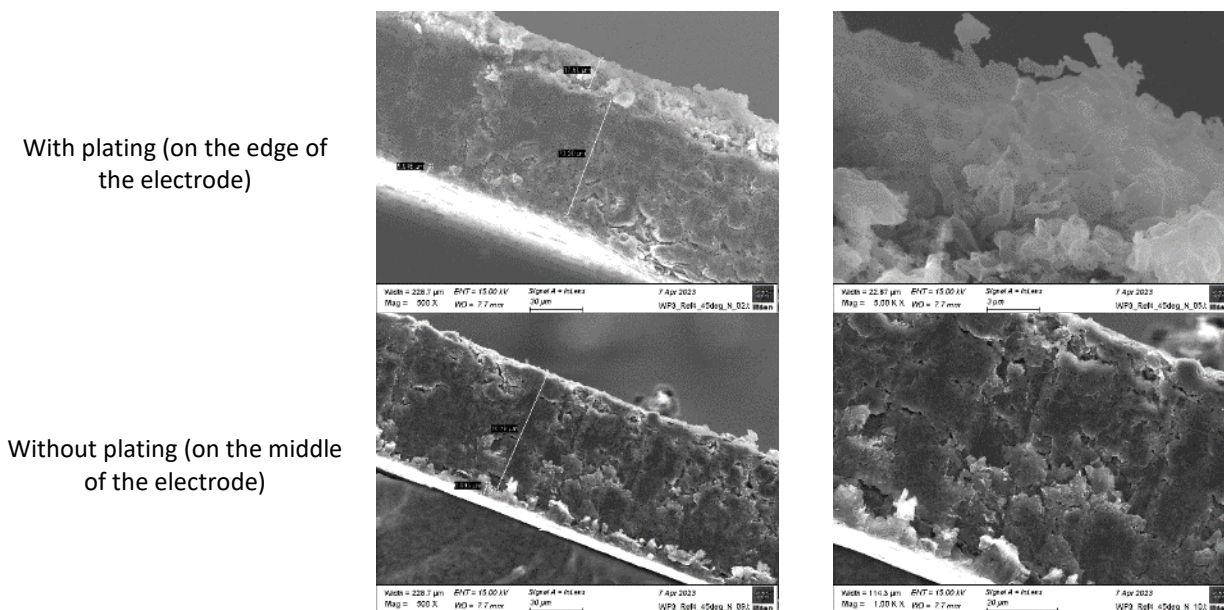


Figure 112 : SEM images – cross-section of the negative electrode cycled at 45°C on the edge (with lithium plating) and on the middle (without plating)

Similarly, EDX measurements were performed on each anodes material and an example is given in Figure 113. The corresponding energy EDX elemental mapping results of the cross-section are shown in Figure 113. The layer of lithium metal is well identified. It is oxygen, fluorine, and phosphorus rich. This conclusion holds for every anode material tested (cells cycled at different temperature). Again, for clarity, not all the measurements are presented in this report and we direct the reader to the Deliverable D3.3 for a complete view of the measurements performed.

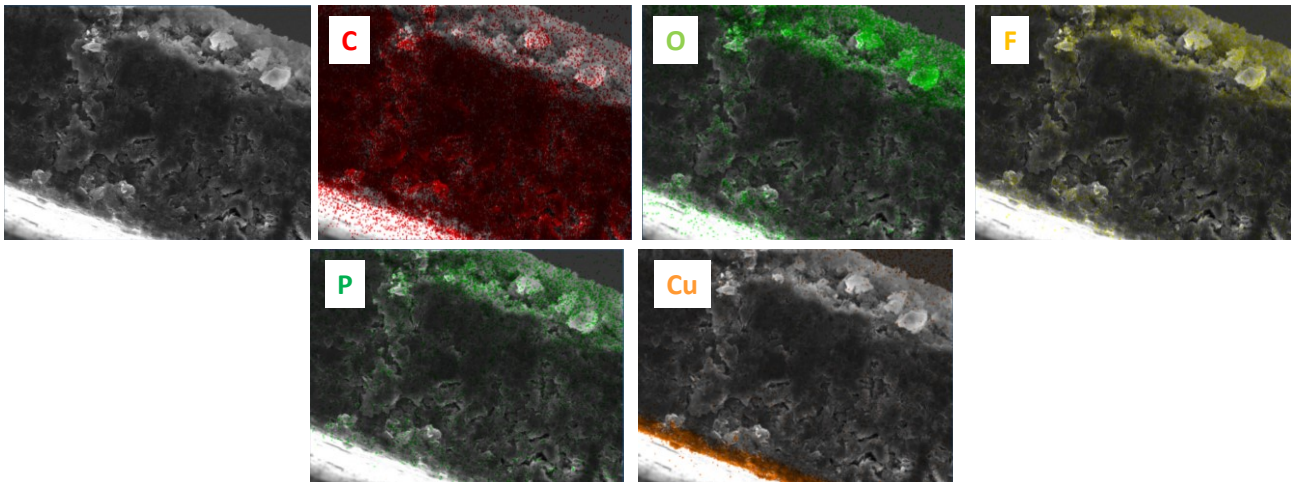


Figure 113 : Energy dispersive X-ray spectroscopy (EDX) elemental mapping of the cross-section of negative electrode cycled at 45°C on the edge (with lithium plating)

## Test in half-coin cell

Electrochemical tests in half-coin cell are illustrated in Figure 114. From these, two capacity values can be determined:

- Reversible capacity ( $C_{rev}$ ), in delithiation for the negative electrode and in lithiation for the positive electrode. It corresponds to the full electrode capacity. The difference of reversible capacity before and after cycling is matching with LAM.
- Residual capacity ( $C_{res}$ ) in lithiation for the positive electrode that allows to know its state of lithiation before and after cycling. The difference of residual capacity before and after cycling is matching with LLI.

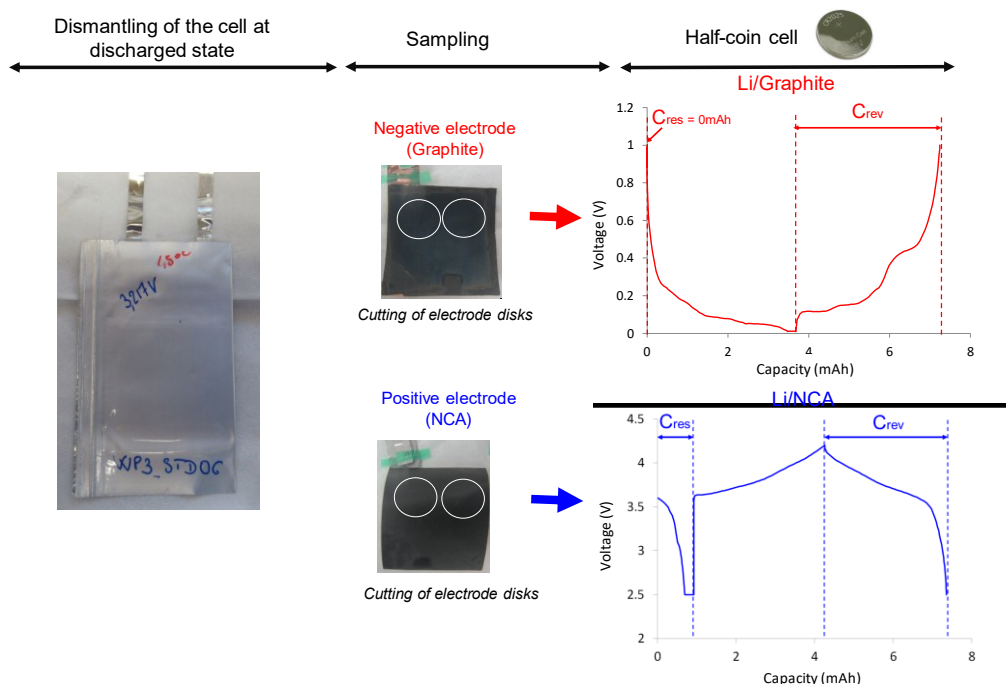


Figure 114 : Illustration of the electrochemical test in half- coin cell.

The formula re expressed below:

$$LAM_{pos} = \frac{C_{rev} \text{ positive after cycling} \times 100}{C_{rev} \text{ positive before cycling}}$$

$$LAM_{neg} = \frac{C_{rev} \text{ negative after cycling} \times 100}{C_{rev} \text{ negative before cycling}}$$

$$LLI = \frac{(C_{res} \text{ positive after cycling} \times 100) - (C_{res} \text{ positive before cycling} \times 100)}{C_{rev} \text{ positive before cycling}}$$

In this study, disk sampling has been performed on the top of the electrodes as schematized in the figure above.

To facilitate the evaluation of the active material degradation and improve processing accuracy, galvanostatic curves obtained at C/10 rate were plotted in  $dQ/dV = f(V)$  to transform inflection points on the potential profile into peaks/valleys as illustrated in Figure 115.

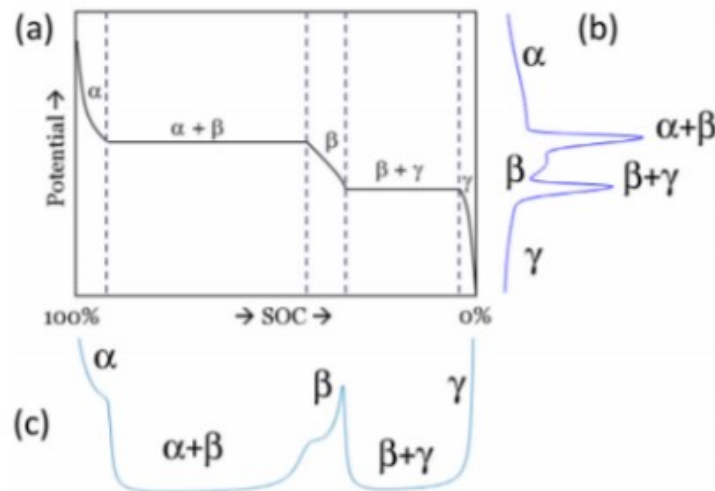


Figure 115 : Correspondence between voltage curve (a), Differential voltage analysis (DVA) curve (b) and Incremental Capacity Analysis (ICA) curve (c)

Here, the authors of this manuscript are aware that the present report shall be concise and therefore, the DVA curves and data analysis will not be presented, but instead, a table resuming all the discoveries made from the SEM images, EDX measurements, and half coin test cell is proposed.

In conclusion, the loss of capacity is caused by LLI degradation mode. LLI is attributed to lithium metal deposition on the negative electrode surface. This deposition covers entirely the surface of the electrode, except at 45°C. At 45°C, the deposition is heterogeneous. At low temperatures, the reference electrode can detect assuredly when lithium is plated in metallic form (high polarization of the potential of the negative electrode that passes below 0 V vs Li and appearance of a plateau).

At 25°C, as soon as the potential reaches 0V vs Li, the lithium deposition occurs: the 0V threshold must be the strict limit. At 45°C, the formation of heterogeneous metallic lithium is not detected. A summary of the discovery is presented in Table 19 below.

Table 19 : Results of the post mortem characterization vs electrochemical profiles

	45°C	25°C	0°C	-10°C
<b>Loss of cell capacity (%)</b>	30%	46%	65%	73%
<b>Visual inspection of the negative electrode</b>	Localized and thick Li-plating on the edge, propagated towards the middle of the electrode (40% of surface covered)	Li-plating on the entire surface, thicker on the edge	Li-plating on the entire surface, very thick	Li-plating on the entire surface, very thick
<b>Lithium deposition morphology</b>	Tubular shape it partially covers the electrode	Tubular shape It seems not dense	Fibrous shape	Foam shape
<b>Negative electrode</b>	+16µm of thickness	+15µm of thickness	No thickness increase	No thickness increase
<b>LAM (%) estimated</b>	3%	9%	45%	17%
<b>LAM (%) measured</b>	0%	2%	5%	6%
<b>Positive electrode</b>	No increase of thickness	No increase of thickness	No increase of thickness	No increase of thickness
<b>LAM (%) estimated</b>	6%	9%	1%	20%
<b>LAM (%) measured</b>	1%	0%	2%	0%
<b>LLI (%) estimated</b>	32%	45%	45%	62%
<b>LLI (%) measured</b>	27%	42%	58%	66%
<b>Negative electrode profile given by the reference electrode</b>	No passage above 0V vs Li, heterogeneous lithium deposition	No passage above 0V vs Li though a covering lithium deposition is observed	Passage above 0V vs Li with a plateau at 0V vs Li	Passage above 0V vs Li with a plateau at -0.075 V vs Li



- **Long term ageing of instrumented LiFUN cell (1.1A.h.) with OF.LumT sensors at high C-rate**

In order to study the long-term ageing of OF/LumT sensor in high C-rate condition, we decide to perform cycling test of one of instrumented cell used for ESRF experiment during the collaboration with BIG-MAP project. Figure 116 shows a photo of sample ESRF-08 with instrumentation. The OF/LumT sensor was inserted in the middle of the electrodes sack at 1 cm from the edge of the electrode on the opposite side of the current collectors. The external temperature was measured by thermocouple in the center of the cell, close to the OF/LumT position, at each collector (positive and negative) and in ambient. The cell was placed between two plates for mechanical constraint. The two red circles show the measurement point for ESRF experiment: close to the fiber tip and in the center of electrodes.

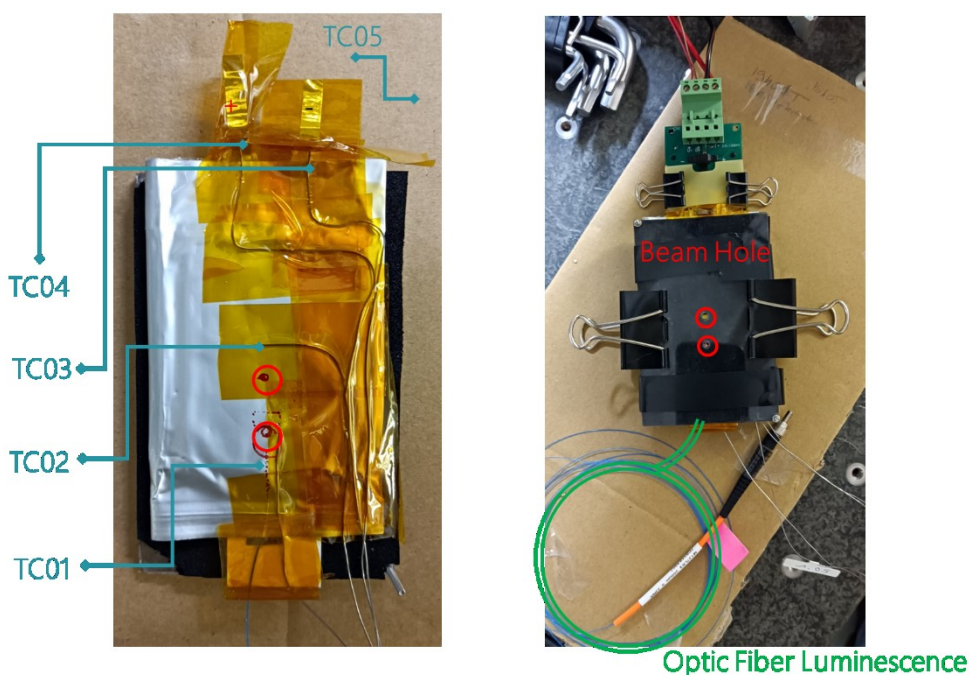


Figure 116 : ESRF-08 sample prepare for ESRF experiment in collaboration with BIG-MAP project

During the experiment at ESRF the cycling protocol apply to the cell is show in the Figure 117. The figure shows the variation over the time of current, potential of the cell and the temperature measured by thermocouples.

The protocol apply to this cell was:

- 1- First a slow discharge at C/5,
- 2- Then a charge and discharge at C/5.
- 3- Then a first discharge at 4C to measure temperature elevation.
- 4- After waiting time, a residual discharge at C/5
- 5- Then the charge at C/5 and discharge at 4C was reproduce a second time with residual discharge at C/5.
- 6- Then a series of cycling with increase charge rate (C, 2C, 3C and 3C) with slow discharge at C/5.
- 7- Finally, a discharge at 4C following by residual discharge



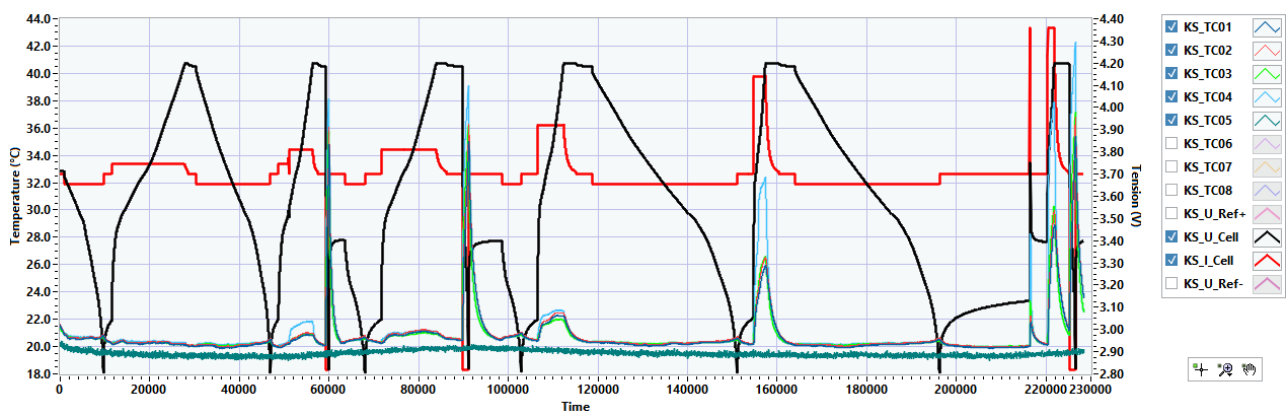


Figure 117 : Cycling test perform during the ESRF experiment on the ESRF-08 sample

## Long term ageing of LIFUN cell with OF/LumT sensors

In order to study the long-term ageing of OF/LumT sensor in high C-rate condition, we decide to perform cycling test of one of instrumented cell used for ESRF experiment during the collaboration with BIG-MAP project. The test protocol is detailed in the Deliverable D3.3, however, a brief description would be that after residual discharge a first checkup at low C-rate (C/5 and C/10) was applied to measure the initial capacity of the cell. Then charge at 2C and discharge at 4C was applied during 150 cycles. The final checkup was the same as the initial checkup to measure the degradation of the cell performances. An overview of the cycling and data harvested is presented in Figure 118. We can conclude on the very good stability of the OF/LumT sensor in high C-rate cycling condition and at high temperature.

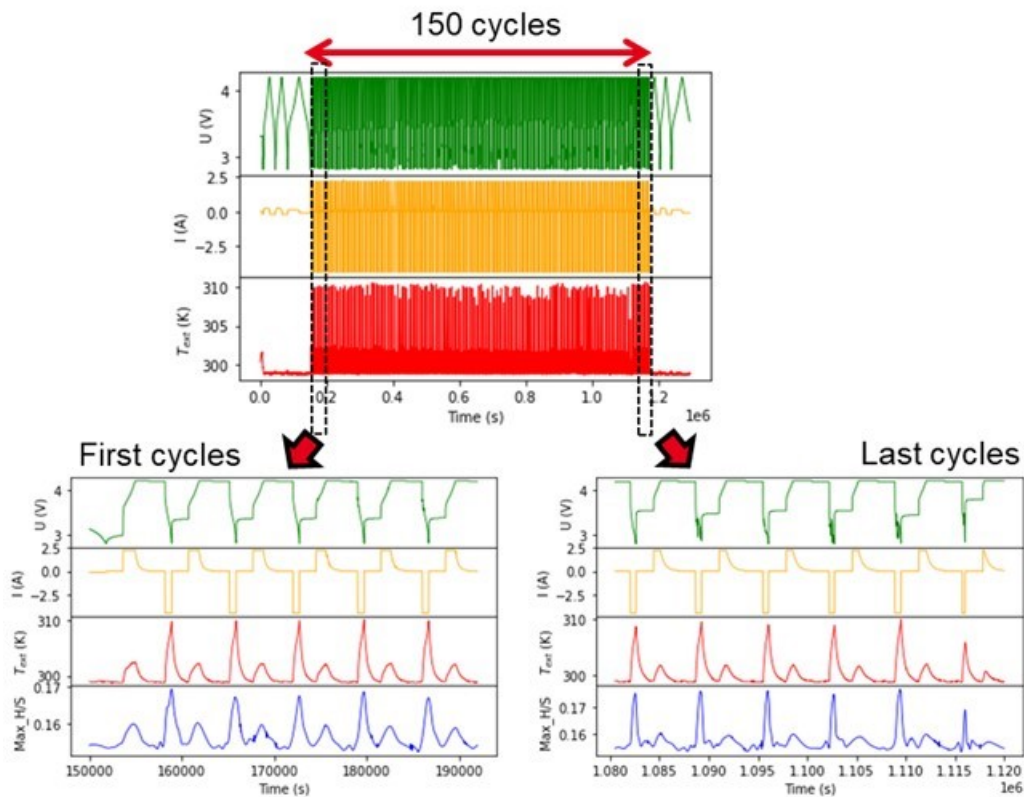


Figure 118 : Ageing of ESRF-08 at 2C (charge) - 4C (Discharge). Variation of the cell potential, cell current, surface temperature and Luminescence ratio from the OF/LumT sensor.

## • Lithium sulfur concentration measurements in LSB batteries

We explored the capability of operando chemical dynamics/states testing of LSBs by putting a 2 mm thick, 12.8 mm diameter polyether ether ketone (PEEK) ring (such that a 1 cm long TFBG can pass through) in the middle of the Swagelok assembly to separate the cathode (sulfur and Super P carbon composite (60/40 wt.%) and anode (lithium). By doing so, the cladding modes of TFBG enable to test the sulfur concentration evolution stemming from generated polysulfide species during cycling (Figure 119a, b) while simultaneously deploying in operando XRD to track the phase transition of the composite electrode (Figure 119). At the upper voltage plateau around 2.4 V, the highest sulfur concentration in the electrolyte was monitored (left panel of Figure 119c) and found to be accompanied by a decrease in the sulfur peak intensity (XRD pattern) resulting from a series of phase transformations, i.e., from solid sulfur to soluble intermediate polysulfides. On the other hand, when the carbonate-based electrolyte was used as a reference (i.e., LP30, right panel of Figure 119c), no concentration gradient was observed in the electrolyte and remained nearly stable due to the fact that no soluble polysulfide intermediates were formed. Instead, this resulted in the formation of insoluble and undetected products, since it is known that there is a nucleophilic reaction between sulfur radical and ethylene carbonate of LP30 to form thiocarbonate-like solid electrolyte interphase. Turning to the lower voltage plateau around 2.1 V, the concentration of dissolved sulfur decreases as a result of the reduction of long-chain polysulfide into shorter chains, leading to insoluble  $\text{Li}_2\text{S}$  compound in the cathode and verified by XRD. Upon charging, the sulfur concentration indicates reversible recovery consistent with the decay of  $\text{Li}_2\text{S}$  peaks until complete disappearance at the voltage  $\sim 2.4$  V, where crystallization of sulfur starts and thus sulfur concentration in electrolyte drops again, even though the deposited solid sulfur in the cathode is featureless by XRD.

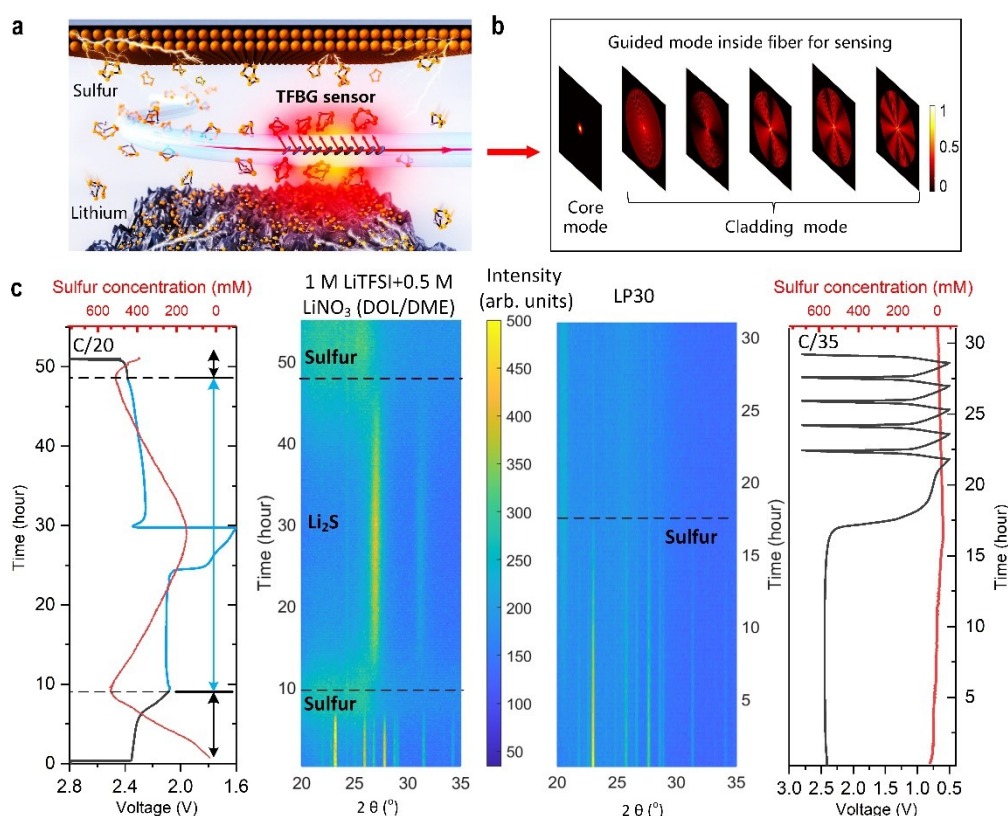


Figure 119 : a) Schematic of a fiber optic sensor immersed in electrolyte for in-situ detection of sulfur concentration originating from the generated dissolved polysulfide and their transport activities (i.e., shuttle effect). b) Backward-propagation guided modes inside fiber for sensing. c) Decoding electrolyte sulfur concentration dynamic of LSB by TFBS and XRD at C/20 (0.275 mA, left panel: polysulfide dissolution allowed (electrolyte of 1 M LiTFSI, 0.5 M LiNO<sub>3</sub> in DOL/DME (1:1, v/v)); right panel: polysulfide dissolution prohibited (electrolyte of LP30: 1 M LiPF<sub>6</sub> in EC/DMC) of sulfur and Super P carbon composite (60/40 wt.%) electrode.

By using TFBGs sensors via the monitoring of both temperature and refractive index metrics, electrolyte-electrode coupled changes that fundamentally control lithium sulfur batteries has been well tracked. Through quantitative sensing of the sulfur concentration in the electrolyte, we demonstrate that the nucleation pathway and crystallization of Li<sub>2</sub>S and sulfur govern the cycling performance, With this technique, a critical milestone is achieved, not only towards developing chemistry-wise cells (in terms of smart battery sensing leading to improved safety and health diagnostics), but further towards demonstrating that the coupling of sensing and cycling can revitalize known cell chemistries and break open new directions for their development. More information can be found in the latest paper of Fu Liu et al.<sup>18</sup>

Table 20. *List of deliverables WP3*

Deliverable Number	Deliverable Title	Lead beneficiary	Type	Dissemination level	Due date (in month)	Status
D3.1	Report electrochemical test results of instrumented cells	1-CEA	Report	Public	24	Submitted
D3.2	Report on the correlation between physical/virtual sensor outputs and the identified physicochemical phenomena of the Li-ion batteries - V1	3-CNRS	Report	Public	24	Submitted
D3.3	Report on the correlation between physical/virtual sensor outputs and the identified physicochemical phenomena of the Li-ion batteries - V2	3-CNRS	Report	Confidential	32	Submitted

Table 21. *Relevant Milestones associate to WP3*

Milestone Number	Milesstone Title	Lead beneficiary	Due date (in month)	Status
MS6	Correlation of at least one output signal from each sensor to a physico-chemical phenomenon of the Li-ion cell	3 – CNRS	32	Achieved with D33

<sup>18</sup> Liu, F., Lu, W., Huang, J. *et al.* Detangling electrolyte chemical dynamics in lithium sulfur batteries by operando monitoring with optical resonance combs. *Nat Commun* **14**, 7350 (2023). <https://doi.org/10.1038/s41467-023-43110-8>

## WP4 - Development of virtual sensors and BMS SoX indicators algorithms

Work package number	4	Leader	INSA					
Work package title	Development of virtual sensors and BMS SoX indicators algorithms							
Short name of participant	FAURECIA	CEA	UAVR	INSA				
Person months per participant	5	23	12	35				
Start month	M1			End month		M36		

### Objectives

The aim of WP4 is to develop virtual sensors and BMS SoX indicators algorithms. The main objectives of this WP are the following:

- Develop numerical electro-chemical and thermal models and algorithms suitable for reference simulations (version 1 in D4.2, D4.3, D4.4 and version 2 D4.7, D4.8, D4.9);
- Reduce the models and develop virtual sensors (E-BASE and T-BASE) for electro-chemical and thermal physics-based models (D4.1, D4.5 and D4.6);
- Provide real-time SoX cell indicators estimation (D4.10);
- Provide real-time algorithms able to reconstruct the desired variables precisely enough at high charge/discharge rates and under different temperature conditions (D4.11).

### Highlights of most significant results

The two main aspects of WP4 concern the development and exploitation (Task 4.1 and Tasks 4.2 and 4.3, respectively) of numerical models of the battery cell. Task 4.1 develops both electrochemical and thermal models for the battery cell, Task 4.2 exploits reduced-order models to reconstruct in real-time the internal state of the battery cell (i.e., develops virtual sensors for the system) and Task 4.3 utilizes the information provided by the physical and virtual sensors in the cell to obtain SoX indicators that inform the charge and discharge of the cell.

The results obtained in Task 4.1 the development and update of electrochemical and thermal models for the battery cell used in this project (D4.2, D4.3 and D4.4 then updated in D4.8, D4.9 and D4.10, respectively). In particular:

- **An electrode (1D+1D) model based on Newman's porous electrode theory** has been developed by the CEA and fully parametrized based on available literature and material properties provided by VARTA, as well as fitting based on experimental data on the battery cell with VARTA materials. This electrode model, implemented in COMSOL, is freely accessible to the partners in the consortium, to validate reduced order models in task 4.2. In the second half of the project, this model has been updated based on experimental data available for the single-layer cell with VARTA materials.
- **A pseudo-3D (p3D) model of the cell** that solves both electrochemical and thermal equations in the different domains (positive and negative electrodes as well as separator) has also been developed by the CEA. As is the case with the 1D+1D model, this model has also been implemented using COMSOL and is accessible to INSTABAT partners for the validation of the electrochemical and thermal behaviour of the cell, for task 4.2. During the second half of the project, this model has been updated based on experimental data collected for single-layer cells with VARTA materials.
- **A 3D thermal model of the cell** has been developed by Faurecia and runs using a MATLAB® script. This model has been parametrized using project data as well as available data from the literature. The simulation is parametrizable with different cell dimensions/thermal properties/boundary conditions/electrical properties. The first simulations aim to reproduce the behaviour of the pouch cells used in the project, in both adiabatic and free convection. In the second half of this project, this model has been updated.

The results obtained in Task 4.2 concern the development of reduced-order models and estimator design for the real-time reconstruction of internal variables, which will then be available to the BMS algorithms (D4.1, D4.5 and D4.6). The models and estimation algorithms concerned are:

- **A reduced electrochemical electrode-electrolyte model** developed by INSA Lyon (D4.1, D4.5 and D4.6) for state estimation purposes. This electrode model is based on a finite-volume scheme specifically developed for

the project, considering the transport coefficient and porosity discontinuities at the interfaces of the different battery domains. This model, presented in D4.6, has been validated against the reference (1D+1D) model presented by the CEA in some charge/discharge scenarios. An updated version has been validated using single-layer cells with Varta materials cycling in CCCV and WLTP cycles at 25°C. Since two different cells were cycled in these conditions, one of the cells was used for the calibration of the model (using only the first discharge available in the CCCV profile data) and then cross-validated using the full CCCV and WLTP cycles in both cells.

- **An electrochemical “virtual sensor” (E-Base)** based on the reduced electrochemical model, developed and updated by INSA Lyon (D4.1, D4.5, D4.6). This estimation structure allows some modularity (depending on the available physical measurements). It can consider as inputs current and voltage to the battery cell, as well as thermal information, Li<sup>+</sup> concentration in the electrolyte and reference electrode information. A more detailed presentation of this is available in deliverable D4.6. An updated version has been validated using single-layer cells with Varta materials cycling in CCCV and WLTP cycles at 25°C. This updated version has also been compiled and integrated into the experimental interface.
- **A reduced (2D) thermal model** developed by UA based on an ANSYS-Fluent battery module with a Multi-Scale Multi-Dimensional model (not considering the microstructure of the battery). This model includes the solution of heat flux equations, as well as electrical field solution, as well as a simplified semi-empirical Newman-Tiedemann-Gu-Kim (NTGK) model parametrized based on experimental data and parameter estimation tools.
- **An electrochemical “virtual sensor” (T-Base)** developed by UA (D4.5, D4.6) in the second half of the project has been presented in D4.6, based on a simplified thermal model presented in D4.5. This virtual sensor uses particle filtering for simultaneous SOC and Temperature estimation. This algorithm has also been integrated into the experimental platform.

#### **Summary of progress towards objectives and details for each task**

### **TASK 4.1 ELECTRO-CHEMICAL AND THERMAL MODELLING AND SIMULATION**

(Leader: CEA; Participants: FAURECIA, INSA, UAVR) (M1-M18; M24-M29)

Task 4.1 is concerned with the development, implementation, and parametrization of reference numerical models of the different phenomena involved in the battery. In this section we will present some results of the different models developed in this task.

- **Electrode (1D+1D) model (D4.2)**

The results of this sub-task consist of the development of a demonstrator version of a 1D+1D porous electrode (Newman) Model using COMSOL (D4.2 and D4.7). A Newman model consists of charge and mass conservation equations in both a liquid and a solid phase in 3 distinct domains, corresponding to the two electrodes and the separator region in the battery. A kinetic model for reaction rates at the particle-electrolyte interfaces is also included in the model. Both the solid and liquid phases are restricted to a 1D representation (thus the 1D+1D model designation). The modelled transport takes place along the thickness of the battery (for the electrolyte) and along the radial direction (for the electrode material particles). The particles in the active material are assumed spherical in this model (although variants with cylindrical particles exist).

By using this 1D+1D model, it is possible to simulate the potential of the lithium-ion battery and predict the cell capacity. Furthermore, internal variables are available in the model, such as local potentials, local lithium concentration, intercalation current, etc.

One of the main difficulties of the model developed here consists of the full parametrization of the Newman model, which requires good knowledge of the materials and the geometry of the cell. The main result of this subtask is, then, a fully parametrized Newman electrode model of the battery based on available properties in the literature, as well as information provided by INSTABAT partners, notably VARTA, for the cell used in the project. This model has further been tuned and validated by comparison to experimental results from WP2 in constant-current charge and discharge scenarios going from 0.1C to 2C charge/discharge rate. The comparisons show good accuracy, as shown in Deliverable D4.7.



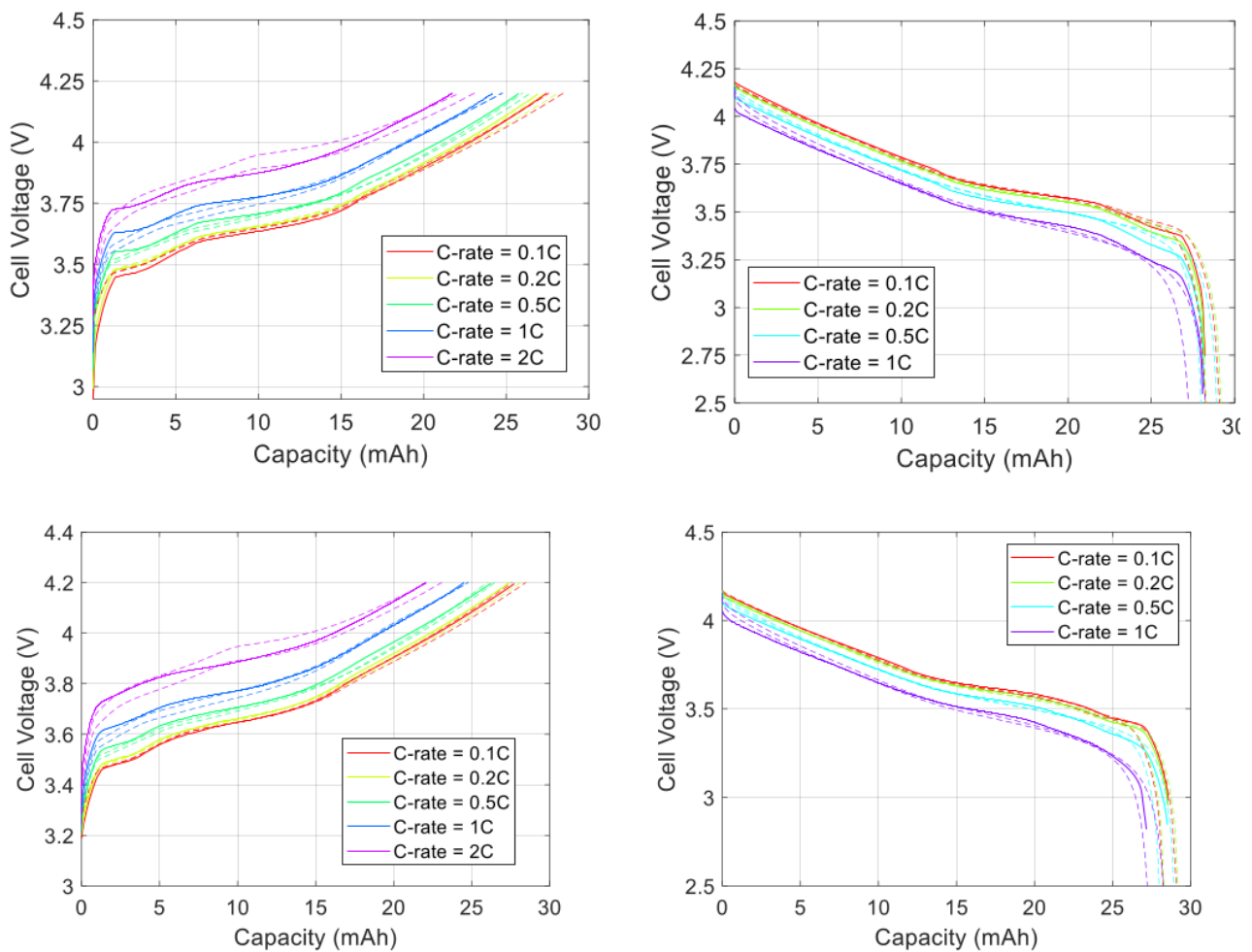


Figure 120: Comparison between experimental curve (dash line) and simulated curve (solid line) for galvanostatic charges (left) and discharges (right) at 25°C, in pouch cell configuration, with the V1 model (top) and with V2 model (bottom).

- **Pseudo-3D (p3D) model of the cell (D4.3)**

The result of this consists of a demonstrator code developed by the CEA and available to INSTABAT partners that implements, using COMSOL, a p3D model of the battery cell (D4.3 and D4.8). This demonstrator allows the validation and development of reduced order models, such as the electrochemical and thermal models developed in task 4.2.

The main addition in the p3D model of the cell, developed as well by the CEA, is the inclusion of in-plane heterogeneities along the cell plane (which are neglected in the 1D+1D model). As is the case of the 1D+1D model, the main challenge consists of the full parametrization of the model. In this case, the parametrization is done using the data of the 1D+1D model, which includes all the necessary transport parameters, except for those concerning the geometry and thermal characteristics of the p3D cell. The main difference in the phenomena modelled in this p3D model with respect to the 1D+1D model includes the in-plane transport of Li ions in the electrolyte phase, as well as a thermal model that was not included in the electrode model. The updated p3D model is presented in D4.8.

Besides the electrochemical information obtained with the p3D model (analogous that obtained with the 1D+1D model, except for the in-plane heterogeneities), this model provides thermal information on the cell, as seen in the next Figure.

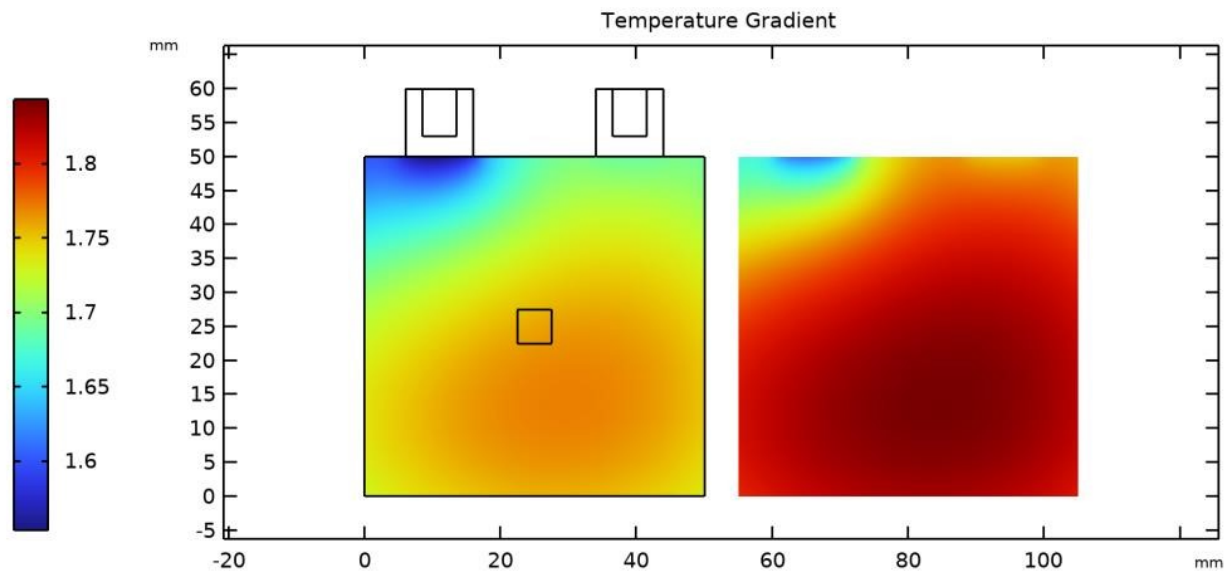


Figure 121: Simulation result: 1C charge at -10°C. Temperature gradient at the end of the charge along the electrodes for the layer in contact with the casing (left) and for the central layer of the stack (right). This is the updated P3D model provided by CEA.

- **3D thermal model of the cell (D4.4)**

The main result in this subtask consists of the development of a parametrized 3D thermal model of a battery cell developed and updated by VARTA (D4.4, D4.9). In this case, the model is run using a MATLAB® script that can be parametrized according to the specific cell geometries and thermal characteristics. Unlike the p3D model previously presented, this includes more specific material properties, as well as a full 3D heat transfer model. As was the case in the previous models, the main difficulty consists of fully parametrizing such a model. This was done based on available material properties from the literature and adapted to the INSTABAT pouch cell under consideration.

Unlike the other models in this Task, this is a purely thermal model, based on a thermal diffusion model with parametrizable boundary conditions representing different scenarios, such as adiabatic conditions or operation with cooling on a particular boundary.

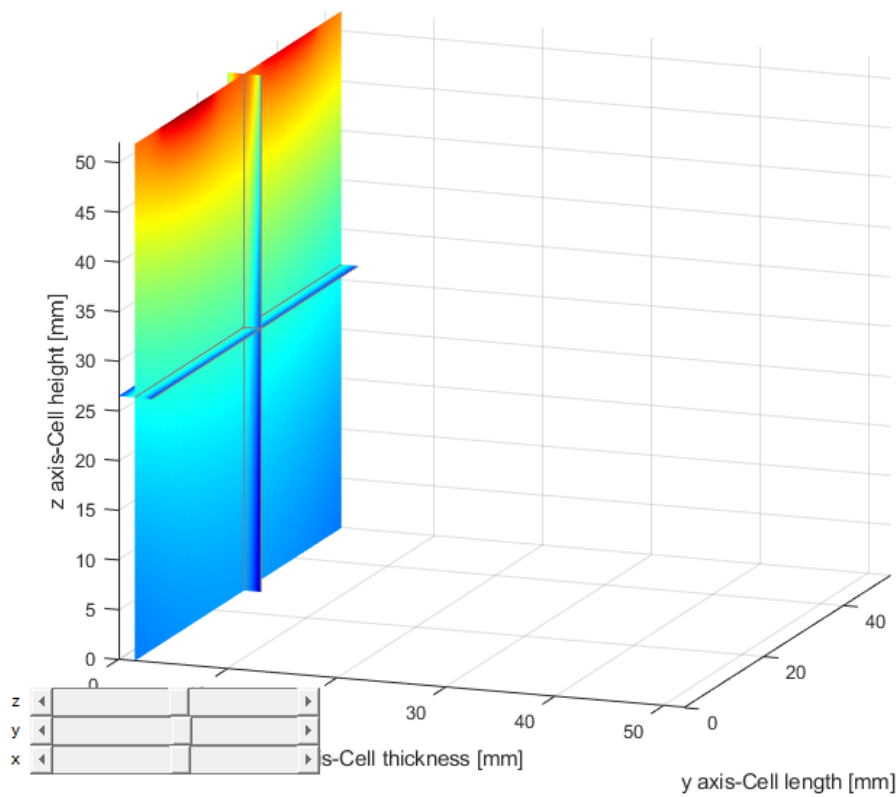
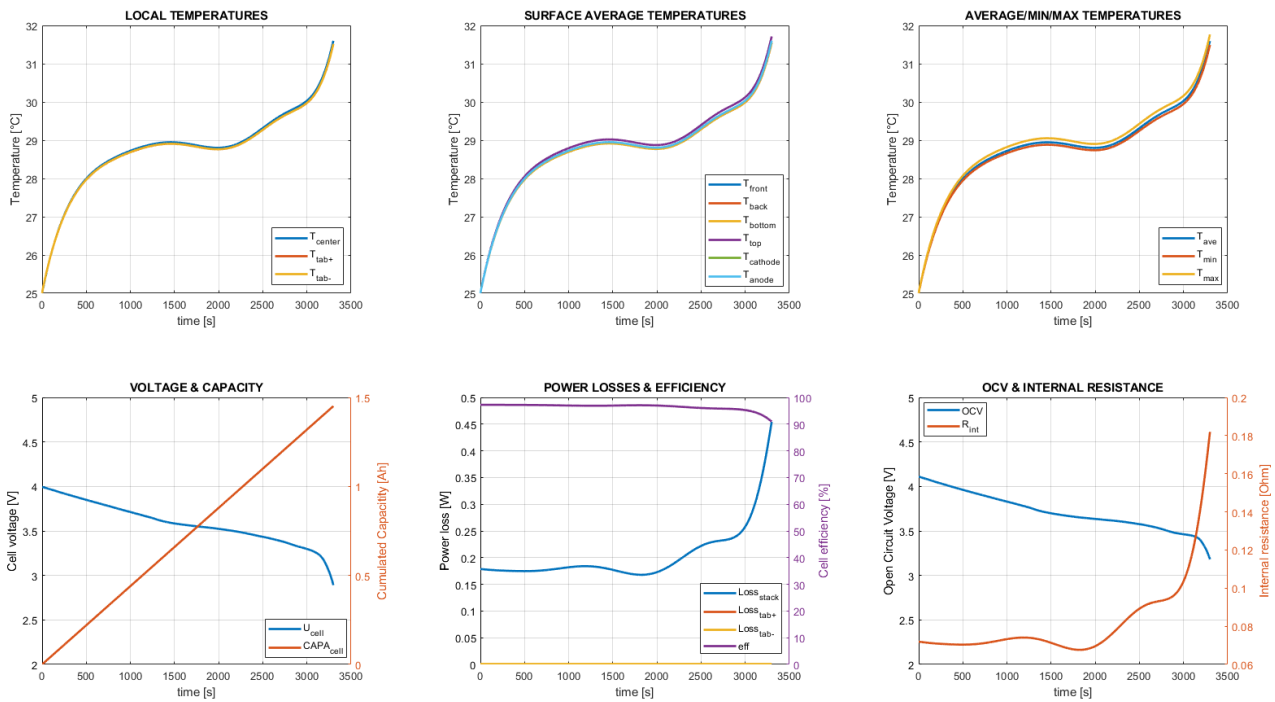


Figure 122: Example of thermal information obtained from the updated 3D model (D4.9) of a sample cell for a 1C constant-current discharge profile at 25°C.

## TASK 4.2 VIRTUAL SENSORS DEVELOPMENT AND IN SILICO TEST

(Leader: INSA; Participants: UAVR, CEA) (M1-M29)

### • Reduced Electrochemical electrode-electrolyte model and E-BASE virtual sensor

The main result in this subtask is the development of a reduced electrode-electrolyte model based on the 1D+1D model developed in task 4.1 and oriented towards the development of real-time reconstruction of internal electrochemical states. The main challenge of this reduced-order model consists of obtaining a modular design where the compromise between model complexity and execution time can be chosen depending on the needs of real-time execution and available resources.

A finite-volume based model reduction, using MATLAB and specifically developed polynomial interpolants was developed to obtain fast and accurate representation of the system. An example showcasing the modularity of the approach is shown in the figure below. All the phenomena in the Newman model can be included (or excluded) from the reduced order model based on the complexity requirements. For instance, a fast simulation (around 5ms per second of real-time) can be obtained by neglecting lithiation heterogeneity in the solid phase.

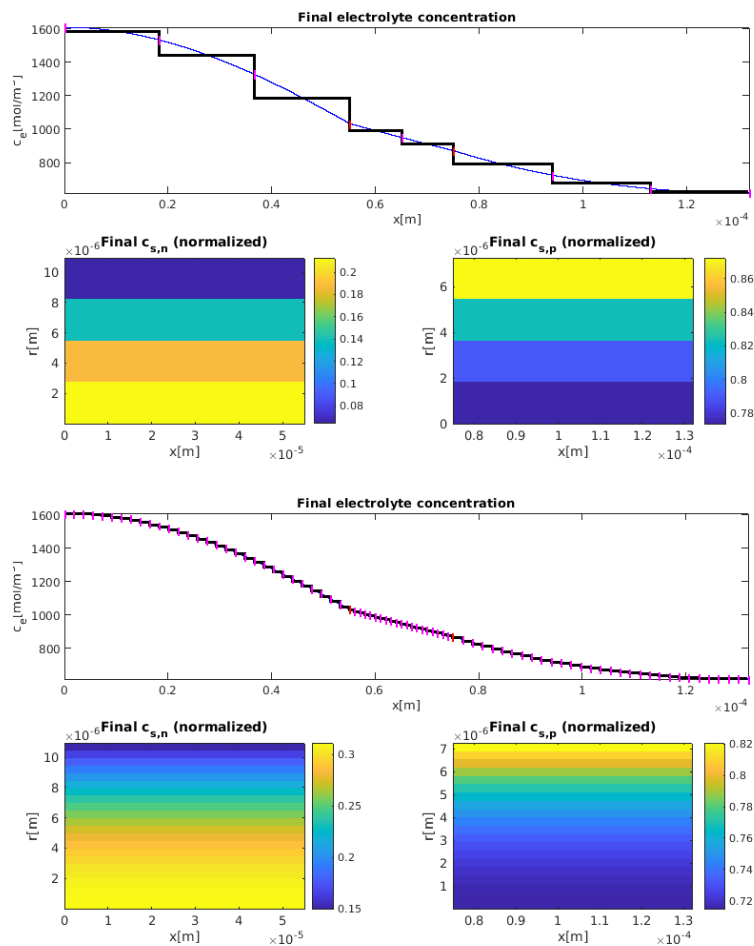


Figure 123: Example of electrochemical information obtained from the reduced order model of a sample cell for a constant-current discharge profile with very low complexity model (left) and high-resolution model (right). In this case, the lithiation heterogeneities are neglected to reduce the computational cost, and a second of simulation in the low complexity model can be simulated in 5ms on average.

A full simulation, including lithiation heterogeneities and providing a full reconstruction of the internal potentials can still be done in approximately 70ms of simulation per second of real-time.

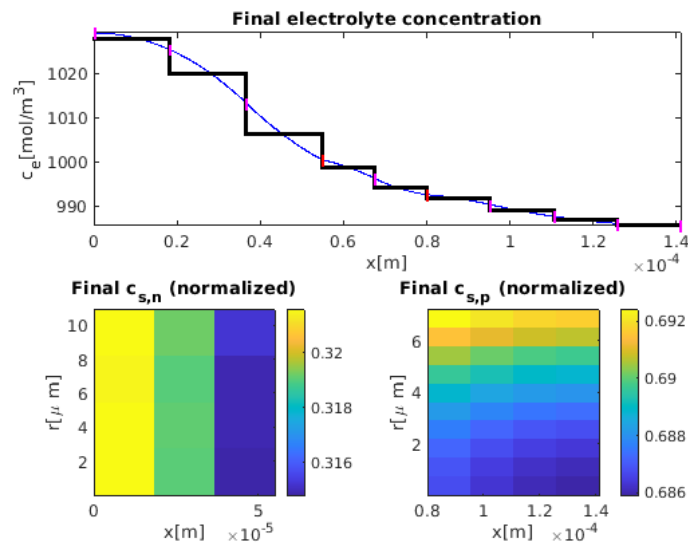


Figure 124: Example of electrochemical information obtained from the reduced order model of a sample from a WLTP cycle at 25°C with experimental data, including heterogeneities in lithiation. A second of simulation in this, more complete model, can be run in approximately 70-80ms on average.

Furthermore, this model has been implemented in such a way as to be able to generate C code and compile to generate a DLL library for integration with WP5. It should be noted that the version integrated into the experimental platform for WP5 does not include the information from the Li-concentration sensor, which is not available at this time. This model was then integrated into a state estimation scheme (E-BASE) detailed in deliverables D4.1, D4.5 and D4.6, and represented schematically in the next figure:

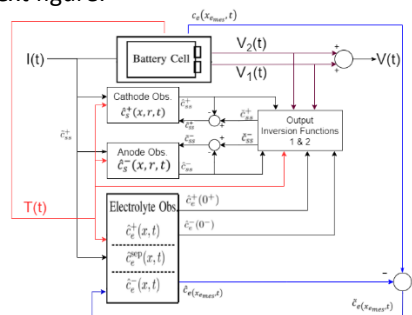


Figure 125: Block diagram of the observer with inclusion of Temperature, Feedback Injection and Reference electrode

- **Reduced 2D and 0D thermal models and thermal virtual sensor (T-BASE)**

The main result in this subtask during the first half of the project was the development by University of Aveiro of a 2D simulation model using ANSYS Fluent battery modules and the parametrization of a Semi-empirical Newman, Tiedemann, Gu and Kim (NTGK) model where the coefficients are identified using experimental data. The model requires the reconstruction of the electric field inside the battery (or electric potential) and uses Arrhenius-type dependencies on the kinetic parameters. An energy conservation equation solved in the domain is used to estimate the heat exchanges and evolution.

The proposed reduction and parameter identification methods were tested based on experimental data using a commercial cell and an example of the available information provided by this model is presented in the following figure:



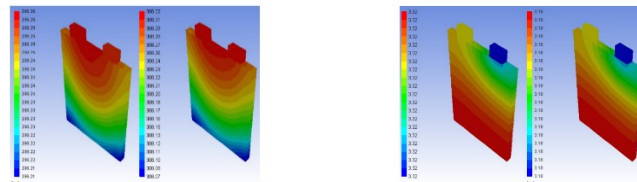


Figure 126: Sample results of the simplified 2D thermal model for different discharge rates. Temperatures on left figure, positive potential on the right figure.

During the second half of the project (D4.5, D4.6). A reduced 0D thermal model was developed by University of Aveiro based on a discrete-time model of the system and a particle filtering approach. This algorithm allows the simultaneous estimation of SOC and temperature on the system. A schematic representation of this algorithm is shown in the next figure.

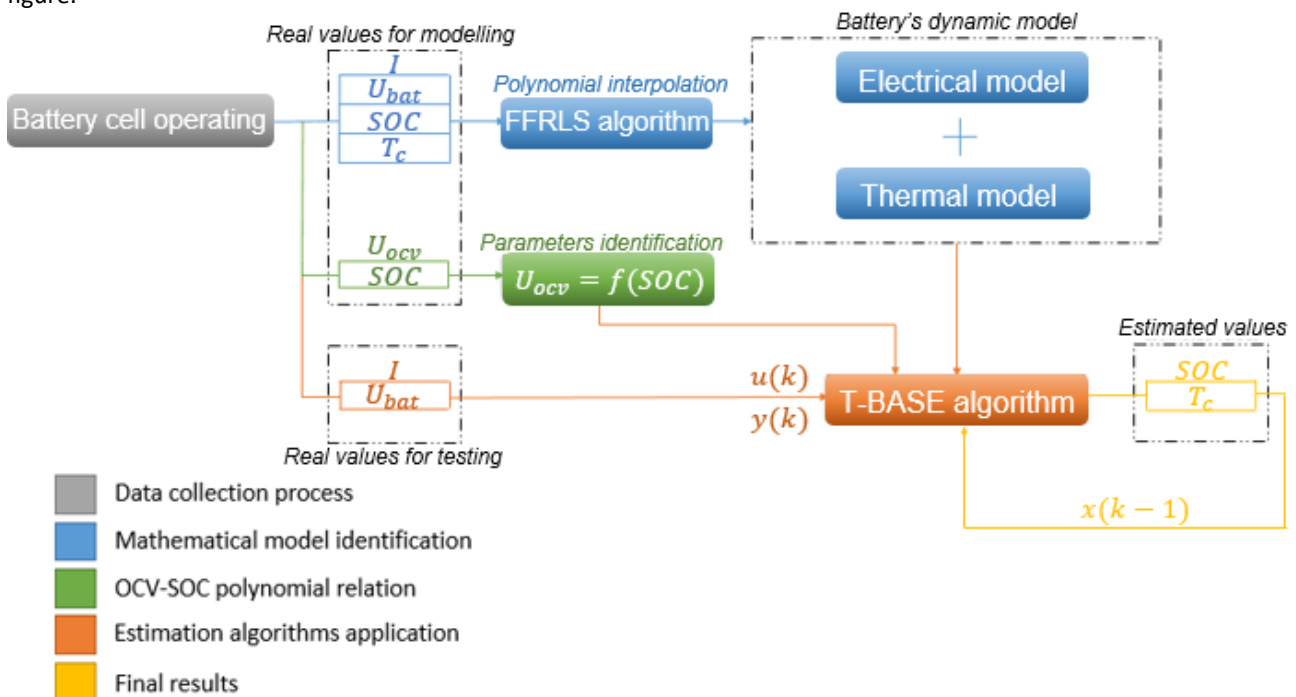


Figure 127: Schematic representation of T-BASE thermal estimation algorithm (in orange), based on a 0-D discrete-time model (in blue) and identification of OCV curve parameters (in green).

## TASK 4.3 DESIGN OF STATE OF CHARGE, HEALTH, POWER, ENERGY AND SAFETY CELL INDICATORS ALGORITHMS

(Leader: CEA) (M23-M36)

Task 4.3 concerns the development of SoX indicators using information from the available sensors in the INSTABAT project. The main work in this work package consisted of developing concepts for State of Charge (SoC), State of Power (SoP) and State of Health (SoH) estimators that exploit the new information available in this project. A strong interconnection between these indicators and the virtual sensors developed in Task 4.2. More details can be found on Deliverables D4.10 and D4.11.

The main proposed structure for SoC and SoP estimators integrates the E-BASE reduced model and a closed loop observer as depicted in the following figure:

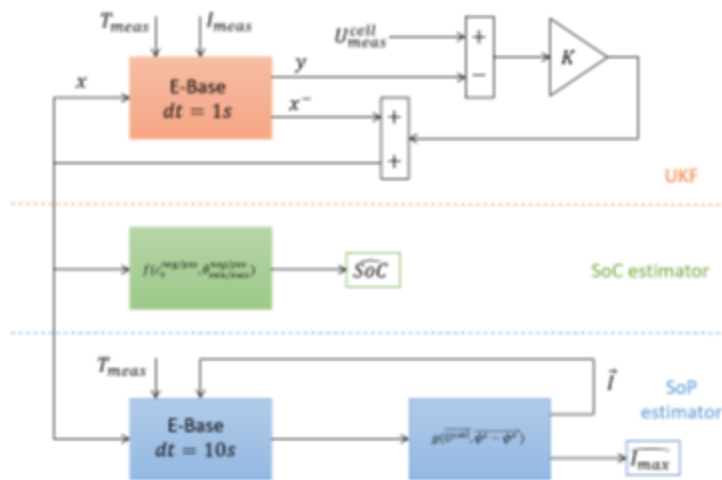


Figure 128: Schematic representation of the integration of E-BASE models and virtual sensor in the development of SoC and SoP estimators based on Unscented Kalman Filtering

One of the novel results is that, by integrating electrochemical information, SoP indicators can integrate Li-plating constraints and not only absolute voltage limits. This is illustrated in the next Figure.

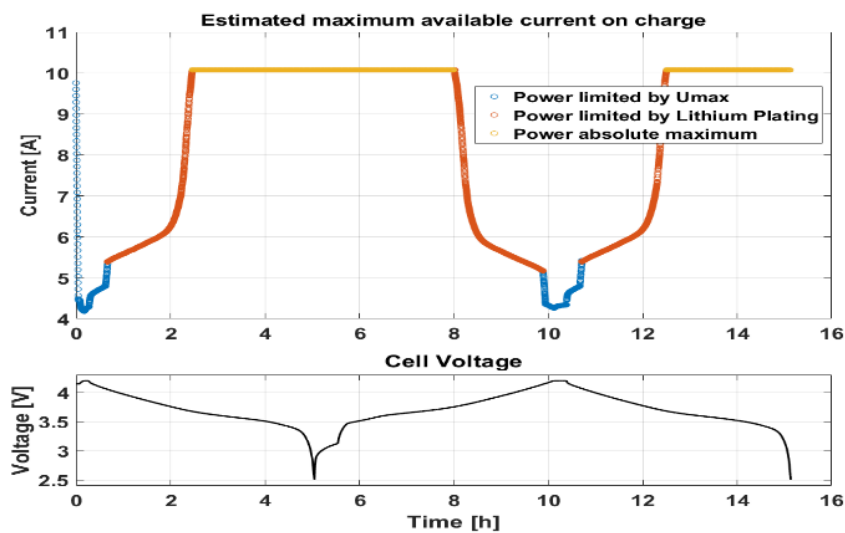


Figure 129: SoP information integrating electrochemical data which allows for limitations based on risk of Li-plating

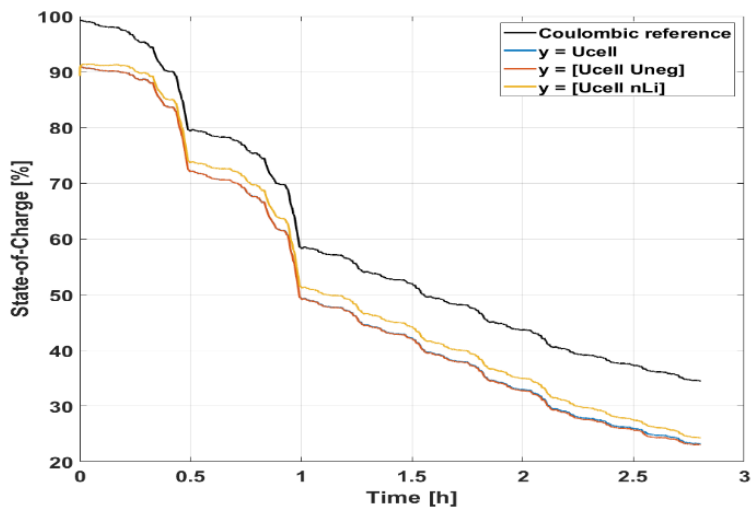


Figure 130: SOC estimation integrating Li-concentration information from the electrochemical model

For State of Health estimation, a first approach using electrochemical information relies on the use of total amounts of cyclable Li estimation. The principle is presented in the next figure:

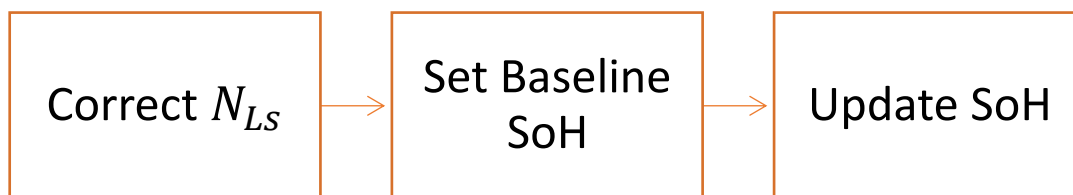


Figure 131: Principle of Electrochemical information for SoH estimation (In particular moles of cyclable Li available)

Table 22. *List of deliverables WP4*

Deliverable Number	Deliverable Title	Lead beneficiary	Type	Dissemination level	Original Due date (in months)	Status
D4.1	Report on generic structure of electrochemical virtual sensor algorithm	6-INSA LYON	Report	Confidential	12	Submitted
D4.2	Version 1.0 of the 1D+1D electrode model	1-CEA	Demonstrator	Confidential	18	Submitted
D4.3	Version 1.0 of the p3D cell model	1-CEA	Demonstrator	Confidential	18	Submitted
D4.4	Version 1.0 of the 3D thermal cell model	4-FAURECIA	Demonstrator	Confidential	18	Submitted
D4.5	Report on temperature dependent electrochemical virtual sensor algorithm (E-BASE and T-BASE)	6-INSA LYON	Report	Public	24+4	Submitted
D4.6	Report on adapted electro-chemical/thermal virtual sensor algorithms compatible with BMS	6-INSA LYON	Report	Public	29+4	Submitted
D4.7	Version 2.0 of the 1D+1D electrode model	1-CEA	Demonstrator	Confidential	29+4	Submitted
D4.8	Version 2.0 of the p3D cell model	1-CEA	Demonstrator	Confidential	29+4	Submitted
D4.9	Version 2.0 of the 3D thermal cell model	4-FAURECIA	Demonstrator	Confidential	29+4	Submitted
D4.10	Preliminary design report of BMS SoX indicators algorithms architecture	1-CEA	Report	Confidential	24+4	Submitted
D4.11	Final design report of BMS SoX indicators algorithms architecture	1-CEA	Report	Confidential	29+4	Submitted
D4.12	Performance analysis report on the BMS SoX estimation algorithms	1-CEA	Report	Public	36+4	Submitted



Table 23. *Relevant Milestones associate to WP4*

Milestone Number	Milestone Title	Lead beneficiary	Due date (in month)	Status
MS2	Coupled electro-chemical and thermal models for state estimation (virtual sensing) ready for validation	6 - INSA LYON	12	Submitted
MS4	BMS SoX algorithms and virtual sensors ready	6 - INSA LYON	29	Algorithms integrated into BMS and Platform -> Validate
MS7	Performances of “lab-on-a-cell” platform available	1 - CEA	36+4	Validate by the last experiment in December 2023 and deliverable D412



## WP5 - Proof of concept multi-sensor platform

Work package number	5	Leader	CEA						
Work package title	Proof of concept multi-sensor platform								
Short name of participant	UAVR	CNRS	IFAG	FAURECIA	VMI	INSA	CEA		
Person months per participant	10	9	4	1.5	9	4	13		
Start month	M4			End month			M36		

### Objectives

The objective of WP5 is the implementation of a proof of concept of the multi-sensor platform. The main objectives of this WP are the following:

- Integrate successfully the sensors into the cell prototype;
- Develop a functional proof of concept of the multi-sensor platform that, combined with appropriate BMS, is able to improve the accuracy of the SoX cell indicators.

### Highlights of most significant results

An accurate and reliable knowledge of the operando key parameters of a Li-ion battery is essential to its optimal use, safety and extended lifespan. The WP5 must use and combine previous WPs results to achieve the implementation of a proof of concept of the multi-sensor platform. First, the knowledge acquired in the WP2 will help for integrating each innovative sensor into an instrumented prototyped cell.

A multi-physics instrumentation platform is necessary to exploit the signals of these sensors and to analyse and process them in real time. Indeed, the INSTABAT multi-sensor platform not only acquire signals from various sensors developed in WP2 but also embed models and algorithms developed in WP4 thanks to WP3 characterization results and finally record all the produced data (raw and processed). Models and algorithms use cross information obtained from different sensors but corresponding to a common phenomenon, which enrich the correlation analysis with the physico-chemical phenomena happening inside the cell.

During the second part of the project, the platform built has been achieved and the cell prototypes manufactured. The lab-scale tests on the assembled test bench with multi-instrumented cell has been done during the last 4 month of the project. Two types of tests was planned, standard cycle based on EV use cases and abusive test. First type is used to evaluate the behaviour of the prototype cell during classical operating conditions and during limited stresses (cycling at extreme conditions and high-power) in an EV context. Abusive tests are used to find out if the innovative sensors can provide early detection of hazardous events or if, on the contrary, they damage the cell.

The database collected by the platform is required to analyse the relevance of physical/virtual sensors by correlating them with internal electro-chemical phenomena but also by evaluating the impact on the performance of BMS and safety indicators.

In the previous description, much of the activities are closely linked to the tasks performed in the other WPs. However, during this first half of the INSTABAT project, we have worked hard to ensure that we will properly interface and integrate outcomes from previous work packages. To this end, the work undertaken last year has consisted of:

- keeping a strong link with sensors developers in WP2 to take into account integration techniques and requirements for Li-ion battery cell
- specifying the sensors interfaces and the required instruments to access measurements
- specifying a way to interface the processing of algorithms and models
- building the platform hardware/software architecture to acquire, process and store signals and data
- Validating platform hardware/software components integration step by step

This preparatory work led to the realization of instrumented cells (with 2 INSTABAT sensors) and a Beta version of the multi-sensor platform that we were able to use during a campaign of characterization tests under X-rays at the ESRF to follow in situ and operando behaviour of Li-ion cells.

The major part of the work for the WP5 has been done during the second part of the project. The integration of all the sensors (physical and virtual) and the SoX indicator has been achieve. Multi-instrumented cells equipped with a simultaneous integration of two physical sensors: RE and FOLum-T has been combined with the platform. The “lab-on-

cell” has been tested on standard a multi-instrumented cells in abuse condition to measure the impact of sensors to the safety of the cell. We haven’t observed any negative impact of the sensors on the safety behaviour.

The performance of the multisensor platform was also tested and validate at the end of the project by testing cell at high C-rate. However, due to the shorter time and the reduce number of sample only few experiment have been performed to validate the proof of concept and measuring the improvement of the performances and safety in all condition that we expected. Despite these partial results, we can conclude that the platform is functional and that it is capable of achieving the objectives set out in the project. Proof-of-concept can be considered to have achieved its objectives. The results also demonstrate the versatility of the platform, which is capable of integrating different types of sensors (physical and virtual) as well as advanced management functions. This platform therefore also meets the BATTERY 2030+ roadmap objectives for coupling sensing and self-healing with a fully integration of all the function in the same tools.

The WP5 progress summary is detailed below

*Progress summary towards objectives and details for each task*

## TASK 5.1 CELL PROTOTYPE FABRICATION AND MULTI-SENSOR HARDWARE INTEGRATION

(Leader: CEA; Participants: CNRS, UAVR, VMI, IFAG) (M4-M36)

As a reminder, the goal of this task is to fabricate a prototype cell that simultaneously integrates multiple INSTABAT sensors in a large pouch cell with a capacity target between 0.3 and 4 A.h based on a chemistry used in WP2, to be delivered Month 24.

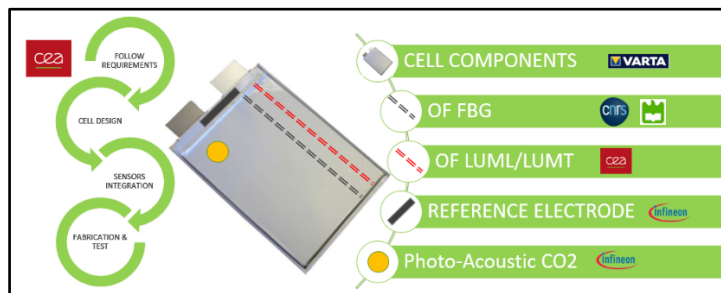


Figure 132: Multi-sensor cell prototype structure

At this time, the work of WP2 is still in progress to optimize sensors integration. VARTA VMI and CEA follow closely WP2 to be ready to transpose the process. However, for the needs of the experiment at ESRF in February 2021, we developed a first prototype of cell which integrated 2 sensors of the project, namely the reference electrode and the thermoluminescence optic fiber. This experiment was planned in collaboration with the BIGMAP project (see Task 7.3). We based our prototype on non-activated commercial LiFun cells used in WP2 which has the NMC-Graphite electrodes couple as targeted in the project. The original cell was disassembled and stacked to obtain a 1.1A.h Li-ion cell equipped with reference electrode and thermoluminescence optic fiber.

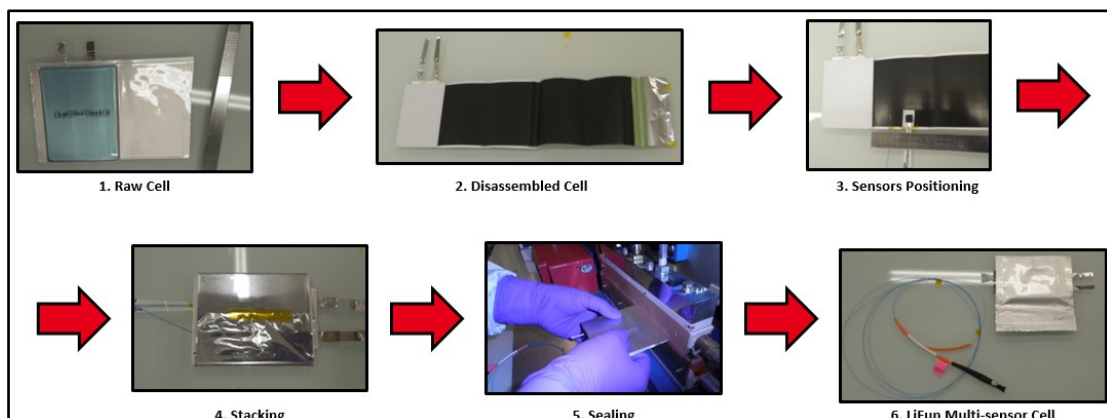


Figure 133: Multi-sensor cell ESRF prototype Process

After activation, we were able to demonstrate that the prototype cell worked even at high speeds without being damaged or disturbed by the integration of sensors and that it had an equivalent nominal capacity over the few cycles of use.

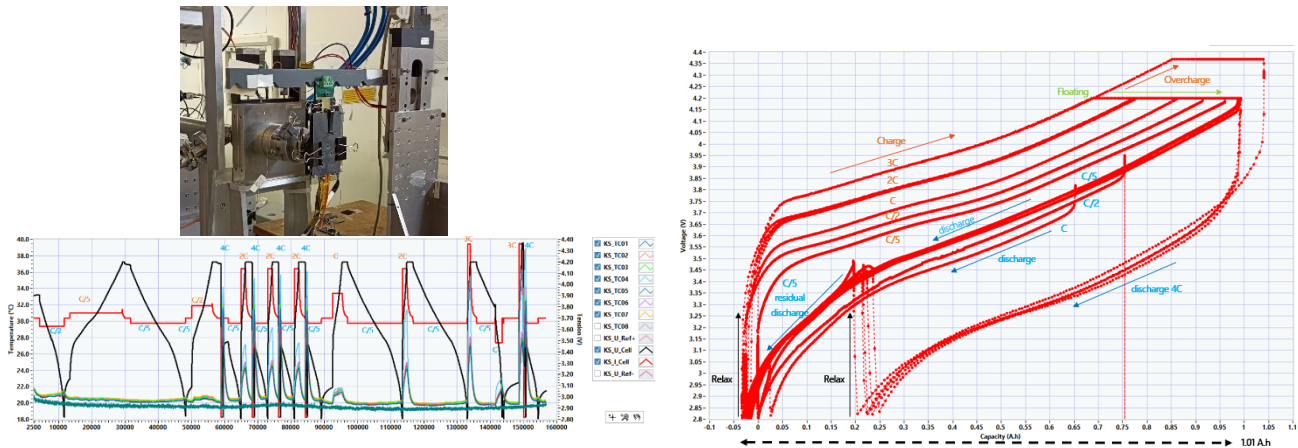


Figure 134: Electrochemical parameters of multi-sensor prototype cell performing cycle during ESRF experiment

During the second part of the project the integration of FO-FBG sensors on the platform was successfully achieved and the platform was used at CEA for testing multi-instrumented cell with FO-LumT, RE and FBG (see WP2 and WP3 paragraph).

Further on, the challenge will be to realize successfully a cell based on the VMI components by adding the Bragg fiber with partner's requirements to have a complete prototype. As we mentioned earlier, reference cell design with these components will be produced and characterized soon (next month) to be compared to the final prototype.

All the sensor hardware was successfully integrated in the platform and tested with instrumented cell or with the hardware equipment associate to sensors.

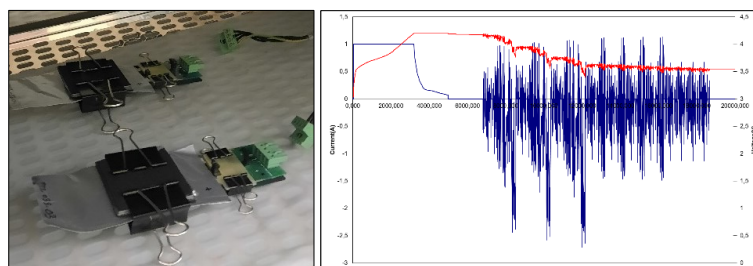
Table 24: Status of sensors development for WP5

Sensor/ Algorithm	Development	Interface	In-operando validation	Status
OF/FBG	OK	OK	OK	Interface with FBG interrogator successful
OF/LUMT	OK	OK	OK	Interface with spectrometer successful / Pre-Processing OK (Calibration required)
OF/LUML	NOK	OK	NOK	Not used but same interface as LUMT
REF Electrode	OK	OK	OK	Interface with voltage measurement device successful
PA CO2	NOK	OK	NOK	Interface by UART communication successful
E-BASE	OK	OK	OK	Interface with automatic generated library (.dll) from Matlab successful
T-BASE	OK	OK	OK	Interface with automatic generated library (.dll) from Matlab successful.
BMS Sensor (U/I/T)	OK	OK	OK	Interface with multimeter measurement device successful
BMS Algorithm	OK	OK	OK	Interface with automatic generated library (.dll) from Matlab successful

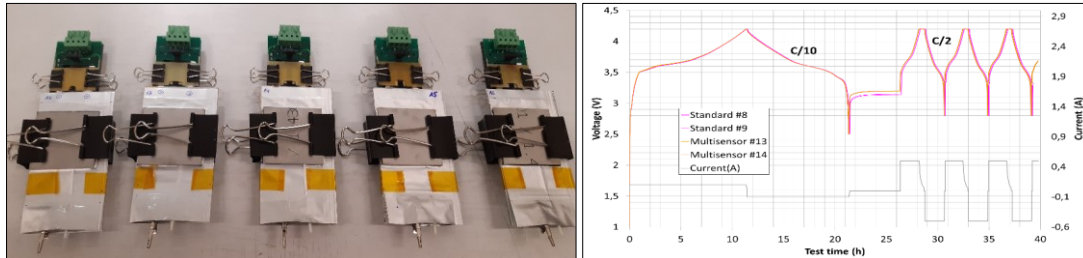
Table 25: Status of sensors for integration into the cells for WP5

Sensor	Integration progress	Status for WP5
OF/FBG	Integration and operation in LiFun /Varta cell	OK for prototype Integration
OF/LUMT	Integration and operation in LiFun /Varta cell	OK for prototype Integration
OF/LUML	Not operable in any battery cell	<b>NOK for prototype Integration</b>
REF Electrode	Integration and operation in LiFun /Varta cell	OK for prototype Integration
PA CO2	Not operable in any battery cell	<b>NOK for prototype Integration</b>

For the WP5 test a series of multi-instrumented cell and standard cell has been manufactured at CEA (see D5.1). Due to the progress of sensor development and the difficulties to integrate the sensors (Table 5), we decide for the demonstration to integrate only two sensors for the test campaign of WP5. A total of 10 operational reference cell without sensor and 8 operational multi-sensor cell with RE and FOTL was made during this task (see Figure 135).



a) Reference cells



b) Multi instrumented cells

Figure 135: Photo and cycling test of cells prepared for WP5 tests: a) reference cells, b) multi-instrumented cell

## TASK 5.2 DATA POST-PROCESSING AND DATA LOGGING

(Leader: IFAG; Participants: CNRS, UAVR, CEA, FAURECIA, INSA) (M4-M36)

### 5.2.1 Platform architecture

#### 5.2.1.1 Hardware

To realize the proof of concept of the multi-sensor platform, it is necessary to find a hardware target able to measure the signals coming from our sensors but also to process them to feed the virtual sensor models and the battery state estimation algorithms. Most of the INSTABAT sensors are of low TRL and require specific non-integrated instrumentation and equipment to acquire their signals. In addition, we did not want to impose strong constraints on algorithm and model developers in terms of computational or memory resources. Consequently, we decided to build a platform based on an instrumentation computer rather than a rapid prototyping target.

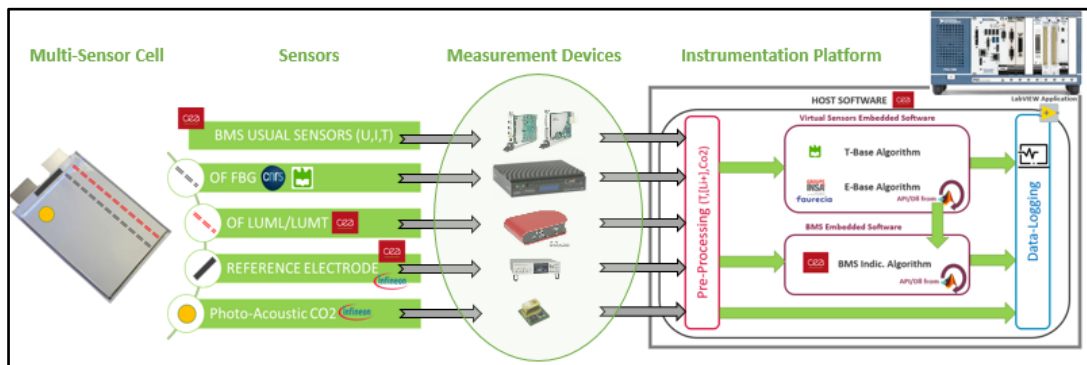


Figure 136: POC multi-sensor platform architecture

The instrumentation computer allows a better connectivity with various equipment I/O and less constraints for software developers. The host software use the LabVIEW environment to perform the following functions:

- Control/command measurement devices to acquire usual BMS sensors and INSTABAT sensor signals
- Pre-process signal to extract battery parameters (ex: temperature from OF spectrum)
- Operate virtual sensors algorithm (E-Base, T-Base) and BMS state indicators calculation compiled in a library
- Synchronize and log all the data produced by the platform

### 5.2.1.2 Software

The software architecture is built around periodic process loops that exchange data by FIFO or Events. Each measuring instrument has its own process with a predefined period to refresh values. In the same way, the processing algorithms are executed in parallel and read/write respectively input/output from and to the data manager at the frequency assigned to them. Additionally, the loop of the data recording process requests the last value in the data manager at the recording period to store them in a secure database. The user interface (HMI) also uses this data stream to refresh visuals and graphics. The loops are synchronized with each other on a common clock but the measurements made by the instruments are not because some of them do not allow it. The data used by the other processes are based on the last value stored in the data manager. Thanks to the low dynamics of the underlying phenomena, this solution is sufficiently efficient. Indeed, the system is limited here by some measuring instruments whose acquisition frequencies cannot be reduced (for example luminescence spectrum could require 1 second of integration to be acquired). We target to refresh and record data manager content at 1 second period to feed algorithms for a proper execution. The adjustment of this timing is possible in the final version of the platform software.

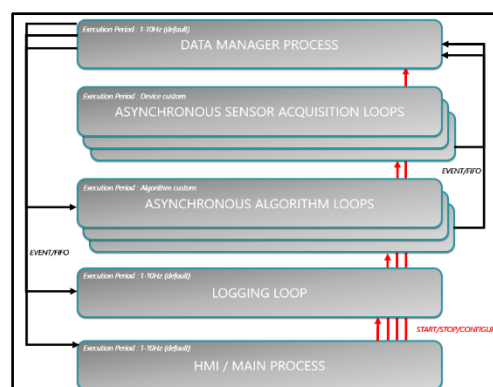


Figure 137: Software architecture

### 5.2.2 Sensor interface

During the first period of the project, a preliminary work consisted in interfacing the LabVIEW environment together with the various instruments necessary to measure the signals of the INSTABAT sensors. The photo-acoustic CO2 sensor has an UART communication interface developed by Infineon. The luminescence optical fiber and Bragg optical fiber requires respectively a compact spectrometer (CSS100 from Thorlabs) and an interrogator (Hyperion Si255 or similar). Both have LabVIEW driver available to control and command them through USB or Ethernet link. Reference electrode



and usual BMS measurement such as cell voltage, current and skin temperature is performed by Keysight precision multimeter 34970A which also has LabVIEW drivers. The integration of FBG interrogator was done during the second phase of the project. So far, all sensors, have been successfully integrated into the software environment. Figure 138 gives an example of the integration into the Labview software.

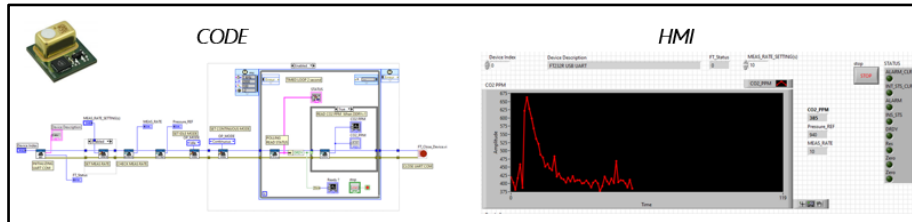


Figure 138: Interface of PAS CO2 sensor with LabVIEW software environment

### 5.2.3 Beta version

For the needs of the ESRF experiment, we have implemented the hardware and software architectures described in the previous chapter integrating the usual BMS and thermoluminescence measurements and pre-processing. It was a good opportunity to validate on a reduced scale our system design. Coupled with the cell prototype, this beta version of the proof of concept of the multi-sensor platform has successfully completed a 90-hour in-situ operando cycling test.

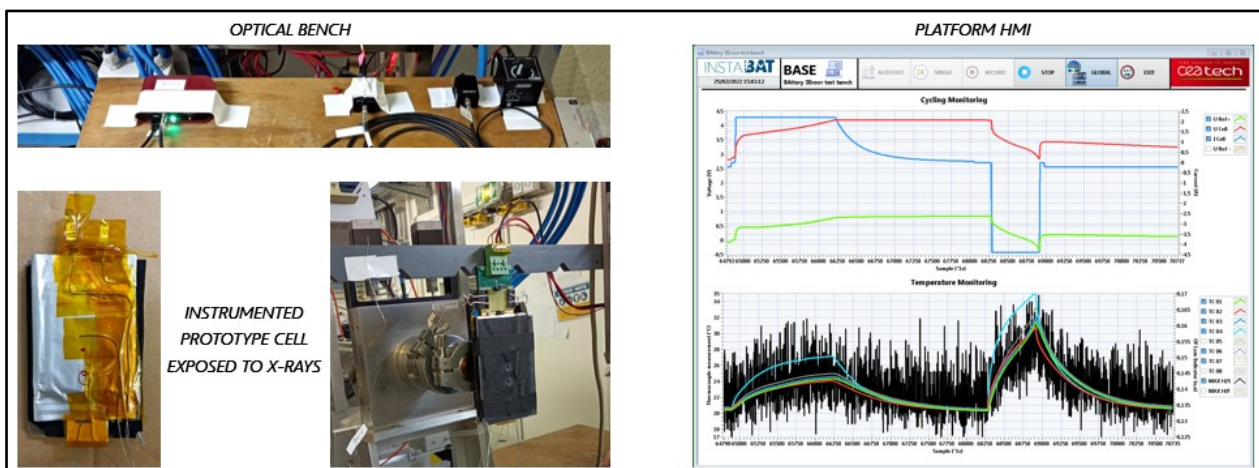


Figure 139: Beta version of multi-sensor platform used for ESRF experiment session

There is still work to be done, especially to interface the Bragg fiber interrogator but also to embed the WP4 algorithms and models into the platform.

### 5.2.3 Final version

During the second phase of the project we finalize the integration of all the function of the platform. The status of the final version of the platform for sensors integration and the BMS function. The detail of this integration was done in D5.3 and D5.4. Table 26 give an overview of the status of the integration of sensors and SoX indicator at the end of the project. Despite of some sensors are not functional (OF/LUML) or not adapted to battery environment (PA CO2) the platform was fully developed to integrate this kind of sensors in the future when they are functional.

Table 26: Status of sensors and SoX integration into the platform

Sensor/ Algorithm	Development	Interface	In-operando validation	Status
OF/FBG	OK	OK	OK	Interface with FBG interrogator successful
OF/LUMT	OK	OK	OK	Interface with spectrometer successful / Pre-Processing OK (Calibration required)
OF/LUML	NOK	OK	NOK	Not used but same interface as LUMT
REF Electrode	OK	OK	OK	Interface with voltage measurement device successful
PA CO2	NOK	OK	NOK	Interface by UART communication successful
E-BASE	OK	OK	OK	Interface with automatic generated library (.dll) from Matlab successful.
T-BASE	OK	OK	OK	Interface with automatic generated library (.dll) from Matlab successful.
BMS Sensor (U/I/T)	OK	OK	OK	Interface with multimeter measurement device successful
BMS Algorithm	OK	OK	OK	Interface with automatic generated library (.dll) from Matlab successful

## TASK 5.3 ADVANCED BMS ALGORITHM INTEGRATION AND OPERATION

(Leader: CEA, Participants: INSA, IFAG) (M24-M36)

As we mentioned before, it will also be necessary to embed the virtual sensor E-Base and T-Base as well as the BMS estimator algorithms. Both are developed using MATLAB® software. Our solution to implement these algorithms on the software platform is to use automatic code generation to create a Windows library (\*.dll) that can be executed by the LabVIEW engine. In this context partners involved in algorithms development must:

- reduce models to minimize the use of computer resources
- adapt algorithm to be time based (executed at each time step)
- define format and datatype of inputs/outputs
- use MATLAB® Coder code generation function to convert MATLAB® code to operable library

The work of WP4 was finished during the second phase of the project and produce all the DLL and algorithm for integration to the platform during the last 2 month before end of the project. The time to integrate all this function in the platform was short for the proof of concept. However, to prepare the work, during the first phase of the project, an initial version of the BMS algorithm estimating SOC/SOH, using the usual cell measurements (voltage, current and temperature) and based on Kalman filter processing was converted to test successfully the connectivity of the LabVIEW environment with the generated library.

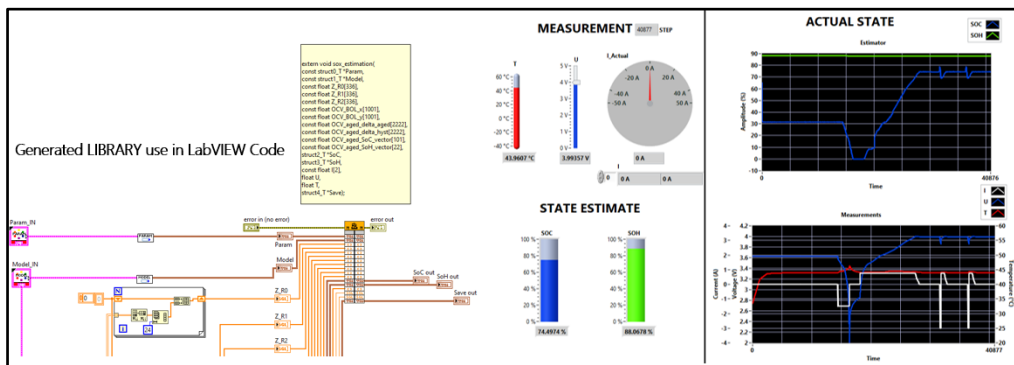


Figure 140: Execution of BMS indicators algorithm library converted with Matlab Coder in the LabVIEW environment

On the other hand, detailed specifications relative to algorithm I/O has been approved and constructed by all partners. The aim of this document was to define what the properties of I/O processing blocks are and how they are supposed to be linked with sensors measurement values. Among required processing blocks inputs, there are physical or structural parameters with configurable values relative to battery cell or sensors. An essential work will be to prepare algorithms integration when a first version would be ready even if it remains still some requirements to be defined.

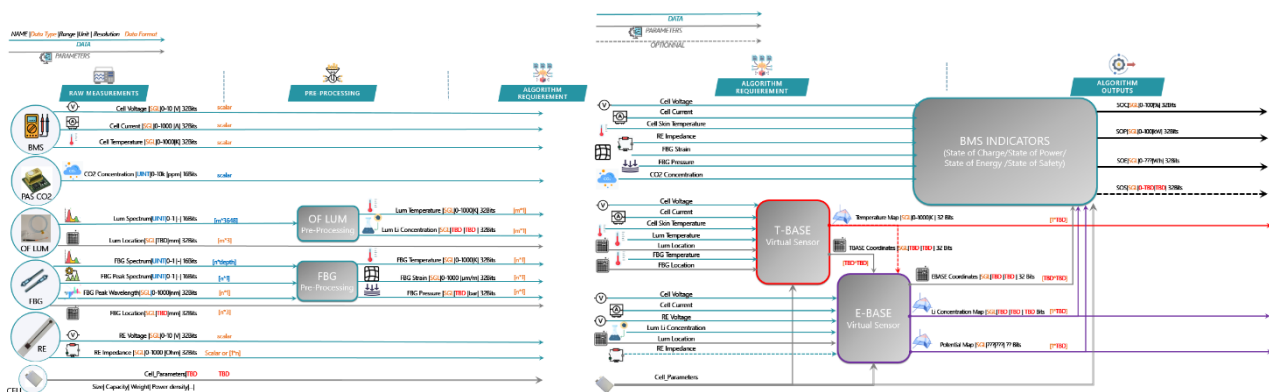


Figure 141: Algorithm integration specification block diagram

During the second phase of the project, when the output from the WP4 was fully developed, the virtual sensors (E-Base and T-Base) and SoX algorithms has been integrated into dynamic libraries format for the platform software. The validation of the integration has been done with multimayer instrumented VARTA cells check-up cycles data acquired during the task 5.4.

## TASK 5.4 LAB-SCALE TESTS ON CELL PROTOTYPE

(Leader: CNRS; Participants: UAVR, CEA) (M24-M36)

Two experimental campaign has been performed for the lab-scale tests on cell prototype in abuse condition and with a representative cycling test. Due to a small amount of cells, the experiment has been designed to maximize the chance to achieve the objective of the project and having datas to evaluate the KPI. The Figure 142 show the synoptic of the lab-scale tests. 4 cells was used for the abuse test: Two reference cells and two cells with OF/LumT and RE sensors. The implementation of FBG sensors weren't available for this test due to the difficulties to integrate all the sensors and the delay of cells preparation. For cycling test, 6 prototypes cell with OF/LumT and RE sensors and 6 reference cells was prepare. Unfortunately due to the difficulties of the integration of sensors only one multi-instrumented cells was alive for the test after fabrication, formation and preparation phase.

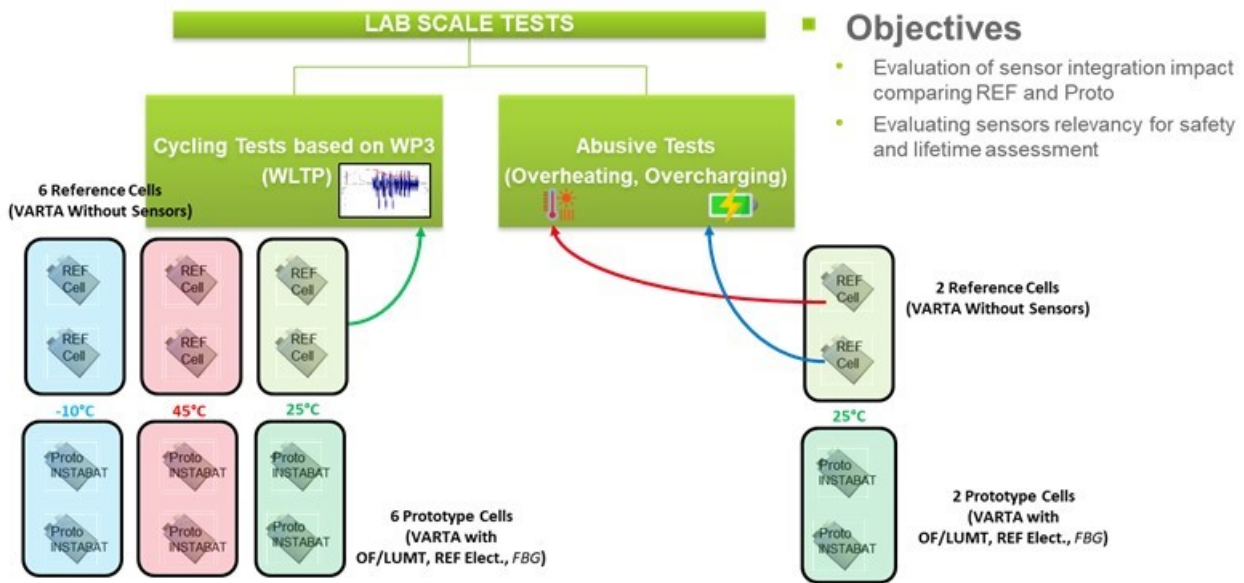


Figure 142: Lab-scale tests on cell prototype synoptic

For the experimental test only one multi-sensor cell can be tested for each condition (abuse test and performance test). For the performance test due to the number of cells, only the 25°C temperature could be performed. The results summary of these two tests (abuse and performance test) is given below.

## • Abuse tests

Two types of abuse test have been performed on the reference and instrumented cells: overcharge and overheating. For the two tests, the initial performances of the cell were measured with a check-up at C/5. Initially, the cells were stored at 30% SOC, the first step consists of a discharge at C/5 up to SOC 0%, then a charge at C/5, a discharge at C/5 and another charge at C/5. With this protocol, we can measure the capacity of the cell and check if all the sensors and the cell are functional. When the cell is charged at SOC 100%, the abuse test can be started.

For the overheating test, the temperature of the cell increases at 6°C/min until runaway. For the overcharge test, C-rate current is maintained to C until runaway with a stop condition at 2C or 2V. During the experiment, all the cells have been instrumented by an external thermocouple on the surface to follow the external temperature of the cell. Cell potential and current have been monitored for both types of cells. All the measurements have been performed and recorded by the platform. All cells are compressed between two rigid plates to apply a small pressure by using strings on both sides.

Figure 143 illustrates photo captures of the cells at the beginning and at the end of the test. We can see for the reference cell a swelling of the pouch during both tests with an opening for overheating. The swelling is due to the production of gases due to the decomposition of the electrolyte by temperature (overheat test) or by overpotential (overcharge test). During the overheat test, we have observed an opening of the non-instrumented pouch cell to exhaust the gas. This exhaust does not generate a flame or explosion.

For the instrumented cell, the behavior is different because no swelling has been observed. It is difficult to conclude with only one test, but the main hypothesis is that the gas could be escaping slowly from the sealing point around the sensor connections between the inner and outer parts of the cell. This area is probably less efficient to keep the gas inside the pouch. But we do not have complementary measurements to validate this hypothesis.



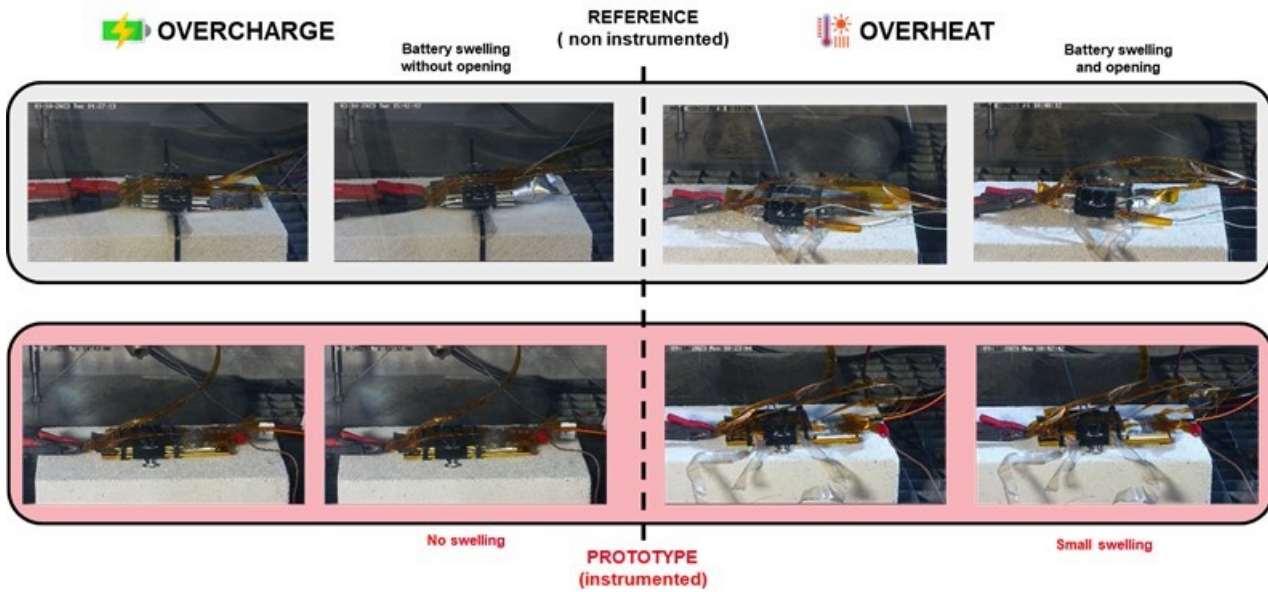


Figure 143: Photo of the cells during abuse test: Left overcharge, right overheat, top reference cells, bottom instrumented cells. The image at left for each case correspond to the beginning of the test and at right the end of the test

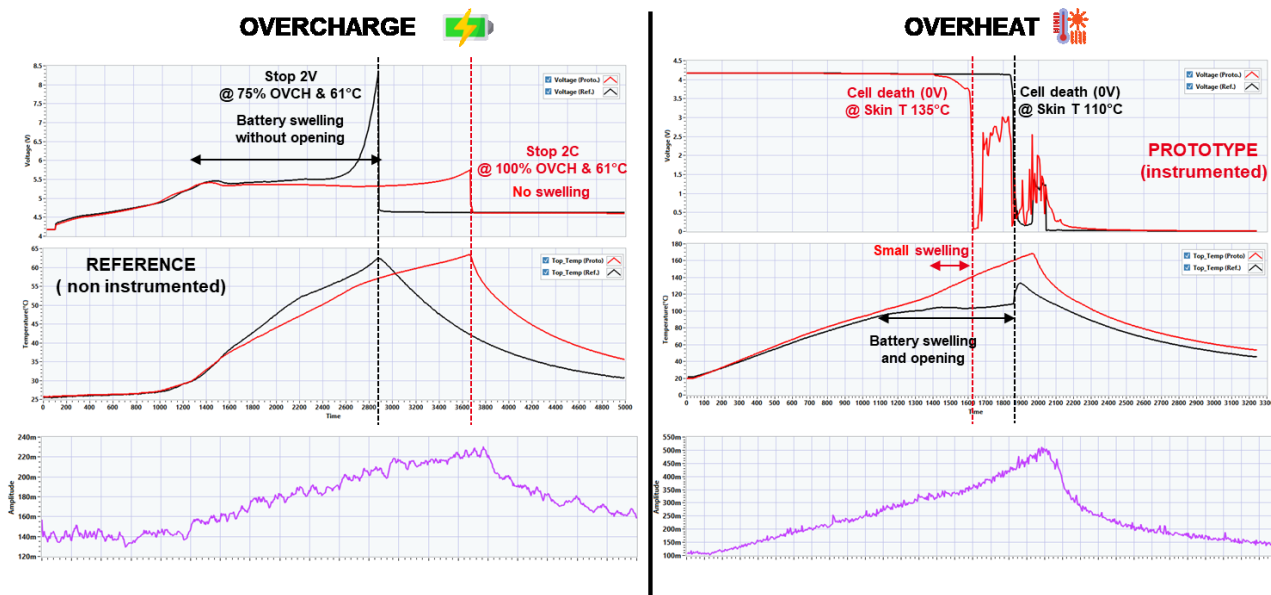


Figure 144: Potential, Temperature and FO/LumT signal during overcharge (left) and overheat test (overheat). In black the curves for the reference cells. In red the curves for instrumented cells

Figure 145 illustrates the interest of the sensors for safety issues. This figure present the potential of the positive and negative electrode measured from RE, the signal from the OFLumT sensor (proportional to the internal temperature) and the external temperature of the cell during the overcharge test. The cell temperature starts clearly to increase when the potential of the negative electrode go below zero. This parameter is directly related to the thermal degradation of the electrolyte and the apparition of the lithium plating<sup>[1]</sup>. Using reference electrode potential is a promising way to detect the overcharge damage. The internal temperature (signal from the FO/LumT in purple) increase before the external temperature and just before the negative electrode potential go below 0V (see blue curve in the figure). These results confirm the performance of the INSTABAT platform is a powerful tool to improve the SOH factor and prevent from ageing by using the signal from the sensors. The other key result of this experiment is that both sensors remain integral and functional under abusive conditions.

[1] J. Vetter et al. Journal of Power Sources 147 (2005) 269–281, doi:10.1016/j.jpowsour.2005.01.006



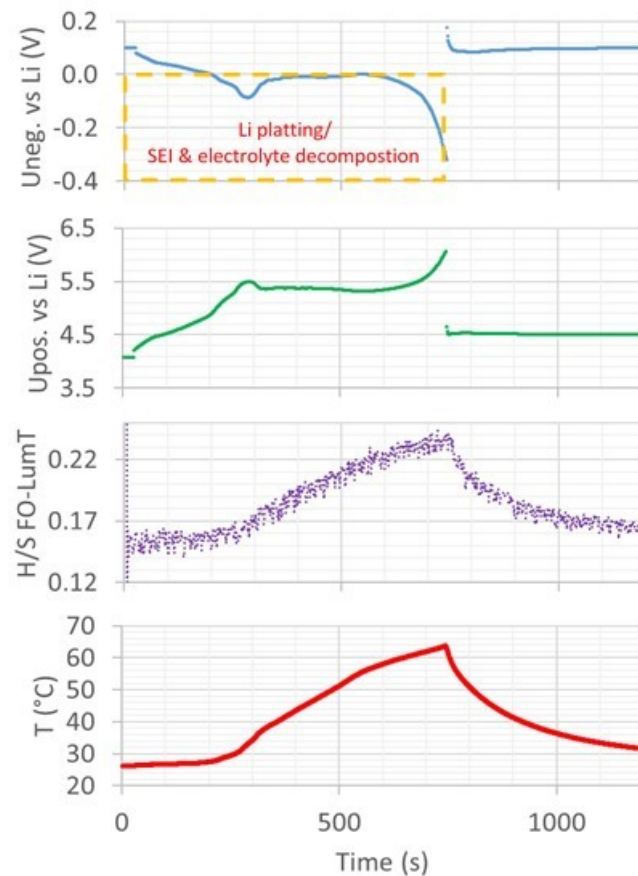


Figure 145: Profiles from sensors during over charging abuse test: Potential vs Li+ of the negative (bleu) and positive (green) electrodes. Signal from the FO/LumT sensors (purple) related to the internal cell temperature and external temperature (red)

A full detail of the results and associate analysis was included into the D5.6.

The main conclusion of these tests are:

- We don't measure any negative impact of the sensors to the cell safety. For both tests the temperature increase rate and swelling were smaller.
- The FO/LumT is functional over all the abuse test with a good accuracy to the external temperature measured by thermocouple. The second result is the FO/Lum-T sensor is stable in the full range of temperature during overheating tests up to 170°C.
- The RE sensor is functional during all the abuse test and give the information of the degradation of the electrodes potential during the abuse condition.
- The exploitation of the results and the design and implementation of State of Safety in the INSTABAT platform was not possible due to the lake of time. These results were obtained at the end of the project.

However they open the way to go further and achieve the initial goal of the project related to improving the safety margin for the future cell technologies.

- **Performances tests**

The performance tests were started at the end of the project (in December 2023) due to the delay to implement all the components, especially algorithm on the platform software. At the end only one instrumented cell was available when we started the performance tests. A comparison will be made between reference cell and instrumented cell with associate BMS regulation using sensor (physical and virtual) signals and SoX indicator. The experiment has been designed to demonstrate the capability of the platform to address the objectives of the project focused on EV use cases. Initially we plan to perform experiments at 45°C to accelerate the cell degradation with a WLTP cycling in discharge and 2C charge (to simulate the EV usage and extreme conditions). Unfortunately, due to a defect in our climatic chamber, we had to carry out the test at 25°C. The detailed results are presented in the deliverable (D5.6).

The platform is fully operational during lab-scale test, performing successfully real-time measurement of cell parameters (temperature, electrode potential, Lithium concentration) thanks to physical and virtual sensors. The measurement usage by the virtual sensor and the SoX algorithm is operational but more detailed analysis is needed to judge their accuracy. The platform is able to monitor properly the cell state and it's clear that this will improve the safety parameter by limiting the critical parameter (potential of the negative to limit the lithium plating, cell temperature to limit degradations, etc...).

- **Conclusion**

in-depth analysis of these lab-scale test results is not yet complete as they were carried out at the very end of the project.

Another noteworthy point is the tests were performed with only one instrumented cell and need to be reproduce.

However, we can consider that lab on cell's proof-of-concept objective has largely been achieved. All the component can be easily integrated and most of them are functional. Measurements of cell key parameter are monitored and recorded in real time. Evaluation of prototype performance and the suitability of innovative sensors could not be completed for the delivery of this deliverable. Initial results are promising, and it is planned to update the detailed analysis for the final review.

The INSTABAT platform achieves its objectives by bringing together all the project partners' work in a single system. This part of the project resulted in a demonstration of multi-sensor platform at TRL 3 that combined at least 3 physical sensors, 1 virtual sensor (E-BASE), but also data post-processing and logging and BMS feature on stand-alone unit. This tool shows great potential for understanding and improving the battery cells usage in terms of safety and lifespan.

The results from the abuse test demonstrate the interest of the platform to manage the safety. The information from sensors are useful to detect early critical degradation phenomena (such as lithium plating, electrolyte and SEI decomposition, active material degradation, etc....). The development and improvement of the State Of Safety was not be possible in the frame of INSTABAT but we have all the pieces for a future development of powerful State of Safety algorithm. Due to his versatility, the INSTABAT platform is able to include this kind of new component (State of Safety and associate BMS function).



Table 27. *List of deliverables WP5*

Deliverable Number	Deliverable Title	Lead beneficiary	Type	Dissemination level	Due date (in month)	Status
D5.1	At least 12 cell prototypes, and report on cell prototype manufacturing	1 - CEA	Demonstrator	Public	28	Submitted
D5.2	Strategy for data logging on a multi-sensor cell	5 - IFAG	Report	Confidential	24	Submitted
D5.3	Communications between physical sensor platform, virtual sensors and BMS established	5 - IFAG	Report	Confidential	29	Submitted
D5.4	Proof of concept multisensor platform / "lab-on-a-cell"	1 - CEA	Demonstrator	Public	30	Submitted
D5.5	Performance analysis of the BMS algorithms in the context of the defined two use cases for EV applications	1 - CEA	Report	Public	36+4	Submitted
D5.6	Report about cell prototype performance	3 - CNRS	Report	Public	36+4	Submitted

Table 28. *Relevant Milestones associate to WP5*

Milestone Number	Milestone Title	Lead beneficiary	Due date (in month)	Status
MS5	"Lab-on-a-cell" platform ready (cell prototype equipped with physical/virtual sensors, and associated BMS algorithms providing SoX indicators in real-time)	1 - CEA	30	validate see D5.4
MS7	Performances of "lab-on-a-cell" platform available	1 - CEA	36+4	validate by the last experiment performed in December 2023 and D5.6

## WP6 - Techno-economic feasibility, adaptability to other cell markets and environmental considerations

Work package number	6	Leader	FAURECIA						
Work package title	Techno-economic feasibility, adaptability to other cell markets and environmental considerations								
Short name of participant	BMW	VMI	CNRS	UAVR	IFAG	CEA	INSA	FAURECIA	
Person months per participant	2.6	6	0.5	0.5	0.5	0.5	0.5	6	
Start month	M24			End month			M36		

### Objectives

The aim of WP6 is to establish the steps necessary to ensure a successful commercialisation of the multi-sensor platform. WP6 will:

- Carry out an industrialisation and scalability study and a preliminary design for an industrial multi-sensor platform.
- Assess manufacturability and techno-economic feasibility.
- Study adaptability to other cell technologies and use cases.
- Provide an environmental assessment, focusing on traceability, second life and recyclability.

### Highlights of most significant results

There are two main tasks for WP6 which are industrialization study and techno-economic analysis including environmental considerations and adaptability to other cell technologies. The results obtained in Task 6.1. were successfully submitted on July 6, 2023, which is led by VARTA, which gives an extensive list of different components, sub-components, processes of multi-sensor platform and their respective suppliers. The results obtained in Task 6.1. were effectively implemented in Task 6.2 and generated three important deliverables which are Deliverable 6.2. Environmental Assessment and Recyclability Analysis, which is submitted on Sept 29, 2023, Deliverable 6.3. Techno-economic Feasibility, which is submitted on 07/12/2023, and Deliverable 6.4. Adaptability Study to Different Cell Technologies, which is submitted on 01/12/2023.

All of the WP6 objectives were achieved by submitting the Deliverables 6.1., 6.2., 6.3., 6.4 and each objective and their associated deliverable are discussed below:

- **Objective 1 Carry out an industrialisation and scalability study and a preliminary design for an industrial multi-sensor platform:** This objective is achieved by submission of Deliverable 6.1. Industrialization Study. The content of the deliverable is the components, processes, and suppliers for battery cell, physical sensors, and virtual sensors.
- **Objective 2 Assess manufacturability of techno-economic feasibility:** This objective is achieved by submission of Deliverable 6.3. Techno-economic feasibility. First order of magnitude cost estimation is given in terms of lab-scale design for multi-sensor platform.
- **Objective 3 Study adaptability to other cell technologies and use cases:** This objective is achieved by submission of Deliverable 6.4. Adaptability of the multi-sensor platform to different cell formats, future cathode, anode, and electrolyte chemistries. The physical and virtual sensors are analyzed in terms of different cell formats and cell chemistries.
- **Objective 4 Provide an environmental assessment, focusing on traceability, second life and recyclability:** This objective is achieved by submission of Deliverable 6.2. Environmental Assessment and Recyclability Analysis. The multi-sensor platform is analyzed in this deliverable in four LCA phases, which are raw material, manufacturing, use-phase, and end-of-life.

Since there no related KPI for this WP and the related milestone MS8 Industrialisation and future of the multi-sensor platform assessed is achieved by four deliverables that were successfully submitted in WP6, which give insights on current information available for industrialization, the missing data that needs to be collected for future of the multi-sensor platform, and perspectives for future projects.

Summary of progress towards objectives and details for each task

## TASK 6.1 INDUSTRIALISATION STUDY

(Leader: VMI; Participants: All) (M24-M30)

The objective of Task 6.1 is to enable identifying the gaps between a proof of concept of the multi-sensor platform and a product that is ready for commercialization. The results of this task were reported on a market research report (D6.1 - Market research on components and manufacturing processes) and this report analyzed market of the components and processes for the multi-sensor platform of the INSTABAT project. For the details of all components and processes, please refer to the deliverable 6.1. In this report, only an excerpt is given here.

Deliverable 6.1 starts with the system approach for lithium-ion multi sensor platform and continues with explaining the proof-of-concept multi-sensor platform architecture, by explaining the component of the multi-sensor platform, which includes parts from a conventional battery cell which are cathode, anode, separator, electrolyte, and housing and four physical and two virtual sensors (software and algorithms) together with their instrumentation platform.

Furthermore, the battery cell components and the process of the battery cell production were explained in detailed. Table 29 highlights an example, cathode component, of how the battery components were explained in deliverable 6.1. As it is seen in Table 29, the deliverable 6.1 gave details on sub-component of the main components, type of the sub-component and manufacturer/supplier for each sub-component.

Table 29 Cathode component of INSTABAT proof-of-concept cell

Main Component	Sub-Component	Type	Manufacturer/Supplier
<b>Cathode</b>	Current Collector	Aluminum	Sumitomo Light Metal, Furukawa Sky, Furukawa Elec, LS Mitron, Nippon Foil Mfg
	Positive Active Material	NMC622	Sumitomo Chemicals, Tanaka Chemicals, Nippon Chemicals Industrial, Toda Kogyo, Nippon Denko, Sumitomo Metal Mining, AGC Semi Chemical, Nichia, Umicore, Showa Denko, Tosho, Nihon Kangaku Sangyo, Mitsui Kinzhou, BASF, Johnson Matthew, Posco International
	Binder	PVDF	Solvay S.A
	Conductivity Agent	Carbon black	Imerys, Denka, Aditya Birla Group (India), Targray, Cabot Corporation, Heraeus
	Arrestor Tabs	Aluminum	Bikar GmbH, Avocet Steel Strip

In addition to the components of the cell, the manufacturing processes for a lithium-ion cell is explained in detailed. The entire manufacturing process of a lithium-ion battery can be divided into three main topics:

- Electrode manufacturing
- Assembly
- Formation

For the detailed description of each step, please refer to the deliverable. Moreover, the processes for each component manufacturing INSTABAT ‘proof-of-concept’ were described in this section of the report. Table 30 gives an illustration for this section.



Table 30 Processes for component manufacturing INSTABAT proof-of-concept

Main Component	Intermediates	Process	Manufacturer/Supplier
<b>Cathode/ Anode</b>	Anode/ Cathode Slurry	Mixing, Kneading	Bühler, Ika, Xiamen Tmax Battery Equipments, Wenzhou Ace Machinery

In the last section of the report, the main components, sub-components and manufacturer/supplier for main component, the intermediates, process, and equipment required for the manufacturing and supplies of the equipment were explained in detail for each physical and virtual sensor of the multi-sensor platform.

Here are some important take-aways from this deliverable:

- The result of the supplier survey shows that for battery components and manufacturing processes, Asia dominates the market. For sensor components, the influence of European manufacturers is greater.
- The most difficult points regarding the manufacturability of the multi sensor platform are the interference of the physical sensors with external factors (temperature, pressure, chemical (corrosive) substances, vibrations) that can cause artifacts
- Improving the accuracy of SoX cell parameters will lead to an increase in the efficiency of battery inverters and electric motors and will minimize the environmental footprint over its whole life cycle.

## TASK 6.2 TECHNO-ECONOMIC ANALYSIS INCLUDING ENVIRONMENTAL CONSIDERATIONS AND ADAPTABILITY TO OTHER CELL TECHNOLOGIES AND USE CASES

(Leader: FAURECIA; Participants: All) (M28-M36)

The main objectives of Task 6.2 are to deliver a techno-economic analysis of the “lab-on-a cell platform”, an overall environmental assessment of the platform, and to study the adaptability to different cell technologies. There are three deliverables that are submitted for this task which will be explained as the sub-task of this section.

### Subtask 6.2.1. Environmental Assessment and Recyclability

The environmental assessment of the lab-on-a cell platform was done using the eco-design approach with *life cycle thinking*, to have a full picture of the multi-sensor platform. Life cycle approach considers environmental aspects throughout the entire life cycle of a product, which can also be seen in Figure 146. It implies that the stages of the life cycle are sequential and interconnected. These stages include raw material supply, manufacturing, consumer use and end-phase of the products. The report has a strong emphasis on use and end-phase stage of the eco-design approach.

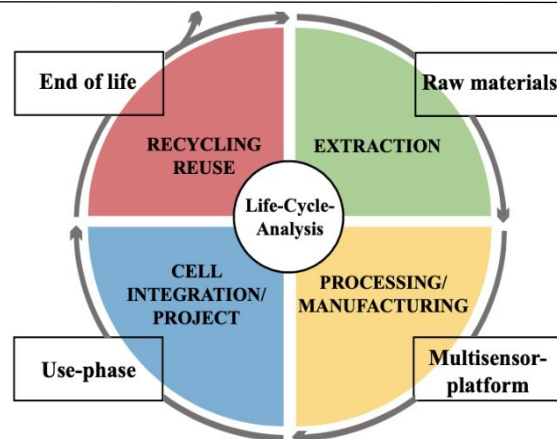


Figure 146: Life cycle approach for environmental assessment

Raw material section of the report identified all resources that can be classified as critical raw material or conflict minerals. Furthermore, the components of the sensors are evaluated in relation to the existing certification of the suppliers such as REACH and RoHS. In this section, it is concluded that the amount of raw materials per sensor is in the range of milligrams and the as the capacity of the cell increases, thanks to the virtual sensors, the amount of critical raw materials will not increase significantly, the detailed can be seen in Table 31 and section 2 of deliverable 6.2.

In the manufacturing section, the important parameters were explained when analyzing the production stage of the life cycle and the ways to minimize the environmental impact of the product. These factors are battery size, capacity, cycle life, battery type, manufacturing energy efficiency, energy consumption, water consumption and waste management. Also, in order to minimize the effect of manufacturing to the environment, renewable electricity can be used as a main energy source, scaling up the new technologies and minimizing the usage of physical sensors through the use of virtual sensors.

Table 31 The among of Critical Raw Materials or Conflict Minerals per Sensor

Sensor Name	Critical Raw Material/Conflict Mineral	The Amount of the Critical Raw Material per sensor	The ratio of Critical Raw Material/Conflict Minerals in 60 Ah Cell
<b>FBG Sensor</b>	N/A	N/A	N/A
<b>RE</b>	Gold	0.21 mg	1.13e-7
	LFP	~ 2.5 mg	1.35e-6
<b>Lithium-ion Luminescence Sensor</b>	Too early to assess	N/A	N/A
<b>Temperature Luminescence Sensor</b>	PTIR545/F	~ 1.66 mg	8.97e-7
<b>PA Sensor</b>	Defined in RoHS and REACH Directives	Most of the critical materials used are well below 1 mg per sensor.	<5.41e-7

In the use phase, the batteries do not emit any pollutants to the air, however, electricity usage can cause emissions. In this section, a scenario that was defined by INSTABAT KPI 11 was used to analyze the use phase of the product. With the better accuracy of SoX values, it will be possible use the battery more efficiently which is coupled with power and energy. Moreover, the more over- and deep-discharge and the dangers associated with these phenomena can be reduced by using the multi-sensor platform. All these accurate data can be also helping the fast-charging capability of the battery.

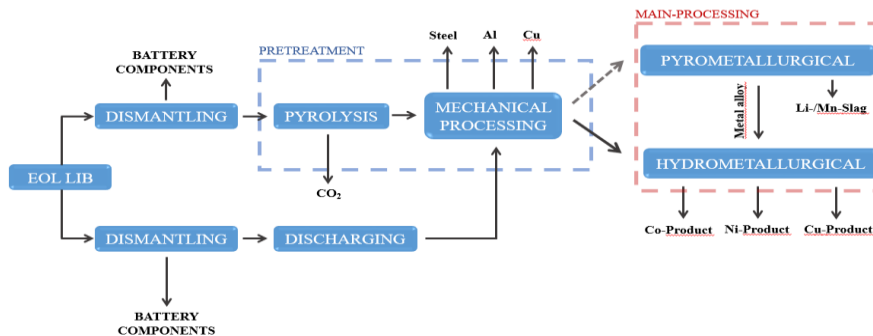


Figure 147: The recycling steps for a lithium-ion cell

In the end-phase section of the report, firstly the different recycling methods for lithium-ion batteries were discussed, specifically pyrometallurgical process, hydrometallurgical process, and direct recycling and afterwards, the possibility of recycling as a unit were discussed. Figure 147 gives a general insight on the recycling steps for a lithium-ion cell. It has been concluded that the additional raw materials of the multi-sensor platform can require additional steps, however due to the low amount of raw material within the multi-sensor platform, the effect of these raw materials might be limited and there is no clear evidence of a side reaction that may lead to toxic effects such formation of additional gases through doped materials. As next step, the re-use of each physical sensor was discussed in this section. It has been concluded that the physical sensors within the cells are very hard to re-use, however, the data unit components can be re-used, if the lifetime of the product allows. Lastly, in the second life section of the report, it has been concluded that the multi-sensor platform can be a big help to second life identification of the cell, since With the help of the in-operando detection by the integrated multi-sensor unit, thermal and cyclic load effects can be recorded and controlled more precisely, and degradation can be detected at an early stage, and longer battery use is to be expected. The collected results can play a major role in the analysis of the SoH and simplify process steps such as SoH analysis and quality classification

## Subtask 6.2.2. Techno-economic Feasibility

The techno-economic feasibility of the INSTABAT project was analyzed in this subtask and deliverable 6.3. The deliverable gives insights on all stages of the techno-economic assessment of the multi sensor platform which can be divided into five steps.

1. **Goal & Scope Definition:** The goal of this feasibility study is to understand technical viability and economical potential of the product and technology. The scope of the assessment is based on life cycle analysis methodology which is also explained in the subtask 6.2.1. The assessment focuses on assessing the lab scale process design and identify the major problems for next projects. The data was collected online was focused on European market whenever, when the information was not found in European market, a global average data was shared in the deliverable. The source of each data was reported in the report.
2. **Inventory Analysis:**
  - a. Defining and checking the quality requirement: The quality requirements were defined and used to collect data for the techno-economic assessment. If the data was found online, the source of each data was reported in the report.
  - b. Collection of Data: Given that the technical data was collected within the project in different work packages, the focus was on the collection of the economic data. Table xx is an example for the economic data and how it was reported within deliverable 6.3. The table has information on the type of economic data, the amount or the cost and the source the information was taken from. The data was collected for utilities, operating labor, sensor raw materials and equipment, software, and multi-sensor implementation.

Table 32 Collection of economic data

Sensor	Amount	Source
<b>Utilities</b>		
Electricity	0.1833 (€/kWh)	Eurostat (2023 first half)
Gas	0.0826 (€/kWh)	Eurostat (2022 second half)
<b>Operating labor</b>		
Average hourly wage in EU	30.50 €	Eurostat (2022)

3. **Calculation of indicators:** In this section capital expenditure and operational expenditure are calculated using the data that was collected in the previous section, which in total concludes as the cost of goods manufactured. The order of magnitude approach is used for cost estimation, given there are currently a lot of unknowns to do a detailed cost calculation.

CAPEX was calculated using Lang factor which relates the purchases equipment cost to total capital investment and fixed capital investment. The formula that is used for this section is:

$$C_{TM} = F_{lang} \sum_{i=1}^n C_{pi}$$

Operational expenditure was determined by using the fixed capital investment, cost of operating labor, cost of utilities, and cost of raw materials. Cost of utilities were calculated based on average values for a large and small factory within Europe. Operating labor costs were defined by average hourly wage in EU times the number of hours within the year, in addition how many people are required to operate the manufacturing. The factors that were used to calculate direct cost can be seen in Table 33.

Table 33: factors used to calculate direct cost

Cost Item	Factor
<b>Variable Costs</b>	
<b>Raw Materials</b>	Calculated in Deliverable 6.4.
<b>Utilities (Electricity+Gas)</b>	Calculated using average values
<b>Operating personnel (a)</b>	Calculated using average values
<b>Supervision and engineering (b)</b>	0.20*a
<b>Maintenance ©</b>	0.05*FCI
<b>Laboratory personnel and consumables</b>	0.15*a
<b>Patents</b>	0.05*OPEX

4. **Interpretation of the Results:** In this section, major cost factors and next steps to improve the cost of INSTABAT multi-sensor platform is defined.

## Subtask 6.2.3. Adaptability of the multi-sensor platform to different cell technologies

Different cell formats, cell chemistries and adaptability of the multi-sensor platform to different cell technologies were reported in this subtask. In this report, only a summary of this deliverable (see D6.4) will be reported. This subtask was analyzed by three main chapter:

1. **Different cell technologies:** This section is divided into cell formats and different cell chemistries
  - a. **Cell formats:** The properties of different cell formats, cylindrical cell, pouch cell, and prismatic cell are explained. Examples of each cell format is given and their safety functions were explained.

- b. **Different chemistries:** This section is divided into two main chapters: Lithium-ion Batteries and lithium-ion batteries. The framework of this section is inspired by classification of different chemistries which is in European Commission JRC Science for Policy Report and OEM announcements (e.g. Tesla, Volkswagen, Stellantis).

Table 34 Classification of different chemistries

Cell generation	Chemistry
<b>Generation 5</b>	<ul style="list-style-type: none"> <li>• Lithium-air batteries</li> </ul>
<b>Generation 4</b>	<ul style="list-style-type: none"> <li>• All-solid-state with lithium anode</li> <li>• Conversion materials (primarily lithium-sulfur batteries)</li> </ul>
<b>Generation 3b</b>	<ul style="list-style-type: none"> <li>• Cathode: HE-NMC, HVS (high-voltage spinel)</li> <li>• Anode: silicon/carbon</li> </ul>
<b>Generation 3a</b>	<ul style="list-style-type: none"> <li>• Cathode: NMC622 to NMC811</li> <li>• Anode: carbon (graphite)+silicon component (5-10%)</li> </ul>
<b>Generation 2b</b>	<ul style="list-style-type: none"> <li>• Cathode: NMC523 to NMC622</li> <li>• Anode: Carbon</li> </ul>
<b>Generation 2a</b>	<ul style="list-style-type: none"> <li>• Cathode: NMC111</li> <li>• Anode: 100% carbon</li> </ul>
<b>Generation 1</b>	<ul style="list-style-type: none"> <li>• Cathode: LFP, NCA</li> <li>• Anode: 100% carbon</li> </ul>

- i. **Lithium-ion Batteries:** The different anode materials (lithium metal, graphite, silicon), cathode materials (LFP, NMC, LNMO) and solid—state electrolytes were explained in detail in this report. This electrochemistry linked with different OEM announcements and market research for future chemistries. A comparison of anode materials that is taken from Deliverable 6.4. can be seen below:



Table 35 Comparison of different anode chemistries for lithium-ion batteries

	Graphite <sup>19</sup>	Lithium metals <sup>20</sup>	Silicon <sup>21</sup>
<b>Properties</b>	synthetic or natural availability  Good specific capacities  Small amount of nanovoids  anisotropic Little microporosity Less interlayer spacing	Highest gravimetric energy density In situ formable	High volume expansion Layered Structure Sustainable High energy density
<b>Specific Capacity</b>	( natural $\approx 335 \frac{\text{mAh}}{\text{g}}$ ) *  ( synthetic $\approx 350 \frac{\text{mAh}}{\text{g}}$ )	$\approx 3861 \frac{\text{mAh}}{\text{g}}$ **	$3579 \frac{\text{mAh}}{\text{g}}$
<b>Swelling</b>	< 10%	***	300 %
<b>Safety-risk</b>	High TRL, very low risks	Very high risk; can be only used with solid-state electrolytes	Very high risk
<b>Voltage (Li<sup>+</sup>/Li)</b>	0.05 – 0.2 V	0 V	0.37 V <sup>22</sup>

ii. **Beyond Lithium-ion Batteries:** Sodium-ion batteries and lithium-sulfur batteries are discussed in this chapter. Their electrochemical behavior and the companies that are currently working on these battery chemistries were reported.

2. **Adaptability of the multi-sensor platform to different cell technologies:** Adaptability of physical sensors and virtual sensors were discussed in terms of different cell formats and different cell chemistries that are explained below and the missing data and work that could be done for possible future projects were defined.
3. **Conclusion:** Perspectives for possible next projects were given for INSTABAT multi-sensor platform.

<sup>19</sup> (a) Kurzweil, Peter, and Otto K. Dietlmeier. *Elektrochemische Speicher: Superkondensatoren, Batterien, Elektrolyse-Wasserstoff, Rechtliche Grundlagen*. Springer-Verlag, 2016 (b) Sarkar, Montajar, Rumana Hossain, and Veena Sahajwalla. "Hard carbons from automotive shredder residue (ASR) as potential anode active material for sodium ion battery." *Journal of Power Sources* 584 (2023): 233577

<sup>20</sup> (a) Kurzweil, Peter, and Otto K. Dietlmeier. *Elektrochemische Speicher: Superkondensatoren, Batterien, Elektrolyse-Wasserstoff, Rechtliche Grundlagen*. Springer-Verlag, 2016 (b) Nzereogu, P. U., et al. "Anode materials for lithium-ion batteries: A review." *Applied Surface Science Advances* 9 (2022): 100233

<sup>21</sup> Nzereogu, P. U., et al. "Anode materials for lithium-ion batteries: A review." *Applied Surface Science Advances* 9 (2022): 100233

<sup>22</sup> Soto, Fernando A., et al. "Computational studies for understanding and developing silicon anodes." *Lithium-Ion Batteries Enabled by Silicon Anodes*. Institution of Engineering and Technology, 2021. 169-202



Table 36. *List of deliverables WP6*

Deliverable Number	Deliverable Title	Lead beneficiary	Type	Dissemination level	Due date (in month)	Status
D6.1	Market research on components and manufacturing processes for industrial multisensory platform	8- VMI	Report	Public	30	submitted
D6.2	Environmental assessment and recyclability analysis	4- FAURECIA	Report	Public	33	submitted
D6.3	Techno-economic feasibility	4- FAURECIA	Report	Confidential	36+4	submitted
D6.4	Adaptability of the multi-sensor platform to different cell formats, future cathode, anode and electrolyte chemistries	4- FAURECIA	Report	Confidential	36+4	submitted

Table 37. *Relevant Milestones associate to WP6*

Milestone Number	Milestone Title	Lead beneficiary	Due date (in month)	Status
MS8	Industrialisation and future of the multi-sensor platform assessed	4- FAURECIA	36+4	submitted



## WP7 - Dissemination, communication and exploitation

Work package number	7	Leader	CEA						
Work package title	Dissemination, communication and exploitation								
Participant number									
Short name of participant	BMW	VMI	CNRS	IFAG	FAURECIA	UAVR	INSA	CEA	
Person	4	1	0.5	0.5	0.5	0.5	0.5	4.5	
months									
per participant									
Start month	M1			End month			M36		

### Objectives

WP7 aims to implement the dissemination, communication and exploitation strategies of INSTABAT. The work under this WP will be carried out at two levels: (1) under the umbrella of the EU large-scale research initiative on Future Battery Technologies102, led by LC-BAT-15 successful consortium and in cooperation with LC-BAT-12 and LC-BAT-14; (2) at INSTABAT individual level. WP7 will be divided into the following complementary activities:

- Dissemination and communication activities to show the attractiveness of the results achieved and their impact towards a target audience composed of already identified key stakeholders;
- Exploitation actions will establish the main pillars for a future market uptake plan of the most promising and mature results generated in the project, thus maximising the opportunities for innovation and business development.
- Implementation of an IPR and Knowledge Management Plan based on the background of each partner and the expected foreground produced in the project. This plan will bear in mind the progress of foreign IP by a continuous observatory of existing and new patents/utility models to ensure freedom to operate.

### Highlights of most significant results

This part outlines the most important results from WP7. During the project, the materials and tools for communication were developed (website, visual identity, etc.). The dissemination and communication strategy was established (deliverable D7.1) during this first period. The communication and dissemination activity was reported in the D7.6, D7.7 and D7.8. The Key exploitation results are identified and the exploitation plan was decided and the results was reported in the D7.5. The coordination with other projects was done through the BATTERY2030+ initiative with active participation to the related activities (see D7.8).

### TASK 7.1. Implementation of dissemination and communication strategy

(Leader: CEA; Participants: All) (M1-M36).

The communication and dissemination strategy was defined at the beginning of the project and detailed in the deliverable D.7.1. During the first period of the project, we achieved some planned actions. The web site and the visual identity of the project was developed. The detail of the web site and the content was detailed in the D7.2. The communication supports such as poster, flyer and booklet were also developed to share the INSTABAT objectives and promote the project. A detailed view of the dissemination and communication activities along the project started were given in the D7.6, D7.7 and D7.8.

#### • Conferences, workshops participation and publications

During the project the results was presented in numbers of conferences and workshop (see Table 38) and publish in articles (Table 39). The last results of the project was not actually published and will be disseminate in future conferences and journal articles. We don't know exactly at this time the number of communication will be done on the project after the end-date.

Table 38: List of conferences and workshops presentation of the INSTABAT results

Authors	Title	Conference	Year
O. Raccurt	INSTABAT: Development of a proof of concept of smart sensing technologies and functionalities, integrated into a battery cell	Battery Innovation Days, Digital online	2021
O. Raccurt	INSTABAT : expo card	Battery Innovation Days, 13-14th September, 2022, Brussel, Belgium	2022
L. Matuck, C. Marques, J. L. Pinto, M. Nascimento	Impact of orientation in thermal and strain performance in an 18650 Li-ion battery via FBG-PANDA sensors	AABC Europe, Mainz, Germany, 13-15th June 2022	2022
O. Raccurt, S. Genies, C. Septet, E. Villemin, M. Guillon, R. Franchi, O. Poncelet, S. Desousa-Nobre	INSTABAT a multisensor smart cell platform for operando and in situ monitoring	International Operando Battery Days, May 16-18th 2022, Grenoble, France	2022
S. Genies, E. Villemin, P. Balfet, O. Raccurt	Electrode de référence pour la technologie lithium-ion pour la gestion de la charge rapide	Journées Electrochimie 2022, 4-7 July 2022, MONS, Belgium	2022
F. Freitas, L. Matuck, J. Bierlich, M. Ferreira, C. Marques, M. Nascimento	Innovative hybrid optical sensing design to simultaneously discriminate pressure and temperature	AOP2022 conference, Guimarães, Portugal, July 18-22, 2022	2022
L. Matuck, J. L. Pinto, C. Marques, M. Nascimento	Evaluation of the orientation impact in thermal behavior of cylindrical Li-ion batteries in different cycling conditions using FBG sensors		2022
M. Nascimento	Optical fiber sensors to track battery safety parameters	1st i3ENERGY workshop, 7th July 2022, Aveiro, Portugal	2022
I. Gandiaga, O. Raccurt, G. Domann	Sensing	Battery2030+ Annual conference, 12 September 2022, Brussel, Belgium	2022
L. Matuck, J. L. Pinto, C. Marques, M. Nascimento	Dual parameters discrimination comparison between two types of optical fiber sensors during the operation of a Li ion battery	ICOFS 27th conference, Optical Fiber Sensors 2022 Alexandria, Virginia United States 29 August–2 September 2022	2023
L. Matuck, J. L. Pinto, C. Marques, M. Nascimento	Dual parameters discrimination comparison between two types of optical fiber sensors during the operation of a Li-ion battery	European Workshop on Optical Fiber Sensors (EWOFs 2023), 2023, Mons, Belgium Proceedings Volume 12643, European Workshop on Optical Fiber Sensors (EWOFs 2023); 126431A (2023) <a href="https://doi.org/10.1117/12.2678091">https://doi.org/10.1117/12.2678091</a>	2023
S. Genies, E. Villemin, P. Balfet, M. Ranieri, O. Raccurt	Reference Electrode as New BMS Sensor	Battery2030+ Annual conference, 9-10 May 2023, Upsala, Sweden	2023
R. Franchi, O. Raccurt, C. Septet, S. Genies	INSTABAT Multi-Sensor Platform		2023
M. M. Arsalan Asif, F. B. Argomedo, V. Heiries	Real time estimation of electrochemical states in Li-ion batteries and exploitation in BMS algorithms		2023
L. Matuck, V. Neto, J. Lemos Pinto, C. Marques, M. Nascimento	From the physical optical fiber sensors data to a predictive virtual sensor		2023
M. Nascimento, L. Matuck, J. Santos, C. Marques, J. L. Pinto	Sensing of Li-ion battery critical safety parameters with customized physical optical fiber sensors		2023
O. Raccurt	Smart Battery From Sensing To BMS: INSTABAT Overview		2023
S. Genies, P. Balfet, E. Villemin, M. Ranieri, C. Septet, O. Raccurt	Why Li(1-x)FePO <sub>4</sub> / LiFePO <sub>4</sub> Is a Good Candidate to be Used As Reference Electrode	244th ECS meeting, October 8-12, 2023, Gothenburg, Sweden	2023

Authors	Title	Conference	Year
A. Bichon, S. Geniès, D. Buzon, P. Balfet, C. Debruyne, E. Villemin, M. Ranieri, C. Septet, R. Franchi, Y.Reynier, P. Azaïs, O. Raccurt	Using a reference electrode inside Li-ion cell as an <i>operando</i> sensor to detect aging mechanisms		2023
O. Raccurt	Multisensor smart cell platform for <i>operando</i> and in situ monitoring, INSTABAT project overview	Workshop Spartacus, Smart sensor Batteries. The future battery generation, Sans Sebastian June 21-22	2023
O. Raccurt	Multisensor smart cell platform for <i>operando</i> and in situ monitoring, INSTABAT project overview	Battery2030+ - Sensing / Self-healing (interface) workshop October, 20, 2023 - Online	2023
M. Nascimento, L. Matuck, S. Genies, R. Franchi, M. Ranieri, P. Balfet, O. Raccurt, J. L. Pinto	Decoupling internal safety parameters during Li-ion pouch cell operation by high-birefringent optical fiber sensors	Submitted to SPIE Photonics Europe, Strasbourg, France, 7-11 April	2024

Table 39: List of publication from INSTABAT already published or under review

Number	Title	Authors	Journal/Book	Year	Status
1	Simultaneous Strain and Temperature Discrimination in 18650 Li-ion Batteries Using Polarization-Maintaining Fiber Bragg Gratings	Matuck, L., Pinto, J.L., Marques, C., Nascimento, M.	Batteries 2022, 8(11), 233, <a href="https://doi.org/10.3390/batteries8110233">https://doi.org/10.3390/batteries8110233</a>	2022	published
2	Dual parameter discrimination using PANDA-FBG sensors at cylindrical Li-ion battery	Matuck, L.C., Pinto, J.L., Marques, C.A.F., Nascimento, M.S.	Proceedings Volume 12643, European Workshop on Optical Fiber Sensors (EWOFS 2023); 126431A (2023) <a href="https://doi.org/10.1117/12.2678091">https://doi.org/10.1117/12.2678091</a>	2022	Published
3	Evaluation of the orientation impact on thermal behavior of cylindrical Li-ion batteries in different cycling conditions using fiber Bragg grating sensors	Matuck, L., Pinto, J.L., Marques, C., Nascimento, M.	Journal of Physics: Conference Series, 2407(1), 012050, <a href="https://doi.org/10.1088/1742-6596/2407/1/012050">https://doi.org/10.1088/1742-6596/2407/1/012050</a>	2022	Published
4	A particle filter-based virtual sensor for estimating the state of charge and internal temperature of lithium-ion batteries: Implementation in a simulated study case	Biazi, V., Moreira, A.C., Pinto, J.L., Nascimento, M., Marques, C.	Journal of Energy Storage, 61, 106814, <a href="https://doi.org/10.1016/j.est.2023.106814">https://doi.org/10.1016/j.est.2023.106814</a>	2023	published
5	Electrochemical State Observer Design for Li-ion Batteries with Heterogenous Electrode Lithiation	Asif, M.M.A., Argomedo, B.	IEEE Control Systems Letter, VOL. 7, 2023, 3199-3204, <a href="https://doi.org/10.1109/LCSYS.2023.3304248">https://doi.org/10.1109/LCSYS.2023.3304248</a>	2023	published
6	Unraveling SEI formation and cycling behavior of commercial Ni-rich NMC Li-ion pouch cells through <i>operando</i> optical characterisation	C. Gervillié-Mouravieff, L. Albero Blanquer, C. Alphen, Jiaqiang Huang, J.-M. Tarascon	Journal of Power Sources, Volume 580, 1 October 2023, 233268, <a href="https://doi.org/10.1016/j.jpowsour.2023.233268">https://doi.org/10.1016/j.jpowsour.2023.233268</a>	2023	published
7	Detangling electrolyte chemical dynamics and evolution in Li-S batteries by <i>operando</i> monitoring with optical resonance combs	J.M. Tarascon, F. Liu, W. Lu, J. Huang, V. Pimenta, S. Boles, R. Demir-çakan	Nature Communications volume 14, Article number: 7350 (2023), <a href="https://doi.org/10.1038/s41467-023-43110-8">https://doi.org/10.1038/s41467-023-43110-8</a>	2023	published
8	Customized Optical Fiber Birefringent Sensors to Multipoint and Simultaneous Temperature and Radial Strain Tracking of Lithium-Ion Batteries	Lucca C. Matuck, Pedro D. Cabrita, João L. Pinto, Carlos A. Marques, Micael S. Nascimento	Advanced Sensor Research, Volume 2, Issue 7 2200046, <a href="https://doi.org/10.1002/adsr.20200046">https://doi.org/10.1002/adsr.20200046</a>	2023	Published





Number	Title	Authors	Journal/Book	Year	Status
9	Optical Fiber Birefringent Sensors	Lucca C. Matuck, Pedro D. Cabrita, João L. Pinto, Carlos A. Marques, Micael S. Nascimento	Cover Frontpage Advanced Sensor Research, 2(7), 2023 <a href="https://onlinelibrary.wiley.com/doi/10.1002/asr.27511219/2023/2/7">https://onlinelibrary.wiley.com/doi/10.1002/asr.27511219/2023/2/7</a>	2023	Published
9	Tracking Li-Ion Batteries Using Fiber Optic Sensors	Micael Nascimento, Carlos Marques and João Pinto	Tracking Li-Ion Batteries Using Fiber Optic Sensors. Smart Mobility - Recent Advances, New Perspectives and Applications. IntechOpen. Available at: <a href="http://dx.doi.org/10.5772/intechopen.105548">http://dx.doi.org/10.5772/intechopen.105548</a> .	2023	Published
10	Thermo-luminescent optical fiber sensor for Li-ion cell internal temperature monitoring	E. Villemin, S. Genies; O. Poncelet; P. Balfet; C. Septet; R. Franchi; M. Guillon; J. Houny; S. Sousa-Nobre, O. Raccurt.	Journal of Power Sources	2023	accepted
11	Outstanding optical fiber hybrid sensing configuration to track internal key safety parameters during operando cylindrical battery	L. C. Matuck, J.P. Santos, F.B. Freitas, N.F. Santos, L.F. B. Fontes, J. Bierlich, C.A. Marques, S. Geniès, J.L. Pinto, M.S. Ferreira, O. Raccurt, Micael S. Nascimento	Energy & Environmental Science Journal	2023	Under review

## • Training activities and communication to student

From the beginning of the project dissemination activities to the students have been done through course and student formation. The list below gives the student number and level of students trained.

- 2 PhD thesis in the Physical Engineering Doctoral Program (in progress);
- 2 Master Science Thesis in the Physical Engineering Course (in progress) + 1 Master Science (expected)
- 1 Bachelor Science Thesis (in progress) + 1 Bachelor Science (expected)
- 1 postdoctoral (2 years)
- 2 Master Science work-study internship
- 1 Master Science internship

From this list UAVR contribute to the training activities and communication to students by involving in the project junior researcher, PhD candidate, Master thesis and Bachelor thesis:

- 1 Junior Researcher (2,5 years);
- 2 PhD Thesis in the Physical Engineering Doctoral Program (which will not be finalised during the INSTABAT timeline) (in progress);
- 2 Master Science Thesis in the Physical Engineering Course (will be finalised during the INSTABAT timeline) (in progress);
- 1 Bachelor Science Thesis (finished).

For INSA Lyon, one PhD student working full time on the project (training or teaching) from the beginning of the project. The PhD defence scheduled for December 19, 2023. INSA Lyon is also starting a new PhD on high-temperature electrolysis for another project who beneficiary to the INSTABAT development of electrochemical battery models. INSA Lyon participating in a master's course on electrified vehicles and part of the topics will cover the power management in hybrid sources, which is somewhat related to the problems dealt with in the project (even if they are closer to the BMS side). The course at INSA Lyon is given on a master specialised on Electric Vehicle: "Mastère Spécialisé Véhicule Électriques (EVE)"<sup>23</sup> for around 7 students/year, 2 years running.

For CEA side 2 young scientists (2 years contract), 1 Master Science thesis and 1 master Science internship are participating from the beginning to the INSTABAT project.

<sup>23</sup> <https://www.insa-lyon.fr/fr/formation/expert-en-vehicules-electrifies>

## TASK 7.2. Exploitation plan

(Leader: VMI; Participants: All) (M12- M36)

During the 1<sup>st</sup> reporting period, a methodology was developed (please refer D 7.4 report) for the identification and evaluation of potential KERs based on the processes shown in the following figure.

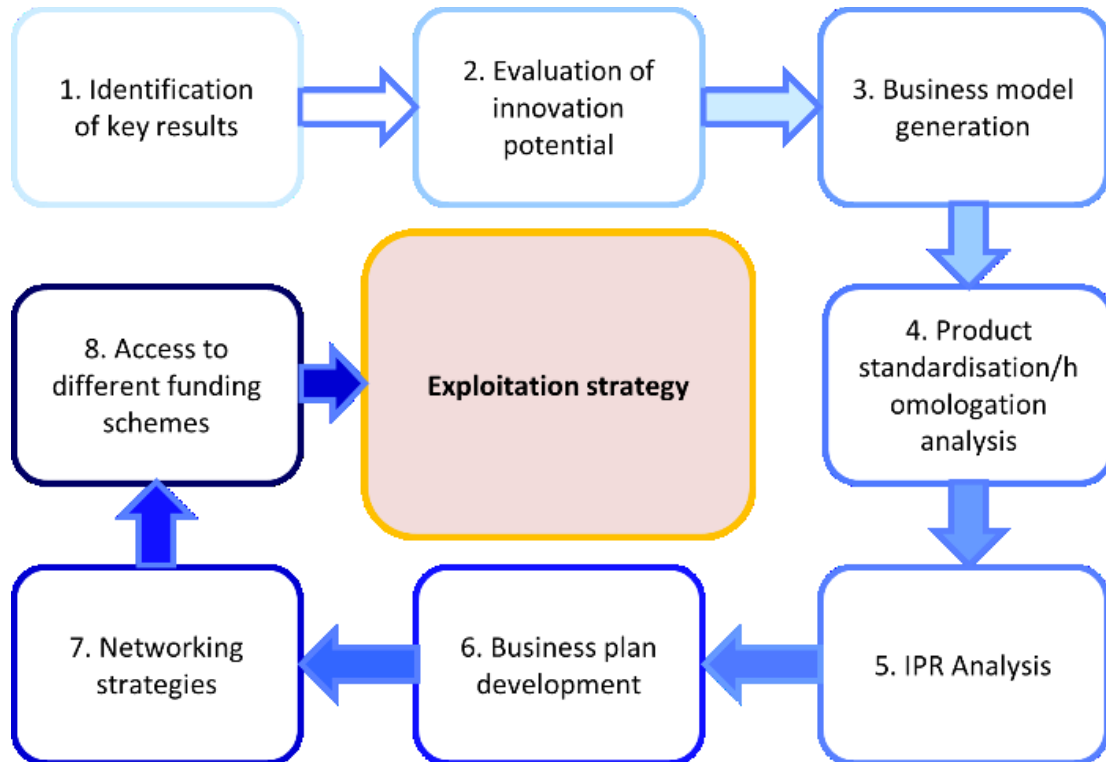


Figure 148: Global overview of the INSTABAT exploitation plan

This general approach in this respect within the INSTABAT project was codified in the D7.4 delivery report. Based on this methodology, a list of 22 KERs was identified at the end of the project, as shown in the following table. The deliverable D7.5 gives the detail of each deliverables and the associate exploitation strategy.

Table 40 Preliminary Key Exploitable Results (KERs) identified during INSTABAT Project by M18

KER-Item	Type of Exploitable Result* (KERs)	Key Result*	Type of Exploitation** CE/SAT***	Ownership	Title	Confidential (YES/No)
KER01	(H)	Training program	(D) Research/SAT	UAVR	PhD thesis	No
KER02	(A)	Product	(D) Research/SAT	UAVR	Customized optical fiber sensors for internal cells parameters discrimination and monitorization	Yes
KER03	(A)	Product	(D) Research/SAT	Consortium	Lab-on-a-battery cell demonstrator	No
KER04	(A) Product/ (B) Process		(D) Research/SAT	Consortium	Industry/Academy collaboration	No
KER05	(H)	Training program	(C) Services/CE	Consortium	Industry/Academy Services	No
KER06	(E)	Methodology	(D) Research/SAT	INSA Lyon	Methodology for development of estimation-oriented (fast) electrochemical models	No
KER07	(D)	Software	(D) Research/SAT	INSA Lyon	E-BASE, state estimation algorithm implementation	Yes
KER08	(D)	Software	(D) Research/SAT	UAVR	T-BASE, Temperature and SOC estimation algorithm implementation	Yes
KER09	(E)	Methodology	(D) Research/SAT	INSA Lyon	Methodology for development of state estimators ("virtual sensors") for reduced electrochemical models	No



KER-Item	Type of Key Exploitable Result* (KERs)	Type of Exploitation** CE/SAT***	Ownership	Title	Confidential (YES/No)
KER10	(D) Software	(D) Research/SAT	INSA Lyon	Fast Finite-Volume Electrochemical Battery Model implementation	Yes
KER11	(D) Software	(B) Selling, Licensing/CE	CEA	Software integrating physical models in charge of predicting internal state of battery cells at electrode and cell scale	YES
KER12	(B) Process	(D) Research/SAT	CEA	Patent filled for process for current collector connection of thin metallic layer supported by polymer film	YES
KER13	(A) Product/ (B) Process	(D) Research/SAT	CEA	Results on stability study of integrated reference electrode	No
KER14	(E) Methodology	(D) Research/SAT	CEA	Comparison methodology for in-situ operando characterisation of multi reference electrodes	No
KER15	(A) Product/(D) Software	(D) Research/SAT	CEA	Multi-sensor cell bench for in-situ operando measurements with embedded processing (BMS)	No
KER16	(B) Process	(D) Research/SAT	Consortium	Process for manufacturing multi-sensor Lithium-ion cell	YES
KER17	(D) Software	(D) Research/SAT	Consortium	In-situ operando characterization database on Lithium-ion cell for cycling and abusive tests	No
KER18	(D) Software	(B) Selling, Licensing/CE	CEA	Software Library integrating reduced order physics-based model together with online sense data to produce improved SOX estimation at BMS Level	YES
KER19	(A) Product	(D) Research/SAT	CEA	Luminescent probe for temperature and Li-ion concentration measurement	YES
KER20	(B) Process	(D) Research/SAT	CNRS	Operando temperature monitoring inside Isolation pad between pouch cells	YES
KER21	(A) Product / (B) Process	(D) Research/SAT	CNRS	Lithium-ion concentration measurements using TFBG	NO
KER21	(A) Product / (B) Process	(D) Research/SAT	CNRS	Temperature and strain measurements using portable mini optical interrogator for EV applications	YES

\*Type of key exploitable result: (A) Product, (B) Process, (C) Model, (D) Software, (E) Methodology, (F) Standardisation, (G) Policy recommendation, (H) Training program

\*\*Type of exploitation: (A) Manufacturing, Assembly, Implementation (B) Selling, Distribution, Licensing, (C) Services e.g. consultancy, training (D) Research

\*\*\*(A, B, C) → commercial exploitable result (CE); (D) → science and technology exploitation (SAT)

## TASK 7.3. Coordination with others EU projects

(Leader: CEA; Participants: All) (M1- M36)

INSTABAT project is on the umbrella of BATTERY2030+ initiative, however natural links were created under the other projects from this initiative such as BIGMAP<sup>24</sup>, HIDDEN<sup>25</sup>, BAT4EVER<sup>26</sup>, SPARTACUS<sup>27</sup> and SENSIBAT<sup>28</sup> (see Figure 149).



Figure 149: BATTERY2030+ largescale initiative and related projects (LCBAT13 and LCBAT14)

- **Participation to the BATTERY2030+ collaboration board meeting**

Coordinator or deputy coordinator of the INSTABAT project was involved in the collaboration board BATTERY2030+ meeting. This biweekly meeting organized by the BATTERY2030+ board is the place for all the stakeholder activities and initiative between partners. During these meetings, a status of the progress of all the projects were presented. We also discussed of the results and cooperation subject between the projects. Some information of workshop and others collaborative activities were presented and discussed. This information is communicated to the INSTABAT consortium after each BATTERY2030+ collaborative board meeting.

- **Participation to the BATTERY2030+ communication board meeting**

INSTABAT coordinator participates regularly to the communication board meeting of BATTERY2030+. The objective is to disseminate the results from INSTABAT to the BATTERY2030+ initiative and participate to the joint communication activities.

Some example of the contribution from INSTABAT projects are listed below:

- 1- A contribution from INSTABAT to the BATTERY2030+ Poster for the Advanced Battery Power Conference (March 29-30, 2022) in Münster.
- 2- A presentation of INSTABAT key results during the internal BATTERY2030+ workshop organised by Lormann Henning the February 14th, 2022 (online).
- 3- Communication of two success stories of the INSTABAT project to Battery2030+ board for the deliverable D111 Project portfolio monitoring.
- 4- Contribution to the letters of BATTERY2030+ initiative
- 5- Participation to the workshop on Sensing and Self-Healing organised by Battery2030+ on the 20th of October 2023

<sup>24</sup> <https://www.big-map.eu/>

<sup>25</sup> <https://www.hidden-project.eu>

<sup>26</sup> <https://www.bat4ever.eu/>

<sup>27</sup> <https://www.spartacus-battery.eu/>

<sup>28</sup> <https://sensibat-project.eu>

The participation to the Battery2030+ communication and board meetings gives the information of all the communication and dissemination activities of BATTERY2030+ initiative and of the other projects (BIG-MAP, SENSIBAT, SPARTACUS, Hidden, and BAT4EVER). This information was shared to the INSTABAT partners along the project.

## • Collaboration between INSTABAT and BIGMAP project

Within BIGMAP, an experimental portfolio of complementary techniques is developed towards the implementation of a multimodal and multiscale characterization platform. Operando synchrotron experiments were realized and analysed according to BIGMAP standards and protocols on INSTABAT pouch cells instrumented with different types of sensors.

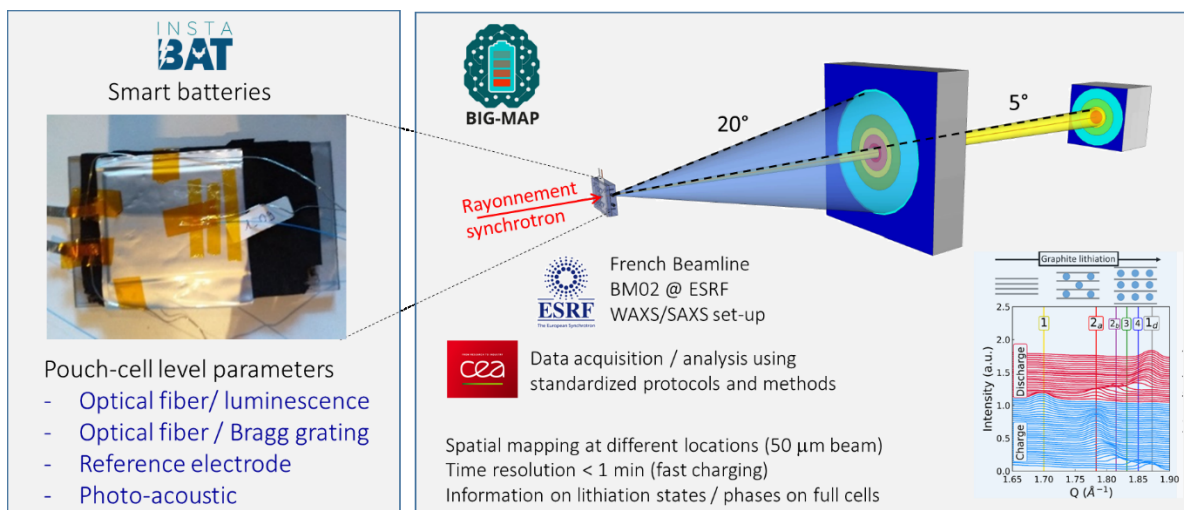


Figure 150: Joint experiment between INSTABAT and BIGMAP project

In the frame of WP2 and WP3 work, Lifun 1.1Ah cells were used for this experimental campaign. CEA has instrumented these cells with OFLumT and RE sensors. Reference cells without sensors were also prepared with one moncell and one multilayer cell to study the effect of the number of layers on the XRD measurement. 3 instrumented cells were prepared from Lifun cell (1.1Ah). One with only OFLumT sensor inside the cell and two with OFLumT and RE sensors inside the cell. Cells are tested in BM02 line at ESRF in operando condition. This work is a collaboration with INSTABAT partners (CEA) and BIGMAP partners (CEA, LEPMI, ESRF)<sup>29</sup>.

The spatially-resolved real-time structural data obtained by X-rays diffraction (phase transitions, strain, local lithiation mechanism) will be cross-correlated to the various sensing data (temperature, local electrode potential), allowing to monitor the potential perturbations of reaction mechanisms due to sensor integration and to correlate micro-to-macro scale performance related to parameter variations along cycling.

The instrumented cells and reference cells are tested in charge and discharge at various rates (from 0.5 to 3 C and from 0.5 to 4 D). Surface temperature was monitoring during the experiment with K-type thermocouples. The signal from sensors giving the internal temperature of the cells (OF LUM-T) and the electrochemistry potential of each electrode (RE) are also recorded.

<sup>29</sup> List of collaborators by partners. CEA: E. Villemin, S. Genies, C. Septet, M. Guillon, O. Ponelet, S. Desousa-Nobre R. Franchi, S. Tardif, S. Lyonard, O. Raccurt ; LEPMI CNRS: C. Villevieille, ESRF : N. Blanc



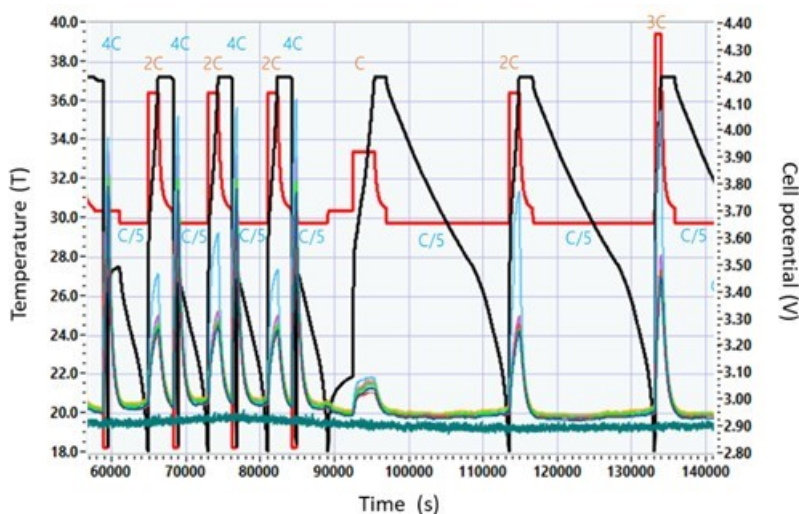


Figure 151: Multi instrumented measurement on LiFun cell (1.1Ah) during ESRF experiment. Cell potential (black), cell current (red), external temperature (blue =  $T_{ab+}$ , green, purple, yellow = cell surface, dark green = ambient)

Figure 151 and Figure 152 show two examples of results from this experiment.

During this experiment we have validated the following steps:

- The instrumentation of cells with 2 sensors (OF LUM-T and RE).
- The cell performance was not modified by the integration of the sensors.
- The setup for, data acquisition and real-time treatment is functional with these 2 sensors
- The measurement of the internal cell parameters with sensors (Temperature, Electrochemistry).
- The local impact of sensor on the cell functioning can be characterized with operando XRD measurements.

A lot of data was collected during the experiment. We are currently analysing the data to correlate the signals from sensors, XRD measurements and electrochemistry phenomena. We will also study the impact of sensors on the cell behaviour.

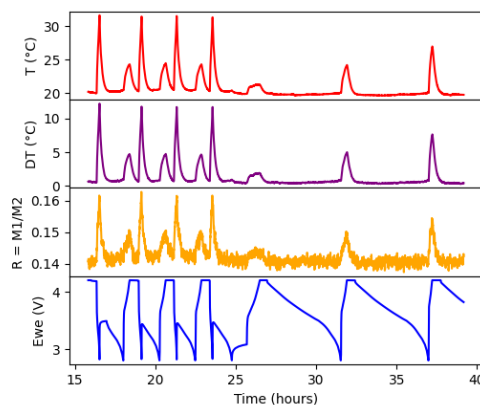


Figure 152: Response of the OFLum-T sensor inside the cell over the time (orange) compared to the surface cell temperature (red), surface heating (purple) and cell potential (blue) during the 4D/1C and 0.5C, 1C, 2C/0.5D cycle. This collective work between INSTABAT and BIGMAP and the results will be valorised through publications.

## • Collaboration between INSTABAT, SPARTACUS and SENSIBAT project

The three project coordinators of INSTABAT, SPARTACUS and SENSIBAT participated in a workshop to discuss about common action and collaboration between the three projects (see D7.8 for more details). During this workshop technical presentation of each project have been done and discussed. The results of these discussions are shared to the partners by each coordinator. We decide of a certain amount of common action:

- 1- Share the ageing protocol in each project to compare and harmonise this part of the work
- 2- Evaluation to show if the INSTABAT multisensor platform could be used or adapted to the sensors from Spartacus and Sensibat.

- 3- Study the possibility to perform common tests on cells.

After this first meeting, we participate to the General Assembly of the SPARTACUS and SENSIBAT project during the year 2022. The objective of this workshop is to:

- 1- Give a full and comprehensive view of the INSTABAT project to the consortium of SENSIGA and SPARTACUS consortium
- 2- Exchange to possible collaboration between each project.

In the same objective, the coordinator of SENSIGA and SPARTACUS participated to a workshop during the INSTABAT General Assembly in 2022 with all the consortium.

The output of this first phase of the collaboration between sensing projects of BATTERY2030+ initiative was the definition of 9 microprojects listed below. For each project, leaders and contact person from INSTABAT, SENSIGA and SPARTACUS was identified.

Table 41: List of micro-project for collaborative works between INSTABAT, SENSIGA and SPARTACUS

N°	Title	Lead person:	Workshop date
1	Exchange of battery cells to compare sensor data	B. Eschelmüller / Jasmin Smajic / Harald Kren	None
2	Data from T-sensors – also by optical sensor technologies	Joris de Hoog / Martin Wenger	None
3	Comparison: Data from Strain/compression sensor – also by optical sensor technologies	Johannes Ziegler	16/06/2023
4	Comparison of approaches to generate models	Didier Buzon, Frederico Bribiesca-Argomodo	None
5	Cost benefit analysis	Jasmin Smajic	None
6	Data management	Lukas Gold	14/06/2023
7	Battery Management systems	Yves Stauffer	None
8	Aging protocols	Olivier Raccurt, Sylvie Genies	None
9	Electronic Hardware	Romain Franchi, Olivier Raccurt, Marco Ranieri	None

However, the process for defining the collaborative topic was quiet long compared to the duration of the project. Despite the participants' willingness to collaborate, it was difficult to implement concrete actions between the three projects. The major difficulty to implement collaborative experiment was the management of the differences between project materials and technologies (cell types and format, active materials, sensor technologies, etc...).

From the 9-micro project in the Table 41 only 2 of them starting with a workshop. During this workshop lot of exchanges was done between the participants and future possible collaboration was defined. The conclusion of these two workshops was detailed below in the D78.

The conclusion of this collaborative action was

- 1- The three project objectives are the same and they are aligned on the BATTERY2030+ roadmap objective for smart-cell part. One of the collaborative areas is to share and compare the results from each project to compare the different approaches. However this comparison is not easy to do due to the differences from each project.
- 2- Somme of approaches such as data management, modelling approaches or Life Cycle Analysis from each of the three projects have been shared between projects during workshops. These exchanges improve the approaches of each project by cross-fertilisation.
- 3- Collaboration between sensing projects on the side of the experiment is difficult to do, but some of recommendation for next project was defined.

All these discussions and collaborative work highlight the challenges and the achievement of each project regarding the roadmap objective. This helped to identify future topics for collaboration, which will be used to build the future collaborative project for the next calls. Lastly, these exchanges helped to coordinate the actions of the three projects and coordinate the actions of the three projects in the relation of the Battery 2030+ roadmap.

### • **Participation to the revision of the BATTERY2030+ roadmap**

From the beginning of INSTABAT project, Olivier RACCURT participates to the working group of BATTERY2030+ for the roadmap revision. During the years 2021 and beginning of the year 2022 several meetings driven by Jana Kumber

(Battery2030+) were organised to discuss and revised the roadmap. The results of this meeting for roadmap revision were shared to the INSTABAT partners for comment and inputs. A publication in Advanced Energy Material was published in May 2022:

J. Aminci et al. "A Roadmap for Transforming Research to Invent the Batteries of the Future Designed within the European Large Scale Research Initiative BATTERY 2030+", Adv. Energy Mater.2022, 12, 2102785, DOI: 10.1002/aenm.202102785.

The revision of the roadmap is a continuous process. We participate as a coordinator of INSTABAT to the meetings with the Battery2030+ community. We participate to the roadmap workshop, organise by Battery2030+ April 23, 2023. Some of the inputs of the sensing part of the new version of the roadmap come from the INSTABAT results. We have redefined the short, medium and long term in relation to the results obtained in the INSTABAT project and the other sensing projects. The new version of the roadmap was published by BATTERY 2030+ jointly to the Battery Europe Association the 26/09/2023<sup>30</sup>.

- **Participation to the building of BATTERY2030+ Projects Data Management Plan**

On behalf of the INSTABAT project, Vincent HEIRIES participated in several meetings (the last one on the 8<sup>th</sup> of April 2022) to define the Data Management Plan. The aim was to harmonise the DMP across all BATTERY 2030+ projects in order to share common ideas and practices. This activity led by Ivano Castelli and Christian Punkt targets to achieve common standards both in terms of data acquisition and battery test protocols. The definition of the related ontology and the related software platforms are supported in the first place by the BIG-MAP project.

- **Participation to the kickoff meeting for energy storage thematic portfolio (EU)**

During the kickoff meeting for Energy Storage Thematic Portfolio (European Union) the programme managers are invited all the European project on this thematic for a presentation of the project activity and results. In this context Kristina Edström and Olivier Raccurt was presented Battery2030+ initiative and INSTABAT project on Monday, 16<sup>th</sup> May 2022 (see below the agenda). This meeting was a good opportunity to communicate around the INSTABAT project and share the results. This presentation has been generating fruitful discussion with IEC programme manager and participants.

---

<sup>30</sup> <https://battery2030.eu/news>



Table 42. *List of deliverables WP7*

Deliverable Number	Deliverable Title	Lead beneficiary	Type	Dissemination level	Due date (in month)	Status
D7.1	Dissemination, Communication and Exploitation Plan	1- CEA	Report	Public	3	Submitted
D7.2	INSTABAT website	1- CEA	Other	Public	3	Submitted
D7.3	Data Management Plan	1- CEA	Report	Public	6	Submitted
D7.4	IPR survey and INSTABAT knowledge management strategy	2- BMW GROUP	Report	Confidential	18	Submitted
D7.5	Exploitation strategy	2- BMW GROUP	Report	Confidential	36+4	Submitted
D7.6	Report on communication and dissemination activities - V1	1- CEA	Report	Public	12	Submitted
D7.7	Report on communication and dissemination activities -V2	1- CEA	Report	Public	24	Submitted
D7.8	Report on communication and dissemination activities - V3	1- CEA	Report	Public	36+4	submitted

## WP8 - Project Management

Work package number	8	Leader	CEA							
Work package title	Project Management									
Participant number										
Short name of participant	BMW	VMI	CNRS	IFAG	FAURECIA	UAVR	INSA	CEA		
Person	months	per	0.5	0.5	0.5	0.5	0.5	0.5	7	
participant										
Start month	M1			End month			M36			

### Objectives

The main objective of WP8 will be to adequately manage and coordinate the project. The WP will also be focused on executing the following specific objectives:

- monitor activities and ensure that the anticipated project outcomes will be in time and in line with the expected results;
- comply with the legal, contractual, financial and reporting requirements of H2020 and EC;
- organise and lead coordination meetings on a regular basis;
- adequately manage the funds of the partners.

### Highlights of most significant results

The project management structures have been set-up and the cooperative work between partners work very well. The consortium working in close cooperation and the interaction between work packages are effective. At the end, the coordination of the project is globally on track to achieve its goals within given contractual timeframe & budget.

During the first period, the coordination of the project suffered from an overload of work for the coordinator (Maud Priour) due to the impact of COVID on CEA activities and the delay of several other projects. The priority has been made for the technical work and the coordination between partners. Nevertheless, this situation impacted the delivery of several management deliverables. Corrective action was taken by CEA to reinforce the coordination by appointing Olivier RACCURT as the new coordinator in February 2022, M. Priour becoming the new deputy coordinator. This action enabled the documents delivery before the date set for the mid-term review.

Finally, the coordination of the project enabled all the tasks to be carried out and the initial objectives to be achieved. Several adjustments had to be made to the schedule to deal with delays in the progress of technical tasks. This led to a 4-month extension in the total duration of the project. We also had to deal with a request from one of the partners to withdraw from the project, but negotiations enabled us to keep the partner until the end, enabling us to complete the associated tasks correctly. Overall, apart from the two points mentioned above, the project management did not suffer any major difficulties during the second phase of the project. The delay in the technical deliverables for WP3 and WP5 is due to the time required to carry out the tests and their analysis, as well as the backlog accumulated during the first phase of the project. However, overall, all the results were obtained at the end of the project, which enabled all the deliverables and milestones to be submitted.

### TASK 8.1. Project administration and management

(Leader: CEA; Participants: All) (M1-M36).

This task lead by CEA covers the activity of administration and management of the project. The description of the “Project Management Handbook” is given on the deliverable D8.1. CEA has also produced a gender equality plan detailed in the D8.2. The coordinator was organised the monthly meeting and general assembly to manage the progress of work. The management of the consortium agreement at the beginning of the project was made on time. During the first period the coordinator is the central contact point for all project partners and monitoring the action with a global view of the project.



To support the collaboration and communication between partners a working space (sharepoint) has been created. For the daily communication between INSTABAT partners and/or the project coordinator tools like email, phone, skype or teams are intensively used.

Monthly meeting with all WP leaders are organized to exchange together on the progress of each WP and coordinates the action. The information from Battery2030+ initiative was shared to the consortium by the coordinator during these meetings.

Online meeting are also organized on WP level by the WP leader.

Following Management Board & General Assembly meetings took place during the project:

- 1- Kick-off meeting 29/09/2020 and 02/10/2020 (online)
- 2- Kick-off meeting on Battery 2030+ initiative 14/10/2020 (online)
- 3- General assembly of Battery 2030+ initiative 07-08/10/2021 (online)
- 4- General assembly of INSTABAT: 23/11/2021 (Grenoble, France)
- 5- General assembly of INSTABAT: 29-30/11/2022 (Aveiro, Portugal)
- 6- Extraordinary Board Meeting : 13-12-2022 (online)
- 7- General assembly of Battery 2030+ initiative 2022 12/09/2022 (Brussel, Belgium)
- 8- General assembly of Battery 2030+ initiative 2023 9-10/05/2023 (Upsala, Sweden)
- 9- Monthly meeting with Coordinator, deputy coordinator  
+ WP leader to manage the progress of work (online)

During the first period of the project, the coordination of the project suffered from an overload of work for the coordinator (Maud Priour) due to the impact of COVID on CEA activities and the delay of several other projects. The priority has been made for the technical work and the coordination between partners. Nevertheless, this situation impacted the delivery of several management deliverables. Corrective action was taken by CEA to reinforce the coordination by appointing Olivier RACCURT as the new coordinator in February 2022, M. Priour becoming the new deputy coordinator. This action enabled the documents delivery before the date set for the mid-term review.

During the second phase of the project, two major difficulties were encountered which required special management by the coordinator.

1. The first concerned the delay in the progress of technical tasks, which had an impact on the achievement of the project's objectives within the allotted time. The consortium decided to request an extension to the project. This was decided at an extraordinary meeting to determine the duration of the extension, which was set at 4 months. Although technically we would have liked to ask for a larger extension, this choice has been constrained by the need to extend the project beyond 2023. This decision was taken collectively at an extraordinary general meeting. Once this decision had been taken, an official request was made by the coordinator to the PO, which enabled the procedure to be launched and led to an amendment to the contract.
2. During the same period, at the start of the second phase, we had to manage a crisis following the announcement by one of our partners (FAURECIA) of its intention to leave the project. This announcement necessitated the convening of an extraordinary general meeting and several meetings for discussions and negotiations between the partner in question, the coordinator, the consortium and the project officer. After a number of exchanges and negotiations, the coordinator succeeded in getting the partner to reverse his decision and remain with the project until the end. However, this period of uncertainty had an impact on project management and the progress of technical tasks. The way the project was managed subsequently enabled us to minimise the impact on the completion of the technical tasks.

Except this two points, there was no difficulties in the coordination.

## TASK 8.2. Governing bodies meetings and interaction with the EC

(Leader: CEA; Participants: All) (M1-M36)

The project coordinator has been in close contact with the project officer and providing regular updates on the progress of the project via email or phone call. One of the first administrative action items at the beginning of the project was the preparation of the preparation of the consortium agreement. The coordinator is responsible to the communication with the project officer and with the partners.

The coordinator was coordinated the whole process for collecting all information needed for the periodic report (technical and financial) in close cooperation with WP leaders.

The project coordinator also prepared the project review meeting which is planned on 20<sup>th</sup> April 2020 (online meeting) with the PO and the expert.

The project coordinator was interacting with the PO for asking project extension for the second phase of the project and the preparation and signature of the amendment.

The project coordinator was interacting with the PO to manage the crisis at the beginning of the 2023 due to the asking from Faurecia (becoming FORVIA) to leave the project. The crisis was solved by the maintaining the FAURECIA participation to the project.

The coordinator was interacting to the PO to prepare the end of the project and the final review meeting.

## TASK 8.3. Risk management and contingency plan monitoring

(Leader: CEA; Participants: All) (M1-M36).

The list of risk was established at the beginning of the project and was based on initial risk determine during the proposal preparation (Table 43). This list was discussed during the monthly meeting and during the general assembly. At this time no new risk was identified from original list from the beginning of the project. The status of each risk was detailed in the (Table 43). Many of these risks have not been encountered or are not considered since they do not correspond to the current advancement of the project. From this list R1 related to the WP1 don't appear and the WP1 is now finished. The R1 is closed. The R2 related to WP2 not appear at this time. From WP2 only R3, R6, R7 and R8 was appear during the first phase of the project. We detail below each of this risk and the risk mitigation measure and results.

Table 43: Risk list, risk mitigation measure and status

Risk	DESCRIPTION OF RISK AND LEVEL OF LIKELIHOOD	WP	PROPOSED RISK-MITIGATION MEASURES	DID YOU APPLY THE RISK-MITIGATION MEASURED (YES/NO)	DID THE RISK MATERIALIZED? (YES/NO)	IF THE RISK-MITIGATION MEASURES COULDN'T BE APPLIED, PLEASE EXPLAIN WHY
R1	Requirements for integration of the multi-sensor platform are not well identified. / Low	WP1	Use partners' (VMI, CEA, and CNRS) valuable expertise on the integration of components such as sensors in the cells.	Not applicable	NO	Not applicable
R2	Some of the key parameters are not capable to be acquired through the sensors. / Medium	WP2	Possible strategies are improving the sensor capabilities, exploring commercial solutions, tuning sensors to measure other parameters.	Not applicable	NO	Not applicable



Risk	DESCRIPTION OF RISK AND LEVEL OF LIKELIHOOD	WP	PROPOSED RISK-MITIGATION MEASURES	DID YOU APPLY THE RISK-MITIGATION MEASURED (YES/NO)	DID THE RISK MATERIALIZED? (YES/NO)	IF THE RISK-MITIGATION MEASURES COULDN'T BE APPLIED, PLEASE EXPLAIN WHY
R3	Signal output from the sensor (any sensor) is too low for detecting key parameters. / Medium	WP2	Routes for amplifying the signal of the sensor will be considered, e.g. by increasing the size of the measurement probes, implementing a higher number of sensing points per probe or multiple sensing probes per sensor.	YES	YES	Not applicable
R4	Implementation of a sensor (any sensor) in a cell disrupt the cell functioning (accelerated degradation, lower performances, etc.). / Medium	WP2	Work towards further miniaturisation and reduction of chemical reactivity of components. Explore different positioning. Increase efforts on other sensor types.	Not applicable	NO	Not applicable
R5	These risks apply to OF/FBG sensor 1. Short lifetime of sensor (fast degradation of polymer fiber). 2. Fibers fragility on handling could make cell assembling process too difficult. / High	WP2	1. Test different polymer materials. 2. Test different structuring strategies such as coating or reinforcement of the fibers.	Not applicable	NO	Not applicable
R6	These risks apply to RE sensor 1. Coating of reference electrode degrades too fast to reach acceptable number of cycles. 2. Parameters signal not stable enough because of electro-chemical instability of the reference electrode material. / High	WP2	1. Manage the coating resistance by improving material stability and/or chemistry. 2. Improve in situ repair strategy and diagnostic by external electro-chemical methods.	YES	YES	Not applicable
R7	This risk applies to OF/Lum sensor Luminescent probes cannot be implemented or	WP2	Explore other luminescent molecules and deposition	YES	YES	Not applicable



Risk	DESCRIPTION OF RISK AND LEVEL OF LIKELIHOOD	WP	PROPOSED RISK-MITIGATION MEASURES	DID YOU APPLY THE RISK-MITIGATION MEASURED (YES/NO)	DID THE RISK MATERIALIZED? (YES/NO)	IF THE RISK-MITIGATION MEASURES COULDN'T BE APPLIED, PLEASE EXPLAIN WHY
R8	do not correctly detect the expected parameters. / High  This risk applies to PA sensor 1. Sensing functionality of the CO <sub>2</sub> sensor cannot be confirmed in the battery cell environment 2. Adaption to the battery cell environment of CO <sub>2</sub> sensor cannot be fully implemented. / MediumMedium	WP2	techniques; explore different strategies of probe positioning (surface, inside porous protective coating); manage and adapt probe chemistry to electrolyte species.  Explore other IR-absorbing gases. Increase efforts on other sensor types.	YES	YES	Not applicable
R9	Physico-chemical phenomena cannot be properly characterised by the mentioned characterisation techniques./Low	WP3	Use of other characterisation techniques not already described in the proposal.	Not applicable	NO	Not applicable
R10	Physico-chemical phenomena cannot be properly correlated to any of the sensors' outputs./ Medium	WP3	Investigate if the physico-chemical phenomena can be indirectly deduced from another sensor output signal.	Not applicable	NO	Not applicable
R11	Post-mortem analysis reveals a negative impact of the sensors on the cell degradation. / High	WP3	Improve integration of sensors and development of sensors materials and chemistry (retroaction on WP2 for sensor development).	Not applicable	YES	Not applicable
R12	Low correlation between virtual sensors outputs and actual values./ Medium	WP3	Perform more validation against models and characterisation tests to improve the virtual sensors.	YES	YES	YES



Risk	DESCRIPTION OF RISK AND LEVEL OF LIKELIHOOD	WP	PROPOSED RISK-MITIGATION MEASURES	DID YOU APPLY THE RISK-MITIGATION MEASURED (YES/NO)	DID THE RISK MATERIALIZED? (YES/NO)	IF THE RISK-MITIGATION MEASURES COULDN'T BE APPLIED, PLEASE EXPLAIN WHY
R13	Interplay between thermal dynamics and electro-chemical parameters might reduce reconstruction accuracy at some points in the battery./ Low	WP4	A modular approach is considered (not beginning with fully coupled dynamics between electro-chemical and thermal models).	Not applicable	NO	Not applicable
R14	Spatially inhomogeneous behaviour may not improve quality of reconstruction when only extremely localised measurements are available./ Medium	WP4	FBG sensor adds previously unavailable information.	Not applicable	NO	Not applicable
R15	Flat open-circuit potential curves and low-sensitivity of other outputs to variable and parameter variation may have a negative impact on sensitivity of the algorithms to measurement and model uncertainties./ High	WP4	Data from reference electrode available, as well as measurements in the electrolyte coming from Li <sup>+</sup> concentration sensor.	Not applicable	NO	Not applicable
R16	Implementation of multiple sensors in a single cell disrupt the cell functioning (accelerated degradation, lower performances, etc.)/ High	WP5	Integrate sensors gradually. Discard defaulting sensor.	Not applicable	NO	Not applicable

- **R3: Signal output from the sensor (any sensor) is too low for detecting key parameters.**

This risk appeared during the work in WP2 for three sensors: OF/FBG, OF/Lum and PAS-CO<sub>2</sub>. For each of these sensors the signal from the first version was too low to give the required accuracy. The mitigation procedure applied was to work on the technical aspect of the sensor to increase some of parameters and improve the sensitivity. In the case of OF/FBG sensors reflectivity had to be increased. For the OF/Lum the sensitivity was improve by study alternative optical probe and by improve the coating procedure on the fiber. For the PAS-CO<sub>2</sub> sensor technical improvement of the electronics was used to improve the sensitivity. The detection limited was reduce from 50 to 2 ppm. This improvement for the three sensors removes the risk and we can say the mitigation procedure gives effective results. The table below resume the mitigation and results.



Risk apparition	Mitigation	Results
OFLumT	Improve optical detection and signal treatment	Detection limit: DT=2°C to DT=1°C
	Change of luminescent material	Higher thermal sensitivity: Sa=0,0012 (cps/°C) to Sa=0,003 (cps/°C)
PASCO <sub>2</sub>	Technical improvement of the sensor	Reduce the detection limit from 50 to 2 ppm (in Ar atmosphere)

- **R6: These risks apply to RE sensor: low stability of RE material.**

This risk appeared at the beginning of work with RE developed in the project with gold coating. The mitigation procedure was applied to identify a solution to protect this material or to change the composition of RE material. Finally, the solution to use LFP coating as reference electrode show a very good stability. The good results from stability test closed this risk and demonstrate the efficiency of the mitigation procedure.

The table below resume the mitigation and results.

Risk apparition	Mitigation	Results
YES	Change of active material for RE	Improve the stability, RE is functional

- **R7: This risk applies to OF/Lum sensor- Luminescent probes cannot be implemented or do not correctly detect the expected parameters.**

This risk appeared during the work on Li<sup>+</sup> optical probe. Several molecules were studied to find the right candidate for Li<sup>+</sup> detection and can be working into the electrolyte. The mitigation procedure was applied by study alternative way to find best optical probe. Based on a deeper study of the state of the art and with the expertise of CEA, a promising optical probe was synthesized and successfully tested in carbonate medium for lithium detection. These good results show that the mitigation procedure was efficient.

Risk apparition	Mitigation	Results
YES	Several optical probes (molecules) was study to find the appropriate candidate with stability in electrolyte	several optical probe was successfully synthesized and tested in electrolyte and bonding in optical fiber

- **R8: This risk applies to PA sensor: Sensing functionality of the CO<sub>2</sub> sensor cannot be confirmed in the battery cell environment, Adaption to the battery cell environment of CO<sub>2</sub> sensor cannot be fully implemented.**

This risk appeared during the WP2 work. The first test of PAS CO<sub>2</sub> sensor into pouch cell does not give conclusive results. The mitigation procedure was applied to understand the reason of this behaviour. It appears that the protocol used to integrate the sensor was not adapted to the sensor specificity. The protocol used damaged the sensor due to vacuum phase. Alternative way to integrate the sensors was propose and applied during the second phase by using specific chamber to evaluate the sensitivity of the sensor to the electrolyte. The results of this analysis show a dependences of the signal of the PAS CO<sub>2</sub> sensor to the vapour electrolyte. Infrared analysis of the absorption spectrum of carbonate

solvent use in electrolyte (EC, DEC, DMC) show an overlap to the CO<sub>2</sub> absorption band use by the PAS CO<sub>2</sub> sensor. With this overlap in the infrared spectrum, the PAS CO<sub>2</sub> sensor can't distinguish CO<sub>2</sub> to electrolyte vapour. Some solution of mitigation was identified during the project but require too much effort to be implemented before the end of the project.

Risk apparition	Mitigation	Results
YES	Change the integration procedure by using : 1- specific chamber and manage the pressure to limit the impact on sensor during integration 2- work on alternative integration way 3- change optical component and wavelength for detection	- Development of new version of sensor to reduce size. Integration was not tested in the cell. Qualification in chamber was not completely successful - New development in optical component is not possible in the frame of INSTABAT project

- **R11: Post-mortem analysis reveals a negative impact of the sensors on the cell degradation. / High**

This risk appeared during the WP3 work for the FO-TL and the RE sensors. We observe around this two sensors more lithium plating for ageing test at low and high temperature. The origin of this defect related to the presence of sensor was clearly identified. It's due to the thickness of the sensor induce geometrical change between electrodes and create locally the condition for lithium plating. This effect can be reduce by reduce the size of the sensor. For Example the optical fiber use for FOTL would be reduce to mitigate this effect. Lithium plating is not present with the FO-FBG sensors. This sensor use a fiber with a smaller diameter. During the project we don't have the possibility to test the mitigation way consisting to reduce the size of the sensor.

In fact, except the apparition of lithium plating locally around the sensor, we don't see any quantifiable negative effect on the performance, ageing and safety of the cell. Of course this results need to be confirm by future study.

Risk apparition	Mitigation	Results
YES	Improve integration of sensors and development of sensors materials and chemistry (retroaction on WP2 for sensor development).	- Improvement of integration can limit negative impact on the integration to the cell performance - The impact of size of sensor (FOTL, RE) to the local degradation was identify by post-mortem analysis and the recommendation is to reduce the thickness of the sensor. (not implemented during INSTABAT)

- **R12: Low correlation between virtual sensors outputs and actual values -> E-BASE**

During the development of E-BASE virtual sensor the first results show a low correlation between outputs and expected values. The analysis of the input data and the model use was done to find the reason. By adjusting some of model parameter and by working on the code the second version of the E-BASE was improve. The mitigation strategy was work in this case.

Risk apparition	Mitigation	Results
YES	Adjustment of the model parameter & change the model definition to improve the representativity	The correlation between E-BASE output and experimental data is not completely achieve and need more work to be improve



Table 44. *List of deliverables WP8*

Deliverable Number	Deliverable Title	Lead beneficiary	Type	Dissemination level	Due date (in month)	Status
D8.1	Project management Handbook	1-CEA	Report	Public	1	submitted
D8.2	Gender equality action plan	1-CEA	Report	Public	6	submitted
D8.3	Periodic report to the EC	1-CEA	Report	Public	20	submitted
D8.4	Periodic report to the EC	1-CEA	Report	Public	36+4	submitted

## 1.3 Impact

Back in 2017, the EC warned about the serious risk for Europe to become irreversibly dependent on battery cells imports, for the rollout of clean mobility, the industry and the stabilisation of power grids integrating high shares of variable renewable energy sources. According to the views of the European Battery Alliance (EBA), if Europe does not act fast, catching up with Asia will become impossible<sup>31</sup>. Just in the field of mobility, given the size of the EU automotive sector (13.3 million jobs, or 6.1% of the total workforce<sup>32</sup>) it is a strategic imperative to reach the EBA's target of 200 GWh/year manufacturing capacity by 2025. The EU could capture a battery market up to €250 billion per year from 2025 onwards to cover an estimated EU need of at least 10-20 Gigafactories. To reach this goal, the EU must bring innovative batteries to the market to attract potential end-users and make them adopt EU batteries. INSTABAT aims at bringing innovation to batteries by including a smart multi-sensor platform into the battery cell ("lab-on-a-cell"). This embedded platform will allow a more effective battery use and control over lifetime through high-accuracy SoX cell indicators. INSTABAT will also advance EU knowledge, by developing/adapting new sensors and reducing the current lack of knowledge about cell internal behaviour. This will prepare the grounds for a highly innovative new generation of batteries. In addition, by prolonging battery life and facilitating battery second life, INSTABAT will have a positive impact on costs and environmental aspects.

### 1.3.1 General impacts

INSTABAT contribute to an improvement of performance and strongly force the development of sustainable battery storage solutions for Li-ion batteries at a more competitive price. This global impact is not only during the project, but more broadly on a long-term basis through the contribution of new technologies. The "lab-on-a-cell" approach developed during the project can be used to develop a new generation of Li-ion and post-Li-ion batteries in the future, which is aligned with the objectives of the Work Programme<sup>33</sup>. Moreover, INSTABAT will contribute to a successful mass introduction of batteries for mobility, allowing for substantial improvements leading to an ultra-high performance. The INSTABAT project is also well aligned with the specific impacts set out in the call LC-BAT-13. The list of 6 general impacts of the project as described below

**Impact 1: Increased quality, reliability and life (QRL) of the battery system by maximizing the performance and safety of the complete battery system over its lifetime, including forecasting the remaining lifetime under different use cases, especially the suitability for possible "second life" usage.**

INSTABAT was given the tools and the way to maximising the QRL of Li-ion batteries via a substantial improvement of the monitoring of battery key parameters<sup>34</sup> during operation. The development of more efficient cell SoX indicators (States of Charge, Health, Power, Energy and Safety) was achieved and we demonstrate the improvement of the BMS function for performance and safety management. With the lab-on-cell concept and new sensor technologies developing in INSTABAT offer the possibility to monitor the key battery parameters with high accuracy.

The more accurate SoX cell indicators offer the possibility to improve the battery usage and lifetime by: (1) reducing battery safety margins, thus allowing less over design and less inefficient use of capacity; (2) increasing battery functional performance thanks to feedback loops from the BMS, based on the SoX indicators, adapting the management of the battery in real-time; (3) forecasting the evolution of SoX through time, including forecasting of the remaining lifetime of the battery; (4) providing triggers for battery self-healing or replacement of defective components; (5) recording data about the cell, granting more efficient second life usage. Therefore, better battery management and wiser use of the battery will be possible. The smart sensors integrated in the battery will act as tools to record the performance, ageing and safety of Li-ion batteries during operation by measuring precisely the degradation phenomena in the core of the cells.

<sup>31</sup> <https://energypost.eu/the-european-battery-alliance-is-moving-up-a-gear/>

<sup>32</sup> [https://ec.europa.eu/growth/sectors/automotive\\_en](https://ec.europa.eu/growth/sectors/automotive_en)

<sup>33</sup> [http://ec.europa.eu/research/participants/data/ref/h2020/wp/2018-2020/main/h2020-wp1820-cc-activities\\_en.pdf](http://ec.europa.eu/research/participants/data/ref/h2020/wp/2018-2020/main/h2020-wp1820-cc-activities_en.pdf)

<sup>34</sup> Temperature and heat flow; pressure; strain; Li<sup>+</sup> concentration and distribution; CO<sub>2</sub> concentration; "absolute" impedance; potential; polarization

Better thermal management of batteries will be enabled by identifying critical zones for the appearance of hot spots thanks to thermal profiles recognition through multi-point and multi-layer monitoring.

The “second life” usage aspect will be ensured, based on a solid and structured lifetime characterisation and data logging. By continuously recording the information generated from the multi-sensor platform, a complete data logging covering the entire life of the battery will be created, granting a more efficient second life usage. The data generated from the battery first life will be key to determine its second life capabilities. In short, our foreseen ambition is to establish the health record of the battery, analogous to personal health records for human beings to estimate its degree of fatigue.

During INSTABAT project, focus was made on two use cases: “High-power charging” and “Cycling at extreme conditions”. The results of these selected use cases for EV applications are to acquire high-power charging profiles and understand how they could be better adapted by monitoring the SoX in real-time. These profiles were considered extreme temperatures to take full advantage of the power and capacity of the cell without any degradation. Cycling at extreme temperatures was also studied. The results show that the multi-sensors used to monitor the cell doesn’t affect the performance and safety and offer the possibility to increase the lifetime by limiting the critical stress factor apparition.

### **Impact 2: Assured best possible performance and lifecycle for a range of applied cell types at lowest cost**

The extra cost of the sensors’ materials, assembly, integration and wiring will be compensated and even reduced by the increase of the total number of cycles (estimated increase of 20% over the battery lifecycle), which is linked to a slower ageing in fast charging (see KPI 13) and better recycling possibilities. In addition to all the improvements in terms of performance and lifecycle already explained in “Impact 1” above, the following aspects have to be considered:

- A more efficient use of the cell capacity will lead to a need for a lower total installed battery capacity to reach the same performance, which will contribute to decrease the cost of the battery.
- A safer use of batteries will contribute to decrease the hazards, e.g. associated with battery usage in EVs and energy storage system applications (thermal runaway, etc.). When a hazard takes place, the cell could be damaged, making the whole battery pack unusable. The costs for replacing battery packs being very high, it is expected that the end-users will consider paying for the “lab-on-a-cell” platform to reduce their exposure to those risks.
- An increase of the lifetime of batteries (due to a more efficient and safer use of batteries) could widen the potential for a second life usage, which means a reduction of the effective cost per cycle as well as a positive impact on environmental aspects.
- Real-time monitoring of key cell parameters with high time and spatial resolution will allow detecting sources of potential problems early on. This could act as a trigger for defective components replacement and self-healing, which would also contribute to increase battery life and thus, reduce its cost.
- The cost of the “lab-on-a-cell” platform could also significantly be reduced in the mid-term as it provides more validation datasets for the models (thanks to the data collected from the sensors). Higher-accuracy and precise models will reduce the need for physical sensors, which will also contribute to reduce the cost of the “lab-on-a-cell” platform.
- The application of the “lab-on-a-cell” was considered for different cell types in the techno-economic analysis conducted as part of Task 6.2.

### **Impact 3: Industrial opportunities for exploiting new concepts and technologies for integrating multifunctional sensor capabilities in the battery cells and for optimizing the performance of the complete battery systems**

INSTABAT was advanced EU knowledge by developing/adapting sensors, enabling in-cell sensing capabilities and reducing current lack of knowledge about internal cell behaviour. These outputs of the project will pave the way for a highly innovative new generation of batteries manufactured by the EU industry.

All the technologies developed during INSTABAT project was validated at lab scale at the end of the project (at least TRL 3) and reaching at a higher TRL when possible. After the project (INSTABAT-EXPANSION), the new technologies will be demonstrated at module and pack level, ensuring the scalability of manufacturing concepts to the features of large battery production lines (TRL 8-9). Some activities, such as new manufacturing processes, new machines and adapted cell and module set-up will be necessary, to ensure the market uptake of these technologies. Therefore, the demonstration at a TRL 8-9 of the technologies and results obtained in INSTABAT (physical sensors, virtual sensors,



validated thermal and electro-chemical models, BMS algorithms, multi-sensor platform or “lab-on-a-cell” approach) will allow generating business opportunities for the exploitation of the new concepts and technologies obtained as a result of this project:

- **Business opportunities for physical sensors manufacturing:** the partners involved in the sensor development will transmit the know-how to industrial partners in order to manufacture the sensors at a larger scale and study all their commercial applications such as: (1) their integration in INSTABAT multi-sensor platforms for mobility applications; (2) their use in other sectors where the safety aspect is important, such as the aeronautics and naval sectors where battery failure can lead to dramatic consequences (in this sense, a letter of interest has been signed by SAFRAN); (3) new applications needing further developments, e.g. adaptation to other cell chemistries and geometries or adaptation of sensors monitoring CO<sub>2</sub> to the monitoring of other gases;
- **Business opportunities for the “lab-on-a-cell” concept:** many battery manufacturers (VMI, who is an INSTABAT partner, but also Lithops and Leclanché who signed letters of interest for the project) would be interested in adopting new solutions for characterising new cell materials and formats, understanding the phenomena taking place at cell level and understanding the interaction between the cell components (anode, cathode, electrolyte, etc.). The lab-on-a-cell could indeed be used as a material characterisation platform. The knowledge obtained at cell level in terms of thermal and chemical behaviour could open the door to new cell designs and materials.
- **Business opportunities for battery manufacturers:** many battery manufacturers are interested in this project due to the improvement opportunities offered in terms of performance and safety of batteries. Indeed, the “lab-on-a-cell” approach would bring them an added value compared to the products offered by their competitors. In this project, the battery manufacturer partner (VMI) will focus on the battery requirements for the mobility applications. However, the multi-sensor platform concept could reach many other applications in the future: (1) aeronautics and naval sectors where safety aspects are critical; (2) stationary applications, such as renewable energy generation or energy storage solutions for industrial plants and household energy storage, where lifetime and performance are fundamental; (3) Industry 4.0., where a higher performance, increased efficiency and lifetime are needed.

INSTABAT will bring a technological competitive advantage to the EU battery industry and opening the door to an innovative new generation of batteries.

#### **Impact 4: Better identification of defective cell components, allowing replacement of components or introduction of local targeted repair mechanisms, such as self-healing, in future cell design and chemistry generations.**

INSTABAT “lab-on-a-cell” can also serve to identify defective components and local spots in the cell that would need repairing. The spatially and temporally resolved monitoring of cell key parameters and their correlation with the degradation phenomena will provide the BMS with a detailed knowledge of the cell so that it could trigger self-healing capabilities or predict the replacement of components if needed.

The sensing technologies developed in INSTABAT could allow to: (1) identify defective components that must be repaired; (2) develop mechanisms within the battery for the on-demand administration of molecules that can e.g. solubilize a resistive deposit such as Solid Electrolyte Interphase; (3) restore a faulty electrode within the battery. This constitutes a transformational change in battery science, as it supposes a great potential for developing supramolecular architectures, which could be physically or chemically cross-linked to heal the electro-chemically driven growth of cracks/fissures in electrode materials. An intimate synergy between intelligent BMS and self-healing capabilities will further secure success and enable EU to lead the world in sustainable technology development.

Collaboration with the LC-BAT-14 consortia on this topic was fundamental for INSTABAT. The “lab-on-a-cell” approach is the first step towards our long-term ambitious vision of combining sensing and stimulus-driven self-healing functionalities within the cell for developing smart cells.

### **Impact 5: Improved knowledge on different factors (use patterns, ambient temperature etc.) impacting on battery performance and characteristics.**

The INSTABAT “lab-on-a-cell” is a powerful tool to gather a vast knowledge on the thermal and physico-chemical degradation phenomena (SEI growth, dendritic formation, etc.) taking place at the cell level. The physical and virtual sensors to be developed in INSTABAT bring in real-time data with a large scope of information never be done before. The monitoring of the evolution of the cell key parameters produce large amounts of data that correlated to battery cell degradation phenomena. This “big-picture” is a major advantages to study more in depth the impact of the use of the battery (cycling patterns, external temperature, etc.) on the battery performance and ageing.

Large amounts of data was collected on Li-ion cells through the characterizations and the tests carried out for the two INSTABAT use cases. The INSTABAT platform is a powerful tools to study the behaviour of cells. This platform can be used for research activities and for cell development to produce a large amount of data. In the future if we have the opportunity to use this platform on a large quantity of cells to produce a large dataset we can imagine to using statistical approaches e.g. to obtain a higher precision for calculating safety limits (higher accuracy for thermal runaway detection...).

### **Impact 6: Provide foundations for collecting large amounts of data that can be used for autonomous discovery of future battery chemistries and for development of advanced modelling approaches to improve current chemistries with a view of optimising cell performance for mobility applications (link with topic LC-BAT-6-2019)**

As already mentioned previously, the “lab-on-a-cell” can also be used as an in operando characterisation platform for battery materials. INSTABAT physical and virtual sensors as well as models and BMS algorithms will be designed keeping in mind that they should be adaptable to other cell geometries and chemistries (for that matter, one test dedicated to another cell chemistry and a broader paper study will be conducted during the project).

Already in INSTABAT, large amounts of data was collected on Li-ion cells through the characterisations and the tests carried out for the use cases. This data was be correlated with the physico-chemical degradation phenomena taking place in the cell. The INSTABAT consortium will share their battery key parameters datasets with the LC-BAT-6 and LC-BAT-12 consortia.

Further tests could provide even larger amounts of data from the heart of battery cells, to allow studying new materials and discovering new cell chemistries beyond Li-ion. In this way, INSTABAT aims at contributing to autonomous material findings and interphase engineering. This would also open the door to develop advanced modelling approaches to improve current chemistries, contributing to a future cell development for mobility applications, in line with the topic LC-BAT-6. The INSTABAT consortium will therefore collaborate with other consortia to provide the foundations for collecting large amounts of data to be used for autonomous discovery of advanced battery chemistries (LC-BAT-12) and for development of advanced modelling approaches to improve current chemistries (LC-BAT-6) with a view of optimizing the cell performance for mobility applications.

## **1.3.2 Impact on the project partners**

The project was creating a collaborative environment for the consortium to accelerate the development of INSTABAT technologies. All the partners of the consortium were improving their own innovation capacities and consolidated their positioning in the battery sector.

- **CEA**

During the INSTABAT project, the research at CEA was contributed to explore new technologies (e.g. luminescence (OF/Lum)) and increased CEA know-how and knowledge in the following areas: reference electrode (RE), cell assembly and testing, battery modelling and BMS. With the achievement of the goals of the project, CEA increase their innovation capacity and consequently gain competitiveness to create more industrial partnerships. The results of this project will enhance CEA's competitiveness in the batteries' field, and thus contribute to Europe's development and positioning in this sector. More broadly, participation in the Battery2030+ initiative has helped create links between European research players and major associations in the Battery fields. This will enable us to generate new collaborations and contribute to the acceleration of European sovereignty in this field.

- **CNRS**

The present project has helped CNRS to enhance its vast knowledge about the characterisation of commercial battery cells, increasing their innovation capacity in cell design for future battery technologies. For CNRS, this project has also contributed to an increase of the understanding and control over batteries, ultimately contributing for extending the lifetime of such systems and enabling more reliable second life applications. The collaborative work developed as part of this project has enabled us to learn about the importance of classifying different battery chemistries in relation to internationally recognized electric vehicle driving tests (WLTP). This learning could serve as a preliminary step towards the integration of batteries in electric vehicles. The collaborative work developed under this project has also where new design packs are emerging. Lastly, this project gave us the opportunity to explore a new class of tilted fiber Bragg Grating Sensors (TFBG's) that provide access to other metrics such ionic gradient via the measurement of changes in electrolyte refractive index. The Li-S system has been used as a proof of concept. Finally, INSTABAT is helping us to strengthen our network of companies and research institutions involved in battery instrumentation technologies.

- **INSA**

INSA's participation to INSTABAT will contribute to develop the basis for future R&D in the area of electro-chemical model exploitation for advanced BMS with potential application to novel chemistries, increasing INSA's visibility in the field and allowing for its participation in new R&D projects. In addition, this project has financed a PhD position in Control Systems and allowed for further development of collaborations in the area of modelling and estimation for electrochemical energy storage systems. Overall, this project has consolidated activities linked to electrochemical systems and dynamical models at INSA and increased collaborative activities. Furthermore, the codes developed for the project can serve as a basis for future, more applied developments with immediate industrial applications.

- **UAVR**

The INSTABAT project will allow UAVR to increase their innovation capacity by facilitating the creation of new partnerships in the future and opening the door to new research projects in the field of INSTABAT. The project will have a positive impact on UAVR's visibility, allowing an increase of their presence at conferences and other events. The collaborative work with relevant industrial partners will facilitate further research in the field of INSTABAT and produce innovative patents related to fiber sensing and battery virtual sensors, creating new market opportunities for industries. In addition, thanks to this project, UAVR will create 4 jobs (3 MSc and 1 PhD thesis in Physical Engineering program).

- **IFAG**

For IFAG, the work done within the INSTABAT project has significantly increased the understanding of the potential but also the challenges regarding the utilization of its microelectronic and –mechanical technologies for CO2 sensing in the context of the battery cell market. With IFAG as WP leader and both, BMW and VMI, being responsible for the deliverables, the collaboration in WP1 provided an excellent opportunity to strengthen the partnership between these three companies. This encompassed in particular a better mutual understanding of the respective general requirements and constraints and provides an excellent basis for future joint projects. The close collaboration with CEA in WP2 and also WP5 was very fruitful and provided IFAG with useful feedback for the development of new generations of its CO2 sensor, which are already much better suited for the target application in battery cells.

- **FAURECIA**

This project is well aligned with FAURECIA's (within FORVIA group) goal to adopt "zero emission vehicles" mobility. Being one of the largest automotive equipment suppliers, FORVIA Group is highly concerned by the battery's environmental performances at the lowest cost in order to offer their customers the most competitive products. This project will contribute to improve FAURECIA's innovation capacity.

- **BMW**

This project will allow BMW to provide better battery packs to customers, at lower cost and with improved functionality, which will lead a stronger market position with increased sales. This effectively impacts a wide range of jobs at BMW, from worker level to highly skilled experts.



---

- VMI

The outcome of INSTABAT will significantly support future material and cell development activities. Using these new methods, a considerable reduction in product development times is expected.

---

## 2 Update plan of the exploitation and dissemination results

The plan for exploitation and dissemination of results as described in the DoA and detailed in the D7.1 is still relevant.

---

### **3 Update of data management plan**

The data management as described in the deliverable D7.3. For the period cover by this report, no modification of the data management plan is required.



## 4 Fellow-up of recommendations and comments from previous review(s)

From the review report receive in Mai 2022 after the midterm review, the recommendation receive are listed below:

(1) to consider a second review of the CO<sub>2</sub> sensor. It seems, in view of the experts, that its implementation in the cell body is a rather challenging task. Therefore, alternative solutions could be an attractive replacement to collect the required information within the cell.

(2) to consider adding additional ports, or a more flexible configuration to the multi-sensor platform (for other types of sensors), or to specialize the multi-sensor platform appropriately, to enhance commercialisation opportunities and the use of these results by other research teams.

(3) to manage the website more actively, for example by providing additional information on future events and upcoming news, taking advantage of the international interest on the website. In addition, it is recommended to consider closer collaboration with the other relevant EU sensor projects (i.e. SPARTACUS, SENSIBAT), which could be attractive for finding and achieving synergies.

(4) to consider putting further effort in near-time publishing of the work results, especially in scientific journals. It could also be useful to motivate students, including master and bachelor students, to get in touch with the project.

The coordinator and the consortium were careful to take these recommendations into account during the second phase of the project.

### 4.1 Answer to the recommendation 1

During the second phase of the project we did not decide to explore alternative technologies for CO<sub>2</sub> sensor as this would have had too great an impact on the project. The strategy explored was to work on reducing the size of the sensor. We have successfully demonstrated that it is possible to significantly reduce the size of this sensor. We believe that the size obtained is compatible with the cell technologies used today like prismatic cells. However, the integration could not be completed due to other limiting factors identified in the meantime, such as the cross sensitivity between the CO<sub>2</sub> and the carbonate gas from electrolyte.

### 4.2 Answer to the recommendation 2

The multi-sensors platform developed in INSTABAT project is a flexible tool. The versatility of the platform was one of the selection criteria in the initial specifications. The software and hardware have been developed to be versatile and to accommodate other types of sensor. However, this adaptation will require future development and will impose certain specifications for the integration of new components. However, these specifications are standard and should not pose any major difficulties.

### 4.3 Answer to the recommendation 3

The website was more actively managed during the second phase of the project. We also took part in more communication activities than in the first phase (see D7.8). When we write this report 9 publication was submitted and 7 was already accepted and published. We participate to 22 scientific conferences and workshop. We also collaborated actively with BATTERY2030+ and other EU sensors project (see WP7 and D7.8).

#### 4.4 Answer to the recommendation 4

The second phase of the project was richer in publications and communication. This is because there were more results in the second phase of the project. In addition, we are continuing and will continue the publication effort even after the end of the project. It is important to make the most of the results obtained. The list of participations in conferences and workshops as well as the publications produced are listed in the deliverable D78.

When this report is writing a number of publication and communication was achieved from the beginning of the project: a total of 10 publications in international journal, one book chapter; 1 article selected for the cover front page of Advanced Sensor Research journal and 22 participation to workshop and conference. For more detail see D7.8.

During all the project we also try to motivate student and young scientist to participate. See "Training activities and communication to student » part of the D7.8.

#### 4.5 Fellow-up of recommendations and comments from final review

From the review report receive in April 2022 after the final review, the recommendation concerning the period cover by the report receive are listed below:

Some deliverable reports need a quality check and others some improvement, mostly in terms of readability, to catch up with the very good scientific work done. Therefore, the following deliverables should be revised and resubmitted: D4.8, D6.1, D7.8 and D8.4.

In deliverable 4.8, the presentation of data is sometimes incomplete. For example, in Figure 16, it is claimed that experimental and simulated data should be compared there. However, it is unclear from the legend, which data is simulated and which experimental.

The abstract does not include the existence of a User Guide for the developed software GUI.

The conclusion (chapter 4) is incomplete, because it only handles the comparison of the model predictions with the experimental results and does not include the description of the GUI, which is a large part of the report. This should be reworked.

Also, the report would benefit from a glossary similar to that in D 4.7.

Deliverable 6.1 would benefit from an abbreviation index.

Also, Table 2 should be revised so that the suppliers are alphabetically listed. A link to the website of the suppliers, or to its full addresses, should be included. You must check if all of the suppliers mentioned in the report are included in Table 2, e.g., the company KELIBER is only mentioned in the text but not in the table. The market research must be better completed. It is to be noted, that on some components, only one or two suppliers are named (i.e.: Solvay for Binder material, Bikar and Avotec for Arrestor tabs), which does not reflect a comprehensive market analysis. There are several content-misleading phonetic typos (inside instead of insight, on-side instead of on-site etc.) which should be corrected, as should a number of dead links.

Deliverable 7.8 claims to be composed of four parts, namely an introduction, the objectives, the dissemination and communication tools and the activities. This is to some extent misleading, as the first two parts are handled within half a page. Especially the objectives are only referenced towards another deliverable within one (!) single sentence. This requires rework, as that approach makes the report user-unfriendly to read. Part 2 has only 2 lines when it should detail, as stated on page 6, paragraph 1.3, "the communication and dissemination objectives for the reporting period are detailed", and not refer to deliverable 7.1. Also, paragraph 1.2 should include what is new in relation to deliverable 7.6. Also, some of the figures (e.g., Fig.10) are illegible due to very small text and a concluding chapter, giving a resume of the deliverable, would be fine.

So, the report in its quality obviously does not live up to the high quality of the activities which are described there, and the quality of most other deliverables.

Some other deliverables don't need to be resubmitted but would benefit significantly from a quality check concerning spelling and grammar and missed reference/figures/ links. Also missing conclusions and an abbreviation index (D2.4,

D3.1, D4.5, D4.6, D4.7, D4.10, D5.2, D5.3, D6.2, D7.7). Details are put down in the comments on the individual deliverables, in the Annex.

## 4.6 Answer to the recommendation from the final review

The deliverables D4.8, D6.1, D7.8 and D8.4 have been corrected in accordance with the experts' recommendations. The new version of the deliverables were submitted on the EU portal.

For the D4.8 some of figures have been modified in order to compare experimental data with simulations. The text was updated to clarify the results analysis and avoid the confusion in the understanding. The abstract was updated to include the description of the GUI.

A glossary has been added to the deliverables as requested. The table 2 of the D6.1 was updated with the link to the web site of suppliers or full address.

The deliverables D2.4, D3.1, D4.5, D4.6, D4.7, D4.10, D5.2, D5.3, D6.2, D7.7 was update according to the recommendation by rewrite conclusion and adding abbreviation index.

The D8.4 (actual report) was updated according to the comment from the reviewer.

## 5 Deviation from Annex 1 and Annex 2

Overall, INSTABAT is on track and there are no deviations from the DoA with important consequences. It is expected that the INSTABAT project will be completed within the scheduled timeframe, reaching the initially set objectives, without requiring more than the allocated resources.

Regarding the identified implementation risks, status and corrective actions are reported in the Task8.3 of this report and in the critical risks section of the Participant Portal.

In the next part, more details are given on deviations at the level of Tasks and at the level of Resources. For all information related to Resources, see **Appendix 1 "Periodic Financial Report"**.

### 5.1 Tasks

Partners	Task	Deviation explanation	Impact on other tasks, on the available resources and the planning
CEA	WP8, WP7	During the first period of the project Internal difficulties at CEA was impact the coordination of the project. The impact of COVID on the global activities of CEA and the charge from others project to the coordinator (Maud Priour) was impact the work in WP8 and induce delay on the delivery of numbers of Deliverables in WP8 and WP7.	The impact of this deviation was essentially on the WP8 and in a little bit on the WP7 activities. This lake of resources for coordination impact the following and deliverance of a number of deliverable of the project (see Table 45). The change of coordinator by CEA in February 2022 made it possible to catch up and provide all the deliverables for the midterm review. For the second period of the project the change in coordination solved difficulties in WP8 and WP7.
CEA, CNRS, UAVR, IFAG	WP2	The development of sensors and they adaptation to the cell environment taking more time than initial planning (OF-Lum, OF-Li and PASCO2).	This deviation of the planning impact the WP3 for the implementation of sensors in cells for ageing study and correlation between sensors signal and degradation mechanisms.
CEA, CNRS, UAVR	WP3	Due to the time shift on the development of sensors the ageing campaign on	This deviation had an impact on the WP4 and the WP5 for validation of the ageing model,



		<p>instrumented cell was shifted in the planning</p> <p>The CO2 sensor in its earlier versions could not be integrated realistically into the pouch cells. It was therefore disregarded in the further course of WP3.</p> <p>The cell fabrication and instrumentation followed by the ageing test taking more time than expected. The consequence was the results arrived late in the project and delay the associate deliverables</p>	<p>the development of virtual sensors and the development of SOX (WP4 and WP5). This deviation was not critical due to the recent results on the development of sensors and the validation of the multiplatform in WP5 (see results from WP3, WP5 and the collaboration work with BIGMAP project: ESRF experiment). In the second part of the project the deviation of the planning for the ageing test and results impact the achievement of the analysis. The consequence was the delay on the submission of the D33.</p>
<b>CEA, INSA, UAVR</b>	WP4	<p>The development of the virtual sensors and the integration into the BMS SoX indicator suffer to the delay from WP3. The experimental data needed to the validation of the model, the virtual sensors and the SoX algorithms come from the WP3. The delay of the achievement of the WP3 task was impact the achievement of WP4 tack.</p>	<p>The consequence of this delay to the availability of the experimental data from WP3 was a delay to the development and the validation of the Virtual sensors and the SoX algorithms. This work can be finalized at the end of the project and impact also the WP5 for the proof of concept validation at the end of the project.</p>
<b>All</b>	WP5	<p>From the first considerations on the multi-sensor platform, we quickly realized that it would be challenging to interface sensors and algorithms with a rapid prototyping platform. It's absolutely necessary to choose a target with a wide variety of physical and communication I/O to interface sensors but also without strong memory or computation resource limitations to interface all processing blocks. Consequently, we decided to base our platform on a flexible, reconfigurable and high performance target hardware such as an instrumentation computer. This architecture is more in line with the level of maturity of the sensors and algorithms developed within the framework of INSTABAT, whose primary objective is to demonstrate the relevance of these technologies rather than their integrability. All the partners have validated the changes compared to the initial proposal. There is no impact on the distribution of resources allocated to the WP5.</p> <p>At the end of the project, the delay on the development of the virtual sensor and the SoX algorithm was impacting the progress of the WP5 for integration of all the functionality in the platform. The tests with a fully integrated platform on multi-instrumented smart cells could only be carried out at the very end of the project for the proof of concept.</p>	<p>It's noteworthy that WP5 advanced faster than expected on the proposal planning during the first phase of the project. The multi-sensor platform validated functional blocks developed for the WP5 have already been used during the experiments at the ESRF and to obtain results for the WP2 and WP3. During the second phase of the project, the impact of the delay for the virtual sensor development and SoX integration into the platform was on the realisation of experiments for the proof of the concept. The consequence was on the time constraint at the end of the project to finalise the proof of concept (D5.5, D5.6 and MS7)</p>



Table 45: List of deliverables already delivery with due date, delivery date and delay. Revised due date for D1.1, D1.2, D2.3, D2.4 and D7.2 was asked after the midterm review.

Deliverable	WP	Due date	Delivery date	Delay (J)	Revised due date	Delivery date	Delay(j)
D1.1	1	31/01/21	12/03/21	40	31/05/22	11/05/22	-20
D1.2	1	28/02/21	12/03/21	12	31/05/22	11/05/22	-20
D2.1	2	30/11/20	04/01/21	35	-	-	-
D2.2	2	31/08/21	30/08/21	-1	31/05/22	09/05/22	-22
D2.3	2	30/11/21	20/01/22	51	31/05/22	09/05/22	-22
D2.4	2	31/08/22	23/09/22	23	-	-	-
D2.5	2	31/08/22	25/09/22	25	-	-	-
D3.1	3	30/04/23	18/04/23	-12	-	-	-
D3.2	3	30/04/23	28/06/23	59	-	-	-
D3.3	3	31/12/23	07/12/23	-24	-	-	-
D4.1	4	31/08/21	30/08/21	-1	-	-	-
D4.2	4	28/02/22	28/02/22	0	-	-	-
D4.3	4	28/02/22	28/02/22	0	-	-	-
D4.4	4	28/02/22	02/03/22	2	-	-	-
D4.5	4	31/08/22	08/09/22	8	-	-	-
D4.6	4	31/05/23	10/07/23	40	-	-	-
D4.7	4	31/05/23	03/03/23	-89	-	-	-
D4.8	4	31/05/23	12/06/23	12	-	-	-
D4.9	4	31/05/23	10/07/23	40	-	-	-
D4.10	4	31/08/22	23/11/22	84	-	-	-
D4.11	4	31/05/23	03/10/23	125	-	-	-
D4.12	4	31/12/23	18/12/23 (*)	-13	08/03/24 (*)	-	-
D5.1	5	30/04/23	12/06/23	43	-	-	-
D5.2	5	31/08/22	19/09/22	19	-	-	-
D5.3	5	31/01/23	19/09/22	-134	-	-	-
D5.4	5	30/06/23	17/11/23	140	-	-	-
D5.5	5	31/12/23	18/12/23	-13	-	-	-
D5.6	5	31/12/23	21/12/23	-10	-	-	-
D6.1	6	30/06/23	06/07/23	6	-	-	-
D6.2	6	30/09/23	29/09/23	-1	-	-	-
D6.3	6	31/12/23	07/12/23	-24	-	-	-
D6.4	6	31/12/23	01/12/23	-30	-	-	-
D7.1	7	30/11/20	22/03/22	477	-	-	-
D7.2	7	30/11/20	11/02/22	438	31/05/22	09/05/22	-22
D7.3	7	28/02/21	11/02/22	348	-	-	-
D7.4	7	28/02/22	14/03/22	14	-	-	-
D7.6	7	31/08/21	31/03/22	212	-	-	-
D7.7	7	31/08/22	13/09/22	13	-	-	-
D7.8	7	31/12/23	20/12/23	-11	-	-	-
D8.1	8	30/09/20	06/04/22	553	-	-	-
D8.2	8	28/02/21	11/02/22	348	-	-	-
D8.3	8	30/04/22	28/04/22	-2	-	-	-
D8.4	8	31/12/23	21/12/2023	-10			

(\*) A first version of the deliverable was submitted on the server but it was rejected by the PO due to missing information. To complete the deliverable additional work was needed to analyse and exploit the results from last experiment of the project with the multi-sensor platform. These experiments were done at the end of December. The additional work was performed by CEA during January and February 2024. A new version of the deliverable D412 was upload on the server the 08/03/2024, one week before the final review meeting.





## 5.2 Use resources

The paragraph below gives the explanation about the deviation of use resources for each partner. We keep on this document the comment of the EC for the first period and the justification given in the mid-term review report (D83). The justification for the situation for each partners at the end of the project is given in a separate paragraph: "Status at the End of the project".

### 5.2.1 CEA

#### For the 1<sup>st</sup> period of the project

##### EC comment:

For CEA: Total costs: budgeted € 575.128,13; claimed in this period € 458.025,76. Deviation -20.36%. Effort in person-months: budgeted PM 51,46 ; claimed in this period PM 35,92. Deviation -30.20%. Please explain.

##### Justification:

Sensors development in the WP2 took more time than initial planned. The consequence is a shift in the planning for the WP2 and WP3 task. Task dedicated to the integration of sensors in cells and test campaign was shifted and explain the deviation of the budget and person-month at lower value.

#### Status at the End of the Project

The situation at the end of the project for CEA is given in the table below. For the project the total budgeted was estimate at €1,150,255 with an effort in Person-month of 89.5. During the period 1 the PM was less than estimate with 35.92 PM and we explain the reason (see previous paragraph). During the second phase of the project, WP2 and WP3 was require more time and effort to achieve the goals of the project. For these reasons, an extension to the project for 4 month was requested and accepted by EC.

The consequence of this extension was increase the amount of PM need to do the work and achieve the goals. The deviation effort in PM is +10% correspond and the deviation for the budget estimate at 14% (budgeted €1,150,255, estimate 1 308 632,30 €).

	Cost		% real vs budgeted	
	€	Person-months	€	Person-months
<b>Budgeted for CEA</b>	1 150 255 €	89,5		
<b>Period 1 (T0 +18)</b>	<b>458 026 €</b>	<b>35,92</b>	<b>40%</b>	<b>40%</b>
<b>Period 1 (T0 +18) with adjustment</b>	<b>557 810,52 €</b>	<b>39,90</b>	<b>48%</b>	<b>45%</b>
<b>Period 2 (M19 -&gt; M40)</b>	<b>750 821,78 €</b>	<b>58,16</b>	<b>65%</b>	<b>65%</b>
<b>Total</b>	<b>1 308 632,30 €</b>	<b>98,08</b>	<b>114%</b>	<b>110%</b>

#### Explanations for Adjustment to Period 1

There was a delay between the moment the cost occurred and when it appeared in our accounting systems. This was especially true for P1 as the end of the reporting period coincided with the CEA's annual closing of accounts. This means that for example, at the time, the hours of work occurred in the months of January and February 2022 were not yet registered and thus not presented in RP1.

The adjustment of 47 492,60€ in personnel unit costs, 4 168,16€ in personnel actual costs and 28 167,05€ in LRI costs reflects this.

**EC comment from the final review:**

1- *“There are personnel costs declared as actual costs, which were not foreseen in the budget. This should have been put under deviations in the Periodic Report. Moreover, there is no justification of the deviations in the large research infrastructure costs (budgeted € 221.000; claimed € 263.632,45). Please explain.”*

2- *“CFS: in the Tables of Procedures, in the procedures A3 FF31 is “Confirmed” while the corresponding option of individual hourly rates is not chosen, which appears inconsistent. FF 32 and 36 are both confirmed, which is not normally consistent. Please explain. In the procedure E1 (exchange rates) both FFs are N/A, with the reason (as stated in the Independent Report) that another option was applied. Please clarify.”*

**Answer:**

**1- Actual costs and LRI costs deviation**

According to the CEA’s usual accounting practices, and confirmed by the independent auditor for the CFS, the use of personnel on non-permanent contracts must be allocated to “actual costs” and not “unit costs”. For this reason, all the costs that concerned the work of non-permanent personnel contracts has been allocated into actual costs. The CEA initially budgeted only unit costs because at the time of the proposal, it was not planned to have personnel on non-permanent contracts working on the project.

LRI reflects the cost of the use of platforms "Liten Battery" and "Leti System". Given that the platforms have been “used” more than planned for INSTABAT (+10% effort in PM), than it is normal that the LRI costs also deviate. Furthermore, the LRI costs are calculated and audited by our statutory auditors. They are based on the costs of the year N-1 and are readjusted when the actual costs for the Year N are known. For example, at the time of the proposal, the available audited hourly rate for use Liten Battery platform was 39.40€. By 2023, the same audited hourly rate was 41.68€.

The deviation of the LRI costs is thus explained both by an increase in the number of hours worked and the cost of each hour worked on our platforms.

**2- CFS**

Reply translated from our statutory auditors:

- We have classified C for FF31 because the CEA reports permanent staff corresponding to Option I as well as expenses for temporary staff such as interns, non-permanent workers, and doctoral candidates corresponding to Option II.
- We have classified C for FF32 and 36 because the portion of staff reported by the CEA includes both employees who use a time reporting system and interns, non-permanent workers, and doctoral candidates who are recruited for a specific project.
- For FF66 and 67, we have corrected the CFS”
- The updated CFS has been uploaded in the reporting period.

## 5.2.2 BMW GROUP

### For the 1<sup>st</sup> period of the project

#### EC comment:

For BMW: Total costs: budgeted € 98.943,13; claimed in this period € 127.407,83. Deviation +28.77%. Please explain.

#### Justification:

BMW's project contribution within the duration of project is not distributed linearly between all funding periods/quarters.

Therefore, a cost overrun (here: +28.77%) within one funding period may occur.

The duration of WP1 „Definition of requirements“ according to the description within GA lasted 6 months (from PM 01 to) PM 06.

As described within BMW's part of the proposal, the main part of the BMW contribution for Project INSTABAT takes place in WP1 (6.0 PM out of 11.1 PM in total = 54,0% of contribution).

Therefore, the amount of € 100.225,88 out of the total of € 127.407,83 for Period 1 are the costs for WP 1 (claimed effort: 6,5 PM).

The difference of € 27.181,95 (= 27,8 % of the remaining project budget of € 97.660,38) is claimed for contributions to WP 7 (1,28 PM) and WP 8 (0,46 PM).

#### Status at the end of the project

For BMW: Total costs: budgeted € 197.886,25; claimed in in total € 201.963,14. Deviation +02.06%.

The Costs for period 2 are € 74.555,31.

The project required more working time than originally planned. As a result, the overall budget was exceeded by 2% despite lower other direct costs.

Due to the COVID situation during the project period, there was an increased exchange via online meetings instead of face-to-face meetings (business trips), which led to increased effort in the management process.

		Grant Agreement PM	TOTAL claimed
Definition of requirements	WP 1	6,0	6,50
Techno-economic feasibility, adaptability to other cell markets and environmental considerations	WP 6	2,6	2,98
Dissemination, communication and exploitation	WP 7	2,0	2,12
Project Management	WP 8	0,5	1,29
		<b>11,1</b>	<b>12,89</b>

## 5.2.3 CNRS

From CNRS side, the budget justification is given below.

### For the 1<sup>st</sup> period of the project

#### EC comment:

For CNRS: Total costs: budgeted € 263.786,88; claimed in this period € 115.626,15. Deviation -56.17%.  
Effort in person-months: budgeted PM 39,36; claimed in this period PM 20,88. Deviation -46.95%.  
Please explain.

#### Justification:

Owing to the pandemic, decision was made to postpone by few months the hiring of Dr. Fu Lui knowing that he was the best candidate for this position with a very strong background in handling optical fibers as well as the physics of optical signal associated with these sensors. This delay thus led to some delay in buying consumables. Finally, and again owing to the pandemic situation, most of the meetings were held virtually, and thus the money previously budgeted for missions was not used as planned.

### Status at the end of the project

The status at the end of the project for CNRS is given in the table below with real data for period 2. The planned total budget for CNRS was €527 573.75, corresponding to 67 PMs.

	Cost		% real vs budgeted	
	€	Person-months	€	Person-months
<b>Budgeted for CNRS</b>	527 573.75	67		
<b>Period 1</b>	<b>115.626,15€</b>	<b>21.2</b>	<b>21.92%</b>	<b>31.64%</b>
<b>Period 2</b>	<b>289.932,05€</b>	<b>38.33</b>	<b>54.95%</b>	<b>57.20%</b>
<b>Adjustment Period 1</b>	<b>9.964,29€</b>	<b>2.28</b>	<b>1.89%</b>	<b>3.40%</b>
<b>Total</b>	<b>415.522,49€</b>	<b>61.81</b>	<b>78.76%</b>	<b>92.24%</b>

#### EC comment from the final review:

for CNRS:

Total costs: budgeted € 527.573,75; claimed € 415.522,49. Deviation -21.24%. Please explain.

CFS: In the report of factual Findings, the amount certified in the CFS is 14 cents less than what was claimed by the beneficiary. In the Tables of Procedures, in the procedure A2 FF 28 is confirmed, while method A has been chosen. In the procedure A4, both Factual findings are confirmed, which is not normally consistent. Please explain. Please send a correct CFS.

#### Justification:

The problem comes from the PM. We budgeted 527573.75 euros (67 PM) and we declared less. The reason is that there have been some changes concerning permanent researchers involved in this project. Dr. Daniel Alves Dalla Corte and Dr Alexis Grimaud left and they have not been replaced.

---

« Concerning the 14 cents: There was a difference because the total had been rounded up on the Portal. We have modified the CFS accordingly.

Concerning question 28: This point does not apply because we apply method A. We have modified the CFS accordingly.

Concerning question A4: we have confirmed all the conclusions because we do have some permanent staff at CNRS who fill in timesheets (the working hours are declared on our software TEMPO), thus points 33, 34, 35 and 36 apply. And we also have some non-permanent staff who fill in both timesheets and a "Declaration on a person working exclusively on a H2020 action", which we use to calculate the salary costs that we declare (point 37 apply). »

## 5.2.4 IFAG

### For the 1<sup>st</sup> period of the project

#### EC comment:

For IFAG:

1. There are personnel costs declared as unit costs, which were not foreseen in the budget. This should have been put under deviations in the Periodic Report. Please explain the reason of this transfer.
2. Average personnel costs: budgeted € 11.061,00; claimed in this period € 6.010,66. Deviation -45.66%. Please explain.
3. Please also provide details about external colleagues reported under other direct costs. Anyway, these costs were not foreseen as other direct costs in Annex 1. Therefore please correct the Use of Resources.

#### Justification:

1. It was our mistake having applied the personnel cost with category a) as actual personnel cost, IFAG uses average hourly rate for personnel cost calculation, the right category should be b) as unit personnel cost. According to Annotated Grant Agreement for cost transfer between category a) and b) there is no amendment required, but if it's wished then we can change the cost category within next amendment run.
2. We have planned the personnel cost of internal and external employees both as personnel cost, total Plan PMs were also for internal and external colleagues. But in last EU audit in 2021 we learned from the EU auditor that the cost for external colleagues in our case should be reported with category other direct cost for service. Therefore, in financial statement we separated the personnel cost for internal and external colleagues in two cost categories, I decided to report also actual PMs for external colleagues in financial statement, as their PMs are also in the Plan PMs. Therefore, the actual average personnel cost in comparison to plan average personnel cost should be calculated in this way: The sum of actual personnel cost and other direct cost /actual PMs  
☐ Average personnel costs: budgeted € 11.061,00; claimed in this period € 10.447,54; Deviation is 5% not 45%.

Cost for external colleagues was foreseen as personnel cost in Annex 1, if it's required we can divide the budget of personnel cost into two cost categories.

#### Status at the end of the project

The status at the end of the project for IFAG is given in the table below. The planned total budget for IFAG was 812,715 €, corresponding to 52 PMs. As explained in the previous paragraph, the personnel effort was split between internal colleagues (reported as "Personnel Direct Costs") and external colleagues (reported as "Other Direct Costs"). The estimated total real cost is just 4% above plan, while the estimated real effort (in PMs) is 15% above plan. The main reason for this slight imbalance in the deviations between cost and effort can be explained as followed: Since the PA sensor in its earlier versions could not be integrated realistically into the pouch cells, it was disregarded in the further course of WP3. On the one hand, this strongly reduced the need for samples to be manufactured and provided to CNRS (thereby decreasing the cost for materials), but on the other hand, this increased the effort invested by IFAG to further decrease the size of the PA sensor (thereby increasing the required PMs). This additional effort was used, for instance, for concept studies on alternative architectures of the PA sensor. Unplanned efforts went also into the consideration of a change of the optical filter to avoid the cross-sensitivity with electrolyte vapor, which was identified by CEA.





	Cost		% real vs budgeted	
	€	Person-months	€	Person-months
<b>Budgeted for IFAG</b>	812 715 €	52		
<b>Period 1 (T0 +18)</b>	<b>475 972 €</b>	<b>34,4</b>	<b>59%</b>	<b>66%</b>
<b>Period 2 (M19 -&gt; M40)</b>	<b>353 169 €</b>	<b>25,5</b>	<b>43%</b>	<b>49%</b>
Total	844 539 €	59,9	104%	115%

**EC comment from the final review:**

*For IFAG: Average personnel costs: budgeted € 11.061; claimed € 6.552,53. Deviation -37.14 %. Please explain.*

**Justification:**

The budget initially included external colleagues within the category of personnel costs. However, subsequent information from the auditor revealed that the cost for external colleagues should be reported under the category of other direct costs for services. If we incorporate the other direct costs for services to calculate the average personnel cost, considering both internal and external colleagues, then the budgeted amount is at €11,061 and the claimed amount becomes €11,279. This adjustment results in a deviation of less than 2%.

## 5.2.5 FAURECIA

### For the 1<sup>st</sup> period of the project

#### EC comment:

- for FAURECIA: Total costs: budgeted € 46.500,00; claimed in this period € 12.500,00. Deviation -73,12%. Effort in person-months: budgeted PM 3,18; claimed in this period PM 0,80. Deviation -74.84%.
- for Faurecia Ger (Third party of beneficiary FAURECIA): There are personnel costs declared as unit costs, which were not foreseen in the budget. This should have been put under deviations in the Periodic Report. Please explain the reason of this transfer. Total costs: budgeted € 69.750,00; claimed in this period € 20.132,08. Deviation -71,14%. Effort in person-months: budgeted PM 1; claimed in this period PM 1,22. Deviation +22.00%.

#### Justification:

1. Faurecia's contribution within the duration of the project is not distributed linearly between all funding periods. Therefore, the deviations of -74.84% for Faurecia and -71,14% for Faurecia Ger were occurred.
  - a. As it is described within INSTABAT proposal, the main part of the Faurecia contribution for INSTABAT project takes place in WP6 and WP6 will start on the third year of the project which has a total effort in person-months as 6 PM (out total of 14 PM for Faurecia).
  - b. Like WP6, our main contribution for WP5 will also start only on second half of the project which corresponds to 1.5PM for 14 PM (Currently, we used only 0.05 PM for the meetings we have attended for WP5).
  - c. We have used the budget for following work packages.
    - i. 0.5 PM for WP1 (out of 0.5 PM) which has been finished after first 6 months of the project.
    - ii. 1.2 PM for WP4 (out of 5 PM): 1.2 PM was used to give the first version of the 3D thermal model and the rest of the budget will be used to give a final version of the 3D thermal model.
    - iii. 0.17 PM for WP8 (out of 0.5 PM): The project will require more program management from Faurecia side, when the workload is higher on second half of the project.
    - iv. 0.10 PM for WP7 (out of 0.5 PM): Similar to WP8, we will require more budget for second half of the project for dissemination, communication and exploitation of the data that we will produce within INSTABAT project.

Since our workload will be higher on the second half of the project, we believe the deviations are normal for each work package.

2. Faurecia and Faurecia Ger use average hourly rate for personnel cost calculation, so the right category should be b) as unit personnel cost. We apologize for our mistake having applied for the personnel cost with the category a).
3. The team of Faurecia for INSTABAT project has changed after INSTABAT proposal submission. During the proposal stage, we have defined Faurecia France taken the management and main workload of this project, however after the proposal, it was decided to give more workload and management of the INSTABAT to Faurecia Ger (third party of beneficiary Faurecia). Due to this reason, the effort in person-months for Faurecia Ger (third party of beneficiary Faurecia) is higher than Faurecia.

### Status at the end of the project

The situation for Faurecia is explained in the table below with the cost for period 2 (M19-M40). For the project, the total budgeted was at €232,500 with an effort in Person-month of 14. During the period 1 the PM was less than estimate and the reasons are explained in the previous paragraphs. During the second phase of the project, WP4 and WP6 required more time and effort to achieve the goals of the project and finish the deliverables before ending the project and due

to this reason, most of the budget was used in second half of the project. The total estimation of PM is higher than what is estimated previously given the 4-month extension, however the total budget is almost reached due the lower travel cost.

	Cost		% real vs budgeted	
	€	Person-months	€	Person-months
<b>Budgeted for Faurecia</b>	232 500 €	14		
<b>Period 1 (T0 +18)</b>	32 632.08€	<b>2,02</b>	<b>14.0%</b>	<b>14.4%</b>
<b>Period 2 estimation (M19 -&gt; M40)</b>	200 647.50€	12,46	86.3%	89,0%
<b>Total (estimation)</b>	<b>233 279.58€</b>	<b>14,48</b>	<b>100,3%</b>	<b>103.4%</b>

#### EC comment from the final review:

*for FAURECIA:*

*Total costs: budgeted € 93.000; claimed € 34.627,50. Deviation -62.77%. Effort in person-months: budgeted PM 6,50; claimed PM 2,20. Deviation -66.15%. Please explain, splitting the beneficiary and its third party.*

*for Faurecia Ger (Third party of beneficiary FAURECIA):*

*Total costs: budgeted € 139.500; claimed € 198.6252,08. Deviation +42.40 %. Effort in person-months: budgeted PM 7,50; claimed*

#### Justification:

The team of Faurecia for INSTABAT project has changed after INSTABAT proposal submission. During the proposal stage, we have defined Faurecia France taken the management and main workload of this project, however after the proposal, it was decided to give more workload and management of the INSTABAT to Faurecia Ger (third party of beneficiary Faurecia). Due to this reason, the effort in person-months for Faurecia Ger (third party of beneficiary Faurecia) is higher than Faurecia.

## 5.2.6 INSA LYON

### For the 1<sup>st</sup> period of the project

#### EC comment:

For INSA LYON: Total costs: budgeted € 142.961,88; claimed in this period € 88.785,58. Deviation -37.90%. Average personnel costs: budgeted € 5.079,00; claimed in this period € 3.317,53. Deviation -34.68%. Please explain.

#### Justification:

The average PM cost of € 5.079,00, given in the initial budget, was calculated based on the salaries of senior researchers and junior researchers, and on an estimation of time for each person. During this first period, most activities have been carried out by the junior researcher (PhD employed to work in the action), who has declared 17 PM on a total of 20.96 PM.

Mian Asif, the junior researcher, has worked on the development of a reduced-order electrochemical model for state-estimation of the battery; as such, the code development and testing process has been carried out in a large percentage by him.

As the salary of the junior researcher is lower than the cost of senior researchers, the declared average personnel cost of this first period is lower than € 5.079,00. This could also explain that the personnel costs we are claiming for this mid-term reporting is lower than half of the personnel budget.

The activities in the second half of the project will concern the fine-tuning of the developed state estimators to obtain the required performances for the specific cell chemistry used in the INSTABAT project. This will undoubtedly require more work by more senior researchers in order to explore new optimized strategies applied to the model and prepare publication of novel results.

Moreover, claimed costs for “other direct costs” are lower than initially planned for two reasons:

Due to COVID context, it was not possible to travel. As a consequence, we only declared € 1 493,00 while we initially budgeted € 14 500 for travels.

The budget foreseen to buy consumables will only be used in the second period of the project. The budget for consumables will help with the validation of the real-time code using a small microcontroller to test the required computational capabilities in order to illustrate the trade off between accuracy of state reconstruction and computational cost of the developed estimators. This cannot be carried out before the production of a code-generation ready version of the code, which will be done in parallel with the demonstrator development by CEA in the second half of the project.

## Status at the end of the project:

The final costs for INSA, after the definitive financial reporting are as follow:

TYPE of EXPENDITURE (as defined by Partner)	TOTAL DURATION FORECAST	ACTUAL FIGURES		
	PLANNED	1ST Period	2ND Period	TOTAL
Total Person-Months (M-M)	41,00	20,96	33,55	<b>54,51</b>
Personnel	208 239,00	69 535,50	172 256,00	<b>241 791,50</b>
Consumables	6 000,00		2 106,05	<b>2 106,05</b>
Equipment	0,00			<b>0,00</b>
Travels & Subsistence	14 500,00	1 492,96	9 582,44	<b>11 075,40</b>
Subcontracting	0,00			<b>0,00</b>
Indirect Costs - Overheads	57 184,75	17 757,12	45 986,12	<b>63 743,24</b>
<b>Total Costs (with IC)</b>	<b>285 923,75</b>	<b>88 785,58</b>	<b>229 930,61</b>	<b>318 716,19</b>

The final costs are slightly above the initial budget (+11.47%). Mostly due to a 16.11% increase in the initially projected personnel costs. This is explained by the extra person-month involvement in the second half of the project. Two main reasons explain this cost: (i) the extension of the project duration (+11.11% total duration), and (ii) unplanned extra work done by INSA relating to the re-parametrization of the open-circuit potential curves for the reduced E-BASE model in order to obtain better agreement with experimental data (required for the final version integrated into the BMS in the multi-sensor platform of WP 5). Overall, the budgetary impact of these two factors was mitigated by the fact that less senior researchers were involved in most of the extra tasks. Furthermore, the consumables and travel expenses were lower than initially projected, mostly due to large differences during the first half of the project (COVID).

---

## 5.2.7 UAVR

### For the 1<sup>st</sup> period of the project

#### EC comment:

Effort in person-months: budgeted PM 37,42; claimed in this period PM 17,21. Deviation -54,01%. Average personnel costs: budgeted € 3.115,00; claimed in this period € 4.635,90. Deviation +48.83%. Please explain.

#### Justification:

The deviations of -54.01 % in Person-Months were due to delays that could not be avoided in the signings of the contracts of Post-Doc and PhD student. The processes, in COVID19 context, took much longer than expected and required a higher effort of the Senior Researcher, originating a deviation of +48.83% in average personnel costs during reported period. In any case, in the end of the project, no significant deviations are expected in total number of person months and personnel costs.

#### Situation at the end of the project

Effort in person-months (M19-M40): rebudgeted PM 43,79 (as explained in previous paragraph); claimed PM44,49 in the 2<sup>nd</sup> period. No significant deviation at the end of the project.  
Personnel costs (M19-M40): rebudgeted (as explained in previous paragraph) €110.200,00; claimed €112.382,44 in the 2<sup>nd</sup> period. No significant deviation at the end of the project.



## 5.2.8 VMI

The data on the use of resources at the end of the project for VARTA is given in the table below.

Table 46: Use of resources of VARTA for INSTABAT project M01\_M40

	<b>Personnel</b>	<b>Consumables</b>	<b>Travel</b>	<b>Depreciation</b>	<b>Overall Costs</b>
<b>Planned</b>	~233 k€ (27 PM)	~19 k€	~7 k€	~25 k€	~284 k€
<b>Actual</b>	~246 k€ (27 PM)	~10 k€	~3 k€	~25 k€	~284 k€
<i>deviation</i>	+6%/ (0%)	-47%	-57%	±0%	±0%

Personnel: The deviation in personnel costs is +6% (no deviation for PM) but it proved necessary to deploy more staff in the "Senior Scientists" category than originally planned.

Consumables: Due to the smaller batch sizes resulting from the degree of maturity, fewer consumables were used than estimated.

Travel: Due to the Covid2019 situation, not all project meetings could be physically attended and therefore less than budgeted travel costs were consumed.

### EC comment from the final review:

*for VMI:*

Total costs: budgeted € 284.322,50; claimed € 284.443,98. Deviation -42,96 %.

Effort in person-months: budgeted PM 27 ; claimed PM 14,37. Deviation -46.78 %. Please explain (figures as stated in the Periodic Report are not correct).

### Justification:

For an explanation of the costs claimed by beneficiary number 8, VMI, please refer to the table with the separate statement of claimed costs for the two accounting periods. It should be noted that in the **1<sup>st</sup>** accounting period, the costs up to **May 17, 2021** are listed for **VARTA Micro Innovation GmbH (PIC 969322456, VMI - [UTRO] VMI, 12.40 PM)** and up to the end of this period for **VARTA Innovation GmbH (PIC 890218277, VMI, 4.18 PM)**. Therefore, only the costs of **VARTA Innovation GmbH (PIC 890218277, VMI, 10.19 PM)** are claimed for the **2<sup>nd</sup>** accounting period. In total, € 284.322,50 was budgeted for beneficiary number 8 VMI and total costs of € 284.443,98 are claimed by beneficiary number 8, VMI.



Table 47: Distribution of person-months and costs claimed by VARTA Micro Innovation GmbH (PIC 969322456, VMI - [UTRO] VMI) and VARTA Innovation GmbH (PIC 890218277, VMI) for the 1st and 2nd reporting periods.

Period Number	1 <sup>st</sup>		2 <sup>nd</sup>		
Period Covered	From 1/Sep/2020 to 28/Feb/2022		From 1/Mar/2022 to 31/Dec/2023		
Beneficiary Number	8	8	8		
Beneficiary Short Name	VMI - (UTRO) VMI	VMI	VMI		
Associated WP	PM	PM	PM	Total / PM	Planned /PM
1	8,22			8,22	8,5
2					
3					
4					
5	4,05	2,13	3,20	9,38	9,0
6			5,87	5,87	6,0
7		1,92	0,91	2,83	3,0
8	0,13	0,13	0,21	0,47	0,5
<b>Total / PM</b>	<b>12,40</b>	<b>4,18</b>	<b>10,19</b>	<b>26,77</b>	<b>27,0</b>
	Beneficiary Short Name	Direct Personal costs / €	Direct other costs / €	Indirect costs / €	Total costs / €
1 <sup>st</sup> Period	VMI - (UTRO) VMI	91.261,90	6.542,65	8.639,61	122.255,69
1 <sup>st</sup> Period	VMI	29.348,77	5.209,66	24.451,14	43.198,04
2 <sup>nd</sup> Period	VMI	76.630,95	18.561,25	23.798,05	118.990,25
<b>FSFS</b>	<b>VMI</b>	<b>197.241,62</b>	<b>30.313,56</b>	<b>56.888,80</b>	<b>284.443,98</b>